



Coordination of Phosphido-boratabenzene Ligands to Transition Metals

Thèse

Viridiana Lizet Pérez Torres

Doctorat en chimie
Philosophiae doctor (Ph.D.)

Québec, Canada

© Viridiana Lizet Pérez Torres, 2016

Coordination of Phosphido-boratabenzen Ligands to Transition Metals

Thèse

Viridiana Lizet Perez Torres

Sous la direction de :

Frédéric-George Fontaine, directeur de recherche

Résumé

Environ 90% des composés produits industriellement sont fabriqués à l'aide de catalyseurs. C'est pourquoi la conception de catalyseurs toujours plus performants pour améliorer les procédés industriels actuels est toujours d'intérêt. De la grande variété de complexes avec des métaux de transition rapportés jusqu'à présent, les complexes zwitterioniques attirent notre attention par leurs activités catalytiques souvent supérieures aux complexes cationiques normaux. Un complexe métallique zwitterionique est un fragment métal-ligand neutre où la charge positive est située sur le centre métallique et où la charge négative est délocalisée sur un des ligands liés au métal.

Nous proposons la synthèse de ligands anioniques phosphine comportant des groupements borates et boratabenzènes. Cette dernière espèce est un cycle à 6 membres où l'un des atomes de carbone est remplacé par un atome de bore et qui est négativement chargé. La capacité de ces phosphines anioniques à se lier à un centre métallique à l'aide de la paire libre du phosphore est due à la nature du lien P-B qui défavorise l'interaction entre la paire libre du phosphore et l'orbitale p vide du bore.

Les propriétés de di-*tert*-butylphosphido-boratabenzène (**DTBB**) comme ligand phosphine anionique hautement donneur et encombré ainsi que la découverte de ses modes de coordination inhabituels pour stabiliser les métaux de transition insaturés ont été étudiés au cours de ce travail. De nouvelles perspectives sur les modes de coordination de phosphido-boratabenzène et la force de l'interaction du lien P-B seront discutées ainsi que les applications catalytiques.

Nous avons d'abord étudié la coordination η^1 avec des complexes de fer, ce qui nous a fourni des données quantitatives précieuses sur la capacité du **DTBB** d'agir comme ligand très donneur par rapport aux autres ligands donneurs bien connus. La capacité du **DTBB** à changer de mode de coordination pour soutenir les besoins électroniques du métal a été démontrée par la découverte d'une nouvelle espèce ferrocenyl phosphido-boratabenzène et sa nucléophilie a été étudiée.

Au meilleur de notre connaissance, aucun exemple d'un ligand boratabenzène coordonné aux métaux du groupe 11 n'existe dans la littérature. Voilà pourquoi

nous avons décidé d'explorer les modes de coordination du ligand **DTBB** avec Cu(I), Ag(I) et Au(I). A notre grande surprise, le ligand **DTBB** est capable de stabiliser les métaux du groupe 11 aux états d'oxydation faibles par une liaison M-P qui est une coordination du type η^1 , un mode de coordination guère observé pour les ligands boratabenzène.

Pendant nos travaux, notre attention s'est tournée vers la synthèse d'un complexe de rhodium(I) afin de tester son utilité en catalyse. A notre grande satisfaction, le complexe Rh-**DTBB** agit comme un précatalyseur pour l'hydrogénation des alcènes et alcynes à la température ambiante et à pression atmosphérique et son activité est comparable à celle du catalyseur de Wilkinson.

Dans un désir d'élargir les applications de notre recherche, notre attention se tourna vers l'utilisation des composés du bore autres que le boratabenzène. Nous avons décidé de synthétiser une nouvelle espèce phosphido-borate encombrée. Lorsqu'elle réagit avec des métaux, l'espèce phosphido-borate subit un clivage de la liaison P-B. Toutefois, cette observation met en évidence la singularité et les avantages de la stabilité de la liaison P-B lors de l'utilisation du fragment boratabenzène. Ces observations enrichissent notre compréhension des conditions dans lesquelles la liaison P-B du ligand **DTBB** peut être clivée. Ces travaux ont mené à la découverte d'un nouveau ligand *ansa*-boratabenzène avec une chimie de coordination prometteuse.

Abstract

About 90% of industrially produced compounds are made using catalysts. This is why the design of ever more efficient catalysts to improve the current industrial processes remains a subject of interest. A wide variety of complexes with transition metals have been reported so far. Amongst the plethora of metal complexes used as catalysts, zwitterionic complexes are of particular interest due to their increased catalytic activity that often surpasses that of their cationic parent complexes. A zwitterionic complex is a neutral metal-ligand fragment where the positive charge is localized over the metal center and the negative charge is delocalized over the ligands.

In order to generate new zwitterionic complexes, we are looking at the coordination chemistry of anionic phosphine ligands bearing boratabenzene functionalities. Boratabenzene is a six-membered heterocycle where one of the C-H fragments has been replaced by a negatively charged B-X fragment. The ability of these anionic phosphines to bind to a metal center by the phosphorous lone pair is due to the nature of the P-B interaction, which disfavours orbital overlap between the lone pair of electrons on phosphorous and the empty p orbital on boron.

The properties of di-*tert*-butylphosphido-boratabenzene (**DTBB**) as a highly donating and bulky anionic phosphine ligand and the discovery of its unusual coordination modes to stabilize unsaturated transition metals has been explored in the course of this work. New insights into the coordination modes of phosphido-boratabenzene and on the strength of the P-B interaction will be discussed. Catalytic applications of the synthesized complexes will also be presented.

First we studied the η^1 coordination of **DTBB** to iron, which had provided valuable quantitative data about the donating capability of the aforementioned ligand against other well-known good donors. The **DTBB**'s capability to change coordination modes in order to support the electronic needs of the metal has been demonstrated by the discovery of a new pendant ferrocenyl-like phosphido-boratabenzene species and its nucleophilicity has been proved.

To the best of our knowledge, no example of a boratabenzene ligand coordinated to group 11 metals has been reported in the literature. This is why we decided to

explore the coordination modes of **DTBB** ligand with Cu(I), Ag(I) and Au(I). To our surprise, the **DTBB** ligand is capable to stabilize group 11 metals in a low oxidation state featuring a M-P bond by means of a η^1 coordination, a scarcely observed coordination mode for boratabenzene ligands.

Looking for applications of boratabenzene complexes in catalysis, our attention turned to the synthesis of a rhodium(I) complex. To our delight, the **DTBB**-Rh complex acts as a precatalyst for the hydrogenation of alkenes and alkynes at room temperature and atmospheric pressure and its activity is comparable to that of Wilkinson's catalyst.

Finally in a desire to expand the concepts of our research, our attention turned to explore the use of alternatives to the boratabenzene moiety. We decided to synthesize a new bulky phosphido-borate species. When reacted with metals, the phosphido-borate undergoes a cleavage of the P-B bond. However, this finding sets forward the singularity and advantage of the P-B bond in boratabenzene moieties. This observations also enrich our understanding of the conditions under which the P-B bond on **DTBB** ligand can be cleaved; evidence that lead to the discovery of a new *ansa*-boratabenzene ligand with promising coordination chemistry.

Table of Contents

Résumé.....	iii
Abstract.....	v
Table of Contents.....	vii
List of Tables	xi
List of Schemes	xii
List of Figures	xiv
List of Equations	xvii
List of Abbreviations	xviii
List of Compounds.....	xx
Acknowledgments.....	xxii
1 Chapter 1 Introduction.....	1
1.1 Catalysis and Charge Effect.....	1
1.2 Boron Compounds, Promising Frameworks for Catalysis.....	6
1.3 Thesis Scope.....	8
2 Chapter 2 Literature Review	11
2.1 Boratabenzene Ring, Structure and Reactivity.....	11
2.2 The Rich Coordination Chemistry of Boratabenzene Ligands	12
2.2.1 η^6 Boratabenzene Metal Complexes	13
2.2.2 Ring Slippage and η^5 Coordination.....	14
2.2.3 η^4 and η^3 Boratabenzene Metal Complexes	15
2.2.4 η^1 Boratabenzene Metal Complexes: New Ligands with an Unusual Coordination Mode	16
2.3 Phosphido-boratabenzene Ligands	18
2.3.1 Phosphine Ligands, Versatility and Utility	18
2.3.2 DPB and DTBB Ligands, a Theoretical Comparison	20
2.3.3 Synthesis of DTBB Ligand	23
2.3.4 Metal Complexes of DTBB and DPB	24
2.4 Boratabenzene Complexes in Catalysis.....	25
2.4.1 Boratabenzene Complexes as Polymerization Catalyst.....	25
2.4.2 Miscellaneous Examples of Boratabenzene in Catalysis	27
3 Chapter 3 Methodology	30
3.1 Experimental Methods	30
3.1.1 Inert Atmosphere Chemistry	30
3.1.2 Pressurized Gas and Cryogenics.....	32
3.2 Characterization Techniques	33

3.2.1	Nuclear Magnetic Resonance spectroscopy (NMR).....	33
3.2.2	Mass Spectrometry.....	38
3.2.3	IR Spectroscopy.....	38
3.2.4	Elemental Analysis.....	39
3.2.5	X-Ray Diffraction.....	40
3.3	Density Functional Theory.....	41
4	Chapter 4 Iron Boratabenzene Complexes.....	43
4.1	Introduction.....	43
4.1.1	η^1 Complexes of Boratabenzene.....	43
4.1.2	Iron Carbonyl Species: Reactivity and Catalytic Applications.....	44
4.1.3	Boratabenzene Metal Complexes: Reactivity with H ₂ O.....	46
4.2	Synthesis and Characterization of CpFe(CO)₂(DTBB) (1).....	49
4.2.1	FT-IR, X-ray and Donating Capabilities of DTBB.....	51
4.3	CpFe(CO)₂DTBB (1) Photodissociation of CO Ligands.....	54
4.3.1	Characterization of CpFe(DTBB) (2).....	55
4.4	Formation of CpFe(C₅H₅B-OH) (3) and CpFe(C₅H₅B)-O-(BC₅H₅)FeCp (4).....	59
4.5	Reactivity of CpFe(DTBB) (2).....	64
4.5.1	Reactivity of 2 with H ₂ O.....	64
4.5.2	Reactivity of 2 with O ₂	66
4.5.3	Reactivity with H ₂	67
4.6	A Word on Borabenzene Decomposition Pathways.....	68
4.7	Conclusion.....	69
4.8	Experimental Details.....	70
	General Procedures.....	70
	CpFe(CO) ₂ (DTBB) (1).....	71
	CpFeDTPBB (2).....	72
	CpFeC ₅ H ₄ B-OH (3).....	72
	CpFe(C ₅ H ₅ B)-O-(BC ₅ H ₅)FeCp (4).....	73
	X-Ray Crystallography Data.....	73
	Crystal data and structure refinement for [CpFe(CO) ₂ (DTBB)] (1).....	74
	Crystal data and structure refinement for [CpFe(C ₅ H ₅ B-OH)] (3).....	75
	Crystal data and structure refinement for [Cp ₂ Fe ₂ (μ -oxo-C ₅ H ₅ B-O)] (4).....	76
5	Chapter 5 Copper Boratabenzene Complexes.....	77
5.1	Introduction.....	77
5.1.1	Two-coordinated Complexes.....	77
5.1.2	Cu(I) Coordination Chemistry.....	78
5.1.3	Cu(I) Species as Phosphine Scavengers.....	80
5.1.4	Cu(I) Cation π -Interaction with Arenes.....	81
5.1.5	Cu(I) Coordination to Cyclopentadienyl Ligands.....	82
5.1.6	Cu-B Interaction with Group 11 Metals.....	83
5.2	Synthesis and Characterization of η^1-Copper Species.....	85
5.2.1	X-ray Structure of 6a and 6b.....	93

5.2.2	DFT Calculations	95
5.3	Boratabenzene Silver Species	97
5.4	Reactivity of DTBB with Gold	100
5.5	Conclusion.....	106
5.6	Experimental Details.....	108
	(η^1 -DTBB)CuCl (5).....	109
	[(η^1 -DTBB) ₂ Cu]K (6a).....	109
	[(η^1 -DTBB) ₂ Cu][Cu(IMes) ₂] (6b)	110
	Proposed structure for complex [(DTBB) ₂ Ag]K (7)	111
	Reaction of DTBB with Me ₂ SAuCl, [Au ₄ (μ - η^2 -PtBu ₂) ₄] (8)	111
5.6.1	X-Ray Crystallographic Data	112
	Crystal data and structure refinement for [Cu(η^1 -DTBB) ₂]K (6a).....	113
	Crystal data and structure refinement for [Cu(η^1 -DTBB) ₂][Cu(IMes) ₂] (6b)	114
	Crystal data and structure refinement for [Au ₄ (μ -PtBu ₂) ₄] (8)	115
	Computational Studies.....	116
6	Chapter 6 Phosphidoboratabenzene-Rhodium(I) Complexes as Catalysts for the Hydrogenation of Alkenes at Room Temperature and Atmospheric Pressure	117
6.1	Context of the Research.....	117
6.2	Abstract.....	118
6.3	Résumé.....	118
6.4	Introduction	119
6.5	Results and Discussion	122
6.5.1	Reactivity of 9 with H ₂	125
6.5.2	Hydrogenation of Alkenes by Complex 9.....	130
6.6	Conclusions.....	132
6.7	Experimental Section	133
	General Considerations	133
	Synthesis of [Rh(C ₂ H ₄)(DTBB)] ₂ (9).....	133
	Reaction of [Rh(C ₂ H ₄ (DTBB)] ₂ (9) with H ₂	134
	Hydride 10	134
	Hydride 11	135
	X-ray Crystallography of 9	135
	Crystal data and structure refinement for [(C ₂ H ₄)Rh(DTBB)] ₂ (9).....	136
	General procedure for hydrogenation reactions	137
7	Chapter 7 On the Stability of the P-B Bond and Two New Ligands	138
7.1	The Di-<i>iso</i>-propylphosphido-triphenylborate Ligand (DiPB).....	138
7.1.1	Introduction: Precedents on Phosphine-boranes	138
7.1.2	Synthesis of Lithium Di- <i>iso</i> -propylphosphido- <i>tri</i> -phenylborate (DiPB)	141
7.1.3	DiPB Reaction with Metals of the Group 10	144
7.2	The Discovery of an <i>ansa</i>-boratabenzene Ligand (<i>ansa</i>-DTBB).....	147
7.2.1	Introduction: Metallocenes and Phosphorous Bridged <i>ansa</i> -ligands	147

7.2.2	The Cleavage of the P-B Bond and The Discovery of an <i>ansa</i> -Boratabenzene Ligand 150	
7.2.3	Preliminary Studies on the Coordination and Reactivity of <i>ansa</i> -DTBB.....	156
7.3	Conclusion: On the Stability of the P-B Bond and the Advantages of Having Boratabenzene.....	158
7.4	Experimental Details.....	161
	Lithium di- <i>iso</i> -propylphosphido-tri-phenylborate (DiPB)	162
	[(PPh ₃) ₂ Ni(μ-PiPr ₂) ₂] (12)	163
	[BPh ₄][Li(THF) ₄]	163
	Potassium ditertbutylphosphido-bisboratabenzene (<i>ansa</i> -DTBB).....	163
	Dipotassium ditertbutylphosphido-bisboratabenzene (13)	164
	X-Ray Crystallography Data	164
	Crystal data and structure refinement for [<i>i</i> Pr ₂ P-BPh ₃] ₂ Li (DiPB).....	165
	Crystal data and structure refinement for [(PPh ₃) ₂ Ni ₂ (μ-PiPr ₂) ₂] (12).....	166
	Crystal data and structure refinement for [<i>t</i> Bu ₂ P-(BC ₅ H ₅) ₂] ₂ K (<i>ansa</i> -DTBB).....	167
8	Chapter 8 Conclusion and Perspective.....	168
8.1	Future Work	172
8.1.1	Iron Boratabenzene Complexes	172
8.1.2	Copper Boratabenzene Complexes.....	173
8.1.3	Rhodium Boratabenzene Complexes.....	174
8.1.4	The DiPB and <i>ansa</i> -DTBB Ligands	174
8.2	Final Words.....	175
9	Bibliography	176

List of Tables

Table 2.1: Selected $\nu(\text{CO})$ stretching frequencies (cm^{-1}) of CO bonds in $\text{LNi}(\text{CO})_3$ complexes of phosphine and carbene ligands, against theoretical values for DTBB and DPB ligands.	21
Table 3.1: NMR frequency table of nuclei studied in this work.	33
Table 4.1: IR CO stretchings for complex 1 and other isoelectronic iron carbonyl complexes.	51
Table 4.2: Selected structural parameters: P-B, Fe-P and P-Fe-CO angles and comparison of 1 with similar iron complexes $\text{CpFe}(\text{CO})_2(\text{DPB})$ (XVI) and $\text{CpFe}(\text{CO})_2(\text{tBu}_2\text{P}\cdot\text{BH}_3)$ (XVII).	53
Table 4.3: Selected distances and angles, comparative of 3 and 4 with similar boratabenzene species.	60
Table 6.1: $T_1(\text{s})$ measurements for complexes $[(\text{DTBB})\text{Rh}(\text{H})_2]_2$ (10) and $[(\text{DTBB})\text{Rh}(\text{H})]_2$ (11) at different temperatures. This table was originally included in the supported information of the publication.	128
Table 6.2: Hydrogenation of alkenes and alkynes using 9 and Wilkinson's catalyst (X).	131

List of Schemes

Scheme 1.1: Catalyst charge effect on the catalytic transformation of <i>p</i> -chloro styrene into the hydrogenation product by catalyst a, the hydroformylation product by catalyst b and polymerization by catalyst c, under the same reaction conditions.	3
Scheme 2.1: Ring insertion by organo-boron halides to cyclopentadienyl ligand by Herberich.....	11
Scheme 2.2: Synthesis of borabenzene neutral adducts reported by Fu.	12
Scheme 2.3: Synthesis of DPB by nucleophilic attack on neutral C ₅ H ₅ B-PMe ₃ (III).	12
Scheme 2.4: Synthesis of DTBB ligand reported by our group in 2009.....	24
Scheme 2.5: Regioselective co-cyclization of alkynes and nitriles catalyzed by LCo(COD) (L = 1-Ph-Cp or C ₅ H ₅ B-Ph).....	26
Scheme 2.6: Scandium catalyst of boratabenzene used in the syndiotactic polymerization of styrene.	27
Scheme 2.7: Boration of octane using (C ₅ H ₅ B-Ph)Rh(C ₂ H ₄) ₂ , reported by Bazan.	28
Scheme 2.8: Intramolecular hydroamination using an Yttrium boratabenzene complex by Chen.....	28
Scheme 2.9: Catalytic dehydrocoupling of amino-boranes with an Yttrium boratabenzene complex, reported by Chen.	29
Scheme 4.1: Photodissociation of CO ligands and reactivity against other ligands.	44
Scheme 4.2: Hydrosilylation of acetophenone by [CpFe(CO) ₂ (PPh ₃)] [PF ₆].	45
Scheme 4.3: Hydrosilylation of esters by [CpFe(CO) ₂ (PCy ₃)] [PF ₆].	45
Scheme 4.4: Dehydrocoupling of phosphine-borane adducts by [CpFe(CO) ₂ (Ph ₂ P•BH ₃)].	46
Scheme 4.5: Synthesis of B,B'-oxo linked dinuclear complex by Herberich et al.	46
Scheme 4.6: Polycondensation of bis-boratabenzene rhodium complex.	47
Scheme 4.7: Ruthenium boratabenzenes reported by Wen et al.	47
Scheme 4.8: Mechanism proposed by Wen et al for the formation of μ-oxo boratabenzene species (XV).....	48
Scheme 4.9 : Synthesis of CpFe(CO) ₂ (DTBB) (1).....	49
Scheme 4.10: Photodissociation of CO ligands and change on coordination of DTBB ligand.	54
Scheme 4.11: Synthesis of CpFe(C ₅ H ₅ B-OH) (3) and Cp ₂ Fe ₂ (C ₅ H ₅ B)-O-(BC ₅ H ₅)FeCp (4) from exposure of CpFeDTBB (2) to traces of water.....	59
Scheme 4.12: Attempted synthesis of iron species 2, 3 and 4 from the photodissociation of CO ligand in 1 using wet THF on a bench-top.....	64
Scheme 4.13: Attempted synthesis of iron complexes 3 and 4 by adding equimolar amounts of water to the pendant phosphine complex 2.....	65
Scheme 4.14: Attempt to hydrolyze the B-O-B bridge on complex 4 to obtain complex 3.	66
Scheme 4.15: Attempt to synthesize 4 from reaction of 2 with an excess of oxygen.	66
Scheme 4.16: Formation of species 4 from the reaction of 2 with H ₂	67
Scheme 5.1: Synthesis of [(η ¹ -DTBB)CuCl]K (5).	85
Scheme 5.2: Synthesis of species 6a [Cu(η ¹ -DTBB) ₂]K.	91
Scheme 5.3: Synthesis of species 6b [Cu(η ¹ -DTBB) ₂][Cu(IMes) ₂].	92
Scheme 5.4: Synthesis of Silver-phosphidoboratabenzene complex [Ag(η ³ -DTBB) ₂]K (7).	98
Scheme 5.5: Reaction of DTBB with Me ₂ SAu and gold-phosphanyl oligomer (8) obtained.	100
Scheme 6.1: Synthesis of [(C ₂ H ₄)Rh(DTBB)] ₂ (9).....	122
Scheme 6.2: Catalytic hydrogenation of alkenes.....	130
Scheme 7.1: Synthesis of [H ₃ P•B(C ₆ F ₅) ₃]Li and phosphido-diborates with BH ₃ and B(C ₆ F ₅) ₃	139
Scheme 7.2: Synthesis of (Et ₃ P) ₂ Pt(H)(Ph ₂ P-BH ₃) by Manners.	140

Scheme 7.3: Attempted adduct formation between $i\text{Pr}_2\text{PCl}$ and BR_3 (R = Et or Ph) neat.	141
Scheme 7.4: Synthesis of DiPB ligand.....	142
Scheme 7.5: Comparison of the reaction of $(\text{PPh})_2\text{Ni}(\text{Br})_2$ with DTBB and DiPB.	144
Scheme 7.6: Synthesis of $[\text{Pt}(\text{DTBB})]$ and reaction of DiPB with PdCl_2	146
Scheme 7.7: Synthesis of $\text{Cp}_2\text{Zr}(\text{H})(\text{PMe}_3)(\text{DPB})$ (XVI) reported by Fu.	150
Scheme 7.8: Reaction of DTBB and $\text{Cp}_2\text{Zr}(\text{H})(\text{Cl})$ and <i>ansa</i> -DTBB.	151
Scheme 7.9: Proposed pathway for the formation of <i>ansa</i> -DTBB.	153
Scheme 7.10: Synthesis of <i>ansa</i> -DTBB ligand.....	154
Scheme 7.11: Proposed coordination of <i>ansa</i> -DTBB to metals of the lanthanide series.	157
Scheme 7.12: Reduction of <i>ansa</i> -DTBB with KC_8	157

List of Figures

Figure 1.1:a) Examples of zwitterions: betaine, glycine and ylides; b) Carbanion and sulfonate based zwitterionic complexes.....	2
Figure 1.2: Phosphino-borate zwitterionic complexes [PhB(CH ₂ PPh ₂) ₃]Ir(H)(η ³ -C ₈ H ₁₃) (A) by Tilley, {Ph ₂ B(CH ₂ PPh ₂) ₂ }Pt(Ph)(THF) (B) by Peters, complexes of the type [RuCl(L)(η ⁶ - <i>p</i> -cymene){PR ₂ (<i>p</i> -Ph ₃ BC ₆ H ₄)}] (C) by Spivack, <i>cis</i> -(PPh ₃) ₂ PtH(Cy ₂ PC ₆ F ₄ BF(C ₆ F ₅) ₂) (D) by Stephan, (Et ₃ P) ₃ PtH(PPh ₂ PBH ₃) (E) by Manners, (Et ₃ P) ₃ Rh(DPB) (F) by Fu.....	5
Figure 1.3: Molecular structure of BF ₃ and its vacant <i>p</i> orbital, which can be attacked by a base to form a borane adduct or if attacked by a nucleophile a borate.	6
Figure 1.4: Borabenzene planar ring and 2 <i>p_z</i> empty orbital.	7
Figure 1.5: Borabenzene and boratabenzene stabilized by Lewis bases and comparison with benzene and cyclopentadienyl.	8
Figure 2.1: Sandwich and triple decker complexes of boratabenzene: [Li(C ₅ H ₅ B-H) ₂]Li(THF) ₄ (IV), [(C ₅ H ₅ B-Me) ₂ Pb] (V), [Cp [*] Ru(C ₅ H ₅ B-Me)RuCp [*]]OTf (VI), ([{1-((η ⁵ -C ₅ H ₅)Fe(η ⁵ -C ₅ H ₅)) -η ⁶ -BC ₅ H ₅ }Co(η ⁵ -C ₅ H ₅)] (VII).....	13
Figure 2.2: Sandwich Fe(C ₅ H ₅ B-PC ₄ Me ₄) ₂ (VIII), piano stool [(CO) ₃ Cr(C ₅ H ₅ (TMS)B-Cl)] ⁻ (IX) and triple-decker [(CO) ₃ Cr(μ-η ⁶ C ₅ H ₅ (TMS)B-Cl)Cr(CO) ₃] ⁻ (X) complexes of boratabenzene.....	14
Figure 2.3: Iron complex with elongated B-M distances: Fe(C ₅ H ₅ B-PC ₄ Me ₄) ₂ (XI) and η ⁵ species Cl ₂ Zr(η ⁵ -C ₅ H ₅ B-H) ₂ (XII).....	15
Figure 2.4: Boratabenzene complexes coordinated η ³ : (η ⁶ -C ₅ H ₅ B-Ph)Ni(η ³ -C ₅ H ₅ B-Ph) (XIII), (η ⁶ -C ₅ H ₅ B-NMe ₂)Sc(η ³ -κ ³ -CBN-(C ₅ H ₅ B-NMe ₂)) (XIV).	16
Figure 2.5 : η ¹ coordination of boratabenzenes: [CpFe(CO) ₂ (DPB)] by Fu, [(H)Pt(IMes) ₂ (C ₅ H ₅ (2-TMS)B-Cl)] by Fontaine.....	17
Figure 2.6: MO diagram of different PR ₃ ligands depicting the M (<i>dπ</i>) orbital donating electron density to the PR (σ*) orbital, which becomes of lower energy as the R substituents contain electronegative atoms. ...	19
Figure 2.7: DPB ligand and DTBB ligand, lone pair on phosphorous and proposed coordination to metals.	20
Figure 2.8: Structures of selected ligands from Table 2.1. N-heterocyclic carbene (ICy), DPB and calculated nickel complex of DTBB.....	22
Figure 2.9: Kohn-Sham orbital representations of the HOMO and HOMO-1 of (DPB) ⁻ and (DTBB) ⁻ ligands determined using DFT.....	23
Figure 2.10: a) Metal complexes of DPB reported by Fu. b) Metal complexes of DTBB reported by Fontaine <i>et al.</i>	25
Figure 2.11: Zr and Cr amido-boratabenzene catalyst reported by Chen.....	26
Figure 3.1: Double manifold Schlenk line and Schlenk tubes used in inert atmosphere chemistry.	30
Figure 3.2: Double station glove box.	31
Figure 3.3: Regression graphic and T ₁ value at 203 K, inversion recovery spectra of Rh hydride (10).....	35
Figure 4.1: Boratabenzene complexes coordinated η ¹ : Cp ₂ Zr(H)(PMe ₃) ₃ (DPB) (I), (PMe ₃) ₃ Rh(DPB) (II), CpFe(CO) ₂ (DPB) (III), (IMes) ₂ Pt(H)(C ₅ H ₄ (TMS)B-Cl) (IV).	44
Figure 4.2: Iron carbonyl complexes similar to 1, CpFe(CO) ₂ (DPB) (XVI), CpFe(CO) ₂ (tBu ₂ P•BH ₃) (XVII), CpFe(CO) ₂ (PhP ₂ P•BH ₃) (XVIII), CpFe(CO) ₂ (PPh ₂) (XIX).	50
Figure 4.3: X-ray structure of 1.....	52

Figure 4.4: ^1H NMR (500 MHz, thf-d_8): comparison between η^1 (a) and η^6 (b) DTBB coordination to Fe.	56
Figure 4.5: Other ferrocenylphosphines: XX, $\text{CpFe}(\text{Cp}(\text{P}t\text{Bu})_2)$ (XXI), FcPPB (XXII).....	57
Figure 4.6: (a) HR-MSAPPI m/z : 343.15 $[\text{CpFeDTBB}+\text{H}]^+$; (b) mMass simulation m/z : 343.14 $[\text{CpFeDTBB}+\text{H}]^+$	58
Figure 4.7: X-ray structure of 3.....	61
Figure 4.8: X-ray structure of 4.....	62
Figure 4.9 : ^1H NMR (thf-d_8 , 500 MHz): reaction mixture of 2 and an equimolar amount of water.	65
Figure 5.1: Selected coordination geometries for Cu(I) species, L = N, S, P donors and X = Cl $^-$, NCS $^-$	79
Figure 5.2: Structure of Cu(I) calix[4]arene.	80
Figure 5.3: Dimeric structure of $[\text{C}_3\text{P}\bullet\text{CuCl}]$ (I) with bridging chloride ligands, monomeric $\text{C}_3\text{P}\bullet\text{CuCl}$ (II) and $\text{C}_3\text{P}\bullet\text{CuCl}$ (III).	81
Figure 5.4: Cation-arene interaction of Cu and benzene (IV) and coordination modes η^2 (V) and η^6 (VI) of Cu(I) and arenes.	81
Figure 5.5: Copper complex with a co-ligand CpCuPBu_3 (VII).	83
Figure 5.6: Examples of Cu-B interactions: copper metalloboratrane (TPB)CuCl (VIII), NHC-Cu-Bpin (IX), and a Cu- η^3 -borataallyl complex (X).....	83
Figure 5.7: Three coordinate coordination network of K^+ on DTBB crystals structure and π -coordination of Li^+ cation to boratabenzene $[(\text{C}_5\text{H}_5\text{B-H})\text{Li}][\text{Li}(\text{THF})_4]$ (XI).....	86
Figure 5.8: Alternative structure proposed for species 5, $[(\eta^3\text{-DTBB})_2\text{Cu}]\text{K}$ (Cu- η^3 -BCC).....	87
Figure 5.9: $[(\text{TXPB})\text{Rh}(\mu\text{-CO})_2\text{Fe}(\text{CO})\text{Cp}]$ (XIIa and XIIb) reported by Emslie, $(t\text{Bu}_2\text{PCCB}(\text{C}_6\text{F}_5)_2)\text{Ni}(\text{cod})$ (XIII), $(\text{Pt}(\eta^3\text{-DTBB})_2)$ (XIV).....	88
Figure 5.10: Mass spectrum (HR-MS APPI, negative ionization) of a benzene solution of complex 5: formulas and calculated masses of identified molecular ions.....	90
Figure 5.11: Proposed structure of the most abundant molecular ions found by HR-MS APPI.	90
Figure 5.12: a) Experimental HR-MS APPI for 6a, $m/z = 505.26$ $[\text{Cu}(\text{DTBB})_2]$. b) Simulation generated using Mmass.	92
Figure 5.13: a) X-ray structure of 6a.	93
Figure 5.14: X-ray structure of 6b.....	94
Figure 5.15: Examples of phosphorous two-coordinated linear Cu(I): XV, XVI.	95
Figure 5.16: Ball and stick representations, structure optimization calculated at the DFT level of theory using the hybrid functional B3PW91, basis set 6-31G(d,p).	96
Figure 5.17: η^3 -DTBB species with Pt.	97
Figure 5.18: ^1H NMR (500 MHz, benzene- d_6 /THF) a) $[\text{Ag}(\eta^3\text{DTBB})_2]\text{K}$ (7), b) DTBB.	98
Figure 5.19: ^{31}P NMR (202.40 MHz, benzene- d_6 /THF) a) $[\text{Ag}(\eta^3\text{DTBB})_2]\text{K}$ (7), b) DTBB.	99
Figure 5.20: ^1H NMR (500 MHz, benzene- d_6 /THF) a) 5 days after addition of Me_2SAuCl , b) 10 min after addition and c) DTBB ligand free.....	101
Figure 5.21: ^{31}P NMR (202.40 MHz, benzene- d_6 /THF) a) 5 days after addition of Me_2SAuCl , b) 10 min after addition and c) $[\text{DTBB}]\text{K}$ ligand free.	102
Figure 5.22: Structure of $\{[\text{Au}(\text{P}t\text{Bu})_2]_6\}$ complex reported by Glueck.....	103
Figure 5.23: X-ray structure of 8.....	104
Figure 6.1: Neutral and anionic boron heterocycles.	119
Figure 6.2: Some borabenzene species related to this study: $[(\text{IMes})_2\text{Pt}(\text{H})(1\text{-Cl-2-SiMe}_3\text{-BC}_5\text{H}_4)]$ (III), $\text{Rh}(\text{PMe}_3)_3(\text{DPB})$ (IV), $\text{Pt}(\text{DTBB})_2$ (V), $[(\text{C}_2\text{H}_4)_2\text{Rh}(\text{C}_5\text{H}_5\text{B-NMe}_2)]$ (VI), $[(\text{C}_2\text{H}_4)_2\text{Rh}(\text{C}_5\text{H}_5\text{B-Ph})]$ (VII), $\text{Ni}_2(\text{DTBB})_2$ (VIII) and $(\eta^3\text{-}(\text{C},\text{B},\text{P})\text{-C}_5\text{H}_5\text{BP}(t\text{Bu})_2)(\kappa\text{-}\eta^2\text{-}\eta^1\text{-C}_8\text{H}_{12}(\text{P}(t\text{Bu})_2\text{BC}_5\text{H}_5)\text{Pt}$ (IX).	121

Figure 6.3: ORTEP plot of 9.	123
Figure 6.4: Selected region of the ^1H NMR spectra (benzene- d_6 , 500 MHz) for the boratabenzene and high field Rh-H resonances for hydride 10 (a) and 11 (b).	127
Figure 6.5: Proposed molecular structures for hydride species $[(\text{DTBB})\text{Rh}(\text{H})_2]_2$ (10) and $[(\text{DTBB})\text{Rh}(\text{H})_2]$ (11).	129
Figure 7.1: Anionic phosphino-boranes: $[\text{Ph}_2\text{PBH}_3]\text{Li}$ (III) and $[\text{Ph}_2\text{P}(\text{BH}_3)_2][\text{K}(18\text{-c-}6)]$ (IV).	140
Figure 7.2: X-ray structure of DiPB.	143
Figure 7.3: X-ray structure of 12.	145
Figure 7.4: Metallocenes: non-bridged, <i>ansa</i> -bridged with main group atoms and <i>ansa</i> - with a donor/acceptor (D/A) bridge (E = C, Si, P, B; R = H, Me, Ph, SMe_2 , PMe_3 ; X = Cl; M = Ti, Zr, Hf; D = NR_2 , PR_2 , SbR_2 , OR, F, C; A = BR_2 , AlR_2 , GaR_2).	148
Figure 7.5: Metallocenes complexes of boratabenzene ligands: $[(\text{C}_5\text{H}_5\text{B-N/Pr}_2)_2\text{ZrCl}_2]$ (VIII), $[\text{Me}_2\text{Si}(\text{C}_5\text{H}_5\text{B-N/Pr}_2)_2\text{ZrCl}_2]$ IX and $[(\text{C}_5\text{H}_5\text{B}-(\text{CH}_3)_2\text{P-BC}_5\text{H}_5)\text{Yb}(\text{N}(\text{SiMe}_3))] \text{X}$	149
Figure 7.6: Structures of <i>ansa</i> ligand coordinated to Yb and K (XI), first evidence of a neutral borabenzene coordinated to an alkali metal (XII) and product of the dissociation of neutral borabenzene from <i>ansa</i> ligand (XIII).	149
Figure 7.7: X-ray structure of <i>ansa</i> -DTBB.	151
Figure 7.8: ^1H NMR spectra showing a comparison between the DTBB and <i>ansa</i> -DTBB ligands.	155
Figure 7.9: Proposed coordination modes of the DPB ligand reported by Fu, the DTBB and the DiPB ligands reported by us.	159

List of Equations

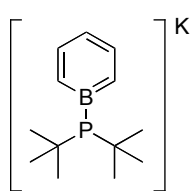
Equation 3.1: Dipole-dipole relaxation T_1 (s).....	34
Equation 3.2: Inversion-recovery sequence used to measure T_1	35
Equation 3.3: Calculation of the IR frequency.....	39
Equation 3.4: Reduced mass calculated for a diatomic molecule.....	39
Equation 3.5: Bragg's law.....	40
Equation 5.1: Disproportionation equilibrium for Cu^+ cation.....	79

List of Abbreviations

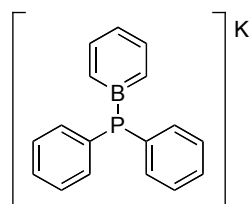
12-c-4	12-Crown-4-ether
Å	Angstrom
APPI	Atmosphere Pressure Photo-Ionization
brs	Broad signal
cat.	Catalyst
cent	Centroid
Cl-boracycle	1-chloro-boracyclohexa-2,5-diene
Cl-boracycle(TMS)	1-chloro-2(trimethylsilyl)-boracyclohexa-2,5-diene
COD	1,5-cyclooctadiene
Cp	Cyclopentadienyl
Cp*	Pentamethylcyclopentadienyl
Cy	Cyclohexane
d	Doublet
D/A	Donor/Acceptor
DFT	Density Functional Theory
EA	Elemental Analysis
EI	Electronic Impact
ESI	Electro Spray Ionization
Fc-	Ferrocenyl-
FLP	Frustrated Lewis Pairs
GC-FID	Gas Chromatography-Flame Ionization Detector
HMB	Hexamethylbenzene
HOMO	Highest Occupied Molecular Orbital
HR-MS	High Resolution Mass Spectroscopy
<i>i</i> Pr	<i>iso</i> -Propyl
IR	Infrared
κ	Kappa (atom bonded to a metal)
LA	Lewis acid
LB	Lewis base
LUMO	Lowest Unoccupied Molecular Orbital
μ	Mu (bridging ligand)
m	Multiplet
M-L	Metal-ligand fragment
MAO	Methylaluminoxane
Me	Methyl
Mes	Mesityl
MO	Molecular Orbital
Mol %	Molar percent

NMR	Nuclear Magnetic Resonance
OTf	Trifluoromethanesulfonate
ov	Overlapped
PHMS	Polymethylhydrosiloxane
ppm	Parts per million
PS	Polystyrene
psi	Pounds per square inch
Py	Pyridine
q	Quadruplet
s	Singlet
t	Triplet
<i>t</i> Bu	<i>tert</i> -Butyl
TMS	Trimethylsilyl
TMSCI	Chlorotrimethylsilane
TOF	Turn Over Frequency
TON	Turn Over Number
η	Hapto

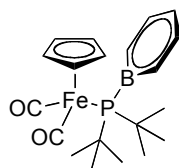
List of Compounds



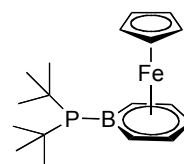
DTBB



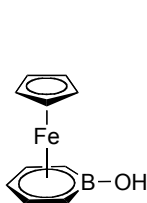
DPB



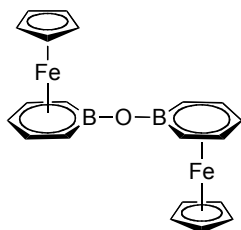
1



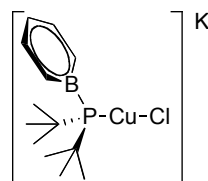
2



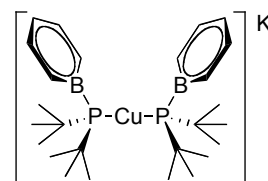
3



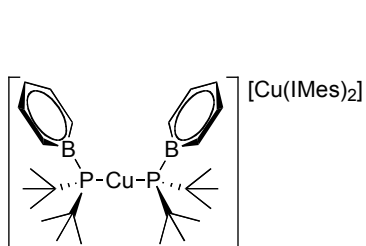
4



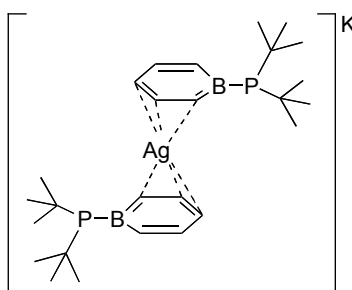
5



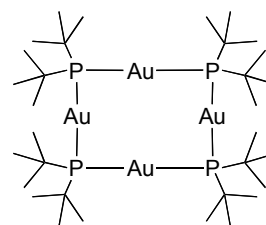
6a



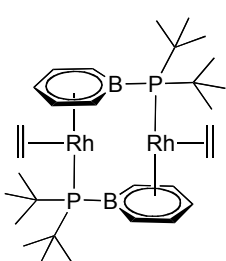
6b



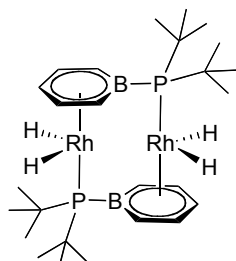
7



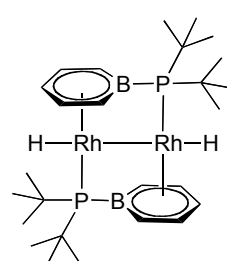
8



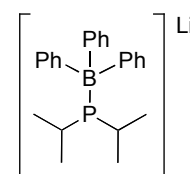
9



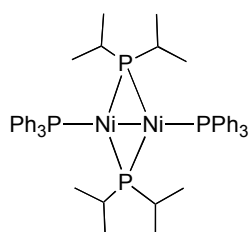
10



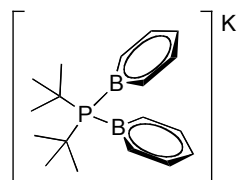
11



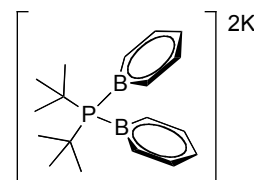
DiPB



12



ansa-DTBB



13

*“Non lucror exposita scientia
per ardua ad astra”*

A mis padres, familia, amigos y Dom.
¡Gracias totales!

Acknowledgments

Little I knew of what my journey would be when I started my PhD. Now, after the 42.2 Km of my doctoral race I wish nothing but to thank all the wonderful people that contributed to my success and cheered me up along the way.

Frédéric-Georges Fontaine, thanks a lot for being patient with me but mostly for pushing me to be a better chemist. To all my colleagues at the group Fontaine past and present, thank you for sharing your knowledge and so many good moments, I wish you all the best.

I would like to acknowledge my colleague and friend Stephanie Barnes whom initiated me on borabenzene and my summer intern François Innes thank you for allowing me to show you the ways of research. To Ambreen Mushtaq and Marc-André Légaré thank you for all the good moments and the even better chemistry conversations.

Merci également au professeur Laurent Maron à L'Université Paul Sabatier, (Toulouse, France) pour la réalisation des calculs de la DFT.

Maintenant j'aimerais remercier les membres du département de chimie qu'ont contribué d'une façon ou d'autre à la réussite de ma recherche: Christian Coté, Sébastien Blanchet, Jean Laferrière, Marylin Marois, Serge Groleau, Mélanie Tremblay, Marie Tremblay et Denyse Michaud. Une mention spéciale à Pierre Audet, qui a investi beaucoup de temps sur le set-up des séquences de RMN, merci énormément j'ai appris beaucoup de toi. Les remerciements sont étendus au professeur T.T.T. Nguyen Dang pour sa patience et engagement a l'enseignement de la chimie théorique, c'était un privilège d'avoir pris vos cours. Un gros merci aux membres des groupes Boukouvalas, Paquin et Leclerc pour leur aide.

I would now like to thank those whom inspired me to keep going with my research. A special mention goes to Dr. Ivan Castillo (Instituto de Química, Universidad

Nacional Autónoma de México, México); I don't think I would be finishing a PhD without your guidance and support, thank you for being my friend and my mentor and for teaching me the ways of research. My dear friends Dr. Lauren Mercier and Dr. Justyna Florek, you both are a great source of inspiration, thank you for standing by my side in the good and bad moments.

Also, I would like to thank all my friends whom provided me constant support despite the time and distance: Karina, Heriberto, Nashely, Mario, Elizabeth, Jessica, Fer, Tania, Oziel, Samuel, Oscar, Daniel, Pepe, Silvia y Vince. ¡Gracias por siempre hacerme reír!

Finalmente quisiera agradecer a mis padres y a toda mi familia, sin su apoyo y cariño nada habría sido posible, los amo infinitamente. Last but not least, a huge thanks to the only man in this world that could bear with my craziness; Dom there is not enough words in English, Spanish or French that could account for how grateful I am to have you by my side, this PhD would have not been possible without your love and understanding.

1 Chapter 1 Introduction

1.1 Catalysis and Charge Effect

Chemistry is implicated in many aspects of our daily lives; about 80 % of the processes in the chemical industry depend upon catalysis.¹ Thus catalysts are involved in the manufacture of almost 90% of the commercially available products.² A catalyst is an additive used in sub-stoichiometric amounts to bring about a reaction at lower temperature than that required for the uncatalyzed thermal reaction.³

Homogeneous and heterogeneous catalysts enable chemical transformations, increase the products' yields and overall make the chemical processes more efficient. Due to the environmental and economical impact of the chemical industry, a cleaner alternative to chemical processes is needed. Green chemistry is an approach that implements chemical principles and methodologies to reduce and prevent pollution as well as developing strategies to reduce risks to human health and environmental impact of chemical transformations.⁴ Hence the use of more efficient catalytic pathways and the appropriate choice of catalyst becomes a key step in the sustainability of modern life-style.

Organometallic compounds have contributed to remarkable breakthroughs in the advancement of catalysis in the past 20 years. Contributions in transformations such as the palladium catalyzed cross coupling,⁵ olefin metathesis,⁶ and asymmetric hydrogenation⁷ have been awarded Noble Prizes.

The catalytic activity of organometallic compounds can dramatically change accordingly to the ligands bonded to the metal centre. In the case of ionic species, the location of the charges within a complex also influences the reactivity of the metal centres, notably in applications such as the Monsanto process for the production of acetic acid⁸ and in the catalytic polymerization of olefins.⁹

The activity of zwitterionic species is one example of the influence of the charge position on the catalytic activity of an organometallic complex. A zwitterion is a compound where the positive and negative charges lie separated within the

molecule in non-adjacent atoms. Aminoacids are examples of zwitterionic compounds: betaine, glycine and other aminoacids derivatives exist as zwitterions. Additionally other neutral compounds with charge separation like ylides are also classified as zwitterions (Figure 1.1, a).¹⁰ In the case of organometallic species, the positive charge is localized over the metal and the negative charge is delocalized over the ancillary ligands, resulting overall in a neutral molecule (Figure 1.1, b).¹¹

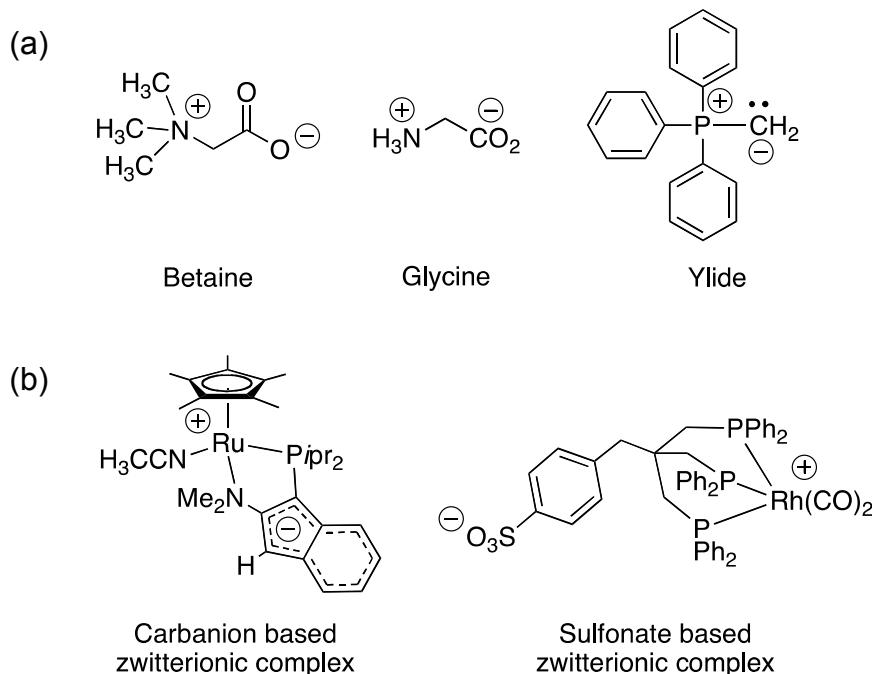
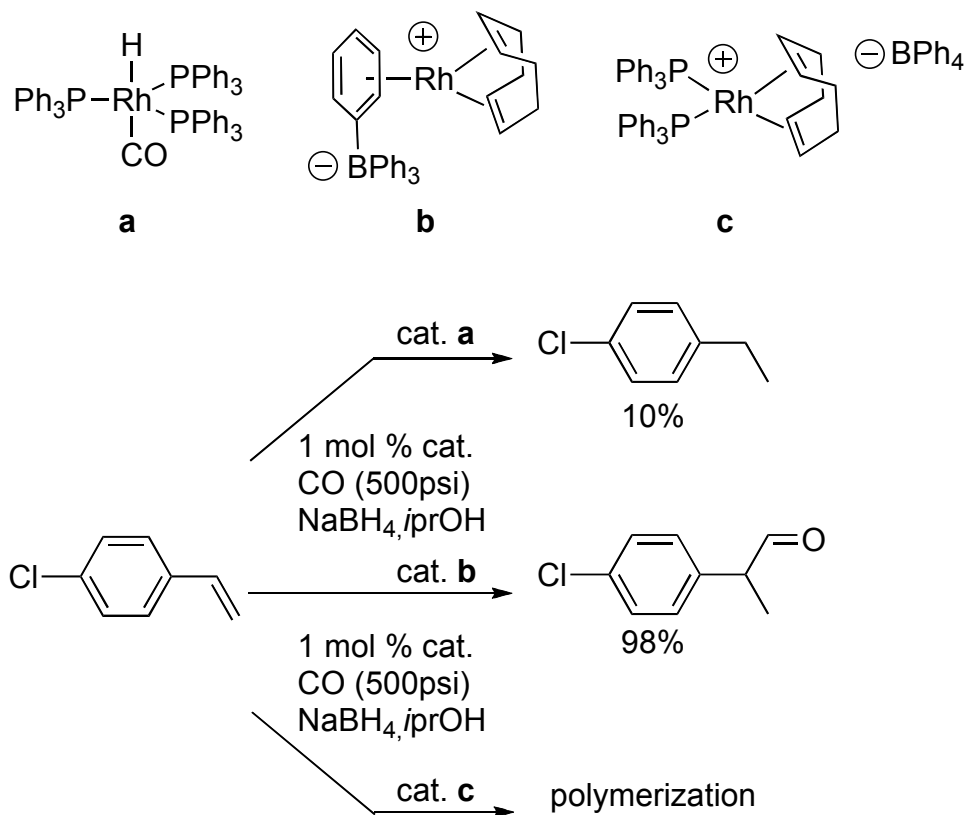


Figure 1.1:a) Examples of zwitterions: betaine, glycine and ylide;¹⁰ b) Carbanion¹² and sulfonate¹³ based zwitterionic complexes.

Different types of zwitterionic complexes exist and they can be stabilized using ligands such as carbanions¹² and sulfonates,¹³ which are capable to support and sequester the negative charge far apart from the metal (Figure 1.1, b).

One class of importance is that of anionic phosphines containing pendant borate fragments. They were notably amongst the first organometallic zwitterionic species to appear in the literature and they have been used in many catalytic applications. Scheme 1.1 shows three organometallic complexes of rhodium(I) with different charge profiles. Pre-catalyst **a** is a neutral molecule capable to hydrogenate *p*-chlorostyrene only in 10% yield.¹⁴ Under the same conditions, the cationic rhodium

catalyst **c** results in an alkene polymerization,¹⁴ whereas the zwitterionic complex **b** affords the targeted branched aldehyde in 93% conversion.¹⁵



Scheme 1.1: Catalyst charge effect on the catalytic transformation of *p*-chloro styrene into the hydrogenation product by catalyst **a**, the hydroformylation product by catalyst **b** and polymerization by catalyst **c**, under the same reaction conditions.

As shown above, zwitterionic complexes exhibit enhanced catalytic activities than their cationic parent complexes for several reasons. Indeed, their solubility in polar and non-polar organic solvents is enhanced compared to the ionic species. Additionally effects of ion-pairing, which in some cases reduce the catalytic activity, are attenuated due to the sequestration of the charge.¹⁶ The fine-tuning of the electronic and steric properties of related cationic complexes of interest has been facilitated using zwitterionic complexes as a study-probe. Thus the investigation of mechanistic details, otherwise difficult to observe due to the low solubility of cationic species, has been possible using zwitterionic complexes.¹⁶

The first reports about phosphino-borates were made by Tilley and Peters,¹⁷ including a tris(phosphino)borate iridium(III) complex (**A**, Figure 1.2) that was able to activate R_3Si-H bonds. Using the same concept, Peters reported a bis(phosphino)borate platinum(II) complex (**B**, Figure 1.2) capable to carry the C-H activation of benzene and toluene.¹⁸ Spivak and collaborators reported a ruthenium arene (**C**, Figure 1.2) featuring a ligand previously reported by Peters,¹⁹ interestingly the presence of the (phosphino)tetraphenylborate enables the dissociation of the chloride ligand, a unique behaviour in ruthenium arene chemistry.²⁰ In 2010 Stephan and collaborators, reported a phosphino-borate ligand (**D**, Figure 1.2) obtained from the reaction of a P/B Frustrated Lewis Pair (FLP) and its utility as a ligand to transition metals, an application newly considered to the FLP chemistry.²¹ In 2003 the Manners group reported the oxidative addition of a P-H bond to Pt(0) to afford a platinum hydride featuring a pendant phosphido-borate ligand (**E**, Figure 1.2).²²

Whereas the use of pendant borates has been a recurrent resource in the chemistry of zwitterionic complexes, other boron compounds such as boratabenzene, a boron heterocycle, have been less developed. The rhodium(I) phosphido-boratabenzene zwitterionic complex (**F**, Figure 1.2), first reported by Fu and collaborators,²³ opens up new avenues to explore on the coordination chemistry and reactivity of such a particular boron compound. The boratabenzene is an interesting framework due to the capability of the aromatic ring to delocalize the negative charge on boron, sequestering the charge apart from the metal centre, the main characteristic of zwitterionic complexes.

With these precedents we decided to explore new alternatives to anionic phosphino-borate ligands by using boron compounds such as boratabenzene. Additionally the catalytic applications of boratabenzene complexes are, so far, limited to polymerization. Hence it becomes an interesting moiety to develop zwitterionic metal complexes.

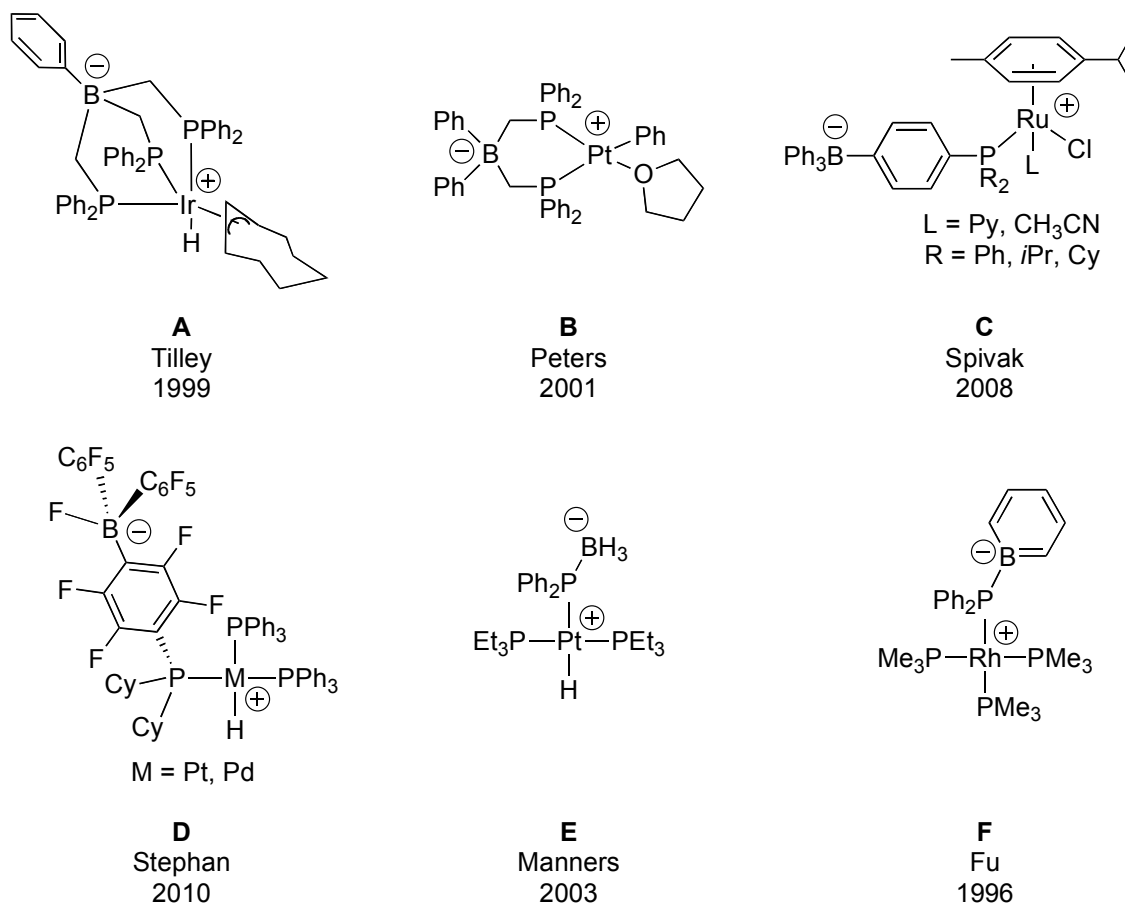


Figure 1.2: Phosphino-borate zwitterionic complexes $[\text{PhB}(\text{CH}_2\text{PPh}_2)_3]\text{Ir}(\text{H})(\eta^3\text{-C}_8\text{H}_{13})$ (**A**) by Tilley,¹⁷ $\{\text{Ph}_2\text{B}(\text{CH}_2\text{PPh}_2)_2\}\text{Pt}(\text{Ph})(\text{THF})$ (**B**) by Peters,¹⁸ complexes of the type $[\text{RuCl}(\text{L})(\eta^6\text{-}p\text{-cymene})\{\text{PR}_2(p\text{-Ph}_3\text{BC}_6\text{H}_4)\}]$ (**C**) by Spivack,²⁰ $\text{cis}-(\text{PPh}_3)_2\text{PtH}(\text{Cy}_2\text{PC}_6\text{F}_4\text{BF}(\text{C}_6\text{F}_5)_2)$ (**D**) by Stephan,²¹ $(\text{Et}_3\text{P})_3\text{PtH}(\text{PPh}_2\text{PBH}_3)$ (**E**) by Manners,²² $(\text{Et}_3\text{P})_3\text{Rh}(\text{DPB})$ (**F**) by Fu.²³

1.2 Boron Compounds, Promising Frameworks for Catalysis

Boron is a metalloid element first discovered in 1808.²⁴ In nature boron can be found in different forms, notably as borax ($\text{Na}_2\text{B}_4\text{O}_7 \cdot 10\text{H}_2\text{O}$) better known for its use in laundry products. Sodium borate pentahydrate, is commonly used in the manufacture of fiberglass and sodium perborate bleach. Another commercially important boron compound is boric acid, used in the manufacture of textile fiberglass and in cellulose insulation as a flame retardant. Boron compounds are also used in the manufacture of borosilicate glasses and enamels.²⁵ More recently boron has found applications in cancer research as radioisotope in boron neutron capture therapy.²⁶ Moreover boron in the form of borate is a micronutrient essential for growth not only in plants but in human nutrition as well.²⁷

Atomic boron possesses three electrons in its valence shell therefore boron compounds such as BF_3 only have six electrons in the valence shell (Figure 1.3). The boron atom does not attain the octet configuration, instead is sp^2 hybridized with a vacant p orbital perpendicular to the plane.²⁸ The empty orbital confers boranes and its derivatives Lewis acidity,²⁹ although in the case of BF_3 the empty orbital can be stabilized by π -donation from the fluoride. The vacant p orbital can also interact with an electron pair from a Lewis base to form neutral adducts or can suffer a nucleophilic attack by an anionic donor resulting in the formation of negatively charged borates (Figure 1.3).³⁰ Because boron is capable to support a negative charge it becomes interesting to explore its use in the synthesis of zwitterionic complexes.

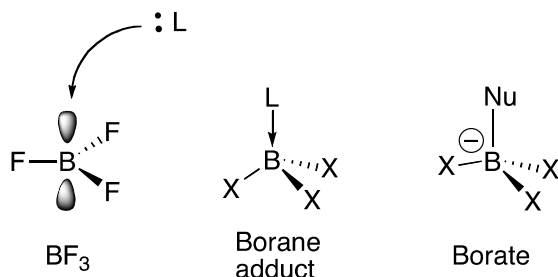


Figure 1.3: Molecular structure of BF_3 and its vacant p orbital, which can be attacked by a base to form a borane adduct or if attacked by a nucleophile a borate.

Amongst the various boron compounds borabenzene (Figure 1.4) has attracted attention since the 1970's when Herberich and collaborators reported for the first time a phenyl-substituted boratabenzene complex (see section 2.1).³¹

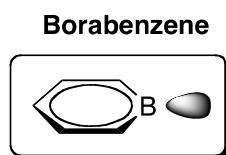


Figure 1.4: Borabenzene planar ring and $2p_z$ empty orbital.

Borabenzene is an aromatic, six-membered ring where one of the C-H fragments has been replaced by boron. The planar 6 electrons π system in borabenzene is similar to benzene. Borabenzene is a very strong Lewis acid because of the presence of one unoccupied LUMO orbital. *Ab Initio* calculations on CO and N₂ adducts, show that the LUMO level is a σ^* orbital of low energy localized on the boron atom.^{32a} The molecule itself is not stable and attempts to isolate it in argon matrixes by flash thermolysis at 10 K have failed.^{32b} In order to isolate the borabenzene, the electronic needs of the boron atom have to be met by stabilization with a Lewis base. When the Lewis base on boron is neutral, such as pyridine (Py), NEt₃ or PMe₃, the molecule is called borabenzene but when an anionic Lewis base is used, such as -Cl, -Ph or -OH, the ring becomes negatively charged and is called boratabenzene (Figure 1.5).

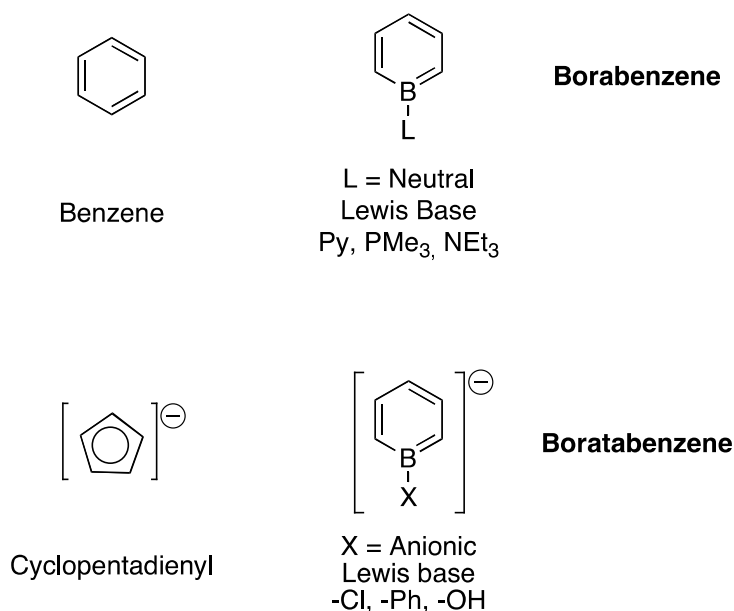


Figure 1.5: Borabenzene and boratabenzene stabilized by Lewis bases and comparison with benzene and cyclopentadienyl.

Boratabenzene, an anionic ligand fragment, attracted our attention as a ligand framework for the synthesis of zwitterionic metal complexes due to its capability of bearing and stabilizing the negative charge by delocalization over the aromatic ring. Additionally the various coordination modes, which will be discussed in latter chapters, can potentially enable the development of new applications in catalysis.

1.3 Thesis Scope

The present work aims to contribute to the knowledge of the unusual coordination chemistry and reactivity of boratabenzene, which has not been as widely explored, compared to other heterocycles containing nitrogen and phosphorous. Particularly our interest lies in the investigation of the scarce η^1 -coordination of boratabenzene ligands. The dissertation is divided in eight chapters and the ninth chapter includes the bibliography.

In chapter 1, an overview of the chemistry that motivated this thesis has been presented.

In chapter 2 the context on which this work fits in the literature and the progression of the field over the last ten years is presented. The fundamental concepts that are key to the proper appreciation of the work in this dissertation are also included.

Chapter 3 is a brief compilation of the methodology and techniques that made possible the development of the present work.

Chapter 4 describes the first example of a di-*tert*-butylphosphidoboratabenzene (**DTBB**) coordinated η^1 through the phosphorous atom to iron, forming a zwitterionic complex. The characterization of the iron species and its transformations in the presence of water allowed for a better understanding of the nucleophilicity and the donating capabilities of the **DTBB** ligand.

Chapter 5 is a relevant contribution to the coordination chemistry of boratabenzene ligands. The first evidences of a boratabenzene ligand coordinated to metals of the group 11 are presented. Notably the copper-coordinated **DTBB** moiety is now part of the short list of η^1 -coordinated boratabenzenes. François Innes, an undergraduate summer intern, is acknowledged for his help during the characterization and recrystallization of the η^1 copper species. All the DFT calculations presented in this chapter were obtained in collaboration with Laurent Maron, at the Université Paul Sabatier in Toulouse, France.

Chapter 6 describes a rhodium-boratabenzene dimer capable to act as a pre-catalyst in the hydrogenation of alkenes at room temperature and atmospheric pressure, showing an activity comparable to that of Wilkinson's catalyst. This chapter has been accepted for publication in the journal *Dalton Transactions*, as an invitation for a special issue on phosphorous chemistry and included in this thesis. The candidate is the first author. The contribution of the authors is as follows: the

experimental work was carried by Viridiana Perez (VP); NMR guidelines and valuable input in the characterization was made by Pierre Audet; the data collection and refinement of X-ray data was made by Wenhua Bi; the manuscript writing and editing was done mainly by myself (VP) and Frédéric-Georges Fontaine revised the document prior to submission. Modifications on the numbering of the compounds, figures and tables of the paper have been done in order to fit the sequence of the dissertation.

In Chapter 7 a phosphidoborate ligand is presented as an alternative to the boratabenzene moiety. Additionally the synthesis of an *ansa*-phosphido-*bis*-boratabenzene ligand is presented. The reactivity of the phosphido-borate and the formation of the *ansa* ligand give a new perspective onto the stability of the P-B bond.

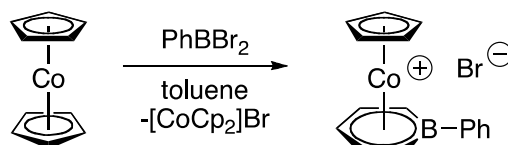
Wenhua Bi is acknowledged for the data collection and refinement of one crystal structure included in chapter 4 and all of the structures in chapters 5 to 7. Thierry Maris (Université de Montréal) is acknowledged for the collection and refinement of two of the structures included in chapter 4.

Chapter 8 offers a conclusion on the study of scarce boratabenzene coordination modes as well as a perspective on future discoveries and applications. Finally the last chapter includes the bibliography consulted for this dissertation.

2 Chapter 2 Literature Review

2.1 Boratabenzene Ring, Structure and Reactivity

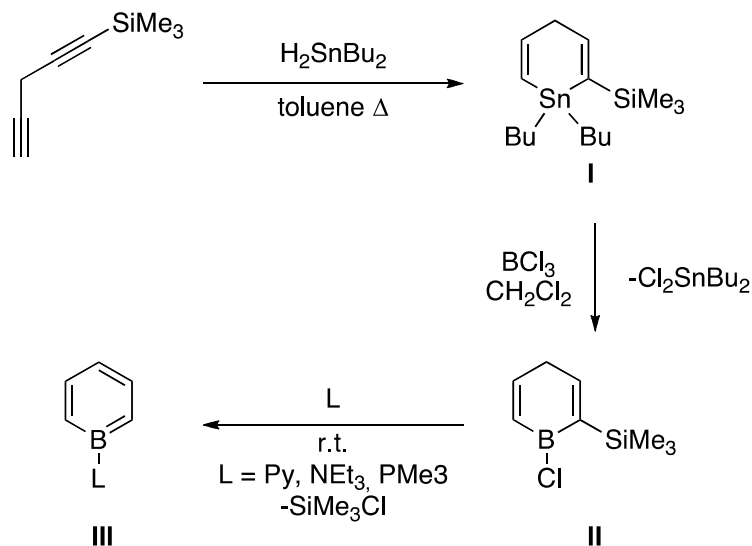
Herberich, reported the first example of a boratabenzene ring in 1970. The synthesis (Scheme 2.1) was achieved by the insertion of PhBBr_2 into one of the Cp rings of $\text{Cp}_2\text{Co(II)}$. The ring expansion of the Cp ligand was followed by the formation of a boratabenzene moiety coordinated to cobalt through the aromatic ring.³¹



Scheme 2.1: Ring insertion by organo-boron halides to cyclopentadienyl ligand by Herberich.³¹

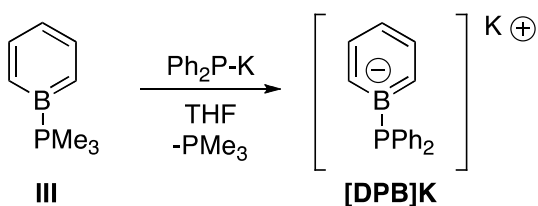
A year later, Ashe reported the synthesis of a phenyl boratabenzene $[\text{C}_5\text{H}_5\text{B-Ph}]\text{Li}$ but using a different synthetic pathway, on which the PhBBr_2 is transmetallated with a stannacycle to yield the $(\text{C}_6\text{H}_5\text{B-Ph})^-$.³³ For a long time, the synthesis of borabenzene and boratabenzene species was laborious, until Fu and collaborators reported a modification of Ashe's synthesis to make easily available neutral borabenzene adducts.³⁴

Scheme 2.2 shows Fu's synthetic pathway to obtain borabenzene and boratabenzene species. The reaction of a commercially available 1-trimethylsilyl-1,4-pentadiyne with H_2SnBu_2 to afford stannacycle species (I). By carrying a transmetallation reaction with BCl_3 , the 1-chloro-2-(trimethylsilyl)boracyclohexa-2,5-diene (Cl-boracycle(TMS)) species (II) can be obtained. Then by reacting the Cl-boracycle(TMS) with a neutral Lewis base at room temperature, the loss of an equivalent of chlorotrimethylsilane allows for the aromatization of the ring to take place. The aromatic character of the ring makes possible the formation of neutral borabenzene adducts (III).



Scheme 2.2: Synthesis of borabenzene neutral adducts reported by Fu.³⁴

Neutral borabenzene adducts (**III**, Scheme 2.3) are particularly useful as starting materials since they can be reacted with nucleophiles, which can attack the boron atom affording boratabenzene salts such as diphenyl-phosphidoboratabenzene (**DPB**). Fu and collaborators found that the nucleophilic attack on borabenzene by an anionic Lewis base proceeds through an associative mechanism.³⁵ Later on, our group proposed that the exchange of neutral ligands undergoes through the formation of borenium intermediates.³⁶



Scheme 2.3: Synthesis of **DPB** by nucleophilic attack on neutral $C_5H_5B-PMe_3$ (**III**).³⁵

2.2 The Rich Coordination Chemistry of Boratabenzene Ligands

Boratabenzene, being an anionic π system, displays coordination chemistry similar to that observed for a cyclopentadienyl ligand. The neutral analogue, the borabenzene moiety, coordinates transition metals through the π system like the

arene ligands. Examples of metal complexes with almost all of the transition metals have been reported.^{32b,37} Some coordination modes are more recurrent than others. The next section is a selection of the most common coordination modes and some examples of rare coordination of the boratabenzene ring.

2.2.1 η^6 Boratabenzene Metal Complexes

As it has been observed with the cyclopentadienyl ligand, boratabenzene has a strong tendency to coordinate to metals through the aromatic ring, where the π cloud donates to the empty d orbitals of the metal. Boratabenzene can also coordinate η^6 to alkaline metals such as lithium (**IV**, Fig. 2.1), obtained from the reduction of adduct **III** with LiAlH_4 .³⁸ Sandwich complexes (**V**, Fig. 2.1) can readily be obtained by salt metathesis with metal halide precursors and a boratabenzene alkali.³⁹ Triple-decker complexes are accessible through electrophilic stacking of the sandwich complexes⁴⁰ or via a transmetallation reaction using a ferrocenylboron halide⁴¹ (**VI** and **VII** Fig. 2.1).

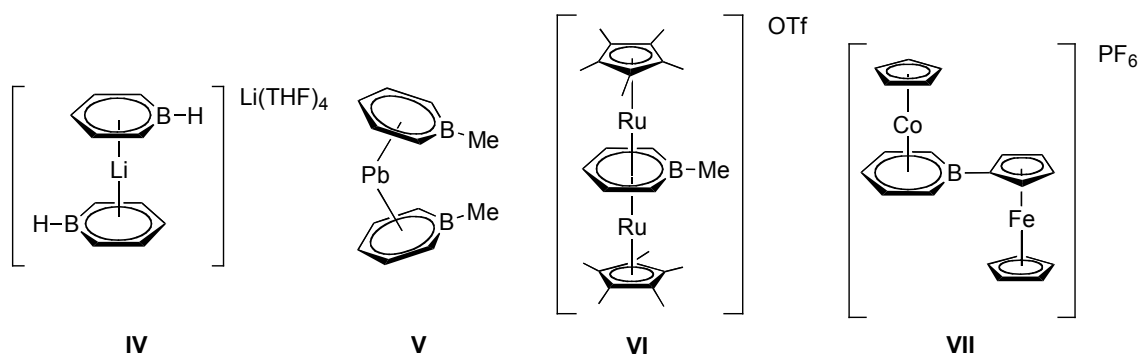


Figure 2.1: Sandwich and triple decker complexes of boratabenzene: $[\text{Li}(\text{C}_5\text{H}_5\text{B-H})_2]\text{Li}(\text{THF})_4$ (**IV**),³⁸ $[(\text{C}_5\text{H}_5\text{B-Me})_2\text{Pb}]$ (**V**),³⁹ $[\text{Cp}^*\text{Ru}(\text{C}_5\text{H}_5\text{B-Me})\text{RuCp}^*]\text{OTf}$ (**VI**),⁴⁰ $([\{1-(\eta^5\text{-C}_5\text{H}_5)\text{Fe}(\eta^5\text{-C}_5\text{H}_5)\} - \eta^6\text{-BC}_5\text{H}_5]\text{Co}(\eta^5\text{-C}_5\text{H}_5)]$ (**VII**).⁴¹

Our group has made a contribution to the library of η^6 coordinated boratabenzene complexes. In 2010, our group reported a new type of ligand. The boratabenzene phosphole (**VIII**, Figure 2.2),⁴² is a ligand which main characteristic is that it retains a quasi-planar position upon η^6 coordination to iron.

I contributed at demonstrating that group 6 piano stool and triple-decker (**IX** and **X**, Figure 2.2) boratabenzen complexes could be isolated using the Cl-boratabenzene ligand.⁴³ These species are interesting since the B-Cl bond might undergo oxidative addition or transmetalation with transition metals. The triple-decker complex afforded the first crystal structure of a Cl-boratabenzene ligand. Additionally this species was shown to be air and moisture stable for several months, unlike the piano stool complex.

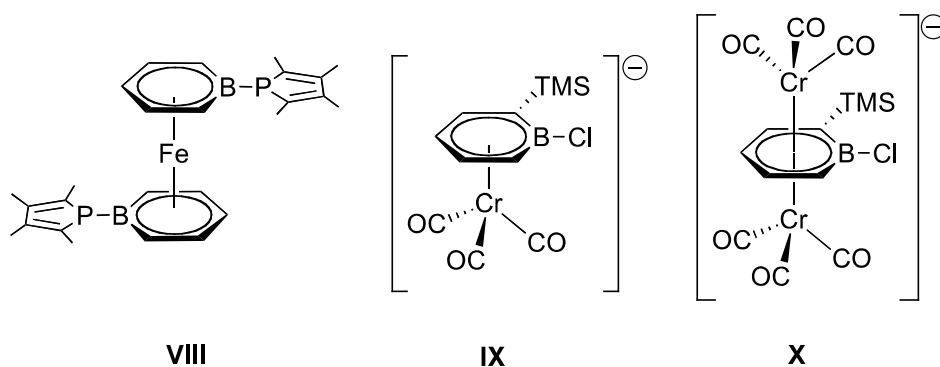


Figure 2.2: Sandwich $\text{Fe}(\text{C}_5\text{H}_5\text{B-PC}_4\text{Me}_4)_2$ (**VIII**),⁴² piano stool $[(\text{CO})_3\text{Cr}(\text{C}_5\text{H}_5(\text{TMS})\text{B-Cl})]^-$ (**IX**) and triple-decker $[(\text{CO})_3\text{Cr}(\mu\text{-}\eta^6\text{C}_5\text{H}_5(\text{TMS})\text{B-Cl})\text{Cr}(\text{CO})_3]^-$ (**X**) complexes of boratabenzene.⁴³

2.2.2 Ring Slippage and η^5 Coordination

Another example reported by our group in 2014, is that of the boratabenzene-mesityl iron sandwich⁴⁴ (**XI**, Figure 2.3); the bulky substituent on boron promotes elongated B-M distances, hence suggesting a certain capability for the ring to slip. Additionally the steric bulk around the boron centre allows the complex to be air and moisture stable, a characteristic rarely observed for boratabenzene compounds.

Complexes adopting a η^5 coordination (**XII**, Figure 2.3) have also been observed;⁴⁵ however examples are less common than those of η^6 , the absence of the interaction between the boron atom and the metal arises as a result of the π -donation from the amide substituent on boron.

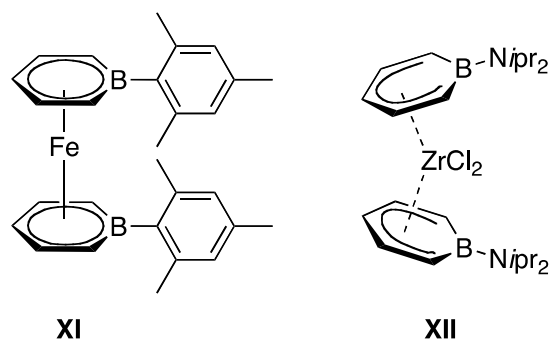


Figure 2.3: Iron complex with elongated B-M distances: $\text{Fe}(\text{C}_5\text{H}_5\text{B-PC}_4\text{Me}_4)_2$ (**XI**)⁴⁴ and η^5 species $\text{Cl}_2\text{Zr}(\eta^5\text{-C}_5\text{H}_5\text{B-H})_2$ (**XII**).⁴⁵

2.2.3 η^4 and η^3 Boratabenzene Metal Complexes

Boratabenzene can coordinate metals in a η^4 and η^3 fashion, but these species are quite rare compared to the number of examples for the η^6 complexes. The localization of the electronic density over a part of the ring, partially breaking the aromaticity has been observed for species such as the nickel sandwich of phenylboratabenzene,^{46,37a} where one of the rings is coordinated η^4 through the C=B-C=C atoms of the aromatic ring (**XIII**, Figure 2.4).

The η^3 coordination, however, is observed more frequently, but this coordination mode often involves the exocyclic fragment of the boratabenzene ring. As shown in Figure 2.4 (**XIV**), a scandium dimethylamido-boratabenzene⁴⁷ was shown to be bonded η^3 through the C=B=N bond, demonstrating that the exocyclic substituent NMe_2 is capable to participate in the interaction with the metal centre. Since the B-N interaction possesses a double bond character, it is involved into π -donation, hence the allyl-like coordination mode.

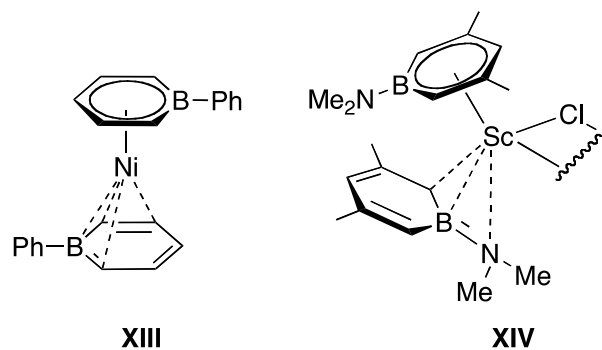


Figure 2.4: Boratabenzene complexes coordinated η^3 : $(\eta^6\text{-C}_5\text{H}_5\text{B-Ph})\text{Ni}(\eta^3\text{-C}_5\text{H}_5\text{B-Ph})$ (**XIII**),^{46,37a}
 $(\eta^6\text{-C}_5\text{H}_5\text{B-NMe}_2)\text{Sc}(\eta^3\text{-K}^3\text{-CBN-(C}_5\text{H}_5\text{B-NMe}_2))$ (**XIV**).⁴⁷

2.2.4 η^1 Boratabenzene Metal Complexes: New Ligands with an Unusual Coordination Mode

The involvement of the substituent on boron in the coordination to transition metals is not only limited to the η^3 coordination. When the Lewis base substituted on boron possesses a lone pair, the aforementioned is also able to bind to metals exclusively, without involving the coordination of the ring.

In 2009 our group reported a Cl-boratabenzene ligand bonded η^1 to Pt through a very unique interaction (Figure 2.5).⁴⁸ The chloride ligand serves as a bridge for coordination to platinum. Nevertheless the B-Cl interaction remains covalent, as shown by DFT calculations. Thus the M-L interaction can be defined as being either a $(\text{Cl-boratabenzene})^-$ species bound to a cationic $[(\text{IMes})_2\text{Pt(H)}]^+$ fragment or a Lewis acidic neutral borabenzene bonded to a neutral $[(\text{IMes})_2\text{Pt(H)(Cl)}]$ moiety via an interaction of one electron pair of the chloride and an empty sp^2 orbital on boron. The reactivity observed for such species is concurrent with these observations, since the platinum complex has shown to release both borabenzene⁴⁹ and Cl-boratabenzene⁴³ accordingly to reaction conditions. Unfortunately the oxidative addition of the B-Cl bond, as it happens with boranes, does not occur for boratabenzene, which might be attributed to the strength of the B-Cl bond, a consequence of the very strong Lewis acidity of the boratabenzene moiety.

Direct B-M bonding is quite rare, up to this day. All the attempts to generate a B-M interaction with a boratabenzene ring failed so far and this coordination mode, of great interest, is highly sought after by our research group.

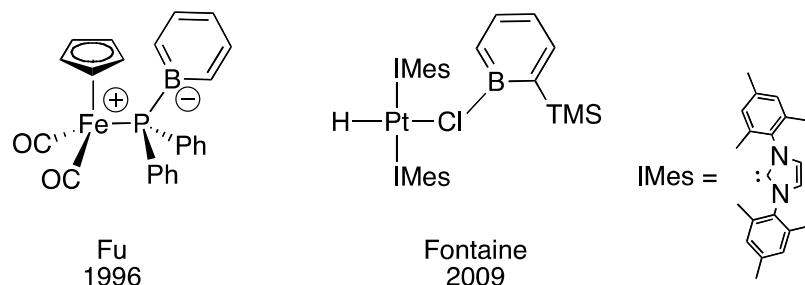


Figure 2.5 : η^1 coordination of boratabenzenes: $[\text{CpFe}(\text{CO})_2(\text{DPB})]$ by Fu,²³ $[(\text{H})\text{Pt}(\text{IMes})_2(\text{C}_5\text{H}_5(2\text{-TMS})\text{B-Cl})]$ by Fontaine.⁴⁸

The very first example of a boratabenzene coordinated η^1 is that of the diphenylphosphido-boratabenzene (**DPB**) reported by Fu in 1996,²³ Figure 2.5 shows an iron complex of **DPB**, featuring a ligand bonded through the lone pair on phosphorous instead of through the aromatic cycle.

DPB is an anionic phosphine, analogous to the widely used PPh_3 . The nature of the P-B interaction is covalent and unlike the amido substituents, the lone pair on phosphorous does not engage in π -donation, instead it remains available to coordinate to a metal centre.⁵⁰

The η^1 coordination mode has been studied, but only at a limited extent. Only four examples were reported in the literature until September 2015. One is the Pt-Cl-Boratabenzene mentioned above; unfortunately the synthesis of such species is expensive and rather sensitive to scale, making further investigations difficult. The remaining examples are metal complexes (Zr, Rh, Fe) of the **DPB** ligand, which will be further discussed in Chapter 4, 6 and 7.²³ Hence it became interesting to further exploit the reactivity and coordination of similar ligand systems which possess the desired characteristics to obtain zwitterionic metal complexes.

2.3 Phosphido-boratabenzene Ligands

In order to appreciate the relevance of designing phosphine ligands negatively charged, a few details on the phosphine structures and uses are mentioned below.

2.3.1 Phosphine Ligands, Versatility and Utility

Phosphines (PR_3) are one of the most common ligands used in organometallic chemistry, because of the abundance of analogues existing and its large versatility. Indeed, exchanging the R groups on phosphorous can modify the electronic and steric properties of the phosphine. These ligands have been shown to stabilize a wide variety of $(\text{PR}_3)\text{M-L}$ fragments and they behave as spectator ligands rather than actor ligands in many transformations.³

When the R substituents on phosphorous are alkyl chains, the inductive effect from the carbon chain increases the electron density on the phosphine, resulting in a very donating, more basic phosphine. Due to destabilization of the $\text{PR}(\sigma^*)$ orbital (Figure 2.6), the phosphine is not able to accept electron density from the M ($d\pi$) orbitals from the metal, an interaction known as back-donation or back-bonding.³

However, exchanging the R group for a fluoride, for example, can lower the energy levels of the $\text{PR}(\sigma^*)$ (Figure 2.6), increasing the donation from the M ($d\pi$) orbitals to the phosphine.³ By back-bonding, PX_3 ligands can stabilize electron rich M-L fragments; however the basicity of the phosphines, in this case, is greatly diminished.

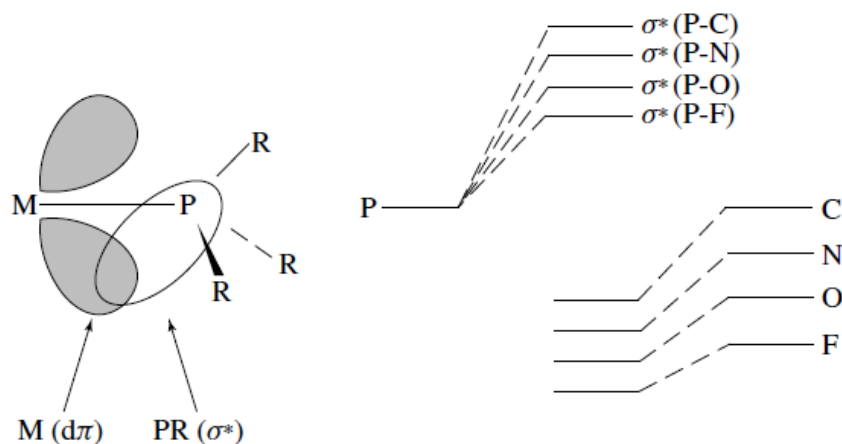


Figure 2.6: MO diagram of different PR_3 ligands depicting the $\text{M} (d\pi)$ orbital donating electron density to the $\text{PR} (\sigma^*)$ orbital, which becomes of lower energy as the R substituents contain electronegative atoms. Figure taken from reference 3.

Comparisons of the electron richness on M-L fragments can be easily undertaken by observing the shifts of $\nu(\text{CO})$ ligands in the IR. First studied by Tolman, complexes of the type $\text{LNi}(\text{CO})_3$ are useful to compare the donating capabilities of the ligand L.⁵¹ Because nickel complexes are not easily obtained for all ligand types, DFT calculations have been shown to provide IR stretching frequencies that are very close to the experimental values, making easier the determination of the donating capability of new phosphines without having to synthesize the metal analogues.⁵²

Additionally the steric bulk of phosphines can be measured by using a space-filling model of the $\text{M}(\text{PR}_3)$ fragment, measuring the cone angle of the R substituents, while folded back; centering the apex of the cone at the metal and standardizing the M-P distance.³ The electronic and steric parameters are useful tools to understand the behaviour of phosphine-metal complexes.

The interest in increasing the electron donating strength of a ligand lies in the possibility to perturb the oxidative addition/reductive elimination equilibrium in favour of the oxidative addition product.³ Similarly the steric bulk can favour the stabilization of unsaturated metal centres in low oxidation states, as we shall see in the present work.

2.3.2 DPB and DTBB Ligands, a Theoretical Comparison

In 2009, B. Macha, a former M.Sc. student in our group, synthesized an analogue to Fu's ligand, the di-*tert*-butylphosphido-boratabenzene (**DTBB**) (Figure 2.7),⁵³ exchanging the phenyl rings for *t*Bu substituents, moieties that provide a strong electronic inductive effect, thus increasing the basicity of the phosphine. Additionally the steric bulk of the alkyl groups could potentially stabilize unsaturated metal centres, leading to new reactivity.

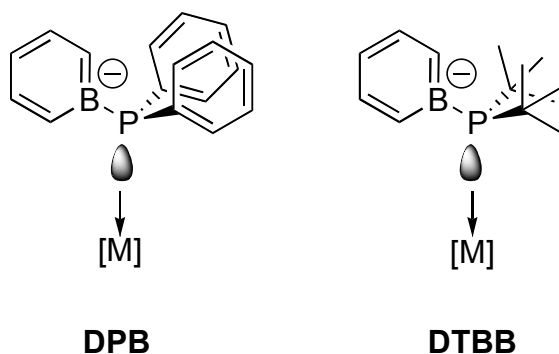


Figure 2.7: DPB ligand³⁵ and DTBB ligand,⁵³ lone pair on phosphorous and proposed coordination to metals.

To further investigate the donating capabilities of the **DTBB** ligand, a theoretical comparison of the **DTBB** and **DPB** against other bulky and very donating ligands was carried out. Theoretical calculations using MPW1PW91 functional 6-311+G(2d) (Ni) 6.311+G(d,p) (C,H,B,O,P) and experimental values of $\nu(\text{CO})$ stretching in the IR spectrum of various ligands compared with **DPB** and **DTBB** are shown in Table 2.1.

Table 2.1: Selected $\nu(\text{CO})$ stretching frequencies (cm^{-1}) of CO bonds in $\text{LNi}(\text{CO})_3$ complexes of phosphine and carbene ligands, against theoretical values for **DTBB** and **DPB** ligands. The values on the table were taken from reference 53.

Ligand	Calculated	Experimental
PF_3	2111.3	2011.8
PPh_3	2067.5	2068.9
$\text{P}(t\text{Bu})_3$	2055.3	2056.1
ICy	2049.8	2049.6
DPB	2035.5	-
DTBB	2026.4	-

^aGaussian 03 MPW1PW91 functional 6-311+G(2d) (Ni), 6-311+G-(d,p) (C,H,B,O,P). Calculated values have been corrected according to the function $\text{exp} = \text{calc} \times 0.9540.35$

CO ligands are particularly useful to evaluate the electron richness of a M-L fragment. The presence of very electron donating ligands increases the back donation from the *d*-filled orbitals of the metal to the π^* of the CO ligand. As the electron richness of the surrounding ligand increases, the back-bonding between the metal and the CO ligand becomes stronger, shifting the stretching bands to lower frequencies.

From Table 2.1, we can observe that phosphine ligands such as PF_3 , an electron acceptor rather than a donor phosphine, shows CO stretchings at 2111 cm^{-1} , while $\text{P}(t\text{Bu})_3$ shifts the bands to a lower frequency (2055 cm^{-1}) as consequence of the inductive electronic effect of the *t*Bu groups. Comparing the **DTBB** to NHC ligands, which are known to be very good donors, **DTBB** shifts the CO bands (Table 2.1) even more than ICy, an N-heterocyclic carbene, (Figure 2.8) and the **DPB** ligand. Because **DTBB** is a very strong donor ligand, the M-L fragment becomes more electron rich, which has a direct effect on the back-bonding between the metal and CO. However comparisons between phosphines and carbenes must be regarded carefully, due to the structural differences between these types of ligands.

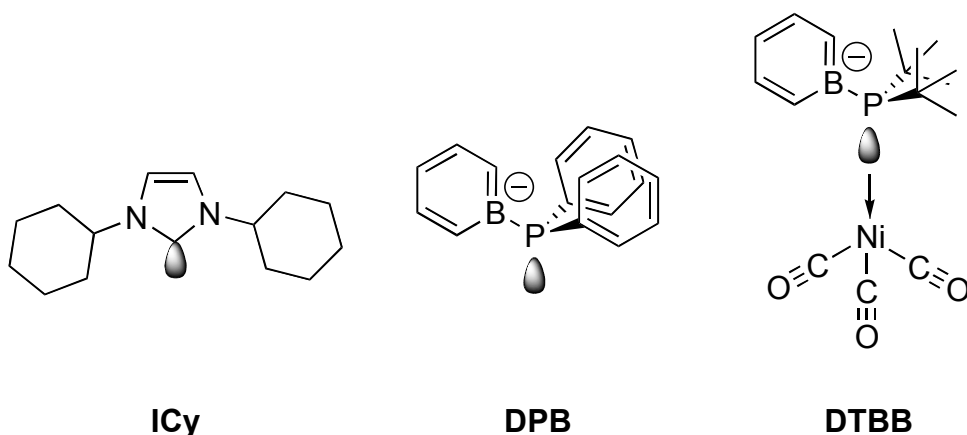


Figure 2.8: Structures of selected ligands from **Table 2.1**. N-heterocyclic carbene (**ICy**), **DPB** and calculated nickel complex of **DTBB**.

Furthermore calculations on the **DPB** and **DTBB** ligands provided more insight into their structure and reactivity. The HOMO level of (**DPB**)⁻ (Figure 2.9) is located over the π -system and is equivalent to the e_{1g} of benzene. The phosphorous lone pair is observed as the HOMO-1, being of lower energy than the HOMO level by 20.7 Kcal \cdot mol⁻¹.⁵³ A similar pattern is observed for the (**DTBB**)⁻ ligand (Figure 2.9). As a consequence of the increased donating capability of *t*Bu groups, the difference between the HOMO and the HOMO-1, is lower in energy (11.3 Kcal \cdot mol⁻¹).⁵³ Hence the **DTBB** ligand is a stronger electron donor than **DPB**. In addition, the steric bulk of **DTBB** might help stabilizing low-coordinated metal centres.

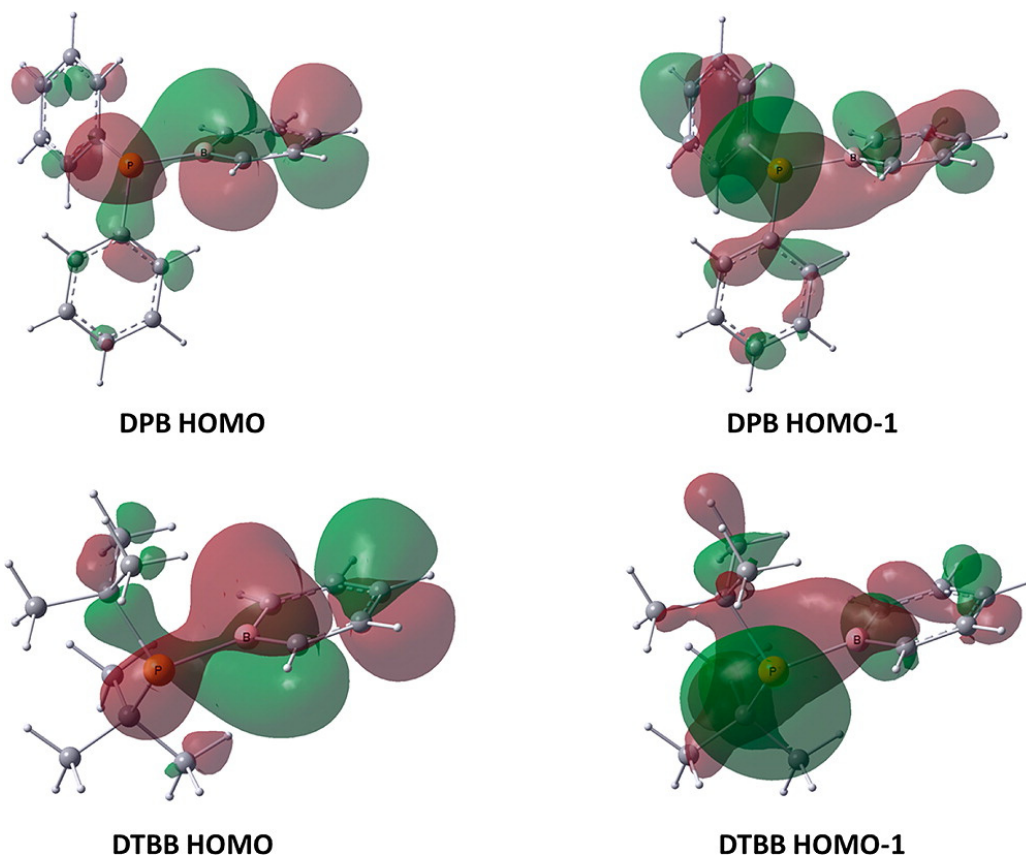
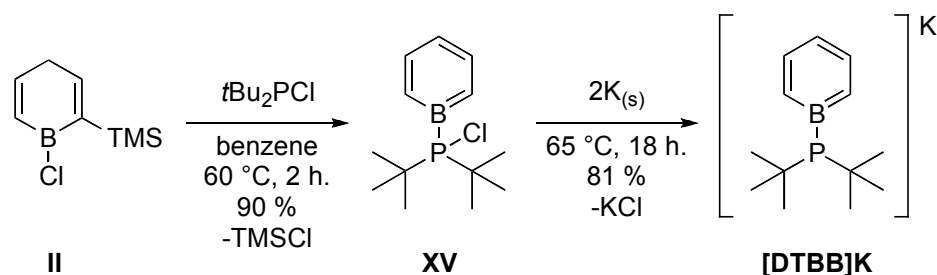


Figure 2.9: Kohn-Sham orbital representations of the HOMO and HOMO-1 of $(\text{DPB})^-$ and $(\text{DTBB})^-$ ligands determined using DFT. Figure taken from reference 53.

2.3.3 Synthesis of DTBB Ligand

The synthesis of **DTBB** ligand⁵³ can be efficiently carried out in good yields. The first step involves the formation of a neutral borabenzene-phosphine adduct. Reaction of Cl-boracycle(TMS) (**II**) (Scheme 2.4) with $t\text{Bu}_2\text{PCl}$, with loss of TMSCl , yields the neutral di-*tert*-butyl-chlorophosphinoboratabenzene (**XV**). Unlike other borabenzene-phosphine adducts like $\text{C}_5\text{H}_5\text{B-PMe}_3$ (**III**), species **XV** is not stable in the solid state and must be quickly used in the following step. Reduction with potassium under reflux, affords the potassium salt of di-*tert*-butyl-phosphidoboratabenzene (**DTBB**).



Scheme 2.4: Synthesis of **DTBB** ligand reported by our group in 2009.⁵³

2.3.4 Metal Complexes of **DTBB** and **DPB**

Metal complexes of phosphido-boratabenzene ligands can be readily obtained by salt metathesis with metal precursors in most cases. As previously mentioned, Fu reported that metal complexes of **DPB** with Fe, Rh and Zr, were bonded η^1 through the phosphorous lone pair (**XVI**, **XVII**, **XVIII**, Figure 2.10).²³

Unlike the **DPB**, η^1 -coordination of the **DTBB** ligand to group 10 metal centres, for example, proved to be difficult due to the nature of the metal precursors (Figure 2.10, b).⁵³ Instead of bonding through the lone pair on phosphorous, the **DTBB** ligand has a strong preference to bind η^6 as observed on the nickel dimer (**XIX**) where the metal centre is coordinated to the aromatic ring. The coordination sphere of the nickel is fulfilled with the phosphorous of a second **DTBB** and results in the formation of a Ni-Ni bond. Attempts to coordinate **DTBB** to Pt(II) resulted in a η^3 bonded **DTBB** sandwich complex (**XX**) when PtCl_2 was used. However when $(\text{COD})\text{PtCl}_2$ was used, **DTBB** coordinates η^3 through the P-B=C bond but a second **DTBB** anion carries a nucleophilic attack on the platinum-coordinated cyclooctadiene (COD) (**XXI**).

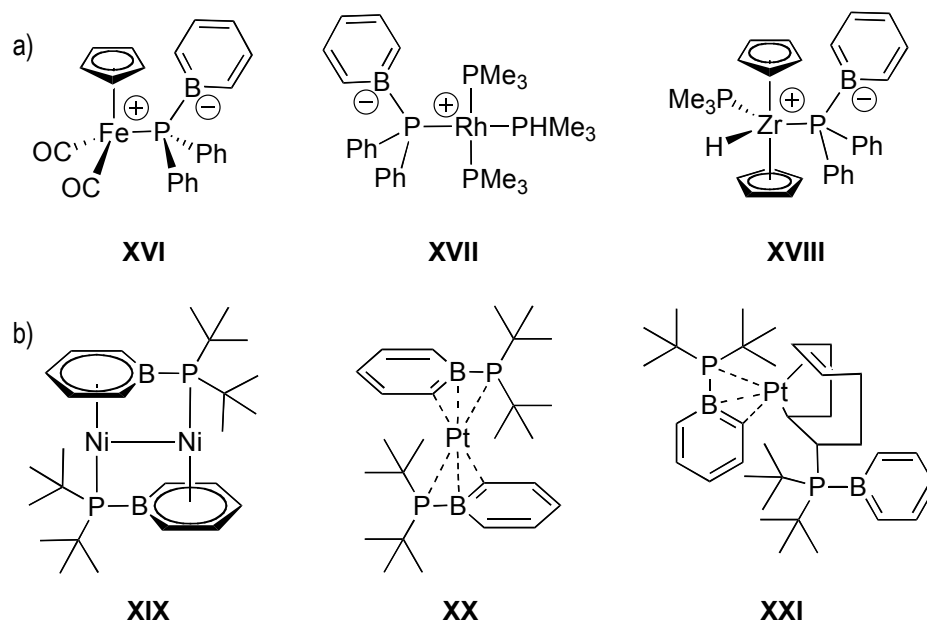


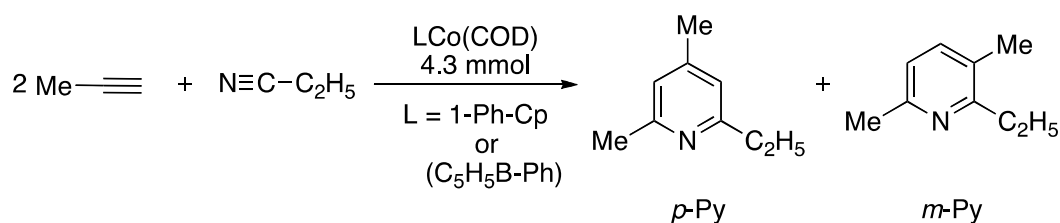
Figure 2.10: a) Metal complexes of **DPB** reported by Fu.²³ b) Metal complexes of **DTBB** reported by Fontaine *et al.*⁵³

2.4 Boratabenzene Complexes in Catalysis

Metal complexes of boratabenzene with almost all the heavy elements have been reported in the literature. In this section some relevant examples of the catalytic activity of boratabenzene complexes are presented.

2.4.1 Boratabenzene Complexes as Polymerization Catalyst

Catalytic co-cyclization of alkynes and nitriles to selectively produce substituted pyridines was carried using a (C₅H₅B-Ph)Co(COD) (Scheme 2.5). The reaction takes place at 120 °C, the product ratio of substituted pyridine *p*-Py/*m*-Py is of 2.52 when phenyl-boratabenzene was used as a ligand. It is notable that a higher activity is observed with the boratabenzene ligand compared to the Cp analogue, which catalyzes the reaction at 140 °C and only produces a *p*-Py/*m*-Py ratio of 1.73. This reactivity can be expanded to the cyclization of acrylonitrile and acetylene to produce 2-vinylpyridine (TON 2164) at 120 °C, in a regioselective way and can be adapted to cyano and amino containing substrates.⁵⁴



Scheme 2.5: Regioselective co-cyclization of alkynes and nitriles catalyzed by LCo(COD) (L = 1-Ph-Cp or C₅H₅B-Ph).⁵⁴

The use of boratabenzene metal complexes as catalyst in polymerization was widely explored during the late 1990's and early 2000's by Bazan. The capability of boratabenzene complexes to selectively produce branched polymers,^{55a} linear oligomers,^{55b,c} dimers of ethylene^{55d} and other alkenes^{55e,f} has been subject of many publications.

Polymerization has also been achieved using metals such as Zr and Cr in excellent yields and low temperatures. A great example is that of the amido-boratabenzene chromium complex, reported by Chen. This chromium catalyst gets activated by MAO and is capable to polymerize ethylene ($170 \times 10^6 \text{ g PE mol}^{-1} [\text{Cr}] \text{ h}^{-1}$) at 30 °C. Its catalytic activity is only limited by mass transport rather than the structure or stability of the catalyst itself.⁵⁶

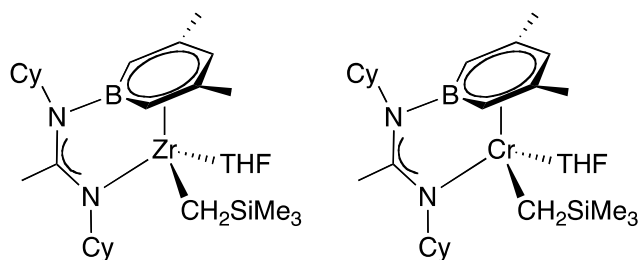
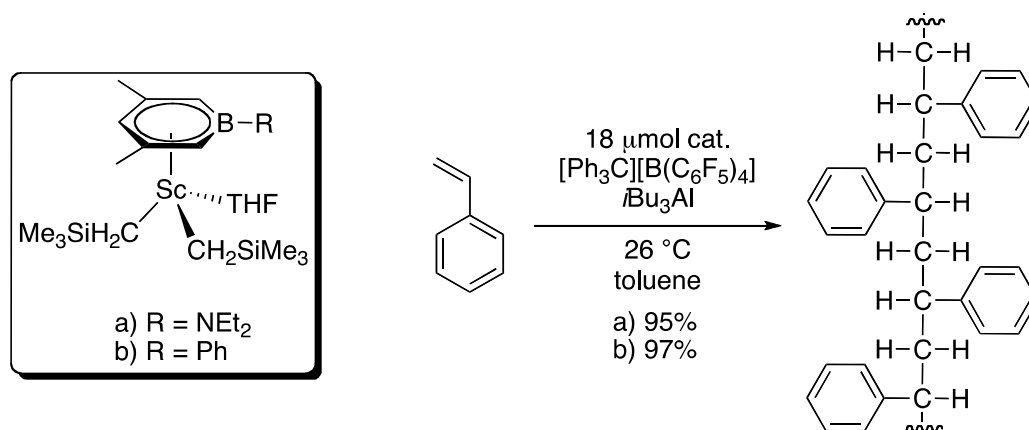


Figure 2.11: Zr and Cr amido-boratabenzene catalyst reported by Chen.⁵⁶

Recently Chen Y. reported a scandium boratabenzene complex which is capable of selectively produce syndiotactic polymerization of styrene in high yields at 26 °C. Indeed, a catalyst featuring an amido-boratabenzene can produce syndiotactic polystyrene in 95% yield (TOF = 1944 Kg PS mol⁻¹ [Sc] h⁻¹) while the phenyl-boratabenzene analogue was even more active affording 97% yield with higher TOF (TOF = 2061 Kg PS mol⁻¹ [Sc] h⁻¹). The difference of reactivity is a consequence of the exocyclic substituent on boron. Since the amido group is involved in π-donation with boron, the amido-boratabenzene complex shows a lower activity than the one containing the free rotating phenyl substituent.⁵⁷



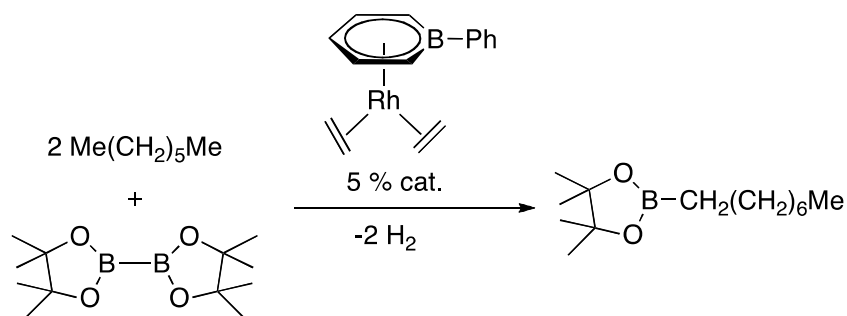
Scheme 2.6: Scandium catalyst of boratabenzene used in the syndiotactic polymerization of styrene.⁵⁷

2.4.2 Miscellaneous Examples of Boratabenzene in Catalysis

Only a small number of examples of catalytic applications other than polymerization have been reported. Nevertheless the scarcity of these examples is not representative of the importance of the transformations.

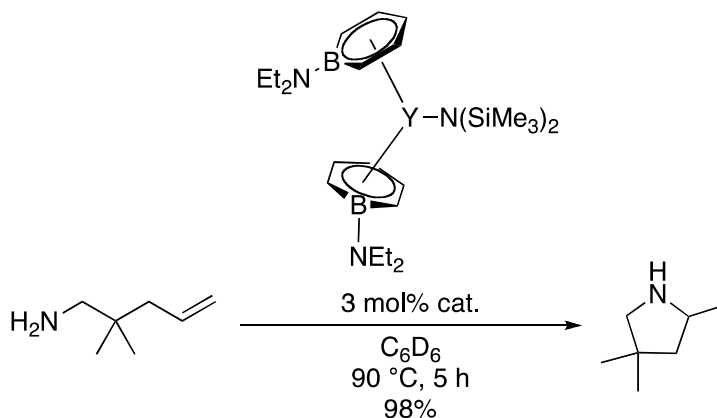
For example, in 2001 Bazan brought about the use of boratabenzene metal complexes a step further than the polymerization catalysis. The C-H activation of octane using pinBBpin is initiated faster by a (C₅H₅B-Ph)Rh(C₂H₄)₂ than by the analog Cp^{*}Rh(C₂H₄)₂. Unfortunately the boratabenzene complex is not thermally stable and if the catalysis is carried at temperatures higher than 95 °C, conversion of the reagents only reaches 15% yield and the catalyst becomes inactive after 24h, unlike the Cp^{*} complex which brings the reaction to completion.⁵⁸

Nevertheless these complexes could provide alternatives to C-H activation for reactions that require temperatures below 95 °C.



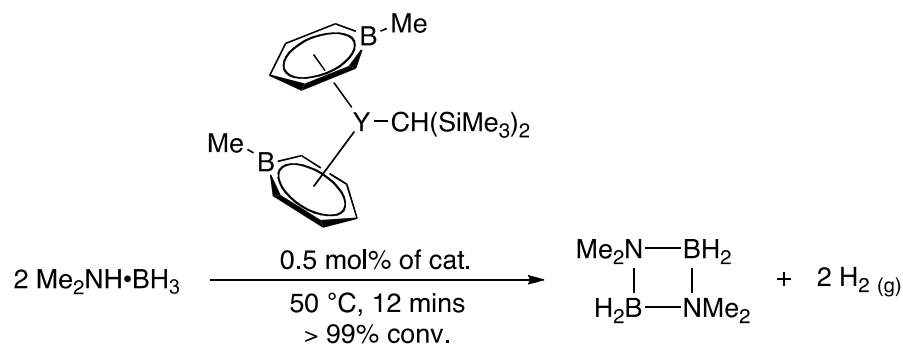
Scheme 2.7: Boration of octane using $(\text{C}_5\text{H}_5\text{B-Ph})\text{Rh}(\text{C}_2\text{H}_4)_2$, reported by Bazan.⁵⁸

Chen has observed the intramolecular hydroamination of amines using an yttrium boratabenzene complex in yields as high as 98%.⁵⁹ The atom-economy of such transformation is of relevance to the commercial availability of nitrogen heterocycles, important precursors in the manufacture of pharmaceutical and fine chemicals.



Scheme 2.8: Intramolecular hydroamination using an Yttrium boratabenzene complex by Chen.⁵⁹

Chen has also reported the dehydrocoupling of amino-boranes using an yttrium boratabenzene complex (Scheme 2.9).⁶⁰ This transformation is of particular relevance since the product of the dehydrocoupling is molecular hydrogen. Such transformations are of current interest as alternative solutions to the upcoming energetic crisis and its environmental impacts.



Scheme 2.9: Catalytic dehydrocoupling of amino-boranes with an Yttrium boratabenzene complex, reported by Chen.⁶⁰

3 Chapter 3 Methodology

3.1 Experimental Methods

3.1.1 Inert Atmosphere Chemistry

Borabenzene compounds are prone to oxidation and hydrolysis by coming in contact with moisture or oxygen in the air. For this reason the use of proper techniques to handle and store air sensitive compounds have been employed.

Developed in the 1900's by Wilhelm Schlenk,⁶¹ Schlenk techniques⁶² are particularly useful to limit the exposure to air by removal of volatiles with vacuum and replacement of the atmosphere by a stream of dry nitrogen gas using double manifold high pressure glass tubes having Teflon valves. Schlenk lines and tubes are helpful during the handling and manipulation of air sensitive and dry chemicals (Figure 3.1).



Figure 3.1: Double manifold Schlenk line and Schlenk tubes used in inert atmosphere chemistry.

The use of stainless steel cannulas allows for the transfer of solvent or solution from one vessel to another, minimizing if not fully avoiding the contact with air by maintaining a positive pressure of N₂ gas.

Furthermore the use of inert atmosphere gloveboxes allows us to manipulate air sensitive chemicals (Figure 3.2). Operations such as weighing and storing chemicals are easily carried inside the box.

The atmosphere inside the glovebox is constantly circulated through a purification unit, which contains molecular sieves to retain water and a copper catalyst to filter off traces of oxygen. The purification system is regenerated easily by several cycles of heating and circulation of H₂/N₂ gas mixture, thus keeping the quality of the atmosphere inside up to <0.01 ppm of moisture and oxygen, allowing the chemist to safely handle very reactive chemicals which otherwise would violently react with air.



Figure 3.2: Double station glove box.

Avoiding the contact of chemicals with air is essential to the organometallic chemist, however solvents and other reagents that are not commercially packed

under argon or nitrogen have to be properly purified and dried before introducing them in the glove box.

The solvents purification is carried by pre-treatment according to reported procedures in the literature⁶³ and pre-drying with the appropriate drying agent. Upon treatment the solvents (THF, ether, hexane, pentane, toluene) are refluxed with either sodium/benzophenone (ketyl) or potassium to be distilled under a stream of nitrogen and stored using Teflon capped Strauss flasks. Solvents used for NMR analysis are stirred under a mirror of Na/K amalgam for 48 h. The solvents are degassed using three cycles of freeze-pump-thaw and vacuum transferred to a Strauss flask.

3.1.2 Pressurized Gas and Cryogenics

Borabenzene compounds are particularly susceptible to oxidation and hydrolysis due to the inherent Lewis acidity of boron. However the use of proper Schlenk techniques, glove boxes and airtight J. Young tubes simplifies the manipulation of these compounds.

In chapter 6, the rhodium dimer was exposed to ≈ 1 atm of H_2 gas, this was only possible using a J. Young tube. These NMR tubes are fitted with a Teflon stopper serving as a valve, allowing the control of the atmosphere inside the tube. The Teflon stopper can be fitted to a glass adaptor with a ground joint that can be connected to the Schlenk line. Manifolds with two ports for J. Young adaptors are available in our laboratory.

In a typical experiment the J. Young tube was loaded with a solution of a metal complex and degassed using three cycles of freeze-pump-thaw, frozen down to 77 K with a N_2 liquid bath. After allowing the sample to thaw for a third time, the solution was frozen again and the liquid nitrogen bath was removed, the Teflon stopper was opened to allow H_2 into the tube for 10 seconds and closed again. The solution was allowed to thaw slowly in order to avoid explosion of the glassware.

It is important to remark that J. Young tubes must not be submitted to pressures higher than five atmospheres of gas to avoid rupture and possible explosion of the glassware. Additional precautions must be taken when the use of liquid nitrogen is needed, since oxygen condenses at atmospheric pressure at 90 K and can cause

unexpected detonations when organics are present in the mixture. Proper fitting of the ground joints with grease and testing of the Teflon stoppers must be performed as a routine procedure to avoid the presence of leaks that could bring oxygen to condensate inside the flask or airtight tube in use.

3.2 Characterization Techniques

3.2.1 Nuclear Magnetic Resonance spectroscopy (NMR)

Structure elucidation through NMR spectroscopy is a major tool in organometallic chemistry, not only for the characterization of the organic ligands but to characterize their coordination modes. In many cases NMR, can also be used to monitor the course of a reaction, to elucidate mechanisms and to study fluxional processes.

Molecules presented in this work contain a variety of NMR active nuclei as shown in Table 3.1.⁶⁴

Table 3.1: NMR frequency table of nuclei studied in this work. Values taken from reference 64.

Isotope	Spin	Abundance (%)	NMR Frequency (MHz) at field 11.743 T
¹ H	1/2	99.98	500
¹³ C	1/2	1.108	125.721
³¹ P	1/2	100	202.404
¹¹ B	3/2	80.42	160.419
¹⁰³ Rh	1/2	100	15.737

Placing a sample in a magnetic field at the frequency of the nucleus under study and exciting the sample with a radio frequency pulse at 90°, forces the nuclear spins to move from their equilibrium position in order to align to the magnetic field. Then a delay is allowed for the spin to relax back to its equilibrium position. This behavior produces a resonance response registered as Free Induction Decay

(FID). A FID plot is recorded using multiple scans to increase the signal-to-noise ratio, resulting in better resolution NMR spectra. Processing the FID with a Fourier Transform (FT) is possible to extract the plotted spectrum.

3.2.1.1 Dipole-dipole Relaxation (T_1)

Special attention is given to species such as the rhodium hydrides described in chapter 6. Metal hydrides are subject of debate when it comes to identifying a terminal or “classical” hydride from the dihydrogen complex, where the H_2 molecule behaves as a σ -bonded ligand. Because there are many limitations with other techniques to properly differentiate between terminal or bridging classical hydrides and dihydrogen complexes, the measurement of the dipole-dipole relaxation is an inexpensive solution to elucidate the nature of the metal-hydrogen interaction. Nevertheless some considerations, well documented in the literature,⁶⁵ must be taken into account when analyzing the data.

Crabtree and Lavin reported in 1985 that H_2 bound to metals was observed as a broad resonance and this broadness was attributed to a rapid dipole-dipole relaxation time, which in other words means a short T_1 (s).⁶⁶ Rapid relaxation is explained because of a short H-H bond distance.

Dipole-dipole relaxation T_1 (Equation 3.1) is proportional to the inverse sixth power of the internuclear distance and can be described using the following equation

$$R = 1/T_1 = 4\gamma^2_H\gamma^2_A\hbar S(S-1)\tau/3r^6_{H,A}$$

Equation 3.1: Dipole-dipole relaxation T_1 (s).⁶⁶

If one of the two dipoles is 1H , in Equation 3.1, γ is the gyromagnetic ratio, which is directly proportional to the magnitude of the magnetic moment of the nuclei A and 1H , S is the spin quantum number and \hbar is Planck’s constant, τ is the molecular correlation time and r is the distance between the two dipoles. Values of τ and r vary with the molecular structure. This is the case of the complexes in chapter 6, since larger molecules move slowly (large τ) and the proton directly bound displays

short r -values. The other factors affecting the T_1 measurements as well as the dipole-dipole contributions from adjacent atoms are properly described in the literature.⁶⁷

T_1 can be measured using the inversion-recovery sequence described in Equation 3.2.⁶⁸

180° pulse – τ (waiting time) – 90° pulse – (collection of the FID and transform)

Equation 3.2: Inversion-recovery sequence used to measure T_1 .

The resulting FID can be transformed using FT resulting in a series of spectra depicting different waiting times (τ). The 180° pulse inverts the magnetization, hence the spectra showing negative signals. The magnetization remains inverted up to the moment on when the 90° pulse is allowed. Eventually the waiting time increases and the 90° pulse results in positive signals as the spins relax towards their equilibrium position. The T_1 value can be calculated by a graphical treatment of the data using a regression analysis (Figure 3.3).

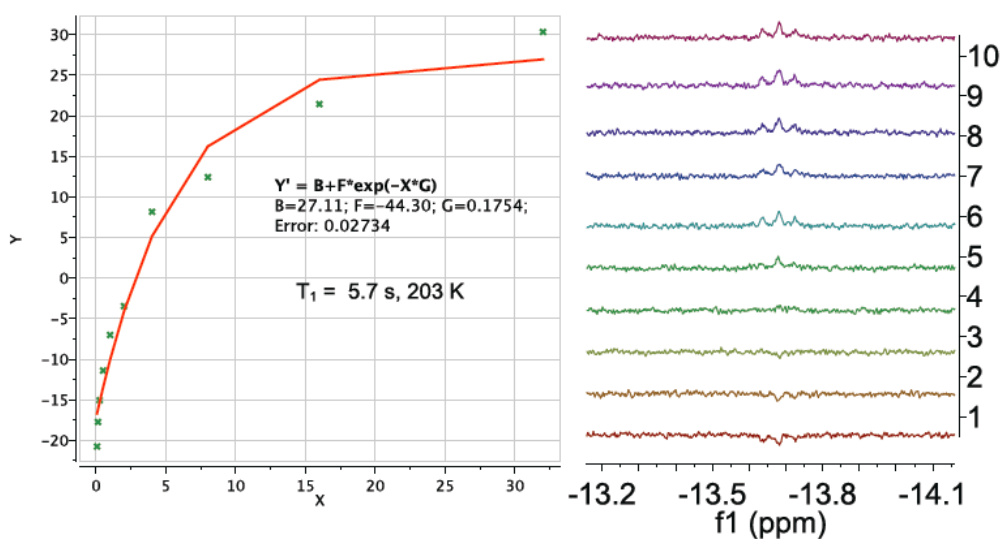


Figure 3.3: Regression graphic and T_1 value at 203 K, inversion recovery spectra of Rh hydride (10).

3.2.1.2 NMR Correlation Experiments

In chapter 6, the characterization of rhodium species was made easier since all atoms in the molecular structures were NMR active. Indeed, it allowed for the mapping of the bonding structure through NMR correlations. NMR correlations such as $^1\text{H}\{^{31}\text{P}\}$ were crucial to set apart the identity of the rhodium hydride species, other impurities and decomposition products and to locate the position of the ligands around the metal centre.

^1H - ^1H correlations are useful in the identification of the borabenzene protons and their coordination mode as will be discussed in chapters 4 and 5 for the iron and copper species respectively, where *g*COSY experiments were used to identify *ortho*, *meta* and *para* protons for the different coordination modes of boratabenzene.

3.2.1.3 Multinuclear NMR: ^{31}P and ^{11}B

Having molecules with multiple NMR active nuclei can be both useful and tedious since acquisition times required to properly obtain the full characterization of a single species are long and often involve several attempts.

^{31}P NMR was the main tool to observe phosphorous-containing ligands presented in this work. The coordination of a phosphorous atom to a metal becomes evident because of the change in the chemical shifts of several parts per million in some cases. It allows for ^{31}P to be an excellent tool to follow the course of reactions as well as the changes in the coordination modes.

Particular attention is made to the phosphide ligand **DTBB**, which shows relatively high shifts because of the localized electron lone pair.

In chapter 4, ^{31}P NMR was crucial to witness the coordination change of η^1 -**DTBB** ligand to a η^6 -coordinated **DTBB** featuring a pendant phosphine. The significant change in the ^{31}P chemical shift upon dissociation of the phosphine was representative of the different coordination environments.

^{31}P resonances of [P-M] fragments, when the metal is not NMR active, are usually observed as sharp lines. However, for most of the species in this work, signals are observed as broad multiplets due to the presence of a P-B interaction. Coupling of both NMR active nuclei enhances the broadening of the signals in both ^{31}P and ^{11}B NMR.

Both ^{10}B and ^{11}B are NMR active nuclei, however ^{11}B yields sharper signals in the spectrum because of its short relaxation time, is easier to observe and more abundant (^{11}B 80.42 %) than ^{10}B (19.58 %).

Because of the quadrupolar moment of ^{11}B , which has a nuclear spin of 3/2, significant effects are observed for the atoms bound to the boron centre or adjacent to it, such as the phosphorous and the *ortho* carbons and protons on the boratabenzene ring. Broadening of the signals is observed in all cases, particularly in ^{13}C NMR where the *ortho* carbons are often not observed, hence the use of ^1H - ^{13}C correlations.

Important information on the coordination environment of the boron centre is obtained from the chemical shift and the splitting of the ^{11}B NMR signals. The ^{11}B chemical shifts of boratabenzene species range from 10 to -60 ppm while species such as those in chapter 4 where the π -contribution from oxygen is present have their chemical shifts vary from 90 to 10 ppm.

It is important to note that the use of airtight J. Young tubes was essential to characterize all the air sensitive species in this work. Since common glass NMR tubes contain borosilicates, a quartz J. Young was used to avoid the background signals when measuring the ^{11}B NMR spectra.

It was unfortunately not possible to acquire the rhodium NMR for species in chapter 6 because the 11.4 T magnet that we have is not capable to reach the low frequency (15.737 MHz) necessary to measure ^{103}Rh .

3.2.2 Mass Spectrometry

Electrospray ionization (ESI) was used when ionic molecules exist in solution, as is the case of the species discussed in chapter 5. The solution being analyzed is directly injected into the instrument's source, for the case of air sensitive compounds used in this work. The solution is then nebulized through a capillary needle by a stream of N₂ gas. The needle is connected to an electrode that applies a steady voltage producing charged particles rather than breaking the molecule. This is why ESI is considered a soft ionization technique. The mass spectrum shows a mass-charge ratio (m/z) of the corresponding molecular ion. These results can be paired with simulations of the spectra that keep in account the abundance of all the isotopes of the elements present, providing a side-by-side comparison of the isotopic patterns that are characteristic of each molecular ion, which is particularly useful with metal complexes.

Atmosphere Pressure Photo-Ionization (APPI) can ionize other molecules that do not possess the characteristics mentioned above; the source of ionization in this case is a UV lamp. This method is useful when multiple bonds and conjugation is present within the molecule, as is the case in chapter 4.

Simulation of experimental spectra can be done using one of several open source softwares available online free of cost. In this work, simulated mass spectra was generated using mMass (ver. 5.5.0, © 2013) mass calculator tool.⁶⁹

3.2.3 IR Spectroscopy

Vibrational spectroscopy provides a great deal of information in the study of metal-carbonyl complexes. It is also a useful technique to follow the course of a reaction, when possible.

The stretching bands representing the vibrational modes of a molecule are observed at a certain position in the IR spectrum. The strength of the bond, measured by a force constant (k) and the reduced mass of the system (m_r), influence the positioning of the bands (ν) (Equation 3.3). The reduced mass, for a

diatomic molecule, can be calculated as shown in Equation 3.4 where m_1 and m_2 represent the atomic weight of the atoms involved in the vibration.³

Non-bonded CO stretching is observed at 2143 cm^{-1} but it can vary from 1700 to 2100 cm^{-1} when coordinated to a metal centre.

$$\nu = \frac{1}{2\pi} \left\{ \sqrt{\frac{k}{m_r}} \right\}$$

Equation 3.3: Calculation of the IR frequency.

$$m_r = \frac{m_1 m_2}{m_1 + m_2}$$

Equation 3.4: Reduced mass calculated for a diatomic molecule.

Upon coordination of the CO ligand to a metal, the intensity of the band increases because of a change in the dipole moment during the vibration, hence the CO molecule becomes polarized. Furthermore this band shifts to a lower frequency if very donor ligands are present on the [M-L] fragment on which the CO ligand is coordinated, this shift is also influenced by the presence of a net negative charge, or if the metal has become more π -basic. The shift of the stretching band is a direct consequence of the back-bonding to the antibonding orbitals of the C-O bonds. A greater back bonding weakens the triple bond lowering the energy of the vibration and shifting the band to a lower wavenumber.

IR spectroscopy becomes an excellent tool for measuring the donating capabilities of ligands, allowing for fine-tuning of the electronic properties.

3.2.4 Elemental Analysis

Elemental analysis of elements C and H are commonly acceptable for the identification of organometallic complexes in the solid state. It is important however

that the values fall in a range of $\pm 0.3\%$ from the theoretical values. In this work, only one boratabenzene complex was characterized using elemental analysis. The main reason is the air and moisture sensitivity of boratabenzene complexes, in consequence is difficult to obtain reliable analysis.

3.2.5 X-Ray Diffraction

X-ray diffraction is one of the foremost tools for structure determination in the solid state, since it provides a tridimensional view of the molecular structure in question.

The wavelength of an X-ray ranges from 0.1 to 1 Å, which is in the order of the length of a chemical bond. When a beam strikes a nuclei possessing sufficient electron density, the beam will be scattered at a certain angle from the incident beam. This is only possible if conditions satisfy the Bragg's law (Equation 3.5).

$$2d \sin \theta = n\lambda$$

Equation 3.5: Bragg's law.

Where λ is the wavelength of the radiation, 2θ is the angle between the incident and diffracted ray, n is an integer and d is the spacing of the unit cells.

The arrangement of the molecules in a tridimensional pattern displays a single unit (unit cell), which repeats along the crystal network. The diffraction pattern and intensity are given by the dimensions and packing of the molecules within the unit cell. This information is summarized in bond distances and angles producing a tridimensional visualization of the molecular structure.

A crystal with specific characteristics is supported on a goniometer, which is then placed between the X-ray source and a charge coupled device (CCD) detector. Then the X-ray beam strikes the crystal from different angles and the data is collected.

The multiple diffracted radiations, so called reflections, are then collected and the data are treated by a statistical method using computational programs and the

chemical knowledge of a skilled crystallographer such as Dr. Wenhua Bi, whom carried most of the diffraction studies presented in this work.

In order to obtain reliable data the crystal must have the correct size and crystallinity, with no impurities embedded or imperfections and it must diffract the X-ray at a considerable intensity. The crystal is protected with an amorphous matrix composed of heavy hydrocarbons such as Paratone N®, which is commonly used. Additionally, air sensitive compounds are also kept under a stream of N₂ and often at low temperatures.

Our research group has a Bruker APEX II area detector diffractometer equipped with a graphite monochromated MoK α radiation source.

The biggest limitation of this elegant technique is the growth of single crystals of a sufficient quality. The craft of growing crystals can be considered as an art rather than a systematic scientific procedure. The growth of good quality crystals involves several attempts under different temperature and solvent conditions and it often takes a lot of time and effort to harvest the results. Moreover the structure obtained from an X-ray diffraction study could not be that of the composition of the mixture as a whole, which is why the interpretation of crystal structures must be paired up with other analysis in solution and solid state.

3.3 Density Functional Theory

The optimized geometries for the copper complexes presented in chapter 5 are the result of calculations performed by Prof. Laurent Maron at Université Paul Sabatier in Toulouse, France. These calculations are based on the methods of Density Functional Theory (DFT).

The following section intends to summarize key concepts of the DFT; a more thorough and instructive introduction to the DFT lies beyond the scope of this work and can be found in the literature.

Density Functional Theory is rooted in quantum mechanics and the computational method has found applications in physics, chemistry and materials science in order

to investigate the structural, magnetic and electronic properties of molecules and materials.

The goal of most quantum chemical approaches is the approximate solution of the Schrödinger equation, the wave function. Solutions to the Schrodinger equations had only been found for a limited number of small molecules.⁷⁰ However by using an approximation on which the electrostatic interactions are omitted, Kohn and Sham arrived to a series of mathematical tools which focuses on the determination not of the wave function but a trial function, also known as a functional (a function of a function). In other words, $f(x)$ is a function of the variable x , while $F[f]$ is a functional of the function f .⁷¹

Theoretical studies based on the Kohn-Sham method are used in calculations for molecular modeling with outcomes of variable accuracy and they can be found in the literature.⁷⁰

4 Chapter 4 Iron Boratabenzene Complexes

In this chapter the first example of **DTBB** ligand coordinated η^1 to a metal centre is presented. Qualitative analyses of the donating capabilities of the **DTBB** ligand as well as the consequences of its nucleophilicity when coordinated to iron are described.

4.1 Introduction

The iron carbonyl species presented in this chapter is the first metal complex where the **DTBB** ligand assumes a η^1 -coordination mode, similarly to the Zr, Rh and Fe species previously reported by Fu. The main interest in looking at this species is to better understand the **DTBB** donating capability as a bulky phosphine.

It was put forward by the photodissociation of the CO ligands, that **DTBB** is a hemilabile ligand, capable to stabilize the metal centre upon the ligand displacement, which opens up the possibility for new reactivity with applications in catalysis.

The nucleophilicity of the pendant **DTBB** is once again demonstrated by its high reactivity with traces of water, yielding two new ferrocenyl-like iron species of boratabenzene with interesting structural properties and which reactivity is yet to be discovered.

4.1.1 η^1 Complexes of Boratabenzene

As mentioned in section 2.2.4, only few examples of η^1 -coordinated boratabenzene complexes have been reported, which are the $\text{CpZr(H)(DPB)(PMe}_3\text{)}$ (**I**), $\text{Rh(PMe}_3\text{)}_3\text{(DPB)}$ (**II**), $\text{CpFe(CO)}_2\text{(DPB)}$ (**III**) reported by Fu²³ and that reported by our group in 2009 featuring a unique Pt-Cl-B interaction $\text{((H)Pt(IMes)}_2\text{(C}_5\text{H}_4\text{(TMS)B-Cl)}$ (**IV**) (Figure 4.1).⁴⁸

Our interest turned to the comparison of complex **III** with an isoelectronic complex featuring the **DTBB** ligand. The presence of the CO ligands would enable us to compare the donating capability of **DTBB** ligand against the **DPB** and other donating ligands, as we shall see in section 4.2.1.

Additionally iron species such as **III** have shown to have interesting coordination chemistry and applications in a variety of catalytic processes.

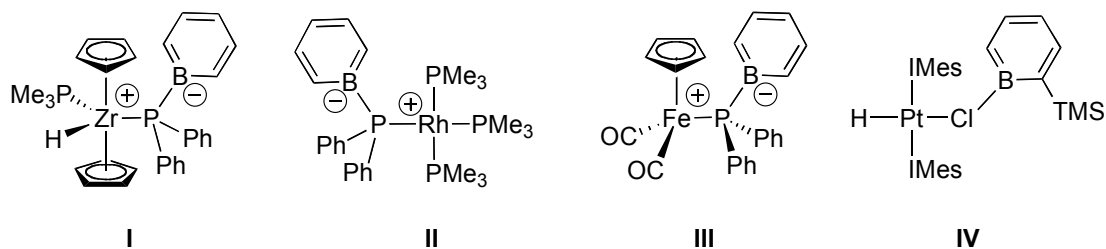
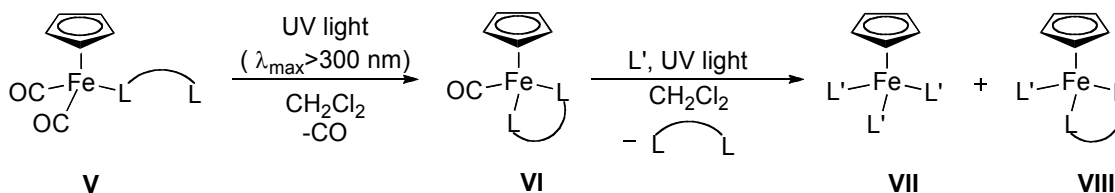


Figure 4.1: Boratabenzene complexes coordinated η^1 : $\text{Cp}_2\text{Zr}(\text{H})(\text{PMe}_3)(\text{DPB})$ (**I**), $(\text{PMe}_3)_3\text{Rh}(\text{DPB})$ (**II**), $\text{CpFe}(\text{CO})_2(\text{DPB})$ (**III**),²³ $(\text{IMes})_2\text{Pt}(\text{H})(\text{C}_5\text{H}_4(\text{TMS})\text{B}-\text{Cl})$ (**IV**).⁴⁸

4.1.2 Iron Carbonyl Species: Reactivity and Catalytic Applications

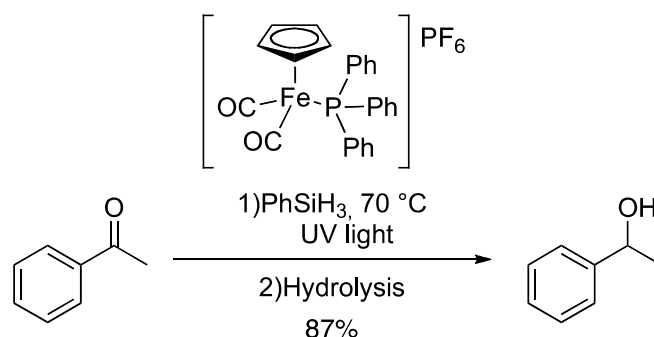
The photodissociation of CO ligands has been observed for iron carbonyl species such as **V** (Scheme 4.1), featuring a bidentate phosphine ligand. Upon irradiation with UV light, dissociation of one carbonyl ligand was observed. As a consequence the second arm of the chelating phosphine occupies the newly created empty site. The carbonyl ligand in species **VI** can undergo another photodissociation, if a second ligand (L') is added and the mixture is again exposed to light. The dissociation of CO yields two products: one involves the complete substitution of all the ligands by L' (**VII**) and the ligand exchange of one CO by L' (**VIII**).⁷²



Scheme 4.1: Photodissociation of CO ligands and reactivity against other ligands.⁷²

Applications to the photodissociation of CO ligands from iron carbonyl complexes has proved useful in the catalytic hydrosilylation of substrates such as acetophenone by iron species $[\text{CpFe}(\text{CO})_2(\text{PPh}_3)][\text{PF}_6]$ (Scheme 4.2). The reaction

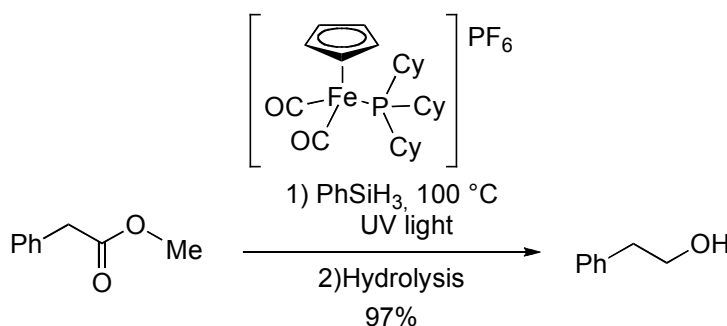
proceeds in relatively mild conditions and the dissociation of CO ligands is triggered by the use of UV light irradiation.⁷³



Scheme 4.2: Hydrosilylation of acetophenone by [CpFe(CO)₂(PPh₃)]⁺[PF₆]⁻.⁷³

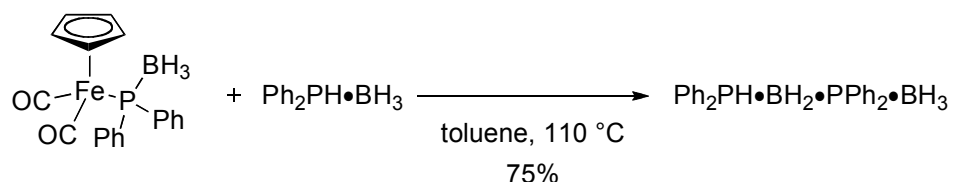
Additionally this reactivity can be extended to the reduction of benzaldehyde derivatives under similar conditions by using visible light. The reactions carried by [CpFe(CO)₂(L)]⁺[PF₆]⁻ (L = PMe₂Ph, PCy₃), proceed in excellent yields and the use of inexpensive silanes such as polymethylhydrosiloxane (PMHS) makes the catalytic reaction an efficient, low cost and low environmental impact process.⁷³

Darcel *et al.* have also worked on the use of iron precatalysts such as [CpFe(CO)₂(PCy₃)]⁺[PF₆]⁻ to carry the unprecedented hydrosilylation of esters using UV light irradiation and obtaining 97% conversion in only 16 hours of reaction (Scheme 4.3). These applications are excellent alternatives to the use of expensive and toxic metals.⁷⁴



Scheme 4.3: Hydrosilylation of esters by [CpFe(CO)₂(PCy₃)]⁺[PF₆]⁻.⁷⁴

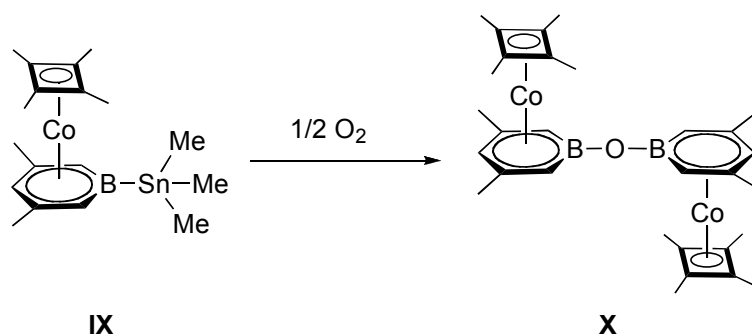
Another relevant application of iron carbonyl complexes featuring phosphino-borane ligands has been reported by Manners. The species $[\text{CpFe}(\text{CO})_2(\text{Ph}_2\text{P}\cdot\text{BH}_3)]$ is capable to carry the dehydrocoupling of $\text{Ph}_2\text{PH}\cdot\text{BH}_3$ in solution. Interestingly the irradiation with UV light do not promote the dissociation of the CO ligands; in order for the dehydrocoupling to happen, the reaction must be heated to $100\text{ }^\circ\text{C}$ (Scheme 4.4).⁷⁵



Scheme 4.4: Dehydrocoupling of phosphine-borane adducts by $[\text{CpFe}(\text{CO})_2(\text{Ph}_2\text{P}\cdot\text{BH}_3)]$.⁷⁵

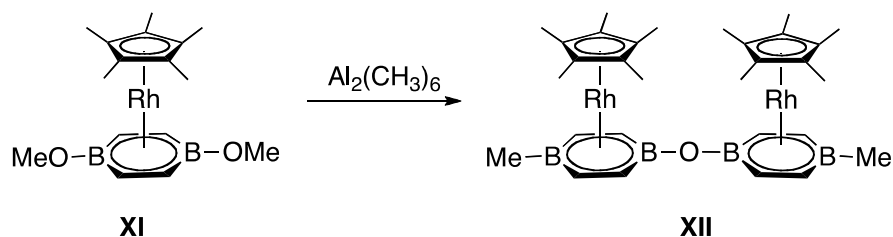
4.1.3 Boratabenzene Metal Complexes: Reactivity with H_2O

The reactivity of boratabenzene metal complexes with traces of moisture and oxygen has been well documented, Herberich reported a μ -oxo bridged boratabenzene, obtained from a solution of **IX** kept for prolonged time and accidentally exposed to traces of air, which yielded crystals of **X** (Scheme 4.5).⁷⁶



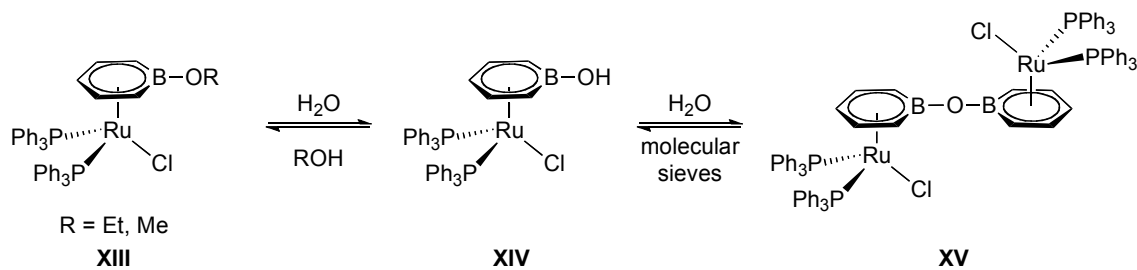
Scheme 4.5: Synthesis of B,B'-oxo linked dinuclear complex by Herberich et al.⁷⁶

Furthermore similar structures have also been observed for bis-boratabenzene rhodium complexes (Scheme 4.6). The polycondensation products are obtained from reaction of species **XI** with $\text{Al}_2(\text{CH}_3)_6$, resulting in the formation of the B-O-B bridged species (**XII**), attributed to hydrolysis during isolation by chromatography.⁷⁷



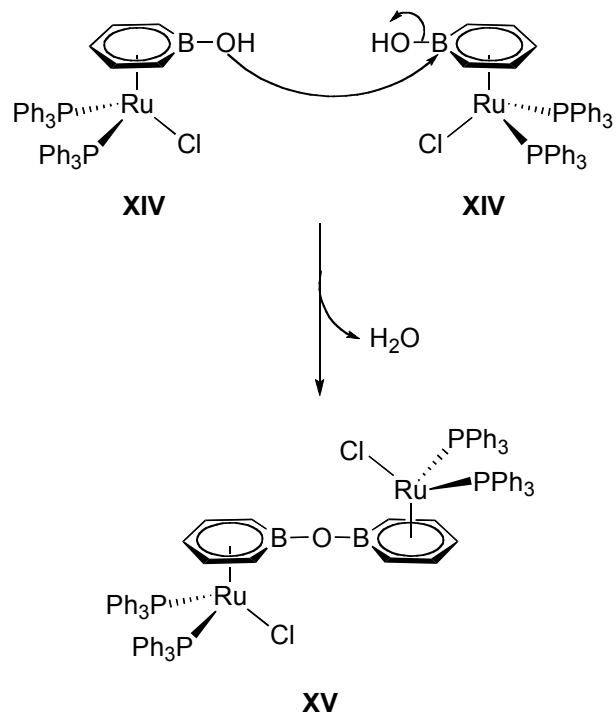
Scheme 4.6: Polycondensation of bis-boratabenzene rhodium complex.⁷⁷

More recently a Ru piano stool complex (**XIV**, Scheme 4.7) was reported by Wen *et al.*⁷⁸ Species **XIV** was obtained by the exchange of an alkoxy group for a hydroxo on a ruthenium η^6 -boratabenzene (**XIII**) in the presence of traces of moisture. Ashe and collaborators have previously reported this behaviour on similar species.⁷⁹ However Wen *et al.* were able to obtain a μ -oxo-boratabenzene complex (**XV**). They observed that species **XIV** and **XV** interconvert with each other by adding or removing moisture from the reaction mixture.



Scheme 4.7: Ruthenium boratabenzenes reported by Wen *et al.*⁷⁸

Furthermore they proposed a mechanism for the formation of the μ -oxo boratabenzene species, shown in Scheme 4.8.



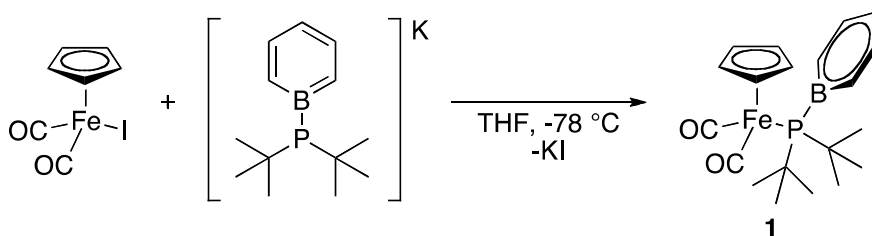
Scheme 4.8: Mechanism proposed by Wen et al for the formation of μ -oxo boratabenzene species (**XV**).⁷⁸

The formation of species **XV** is possible by the nucleophilic attack of the -OH substituent on boron of complex **XIV** to the electrophilic boron of a second molecule of the piano stool complex, elimination of a molecule of water results in the formation of the B-O-B bridge.

4.2 Synthesis and Characterization of CpFe(CO)₂(DTBB) (**1**)

In order to demonstrate that **DTBB** is indeed capable to bond to a metal centre through the lone pair on phosphorous without involving the π system, we decided to react **DTBB** ligand with CpFe(CO)₂I, a metal precursor well known to form sigma complexes by salt metathesis.

Indeed, a salt metathesis reaction between **DTBB** ligand and CpFe(CO)₂I in THF at -80 °C provided a deep red solution and upon filtration of the KI salts, yellow needle-like crystals of complex **1** were isolated (Scheme 4.9).



Scheme 4.9 : Synthesis of CpFe(CO)₂(DTBB) (**1**).

Complex **1** displays a **DTBB** ligand coordinated η^1 to Fe by the empty pair on phosphorous, as expected. Compared to previous work in our group⁵³ the ligand prefers this coordination mode rather than a π -coordination, since 2 electrons are needed to attain saturation on the coordination sphere of the 16-electron fragment [CpFe(CO)₂]⁺. At this point complex **1** is the first evidence of the very bulky **DTBB** ligand to coordinate η^1 , similarly to those examples reported by Fu.²³

Species **1** was fully characterized in solution by multinuclear NMR spectroscopy. ¹H NMR shows signals for the boratabenzene ring at δ = 7.15, 6.72, 6.27 for the *ortho*, *meta* and *para* boratabenzene protons respectively. These chemical shifts are consistent with a η^1 -coordinated boratabenzene ring such as CpZr(H)(DPB)(PMe₃) (**I**), Rh(PMe₃)₃(DPB) (**II**), CpFe(CO)₂(DPB) (**III**)²³ and (H)Pt(IMes)₂(C₅H₄(TMS)B-Cl) (**IV**) (Figure 4.1).⁴⁸

A singlet at 5.22 ppm, integrating for 5H, suggests the presence of a cyclopentadienyl ring coordinated to iron and a doublet at 1.49 ppm, integrating for 18H corresponds to the *t*Bu groups on **DTBB** coordinated to iron through the phosphine lone pair.

While related complex **XVI** shows a broad signal at 19.5 ppm by ^{31}P NMR spectroscopy, species **1** displays a resonance at 66.1 ppm. This chemical shift is similar to the complexes with phosphanyl borohydride ligands, which display phosphorous resonances at higher fields such as **XVII** (81.4 ppm),⁸⁰ and **XVIII** (31.5 ppm),⁸¹ while the phosphido-iron complex **XIX** shows a resonance at 8.3 ppm (Figure 4.2).⁸² It is however difficult to compare the electron donating properties based only on the phosphorous chemical shifts.

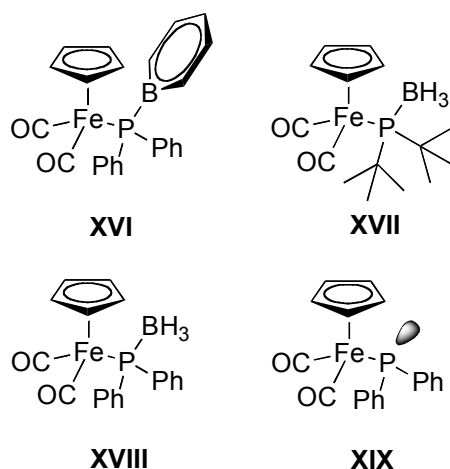


Figure 4.2: Iron carbonyl complexes similar to **1**, $\text{CpFe}(\text{CO})_2(\text{DPB})$ (**XVI**),²³ $\text{CpFe}(\text{CO})_2(\text{tBu}_2\text{P}\cdot\text{BH}_3)$ (**XVII**),⁸⁰ $\text{CpFe}(\text{CO})_2(\text{PhP}_2\text{P}\cdot\text{BH}_3)$ (**XVIII**),⁸¹ $\text{CpFe}(\text{CO})_2(\text{PPh}_2)$ (**XIX**).⁸²

The ^{11}B NMR of **XVI** shows a resonance at 32 ppm while complex **1** displays a broad multiplet at 29.1 ppm, however in the case of boratabenzene, the π delocalization of the ring is the main contribution to the electronic density on boron. This is further evidence of the covalent character of the P-B interaction and the phosphorous lone pair's engagement in the P-Fe bond rather than in π -bonding with boron.

The presence of the carbonyl ligands was confirmed by ^{13}C NMR, observed as a doublet at 215.6 ppm, the chemical shift is in accordance with metal coordinated CO ligands, such as in the related complex reported **XVI** by Fu (214.0 ppm)²³ and other phosphide complexes such as **XVII** (215.5 ppm),⁸⁰ **XVIII** (212.5 ppm)⁸¹ and **XIX** (216.4 ppm).⁸²

4.2.1 FT-IR, X-ray and Donating Capabilities of DTBB

The presence of CO ligands was further investigated by FT-IR spectroscopy. Complex **1** shows two stretching frequencies for the carbonyl ligands at 1966 and 2020 cm^{-1} , compared to the **DPB** that displays analogous frequencies at 1989 and 2035. This is evidence of **DTBB** greater electron richness when compared to the diphenyl analogue. Furthermore the **DTBB** ligand donating capabilities can be compared to similar cyclopentadienyl iron complexes (Table 4.1) bonding to ligands such as PPh_3 (2025, 2070 cm^{-1})⁸³ and PPh_2 (1966, 2015 cm^{-1}).⁸⁴ The C-O stretching frequencies can be related to the amount of back bonding and electronic surroundings of the metal. **DTBB** shows C-O stretchings at low frequencies, this implies that **DTBB** is indeed much more donating than the widely used PPh_3 and its donating capability resembles that of phosphide ligands. Nevertheless it should be considered that the latest species possess a second free electron pair available for donation to the metal centre.

Table 4.1: IR CO stretchings for complex **1** and other isoelectronic iron carbonyl complexes.

	$\nu(\text{CO})$ (cm^{-1})	Reference
$[\text{CpFe}(\text{CO})_2(\text{PPh}_3)]\text{Cl}\cdot 3\text{H}_2\text{O}$	2025, 2070 (Nujol)	83
$\text{CpFe}(\text{CO})_2(\text{PPh}_2)$	1966, 2015 (cyclohexane)	84
$\text{CpFe}(\text{CO})_2(\text{DPB})$	1982, 2024 (KBr) 1989, 2015 (CH_2Cl)	23
$\text{CpFe}(\text{CO})_2(\text{PtBu}_2\cdot\text{BH}_3)$	1982, 2029 (MeCN)	80
$\text{CpFe}(\text{CO})_2(\text{PPh}_2\cdot\text{BH}_3)$	1980, 2029 (toluene)	81
$\text{CpFe}(\text{CO})_2(\text{SiPh}_2\text{Me})$	1994, 1938 (MeCN)	80
$\text{CpFe}(\text{CO})_2(\text{DTBB})$	1966, 2020 (Nujol)	<i>This work</i>

Crystals of **1** suitable for X-ray diffraction studies were obtained upon cooling a THF solution of the complex at $-30\text{ }^\circ\text{C}$. It was shown to crystallize in a monoclinic $C2/c$ space group.

The P-B distance of 1.999(2) Å in complex **1** (Figure 4.3) suggests the presence of a covalent bond. Indeed, dative interactions between P-B have been observed to display long distances (2.15 Å)⁸⁵ while bonds ranging between 1.90 to 2.00 Å are representative of a rather long covalent bond, essentially an intermediate between a single and a double bond.⁸⁶ Also it is important to remark how the phosphorous atom does not engage in π donation with boron and rather forms a covalent bond. The reason is the poor overlapping between phosphorous orbitals and boron. Compared to other boratabenzenes species such as amido-boratabenzene, the overlapping between B-N orbital is more effective due to the nuclear size, both elements being in the second period, hence the interaction with phosphorous, a bigger nucleus, does not have a tendency to engage in π -donation with boron. Furthermore, the phosphine species are known to greatly prefer a sp^3 environment rather than a sp^2 .⁸⁷

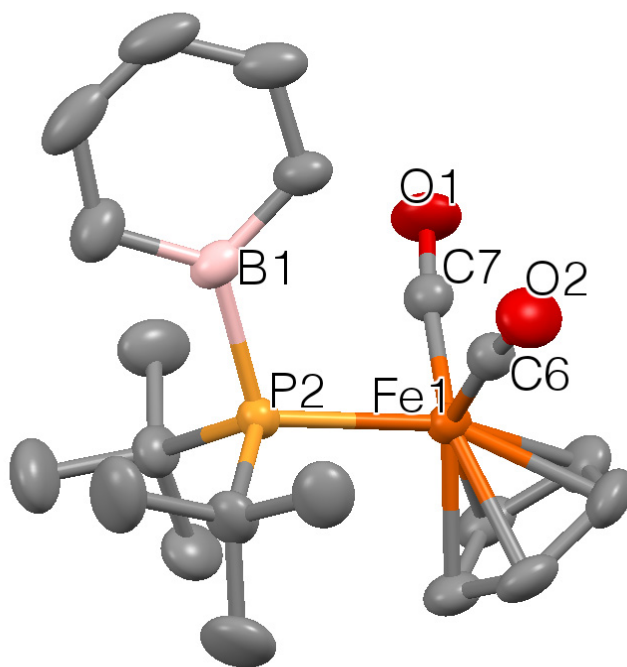


Figure 4.3: X-ray structure of **1**, thermal ellipsoids drawn at the 50% probability level ($R_1 = 3.16\%$). Hydrogen atoms are omitted for clarity. Selected bond distances (Å) and angles ($^\circ$): B1-P1 1.990(2); Fe1-P1 2.357(6); Fe1-C7 1.771(2); Fe1-C6 1.766(2); P1-C8 1.918(2); P1-C12 1.925(2); C7-O1 1.140(2); C6-O2 1.138(3); B1-P1-C12 105.4(1); B1-P1-C8 106.8(1); C8-P1-C12 110.3(1); Fe1-P1-C8 111.46(7); Fe1-P1-B1 110.55(7); Fe1-P1-C12 112.05(7); C6-Fe1-P1 90.35(7); C7-Fe1-P1 89.97(6).

Phosphido ligand **XVI** displays a P-B distance of 1.966(8) Å, only 0.03 Å shorter than the P-B distance on complex **1**. Additionally the length of the Fe-P bond in **1** is 2.357(6) Å, considerably longer than the one observed in **XVI** (2.267(2) Å), presumably an effect of the bulky *tert*-butyl groups. The angles between Fe-P-B and P-Fe-CO in **1** (110.5(7) and 90.3(7) Å respectively) are significantly smaller than in the analogues **XVI** and **XVII** (Figure 4.2), which sets in evidence the steric demands of the bulky *t*-butyl groups (Table 4.2).

Table 4.2: Selected structural parameters: P-B, Fe-P and P-Fe-CO angles and comparison of **1** with similar iron complexes CpFe(CO)₂(DPB) (**XVI**)²³ and CpFe(CO)₂(*t*Bu₂P•BH₃) (**XVII**).⁸²

Bond distances (Å) and angles (°)	XVI	1	XVII
P-B	1.966(8)	1.990(2)	1.964(3)
Fe-P	2.267(2)	2.357(6)	2.340(7)
Fe-P-B	115.3(3)	110.5(7)	108.4(2)
P-Fe-CO	95.4(3)	90.3(7)	89.7(8)

Point groups and R₁ values for complexes in the table can be seen in reference 88

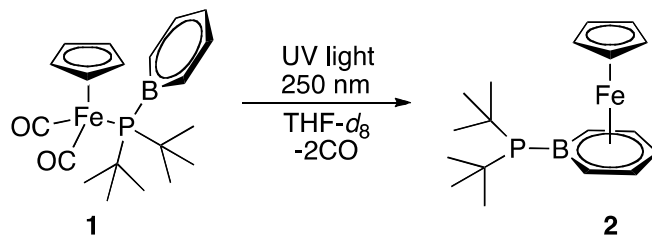
DTBB ligand was conceived as a very bulky and very electron rich ligand, since the *t*Bu groups have a much stronger inductive effect than the electron withdrawing phenyl rings, despite the elongated distance of P-Fe. The IR shifts of the CO stretchings along with the Fe-CO distances are a consequence of effective back-bonding between the [CpFe(**DTBB**)] fragment and the CO ligands. These results further confirm previous studies by B. Macha,⁵³ suggesting that **DTBB** is a ligand with exceptional donating capabilities.

To our delight, the hypothesis on what ligand **DTBB** was conceived proves true with the experimental results that successfully compare to those of the calculations reported by B. Macha and discussed in section 2.3.2.⁵³

4.3 CpFe(CO)₂DTBB (**1**) Photodissociation of CO Ligands

Whereas **1** proves to be stable at the solid state and in solution, when exposed to light, the deep red solution turns brown. It was possible to observe by ¹H NMR a borabenzene species attributed to decomposition. One of the possible features explaining the decomposition of species **1** is the photodissociation of the CO ligands.

In section 4.1.2 we presented an iron carbonyl complexes capable to dissociate CO upon exposure to UV light. Similarly when a deep red solution of **1** in THF-*d*₈ was exposed to short wave UV light (250 nm) inside an airtight J-Young quartz tube for 21 h, the solution changed from deep red to bright yellow. The photodissociation of the CO ligands was observed not only by the change in color but also by a shift in the proton resonances to generate a η⁶-di-*tert*-butylphosphidoboratabenzene species, where the phosphine substituent on boron remains pendant (Scheme 4.10).



Scheme 4.10: Photodissociation of CO ligands and change on coordination of DTBB ligand.

The cyclopentadienyl ligand is well known to be a good spectator ligand,³ because it is firmly bound to metals and apart from some exceptions is somehow inert to nucleophilic⁸⁹ and electrophilic attack.⁹⁰ Changes in the hapticity of this ligand had also been observed under certain electronic modifications in the coordination sphere⁹¹ and by photodissociation of ligands such as CO.⁹²

Furthermore, hapticity changes in 18 electron complexes can be facilitated by the presence of ligands such as cyclopentadienyl (Cp), which can change from η⁵- to η³- coordination, resulting in a reduction in the overall electron count by two units.⁹³

Upon photodissociation of two CO ligands from complex **1** it would be possible for the boratabenzene moiety to coordinate η^6 in order to stabilize the Fe(II) centre and generate species **2**. The passage from $\eta^1 - \eta^6$ demonstrates **DTBB**'s capability to act as a highly versatile ligand. Boratabenzene's hemilability makes it an exceptional ligand and it is precisely this behaviour that could lead to interesting reaction pathways.

Possible catalytic pathways involving the dissociation of CO to create an empty coordination site available for a substrate could be envisaged. Moreover compound **2** is the first ferrocenyl-type phosphido-boratabenzene ever made. Whether the phosphine remains donating or not and its possibility to serve as a ligand to other metals, is worth to be investigated.

4.3.1 Characterization of CpFe(DTBB) (**2**)

Figure 4.4 shows a comparison between species **1** before and after exposure to UV light, putting in evidence the appearance of species **2**. ^1H NMR aromatic resonances were observed at $\delta = 5.51, 5.42, 4.57$ for the *ortho*, *meta* and *para* boratabenzene protons, respectively. The Cp ligand is now observed at 4.30 ppm and the *t*Bu groups at 1.30 ppm. The dissociation of the CO ligands was further confirmed by the absence of the previously observed doublet at 215.6 ppm in ^{13}C NMR.

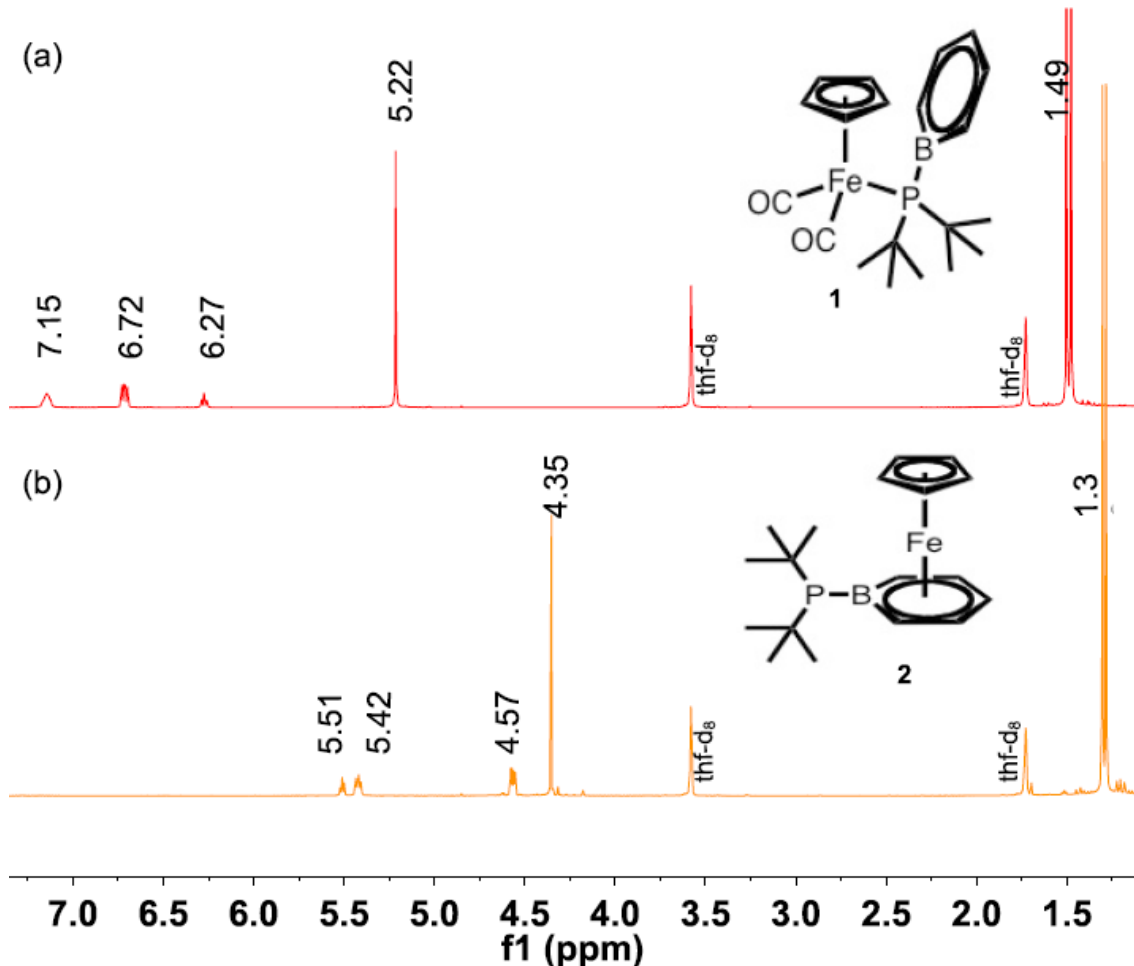


Figure 4.4: ^1H NMR (500 MHz, thf-d_8): comparison between η^1 (a) and η^6 (b) DTBB coordination to Fe.

The change in hapticity can also be observed by looking at the ^{31}P resonance of complex **2**, which displays a broad signal at 3 ppm assigned to a pendant phosphine; entirely different than that of the precursor **1**, where the phosphorous is directly bonded to iron (66.1 ppm). Such is the case of other pendant phosphines, which tend to display resonances more towards low frequencies, examples are: $[\text{Cp}^*\text{Ru}(\eta^6\text{-C}_6\text{H}_4(2\text{-Me})\text{P}(\text{C}_6\text{H}_4)_2)^+]$ (-36.7 ppm)⁹⁴ and Mo complex $\text{Mo}(\eta^6\text{-PhPMePh})(\text{PMePH}_2)_3$ (-31 ppm).⁹⁵

Ferrocenyl pendant phosphines such as those reported by Erker in 2014 (**XX**, Figure 4.5) having a tricoordinated, highly Lewis acidic, borane tethering a pendant phosphine with a P-B dative interaction, displays a ^{31}P resonance at 3.4 ppm.⁹⁶

In contrast, $\text{CpFe}(\text{Cp}(\text{P}t\text{Bu})_2)^{97}$ (**XXI**, Figure 4.5) shows a phosphorous resonance rather different (27.5 ppm) than the one observed for complex **2** (3 ppm).

Emslie and collaborators reported the ferrocenylphosphineborane FcPPB (**XXII**, Figure 4.5); this iron complex shares some structural similarities with species **2**. Interestingly the FcPPB has donating capabilities as a Z ligand and is considered to be a good electron donating ambiphilic ligand fragment.⁹⁸ FcPPB shows ^{31}P NMR shifts of 19.7 ppm, corresponding to the phosphorous atom featuring a P-B interaction and a ^{11}B resonance at 17 ppm. Complex **2** displays a ^{11}B signal at 20.8 ppm and phosphorous signal at 3 ppm, which appears to be at higher field than those observed for FcPPB.

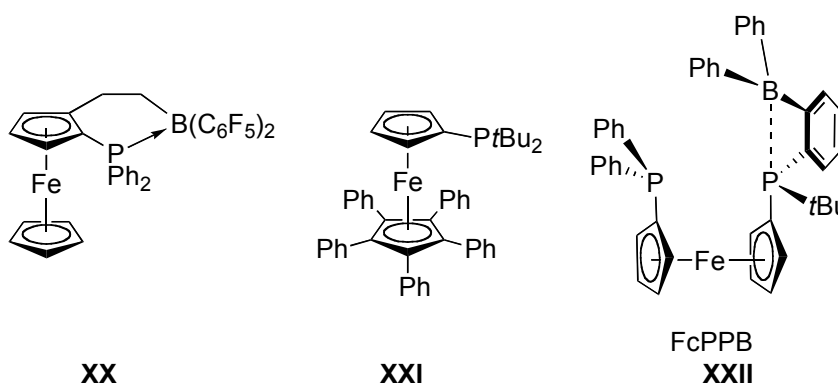


Figure 4.5: Other ferrocenylphosphines: **XX**,⁹⁶ $\text{CpFe}(\text{Cp}(\text{P}t\text{Bu})_2)$ (**XXI**),⁹⁷ FcPPB (**XXII**).⁹⁸

Thus pendant phosphine **2** can be considered as a new highly donating Fc-phosphido-boratabenzene ligand. This enhanced donating ability is related with the complexes high reactivity against moisture and oxygen, as will be discussed in the following sections.

Species **2** was further characterized by HR-MS using APPI ionization showing a mass corresponding to m/z : 343.15 $[\text{CpFe}(\text{C}_5\text{H}_4\text{B-P}t\text{Bu}_2)+\text{H}]^+$, the isotopic pattern corresponds to the calculated mass spectra (Figure 4.6).

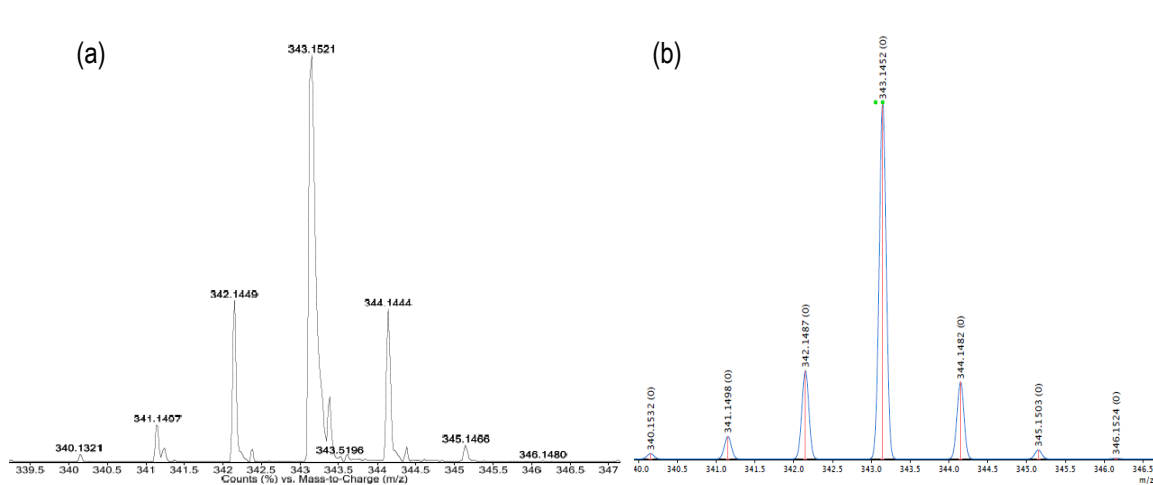
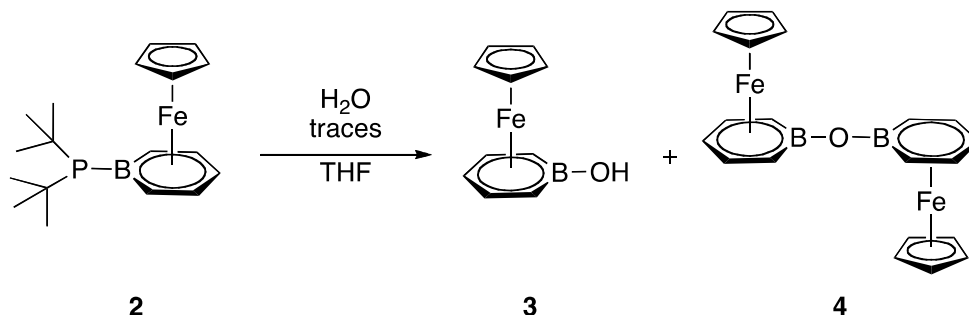


Figure 4.6: (a) HR-MSAPPI m/z : 343.15 [CpFeDTBB+H]⁺; (b) mMass⁶⁹ simulation m/z : 343.14 [CpFeDTBB+H]⁺.

Several attempts to recrystallize species **2** failed to afford suitable crystals for X-ray diffraction studies of complex **2**. In fact, species **2** proved to be extremely sensitive to hydrolysis and only degradation products were obtained.

4.4 Formation of CpFe(C₅H₅B-OH) (3) and CpFe(C₅H₅B)-O-(BC₅H₅)FeCp (4)

Pendant ferrocenyl-like phosphine **2**, appears to be extremely sensitive to traces of moisture, more so than other boratabenzene complexes (Section 4.1.3). All attempts to isolate species **2** in the solid state resulted in the formation of species **3** and **4** (Scheme 4.11), which were obtained from the mixture as crystalline needles.



Scheme 4.11: Synthesis of CpFe(C₅H₅B-OH) (**3**) and CpFe(C₅H₅B)-O-(BC₅H₅)FeCp (**4**) from exposure of CpFeDTBB (**2**) to traces of water.

Aromatic signals of **3** shift to a higher field, in accordance with the η^6 coordination⁵³ of boratabenzene ring δ 4.94 (*m*-H), 4.80 (*p*-H) and 3.79 (*o*-H), while the Cp ligand is observed as a singlet at 3.84 ppm. The phosphine appears to be no longer coordinated on boron, with only broad resonances observed around 1.36 and 0.92 ppm corresponding to *t*Bu₂PH along with other decomposition products. Because of *t*Bu₂PH low boiling point no ³¹P NMR resonance is observed upon evaporation of the solvent. The ¹¹B NMR shows a broad multiplet at 23.3 ppm.

Similarly species **4** was characterized in solution and chemical shifts are in accordance to those of **XV**. Species **4** displays typical chemical shifts of a η^6 -coordinated boratabenzene with proton signals at 5.14, 4.93 and 4.43 ppm, corresponding to both the boratabenzene rings coordinated on the iron centres. The two cyclopentadienyl ligands are observed as a singlet at 3.98 ppm. Despite the triple-decker conformation of species **4**, no fluxional behaviour is observed since signals resolve well at room temperature. ¹¹B NMR shows a broad singlet at 23.2 ppm.

Complex **3** and **4** were successfully characterized spectroscopically in solution by multinuclear NMR and further confirmed by HR-MS using APPI ionization: m/z : 214.02 [CpFe(C₅H₄B-OH)]⁺ and 410.09 [CpFe(C₅H₅B)-O-(BC₅H₅)FeCp]⁺.

Crystals of complexes **3** and **4** were obtained from solutions of **2** in benzene left for slow evaporation. Iron species **3** recrystallizes as red needles in a hexagonal crystal system of the space group *P*32. Interestingly, three independent molecules are found within the unit cell. Complex **4** crystalizes as red needles in a monoclinic crystal system belonging to the space group *P*2₁/*c*. Table 4.3 shows a comparison of **3** and **4** to similar complexes of Ru⁷⁸ and Co.⁷⁶

Table 4.3: Selected distances and angles, comparative of **3** and **4** with similar boratabenzene species.^{76,78}

Bond distances (Å) and angles (°)	3	XIV	4	XV	X
B-O	1.420(7)	1.383(4)	1.391(5)	1.378(6)	1.370(1)
M-B	2.278(9)	2.543(3)	2.288(5)	2.517(5)	2.280(1)
M-B-O	134.1(5)	141.5(2)	134.0(3)	135.9(3)	133.8(7)
M-C _{ortho}	2.148(8)	2.306(3)	2.125(5)	2.289(4)	2.109(8)
	2.157(6)	2.278(3)	2.140(9)	2.331(4)	2.140(1)
B-O-B	-	-	133.0(4)	130.9(4)	131.1(8)

Point groups and R₁ values for complexes in the table can be seen in reference 99

The B-O distance of **3** (1.420(7) Å) (Figure 4.7) and **4** (1.391(5) Å) (Figure 4.8) are well in accordance to what is observed for similar species such as the ruthenium (**XIV**) (1.383(4) Å), (**XV**) (1.378(6) Å) and cobalt species (**X**) (1.370(1) Å) (Table 4.3). Furthermore, these distances are representative of π-donation from the heteroatom substituent on boron, as it has been observed in boratabenzene species with a B-N interaction where the π-bonding becomes evident as the distances shorten and resemble those of a double bond.^{50,55e} Moreover the B-O distances of **3** is in the range observed for other boron compounds with B=O bonds, such as the gaseous B₂O₃ molecule where the distances range from 1.21 to

1.55 Å.¹⁰⁰ This suggests that the oxygen atom in **3** is engaging in a double bond with boron.

It is important to note that both B-O distances in complex **4** vary by only 0.01 Å and these distances are shorter than the B-O distance observed on species **3**. Additionally the B-O distances in **4** are also within the range of B=O double bonds, as mentioned above. This would suggest that the two free electronic pairs from the μ -O bridge in complex **4** are engaging in π donation with each of the boron centres, however the B-O-B angle of 133.0(4)° rather than the 180° angle expected for a linear B=O=B interaction, suggest that the central oxygen might not engage both electron pairs in a π interaction with boron.

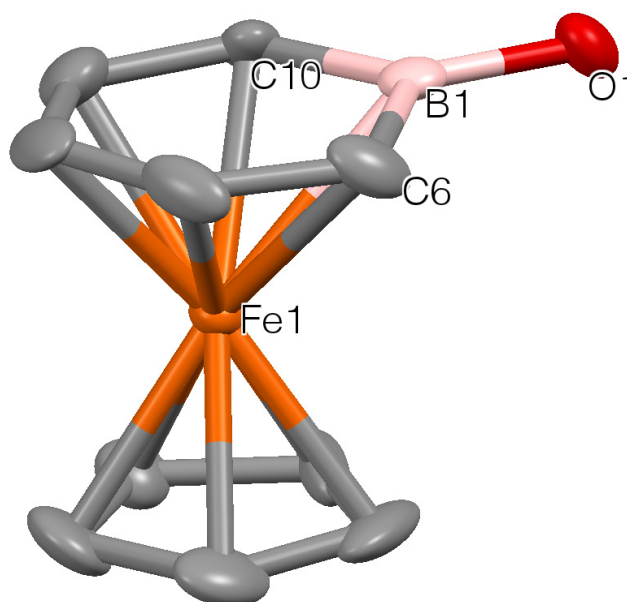


Figure 4.7: X-ray structure of **3**, thermal ellipsoids drawn at the 50% probability level ($R_1 = 3.28\%$). Hydrogen atoms are omitted for clarity. Three molecules are present in the unit cell; values are given for only one of them. Selected bond distances (Å) and angles (°): B1-O1 1.420(7); B1-Fe1 2.278(9); C6-Fe1 2.144(8); C7-Fe1 2.07(1); C8-Fe1 2.041(7); C9-Fe1 2.066(7); C10-Fe1 2.157(6); O1-B1-Fe1 134.1(5), C10-B1-O1 119.0(6); C6-B1-O1 126.2(6); C10-B1-C6 114.5(6).

Metal-boron distances often vary with the size of the substituent on boron and elongated M-B distances and angles are indicative of a certain lability of the bond. Large M-B distances have also been observed when the substituent on boron is very bulky; such is the case of the $[\text{Fe}(\text{C}_5\text{H}_5\text{B-Mes})_2]$ iron sandwich reported by our

group (Section 2.2.2), with a Fe-B distance of 2.395(2) Å and an Fe-B-C_{Mes} of 141.0(1) and 149.9(1)°.⁴⁴

The Fe-B distance observed in **3** (2.278(9) Å) is shorter than the Ru-B (2.543(3) Å) distance of the piano stool complex **XIV** (Table 4.3). Similarly the Fe-B-O angle in **3** (134.1(5)°) is shorter than the Ru-B-O in species **XIV** (141.5(2)°). The elongated distances and angle suggest a combination of the electronic and steric effects of the phosphine ligands in the ruthenium⁷⁸ (**XIV**) as well as in the aforementioned iron sandwich [Fe(C₅H₅B-Mes)₂].⁴⁴ In exchange the highly donating Cp ligand in **3** appears to favour a stronger interaction between the [CpFe] fragment and the [C₅H₅B-OH] ligand. A similar situation is observed for **4** (Figure 4.8), which shows shorter Fe-B (2.288(5) Å) distance and Fe-B-O angle (134.0(3)°) than the ruthenium species (**XV**) (2.517(5) Å; 135.9(3)°). However **4** shows a slightly longer distance Fe-B and Fe-B-O angle than the cobaltocene complex **X** (Co-B = 2.280(1) Å; Co-B-O = 133.8(7)°).

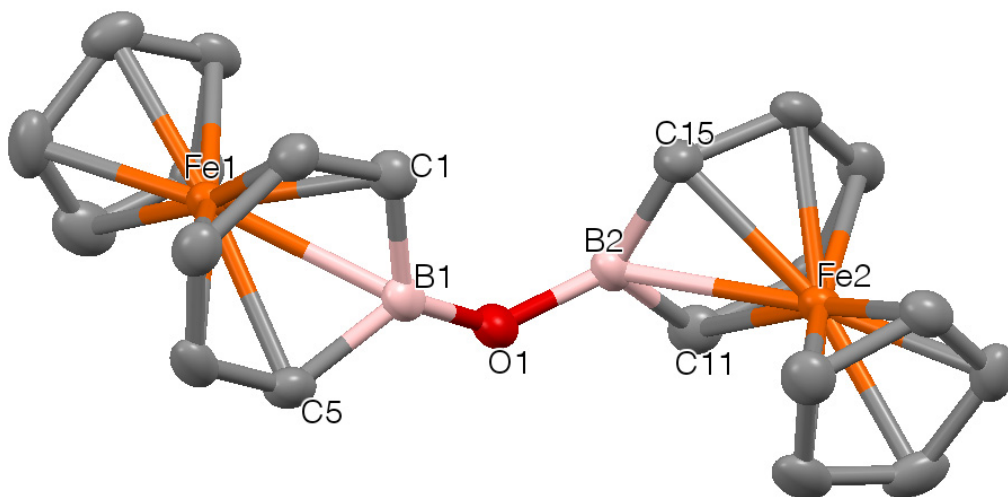


Figure 4.8: X-ray structure of **4**, thermal ellipsoids drawn at the 50% probability level ($R_1 = 4.67\%$). Hydrogen atoms are omitted for clarity. Selected bond distances (Å) and angles (°): B1-O1 1.391(5); B2-O1 1.402(6); Fe1-B1 2.288(5); Fe2-B2 2.307(5); Fe1-C1 2.125(5); Fe2-C15 2.127(4); Fe1-C5 2.140(4); Fe2-C11 2.139(5); B1-O1-B2 133.0(4); Fe1-B1-O1 134.1(3); Fe2-B2-O1 134.0(3); C1-B1-O1 126.1(4); C15-B1-O1 127.1(4); C1-B1-C5 113.1(4); C15-B2-C11 112.3(4).

Complex **3** has Fe-C_{ortho} distances (Fe1-C6 2.144(8) and Fe1-C10 2.157(6) Å) shorter than those observed for the ruthenium species **XIV** (2.306(3) and 2.278(3) Å). Likewise the Fe-C_{ortho} distances on **4** (Fe1-C1 2.125(5) and Fe1-C5 2.140(4) Å)

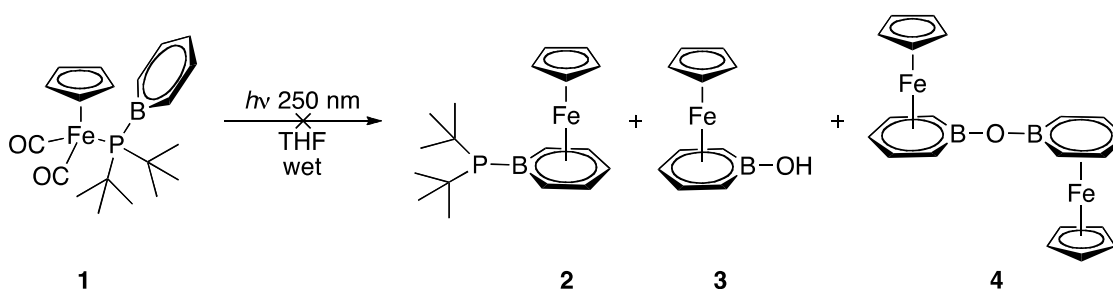
are shorter than those observed for the ruthenium complex **XV** (2.289(4) and 2.331(4) Å) but somehow comparable with the cobalt species **X** (2.140(1) and 2.109(8) Å) (Table 4.3). The elongated distances on one of the ortho carbon of each species described above are suggestive of a coordination mode closer to the η^5 than a η^6 . Furthermore the repulsion of the localized electronic density on one of the ortho carbons of boratabenzene can be observed by the torsion angles described by the atoms C1-B1-O1-B2 and B1-O1-B2-C15 in species **4**. The ortho carbons C1 and C15, where a partial negative charge would allocate, are further apart from the metal, in order to diminish the repulsive interaction between them. This is also observed on the structure of the cobalt complex **X** but that is not the case for the ruthenium species **XV**. This structural interaction also influences the V-shape angle of the B-O-B bonds in complex **4** (133.0(4)°), which is larger than the angle observed for the cobalt (131.1(8) °) and ruthenium (130.9(4) °) species and other boron compounds like B₂O₃ (132°).¹⁰⁰

4.5 Reactivity of CpFe(DTBB) (2)

In order to investigate the availability of electronic density on the pendant phosphine **2** and furthermore its reactivity, several reactions were undertaken.

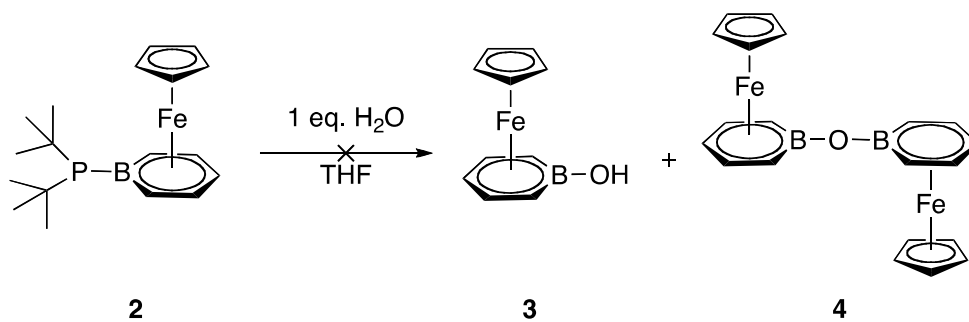
4.5.1 Reactivity of **2** with H₂O

Synthesis was attempted by dissolving CpFe(CO)₂DTBB (**1**) in wet THF, outside of the glove box on a bench top. The solution was placed in a septum-sealed Quartz UV cell and exposed to UV light for 18h. The reaction did not yield the expected product **2**, **3** or species **4** (Scheme 4.12). Instead several unidentified signals are observed as well as numerous signals in the aliphatic region. The ³¹P shows two main peaks at 103.7 and 63.5 ppm, assigned to phosphine oxides.



Scheme 4.12: Attempted synthesis of iron species **2**, **3** and **4** from the photodissociation of CO ligand in **1** using wet THF on a bench-top.

Contrary to what Wen *et al* reported for their ruthenium complexes,⁷⁸ iron boratabenzene complex **2** does not result into formation of **3**, nor **4**, when equimolar amounts or excess of H₂O were added (Scheme 4.13). Indeed, all the boratabenzene signals disappear in the proton NMR and only a broad peak at 3.91 ppm is observed (Figure 4.9). ³¹P NMR of the aforementioned mixture only shows a signal corresponding to *t*Bu₂PH. A similar behaviour has been observed for [(C₆Me₆)-Fe(C₅H₅B-OH)], for which only broad signals for the (C₆Me₆) ligand are observed by proton NMR as a result of a rapid proton relaxation.¹⁰¹ However increasing the relaxation time during the acquisition of the ¹H NMR did not help to resolve the spectrum. Addition of an excess of water yielded the same results.



Scheme 4.13: Attempted synthesis of iron complexes 3 and 4 by adding equimolar amounts of water to the pendant phosphine complex 2.

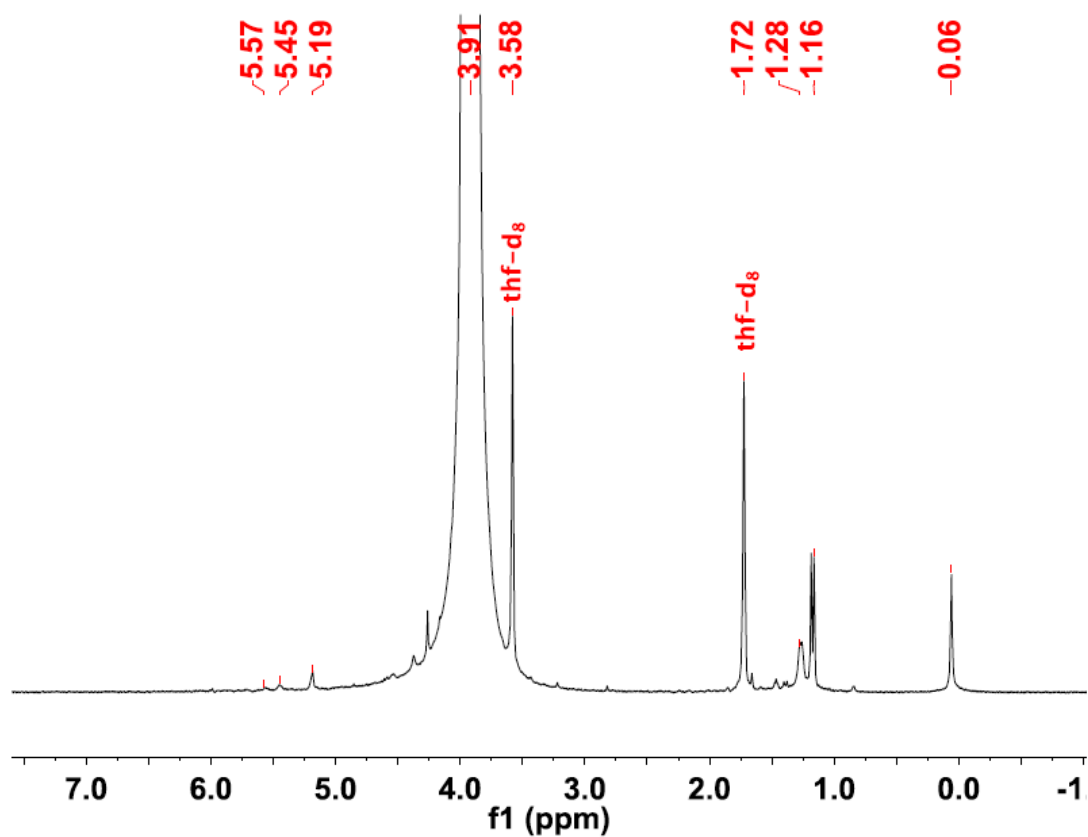
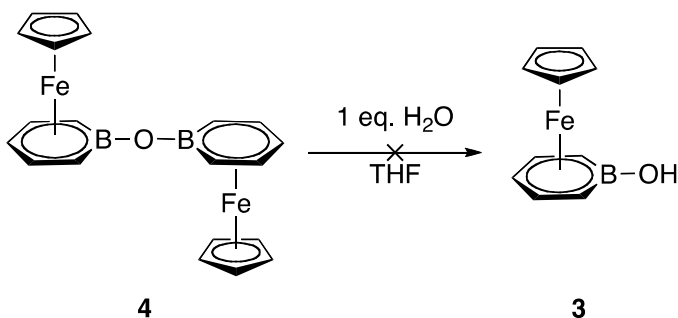


Figure 4.9 : ¹H NMR (thf-d₈, 500 MHz): reaction mixture of 2 and an equimolar amount of water.

Attempts to hydrolyze the B-O-B bridge in complex **4** to obtain the B-OH species **3** by adding water, resulted in the same broad signals as mentioned above.



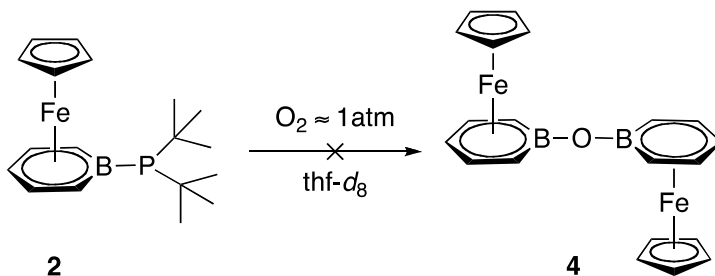
Scheme 4.14: Attempt to hydrolyze the B-O-B bridge on complex **4** to obtain complex **3**.

Upon exposure to water, boratabenzene ligand in complex **2** could undergo decomposition.^{102,103} Isolating crystals from the sample exposed to water would help to identify the decomposition products. Unfortunately recrystallization attempts did not yield good quality crystals.

4.5.2 Reactivity of **2** with O₂

In Section 4.1.3 a cobalt boratabenzene complex with a μ -oxo interaction reported by Herberich was described. The cobalt species was reported to be the result of the exposure of the parent species to traces of oxygen. Based on these precedents we decided to explore the reactivity of species **2** with oxygen.

A degassed solution of **2** was exposed to an excess of O₂ (≈ 1 atm) (Scheme 4.15) simply by exchanging the nitrogen atmosphere by oxygen. As expected, the formation of species **4** was not observed. In fact, two sets of aromatic peaks for unidentified borabenzene species were observed.



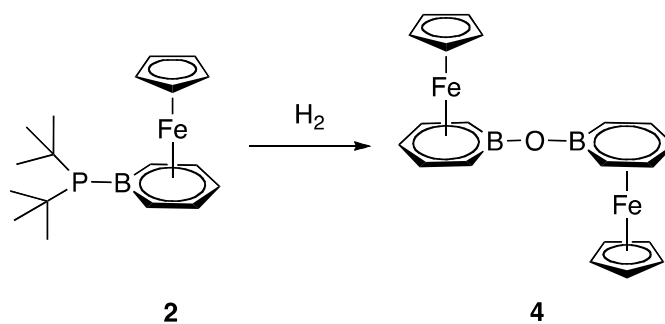
Scheme 4.15: Attempt to synthesize **4** from reaction of **2** with an excess of oxygen.

^{31}P NMR of the reaction mixture shows a slightly broad signal at 63.5 ppm, this chemical shift correlates to that of phosphine oxide $t\text{Bu}_2\text{P}(\text{H})\text{O}$.¹⁰⁴ Comparing the chemical shifts with species **3** and **4**, the observed products of the reaction with oxygen are nothing similar. This result confirms that species **3** and **4** are indeed products obtained from the hydrolysis of species **2**, rather than the product of an oxidation reaction.

4.5.3 Reactivity with H_2

Because the precious and expensive metals of the groups 9 and 10 mainly dominate hydrogenation chemistry, an alternative to hydrogenation catalyst using inexpensive; earth abundant metals such as iron motivated us to explore the reactivity of **2** with hydrogen.

Upon reaction of a benzene- d_6 solution of **2** with ≈ 1 atm of H_2 (Scheme 4.16), a mixture of unreacted species **2** along with signals corresponding to the μ -oxo boratabenzene **4** are observed. Species **4** possibly formed due to contamination of H_2O in the hydrogen gas used. Additionally signals corresponding to $t\text{Bu}_2\text{PH}$ were observed (m, 3.57 ppm, PH; d, 1.40 ppm, $t\text{Bu}_2$). On the ^{31}P NMR, a signal corresponding to **2** (1.0 ppm) is still observed along with a sharp peak at 19.4 ppm assigned to $t\text{Bu}_2\text{PH}$. Recrystallization attempts of the mixture yielded only species **4**.



Scheme 4.16: Formation of species **4** from the reaction of **2** with H_2 .

4.6 A Word on Borabenzene Decomposition Pathways

In order to properly assess the challenges of studying boratabenzene complexes, coordination modes and reactivity, we must explore all different outcomes. Decomposition, the less desired outcome is always a great risk in boratabenzene chemistry. To undertake the endeavour of understanding how boratabenzene behaves, we must learn about its decomposition pathways.^{102,103}

In this chapter we have studied iron complexes sensitivity to moisture and oxygen, observed and characterized some of the products of these reactions. But such reactivity depends not only on the Lewis base on boron but on the [M-L] system on which the boratabenzene ligand is supported.

Despite its Lewis acidity, when the boron centre is sterically protected as it has been shown by our group on a $\text{Fe}(\text{C}_5\text{H}_5\text{B-Mes})_2$ (Mes = Mesityl) sandwich, the exchange of the substituent on boron in the presence of water does not occur.⁴⁴ Likewise a chromium bimetallic triple-decker complex of chloro-boratabenzene has been shown to be air stable in solid state,⁴³ which is further evidence on how stability is modulated by the ligand-metal system.

Complex **1** is as well an air and moisture stable metal complex and it should be noted that in the case of species **1** the lone pair on phosphorous is engaged in a bond with iron. Upon formation of the pendant phosphine **2** the lone pair becomes available and highly nucleophilic. The nucleophilicity of the phosphido fragment favours the proton abstraction from water, originating a $[\text{CpFe}(\text{C}_5\text{H}_5\text{B-P}(\text{H})\text{tBu}_2)]^+$ cationic adduct. The bulky tBu_2PH , now engaged in a dative bond with boron, is prone to act as a leaving group while the boron undergoes a nucleophilic attack by an OH^- . This behaviour leads to the formation of species **3** and **4**.

Interestingly any other **DTBB** metal complexes with metals from the group 9 to 11, presented in upcoming chapters (Chapters 5 and 6), have shown to exchange the base on boron by exposure to similar conditions. Thus the presence of the Cp ligand and the availability of the lone pair on phosphorous seem to play a role into this reactivity.

It is important to note that, during the course of this work, several unidentified decomposition products have been observed, but because boratabenzene can decompose in such intricate pathways, it becomes interesting to keep track and study the decomposition products. Such has been the case of species **3** and **4** in this chapter.

4.7 Conclusion

In this chapter we have shown the first example of a **DTBB** coordinated to a metal centre through the lone pair on phosphorus, a η^1 boratabenzene ligand. Hence complex **1** is now another example of the very few unusual coordination modes of boratabenzene.

We have been able to demonstrate **DTBB** greater donating capability, compared to other good donor ligands and furthermore we have shown **DTBB**'s flexibility as an hemilabile ligand, which opens up a series of opportunities and pathways that could lead to interesting and useful reactivity in catalysis.

In summary a family of entirely new iron complexes of boratabenzene have been characterized by spectroscopy and X-ray diffraction and some of their properties have been investigated.

4.8 Experimental Details

General Procedures

All manipulations were carried out under inert atmosphere, unless otherwise is specified, using standard Schlenk techniques and inert atmosphere glovebox.

Solvents were distilled under N₂ atmosphere over sodium/benzophenone (THF) or stirred over Na/K amalgam and vacuum-transferred (benzene-*d*₆), thf-*d*₈ was pre-dried with CaCl₂, degassed using three cycles of freeze-pump-thaw, dried and stored under activated 5 Å molecular sieves. Water used in reactions under inert atmosphere was degassed by three cycles of freeze-pump-thaw prior to bubbling of N₂ for 30 min inside a Schlenk round bottom flask. The volume needed was withdrawn using a purged stainless steel needle and a syringe.

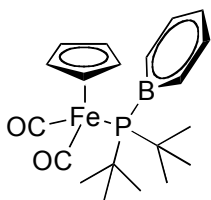
The CpFe(CO)₂I was obtained from Sigma Aldrich and used as received. H₂ gas UHP 5.0 and O₂ gases were purchased from Praxair. The potassium di-*tert*-butylphosphidoboratabenzene (**DTBB**) was prepared following the reported procedure.⁵³

Multinuclear NMR spectra were recorded in sealed J.-Young NMR tubes on an Agilent Technologies NMR spectrometer, ¹H NMR (500 MHz), ¹³C NMR (125.721 MHz), ³¹P NMR (202.404 MHz), ¹¹B NMR (160.419 MHz). NMR correlation experiments *g*HSQCAD and *g*COSY were used to elucidate ¹³C-¹H, ¹H-¹H correlations. Chemical shifts are quoted in ppm relative to external SiMe₄ (¹H, ¹³C), H₃PO₄ (³¹P), BF₃•Et₂O (¹¹B) references with n-bond *J* couplings being quoted in Hz. NMR signals are referred as (s) singlet, (d) doublet, (t) triplet, (m) multiplet, (dd) double of doublets, etc. It should be noted that due to 3/2 spin of NMR active ¹¹B, the resulting spectra are naturally broad. In addition, spectra of ³¹P nuclei bonded to ¹¹B also experience quadrupolar broadening of their signals, which can often cause imprecise coupling values. Spectroscopic data for **DTBB** can be found in the literature.⁵³

Elemental Analysis was carried at the “Laboratoire de Chimie Analytique” at Université Laval. HR-MS spectra were recorded with an Agilent Technologies 6210 LC Time of Flight Mass Spectrometer. Spectra were obtained by direct injection

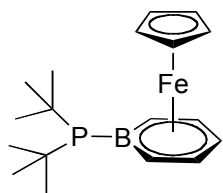
into the nebulizer of solutions of the corresponding species using ESI-MS or APPI-MS ionization in positive and negative modes. FT-IR spectra were obtained with a Nicolet Bomem Magna-850; solid was suspended in Nujol previously degassed by bubbling N₂ and the samples were prepared inside an inert atmosphere glovebox.

CpFe(CO)₂(DTBB) (1)



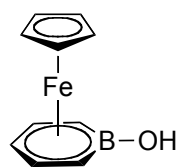
In a 15 mL Schlenk tube equipped with a magnetic stirrer, **DTBB** ligand (0.053 g, 0.202 mmol) was dissolved in 5.0 mL of THF. This yellow solution was added dropwise over 5 min to a previously cooled -78 °C dark solution of CpFe(CO)₂I (0.049 g, 0.202 mmol) dissolved in 2.0 mL of THF. Reaction mixture became red with the presence of a white precipitate. The solution was left to warm up to room temperature and stirring overnight. The reaction mixture was then filtered through cannula, the remaining red solution was kept in a Schlenk tube at -30 °C for 4 days. Yellow crystals like needles were isolated and dried under vacuum. Yield = 0.040 g, 60%. **¹H NMR** (500 MHz, thf-*d*₈): δ 7.15 (brm, 2H, *m*-C₅H₄B-*PtBu*₂), 6.72 (dd, *J* = 9.7, 6.0 Hz, 2H, *o*-C₅H₄B-*PtBu*₂), 6.27 (t, *J* = 7.1 Hz, 1H, *p*-C₅H₄B-*PtBu*₂), 5.22 (s, 5H, Cp), 1.49 (d, *J* = 13.5 Hz, 18H, C₅H₄B-*PtBu*₂). **¹³C NMR** (125.72 MHz, benzene-*d*₆): δ 215.6 (d, 2C, CO), 133.0 (d, *J* = 14.1 Hz, 2C, *m*-C₅H₄B-*PtBu*₂), 116.9 (brs, 1C, *p*-C₅H₄B-*PtBu*₂), 87.8 (s, 5C, Cp), 38.7 (d, *J* = 11.5 Hz, 2C, CH *tBu*₂), 32.8 (d, *J* = 2.2 Hz, 6C, CH₃ *tBu*₂). **³¹P NMR** (202.40 MHz, thf-*d*₈): δ 66.5 (brm, CpFe(CO)₂(DTPBB)). **¹¹B NMR** (160.41 MHz, thf-*d*₈): δ 30.4 (brm, CpFe(CO)₂(DTPBB)). **EA:** Exp. = %C = 59.81; %H = 7.03; Calc. = %C = 60.35; %H = 7.09. **FT-IR:** (cm⁻¹) 2920, 2852, 2021, 1966, 1943.

CpFeDTPBB (2)



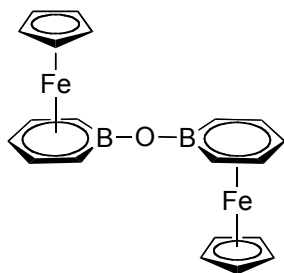
Inside a quartz J. Young NMR tube, **1** (8.0 mg, 0.020 mmol), yellow powder, was dissolved in 1.0 mL of THF. The deep red solution was then exposed to UV light (254 nm) for 24 h. The resulting yellow solution was evaporated under vacuum inside the tube. The red solid obtained was then re-dissolved in benzene- d_6 for characterization. Yield by NMR 100 %. Attempts to isolate and recrystallize compound **2** resulted in the formation of hydrolysis and oxidation products **3** and **4**. **^1H NMR** (500 MHz, thf- d_8): δ 5.51 (t, $J = 5.6$ Hz, 1H, $p\text{-C}_5\text{H}_4\text{B-PtBu}_2$), 5.42 (t, $J = 6.0, 8.1$ Hz, 2H, $m\text{-C}_5\text{H}_4\text{B-PtBu}_2$), 4.57 (dd, $J = 8.6, 4.0$ Hz, 2H, $o\text{-C}_5\text{H}_4\text{B-PtBu}_2$), 4.35 (s, Cp, 5H), 1.30 (d, $J = 10.0$ Hz, 18H, $\text{C}_5\text{H}_4\text{B-PtBu}_2$). **^{13}C NMR** (125.72 MHz, thf- d_8): δ 90.6 (d, $J = 7.0$ Hz, $m\text{-C}_5\text{H}_4\text{B-PtBu}_2$), 83.9 (observed by $g\text{HSQCAD}$, $o\text{-C}_5\text{H}_4\text{B-PtBu}_2$), 79.5 ($p\text{-C}_5\text{H}_4\text{B-PtBu}_2$), 72.2 (Cp), 33.6 (CH_3 on PtBu_2), 33.9 (C on PtBu_2). **^{31}P NMR** (202.40 MHz, thf- d_8): δ 3.0 (brm, $\text{CpFe}(\text{C}_5\text{H}_4\text{B-PtBu}_2)$). **^{11}B NMR** (160.41 MHz, thf- d_8): δ 20.8 (brm, $\text{CpFe}(\text{C}_5\text{H}_4\text{B-PtBu}_2)$). **HR-MS** (APPI): $m/z = 343.15$ [$\text{CpFe}(\text{C}_5\text{H}_4\text{B-PtBu}_2)$] $^+$.

CpFeC₅H₄B-OH (3)



^1H NMR (500 MHz, benzene- d_6): δ 4.94 (dd, $J = 7.6, 5.8$ Hz, 2H, $m\text{-C}_5\text{H}_4\text{B-OH}$), 4.80 (t, $J = 5.5$ Hz, 1H, $p\text{-C}_5\text{H}_4\text{B-OH}$), 3.84 (s, 5H, Cp), 3.79 (d, $J = 8.7$ Hz, 2H, $o\text{-C}_5\text{H}_4\text{B-OH}$), 2.37 (brs, 1H, B-OH). **^{13}C NMR** (125.72 MHz, thf- d_8): δ 90.9 (s, 2C, $m\text{-C}_5\text{H}_4\text{B-OH}$), 75.1 (s, 1C, $p\text{-C}_5\text{H}_4\text{B-OH}$), 70.4 (s, 5C, Cp), 68.4 ($o\text{-C}_5\text{H}_4\text{B-OH}$ found by HSQCAD). **^{11}B NMR** (160.41 MHz, benzene- d_6): δ 23.3 (brm, $\text{CpFe}(\text{C}_5\text{H}_4\text{B-OH})$). **HR-MS** (APPI): $m/z = 214.02$ [$\text{CpFe}(\text{C}_5\text{H}_4\text{B-OH})$] $^+$.

CpFe(C₅H₅B)-O-(BC₅H₅)FeCp (4)



¹H NMR (500 MHz, benzene-*d*₆): δ 5.13 (dd, *J* = 9.2, 5.5 Hz, 4H, *m*-C₅H₄B-O-BC₅H₄), 4.93 (dd, *J* = 5.5 Hz, 2H, *p*-C₅H₄B-O-BC₅H₄), 4.43 (d, *J* = 9.2 Hz, 4H, *o*-C₅H₄B-O-BC₅H₄), 3.98 (s, 10H, Cp). **¹³C NMR** (125.72 MHz, benzene-*d*₆): δ 91.4 (s, 4C, *m*-C₅H₄B-O-BC₅H₄), 75.3 (s, 2C, *p*-C₅H₄B-O-BC₅H₄), 72.2 (*o*-C₅H₄B-O-BC₅H₄ found by *g*HSCAD), 70.4 (s, 10C, Cp). **¹¹B NMR** (160.41 MHz, benzene-*d*₆): δ 23.2 (brm, CpFe(C₅H₄B-OH)). **HR-MS** (APPI): *m/z* = 410.09 [CpFe(C₅H₄B-O-BC₅H₄)]⁺.

X-Ray Crystallography Data

Crystals of compounds **1** and **3** were mounted on a glass fibre using Paratone N® hydrocarbon oil. Measurements were made on a Bruker APEX II area detector diffractometer equipped with graphite monochromated MoK α radiation. The program used for retrieving cell parameters and data collection was APEX 2.¹⁰⁵ Data were integrated using the program SAINT,¹⁰⁶ and corrected for Lorentz and polarization effects. The structure was solved and refined using SHELXS-97.¹⁰⁷ All non-H atoms were refined anisotropically. The hydrogen atoms were placed at idealized positions.

Measurements for crystals of compound **4** were made on a Bruker Venture Metal-jet diffractometer equipped with a molten GaK α anode radiation source. The program used for retrieving cell parameters and data collection was Olex2,¹⁰⁸ the structure was solved with the XT¹⁰⁹ structure solution program using Direct Methods and refined with the XL¹⁰⁹ refinement package using Least Squares minimisation.

Crystal data and structure refinement for [CpFe(CO)₂(DTBB)] (1)

Empirical formula	C ₂₀ H ₂₈ BPO ₂ Fe
Formula weight	398.05
Temperature	296(2) K
Wavelength	0.71073 Å
Crystal system	Monoclinic
Space group	C 2/c
Unit cell dimensions	a = 28.7228(16) Å α = 90° b = 8.2578(4) Å β = 94.1940(10)° c = 16.7830(9) Å γ = 90°
Volume	3970.1(4) Å ³
Z	8
Density (calculated)	1.332 mg/m ³
Absorption coefficient	0.850 mm ⁻¹
F(000)	1680
Crystal size	0.28 x 0.04 x 0.02 mm ³
Theta range for data collection	1.42 to 26.37°
Index ranges	-35 ≤ h ≤ 35, -10 ≤ k ≤ 10, -20 ≤ l ≤ 20
Reflections collected	18037
Independent reflections	4071 [R(int) = 0.0374]
Completeness to theta = 25.242°	100.0 %
Absorption correction	Semi-empirical from equivalents
Max. and min. transmission	0.9832 and 0.7967
Refinement method	Full-matrix least-squares on F ²
Data / restraints / parameters	4071 / 0 / 232
Goodness-of-fit on F ²	1.005
Final R indices [I > 2σ(I)]	R1 = 0.0316, wR2 = 0.0739
R indices (all data)	R1 = 0.0448, wR2 = 0.0802
Largest diff. peak and hole	0.372 and -0.174 e.Å ⁻³

Crystal data and structure refinement for [CpFe(C₅H₅B-OH)] (3)

Empirical formula	C ₁₀ H ₁₁ BOFe	
Formula weight	213.85	
Temperature	150(2) K	
Wavelength	0.71073 Å	
Crystal system	Hexagonal	
Space group	P32	
Unit cell dimensions	a = 19.689(3) Å	α = 90°
	b = 19.689(3) Å	β = 90°
	c = 6.1836(9) Å	γ = 90°
Volume	2076.0(5) Å ³	
Z	9	
Density (calculated)	1.539 mg/m ³	
Absorption coefficient	1.583 mm ⁻¹	
F(000)	990	
Crystal size	0.320 x 0.08 x 0.08 mm ³	
Theta range for data collection	1.19 to 28.31°	
Index ranges	-26 ≤ h ≤ 26, -26 ≤ k ≤ 26, -8 ≤ l ≤ 8	
Reflections collected	22033	
Independent reflections	6875 [R(int) = 0.0362]	
Completeness to theta = 25.242°	100.0 %	
Absorption correction	Semi-empirical from equivalents	
Max. and min. transmission	0.881 and 0.859	
Refinement method	Full-matrix least-squares on F ²	
Data / restraints / parameters	6875 / 2 / 347	
Goodness-of-fit on F ²	1.044	
Final R indices [I > 2σ(I)]	R1 = 0.0328, wR2 = 0.0681	
R indices (all data)	R1 = 0.0366, wR2 = 0.0697	
Largest diff. peak and hole	0.619 and -0.262 e.Å ⁻³	

Crystal data and structure refinement for [Cp₂Fe₂(μ-oxo-C₅H₅B-O)] (4)

Empirical formula	C ₂₀ H ₂₀ B ₂ OFe ₂	
Formula weight	409.68	
Temperature	100 K	
Wavelength	1.34139 Å (GaKα)	
Crystal system	Monoclinic	
Space group	P2 ₁ /c	
Unit cell dimensions	a = 7.5971(5) Å	α = 90°
	b = 10.6406(5) Å	β = 93.827(3)°
	c = 20.6497(12) Å	γ = 90°
Volume	1665.55(17) Å ³	
Z	4	
Density (calculated)	1.634 mg/m ³	
Absorption coefficient	9.409 mm ⁻¹	
F(000)	840.0	
Crystal size	0.094 x 0.077 x 0.031 mm ³	
Theta range for data collection	7.466 to 109.958°	
Index ranges	-9 ≤ h ≤ 9, 0 ≤ k ≤ 12, 0 ≤ l ≤ 25	
Reflections collected	3160	
Independent reflections	3160 [R(int) = 0.0778]	
Data / restraints / parameters	3160 / 0 / 227	
Goodness-of-fit on F ²	1.099	
Final R indices [I > 2σ(I)]	R1 = 0.0467, wR2 = 0.1281	
R indices (all data)	R1 = 0.0516, wR2 = 0.1313	
Largest diff. peak and hole	0.54 and -0.47 e.Å ⁻³	

5 Chapter 5 Copper Boratabenzene Complexes

In this chapter the first examples, to the best of our knowledge, of boratabenzene ligand coordinated to group 11 metals are presented.

5.1 Introduction

Boratabenzene derivatives have been coordinated to most transition metals. The only metals that are not known to coordinate this heterocyclic ligand are those from the groups 11 and 12.^{32b,37a}

Group 11 elements are of particular interest in catalysis and materials chemistry. Indeed, organo-copper compounds are reactive species used in key chemical transformations such as the Corey-Posner reaction where an organo-copper is involved in the formation of C-C bonds.¹¹⁰ Organometallic complexes featuring Cu-Cu interactions have been used as hydrogenation catalyst, a relevant feature regarding the affordability of copper compared to precious metals from the group 9 and 10, which dominate hydrogenation catalysis.¹¹¹

In this chapter, boratabenzene complexes of the group 11 are presented. The first example, to the best of our knowledge, of a copper boratabenzene complex has been synthesized. The linear two-coordinated Cu(I) bis-**DTBB** cationic complex, features the so desired η^1 coordinated **DTBB**. The steric bulk and electron richness of the boratabenzene ligand, successfully stabilizes the unusual Cu(I) unsaturated metal centre.

5.1.1 Two-coordinated Complexes

Two-coordinated complexes, so-called open shell,^{112a} which have coordinatively unsaturated metal centres, are unusual for almost all the transition metals. In fact, only a few exceptions are observed for the group 10. Such is the case for Au(I) complexes which mostly are two-coordinated, unlike Cu (I) and Ag(I) for which tri- and tetra-coordinated modes are more common.^{112b} Their coordination chemistry has been poorly explored but is potentially rich. Because the metal centre is present in a low oxidation state and its coordination sphere is not saturated, they can undergo several transformations such as substitution, addition or oxidation.

The study of such systems is essential to understand the chemistry of well-defined catalytic sites inspired in enzymes and many other biological systems, as well as possible applications for the synthesis of nanomaterials.

The main challenge in this chemistry is to achieve unsaturation of the metal centre. This is only possible by the aid of very bulky ligands to stabilize the unsaturated metal centre. To successfully obtain unsaturated metal-ligand fragments, it is essential to prevent decomposition by disproportionation and the formation of aggregates of extended ionic lattices. Disproportionation can change the metals coordination number from 2 to 4 and even 6. For these reasons the use of bulky ligands arises as an effective strategy.¹¹³

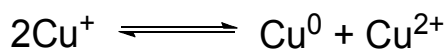
The low oxidation state of two-coordinated metal species and the empty sites available for other ligands to coordinate, make them highly sensitive to moisture and air, regardless of the steric protection from bulky ligands. However this feature is what makes them good candidates for the activation of small molecules such as O₂, N₂O and CO.¹¹² Additionally part of their reactivity is the formation of complexes with Lewis bases such as THF, pyridine or phosphines.¹¹⁴ However, additional stability can be observed for *d*¹⁰ complexes of Cu(I) and Ag(I) since their filled *d* orbitals will favour *sp* hybridization.

5.1.2 Cu(I) Coordination Chemistry

For a better understanding of the bonding and structures of copper complexes presented in this chapter, a brief description of Cu(I) interactions with phosphines, arenes and cyclopentadienyl ligands is presented.

Cu(I) is a precursor of the silent partner in type III copper proteins and its biological importance has been summarised elsewhere.¹¹⁵ Despite its relevance in coordination chemistry, the study of Cu(I) species remains limited due to their thermal instability and their tendency to oxidize to Cu(II).¹¹⁶

The Cu(I) cation can decompose in aqueous media by disproportionation forming Cu(0) and Cu(II) species (Equation 5.1); as a consequence Cu(I) compounds must be handled under strict inert conditions.¹¹⁷



Equation 5.1: Disproportionation equilibrium for Cu^+ cation.

The Cu(I) cation behaves as a soft Lewis acid and can form complexes with soft Lewis basic ligands containing donor atoms such as S, P or I⁻.

The coordination chemistry of mononuclear Cu(I) species is dominated by examples of four-coordinated species, however examples of three-coordinated Cu(I) complexes in trigonal, T-shaped and planar geometries are also known (b, Figure 5.1). Very few five-coordinated examples exist and six coordination or above are unknown. Two-coordinated linear complexes as shown in (a) Figure 5.1 have also been reported.¹¹⁷

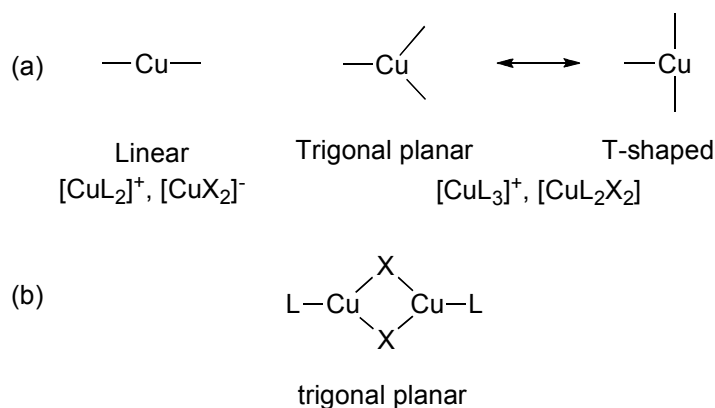


Figure 5.1: Selected coordination geometries for Cu(I) species, L = N, S, P donors and X = Cl⁻, NCS⁻.

Linear two-coordinate Cu(I) species are of particular interest because they allow the bioinorganic chemist to study the coordination chemistry of artificial systems that emulate the Cu(I) centres in proteins. A good example is supramolecular structures such as the calix[4]arene (Figure 5.2), this ligand stabilizes a two-coordinate Cu(I) centre with two biomimetic imidazolyl pendant arms (Cu-N 1.867(9) Å; N-Cu-N 178.5(4)^o).¹¹⁸ Several other examples are reported in the literature but mainly using nitrogen,¹¹⁹ oxygen,¹²⁰ halides,¹²¹ sulphur¹²² donors or carbenes.¹²³ Hence copper boratabenzene species presented in this work provides

another point of reference for the use of bulky phosphines to stabilize Cu(I) centres in a linear arrangement.

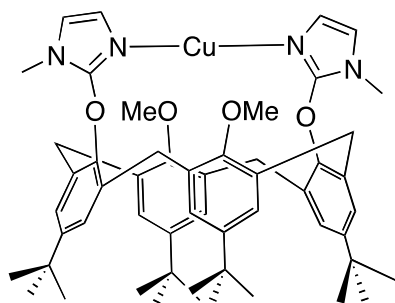


Figure 5.2: Structure of Cu(I) calix[4]arene.¹¹⁸

5.1.3 Cu(I) Species as Phosphine Scavengers

Due to Cu(I) great affinity to coordinate phosphine ligands, copper halides are often used in organometallic chemistry as phosphine scavengers to increase the rate of a catalytic reaction. A phosphine scavenger or a “phosphine sponge” reagent is a Lewis acid that can be added to reaction mixtures in order to remove free phosphine ligands that otherwise would affect the course of the desired reaction.¹²⁴ The use of copper halides as phosphine scavengers has found applications in Stille cross-coupling¹²⁵ reactions and as an initiator in olefin metathesis by Grubs catalyst.¹²⁶

Despite the recurrent use of copper halides as phosphine scavengers, the resulting adducts of the form $R_3P \cdot CuX$ ($R = \text{alkyl, aryl}; X = I^-, Cl^-, Br^-$) are ill defined in the literature.^{126c} Their monomeric or oligomeric structure depends upon the molar ratio of $R_3P:Cu(I)X$ as well as the bulkiness of the phosphine.¹²⁷ Examples of the remaining group 11 metals have also been reported; however their characterization remains limited to the infrared spectra and in some cases X-ray studies.¹²⁸ Figure 5.3 shows the dimeric structure of $Cy_3P \cdot CuCl$ (I) with bridging chlorides, confirmed by X-ray crystallography.¹²⁹ Nevertheless other structures have been proposed such as II and III (Figure 5.3), which can be formed accordingly to the molar ratio of PCy_3 available in the reaction media^{126c} and the amount of $CuCl$ solubilized in function of the solvent used.^{125a} Other alkyl phosphines such as PMe_3 have been

shown to form dimers, tetramers and ionic monomers with the metals of the group 11.¹²⁸ Interestingly the ionic monomers are unstable and it is difficult to properly characterize them.

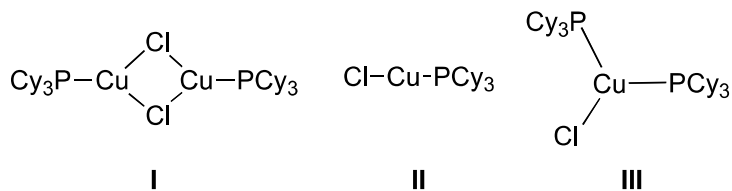


Figure 5.3: Dimeric structure of $[\text{Cy}_3\text{P}\cdot\text{CuCl}]$ (I) with bridging chloride ligands,¹²⁹ monomeric $\text{Cy}_3\text{P}\cdot\text{CuCl}$ (II) and $(\text{Cy}_3\text{P})_2\cdot\text{CuCl}$ (III).^{126c}

5.1.4 Cu(I) Cation π -Interaction with Arenes

The cation π -interaction is a non-covalent interaction between a cation and a π -system¹³⁰ and is a driving force in molecular recognition processes¹³¹ in biological¹³² and artificial systems.¹³³ It has been observed that Cu(I) forms a π -complex with benzene (IV, Figure 5.4) and that the experimental bonding energy is of $50.0 \text{ kcal}\cdot\text{mol}^{-1}$.^{133b} Guo and collaborators have reported a theoretical study comparing Cu^+ and other cations such as Li^+ , Na^+ and K^+ , thus allowing a better understanding of the details on the Cu(I)- π -system interaction. Using B3LYP/6-311+G(d,p) method, they have found that the interaction energy of Cu^+ with η^6 -benzene is stronger than that of Li^+ , Na^+ and K^+ and the strength of such interaction correlates with the size of the cation.^{133b}

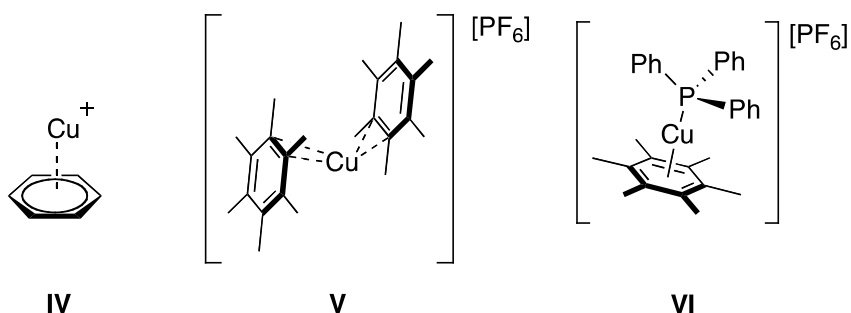


Figure 5.4: Cation-arene interaction of Cu and benzene (IV)^{133b} and coordination modes η^2 (V)¹³⁴ and η^6 (VI)¹³⁵ of Cu(I) and arenes.

They attributed the strength of such interaction to electron donation from the metal's d -filled orbitals onto the σ^* or π^* orbitals of the alkene, resulting in an elongation of the C-C bonds, while the π system donates onto the $4s$ empty orbital of Cu(I), hence the stabilization of such interaction. Interestingly they have concluded that the Cu(I)- π interaction is not of electrostatic character but it is affected by the presence of counterions.^{133b}

Another type of interaction observed for group 11 metals is that of η^2 -coordination with arenes, (**V**, Figure 5.4) this type of interaction is favoured because it diminishes the repulsion between the filled d orbitals and the filled π arene orbitals.¹³⁴

In contrast, calculations on the gas phase show that the more favourable coordination is η^6 (**IV**, Figure 5.4) while the presence of counterions favours the coordination η^2 (**V**, Figure 5.4) with the aromatic system.^{133b}

Contrary to Guo's work published in 2005, Hayton and collaborators have published in 2015 the first unsupported η^6 Cu(I) arene. In this recent publication, they have shown that the η^6 interaction is in fact more stable than η^2 in the gas phase. Additionally they have found that the presence of counterions and the addition of a co-ligand favour the η^6 coordination of arenes to Cu (**VI**, Figure 5.4).¹³⁵ They have proved that the steric and solvent effects play a dominant role on the final bonding. They concluded that there is an electrostatic component attributed to the interaction η^6 -Cu-arene and that this is usually a weak interaction as a consequence of the contracted $3d$ orbitals. Comparison of Cu and Fe complexes¹³⁵ shows how much weaker the Cu-arene interaction is for copper compared to that on Fe, where the energy levels of the $3d$ orbitals of the metal centre match better the π^* orbitals of the arene, promoting the stabilization by back-bonding.

5.1.5 Cu(I) Coordination to Cyclopentadienyl Ligands

As mentioned in section 1.2, the boratabenzene ligand displays coordination chemistry similar to the cyclopentadienyl ring (Cp), hence the use of Cp complexes for comparisons on the coordination of boratabenzene ligands.

CpCu complexes stabilized by a phosphine co-ligand (Figure 5.5) have been observed.¹³⁶ However elongated distances between Cu-C_{cent} of the Cp ring are evidence of a poor overlap between the e₁, e₂ orbitals of Cp and the 3d filled orbitals of Cu. This is due to the contraction of the orbitals, which is more evident towards the right of the transition metal series, resulting in a lack of π* orbitals on the copper centre available for back-bonding with the Cp ligand. In consequence, the presence of a co-ligand has an important impact on the stabilization of copper complexes. Phosphines used as co-ligands have a stronger tendency to stabilize the [η⁵-CpCu] fragment compared to the carbonyl and isocyanide ligands, which form unstable complexes with the [η⁵-CpCu] fragment.^{136a}

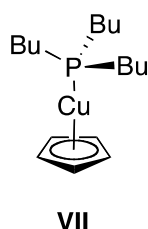


Figure 5.5: Copper complex with a co-ligand CpCuPBu₃ (**VII**).^{136a}

5.1.6 Cu-B Interaction with Group 11 Metals

Cu-B interaction have only been confirmed when the ligand's geometric restrictions forces this interaction, such is the case of a metallaboratrane cage (**VIII**, Figure 5.6) reported by Bourissou¹³⁷ or if NHC ligands are used such as the case of NHC-Cu-Bpin which shows a weak Cu(I)-B interaction (**IX**, Figure 5.6).¹³⁸

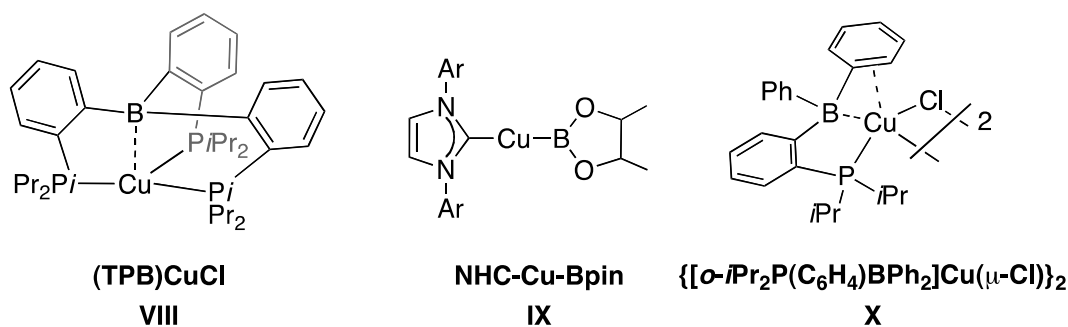
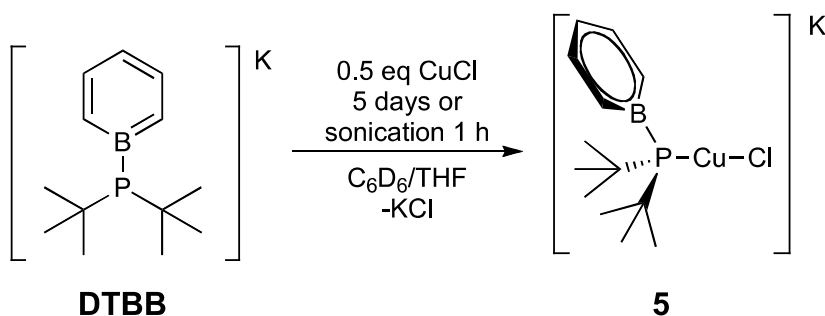


Figure 5.6: Examples of Cu-B interactions: copper metallaboratrane (TPB)CuCl (**VIII**),¹³⁷ NHC-Cu-Bpin (**IX**),¹³⁸ and a Cu-η³-borataallyl complex (**X**).¹³⁹

Mono-phosphino boranes of the type $o\text{-}i\text{Pr}_2\text{P}(\text{C}_6\text{H}_4)\text{BPh}_2$ (**X**, Figure 5.6) display a Cu-BCC coordination with the arene substituent on boron and notably involving a direct Cu-B interaction, confirmed by X-ray diffraction.¹³⁹

5.2 Synthesis and Characterization of η^1 -Copper Species

In a J. Young tube, 0.5 equiv. of CuCl were suspended in benzene- d_6 and 1 equiv. of **DTBB** dissolved in THF was added (Scheme 5.1), within minutes of addition a new product was observed by NMR. However when the reaction was left without stirring on the bench top, the starting material was fully consumed only after five days, while sonication of the mixture for one hour brings the reaction to completion. The product obtained from the reaction was formulated to be a **DTBB** η^1 bonded to a [CuCl] fragment (**5**, Scheme 5.1). Species **5** displays a structure consistent to species mentioned in section 5.1.3 of the type $[\text{R}_3\text{P-Cu-Cl}]$.^{127,129}



Scheme 5.1: Synthesis of $[(\eta^1\text{-DTBB})\text{CuCl}]\text{K}$ (**5**).

The ^1H NMR data shows the signals for the boratabenzene ring at δ 7.43 (*meta*-H), 7.10 (*ortho*-H), 6.53 (*para*-H) and what appears to be a virtual triplet corresponding to the *t*Bu ligands at 1.47 ppm ($J = 6.47$ Hz). The ^{31}P NMR displays a broad singlet at 17.1 ppm, while the ^{11}B NMR shows a broad multiplet at 27.6 ppm.

The proton resonances of the boratabenzene ring in species **5** are slightly shifted towards high field, suggesting an interaction of the boratabenzene ring with the counterion K^+ , rather than a non-coordinated ring. This interaction has been observed as the formation of honeycomb structures and three-coordinated K^+ cations on the coordination networks that the **DTBB** ligand forms within the crystal structure (Figure 1.1).⁵³¹⁴⁰ Other evidences of such interaction had also been observed for alkali metal cations such as Li^+ , which can form a sandwich type structure with $(\text{C}_5\text{H}_5\text{B-H})^-$ ligand (Figure 5.7).^{32b}

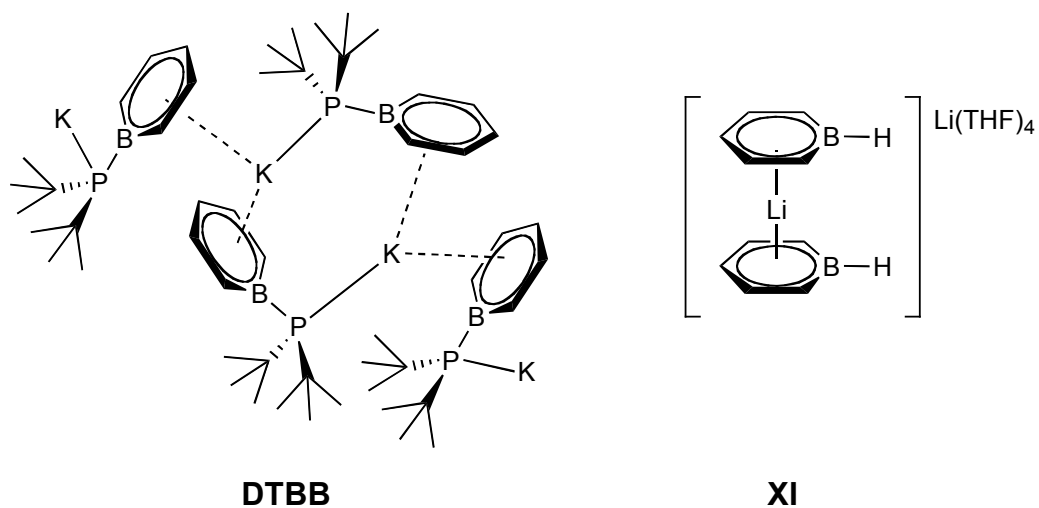


Figure 5.7: Three coordinate coordination network of K^+ on **DTBB** crystals structure^{53,140} and π -coordination of Li^+ cation to boratabenzene $[(\text{C}_5\text{H}_5\text{B-H})\text{Li}][\text{Li}(\text{THF})_4]$ (**XI**).^{32b}

Alternatively the formation of a species featuring two **DTBB** ligand coordinated η^3 through the B=C-C bonds has also been proposed (Figure 5.8), based on similar coordination modes observed for **DTBB** ligand and other ligands with similar structures. The coordination of **DTBB** as a η^6 has been ruled out due to the electron richness of the boratabenzene ring, which has been set in evidence by the previously reported π -coordinated **DTBB** examples to Ni,⁵³ Fe (section 4.3.1) and Rh (Chapter 6). The lack of available *d* orbitals on Cu(I) to accommodate the electronic density of the boratabenzene ring, makes impossible the interaction with the filled π orbitals from the ring, hence making the coordination η^2 - η^6 very weak and as shown by calculations, of electrostatic character.¹³³⁻¹³⁶

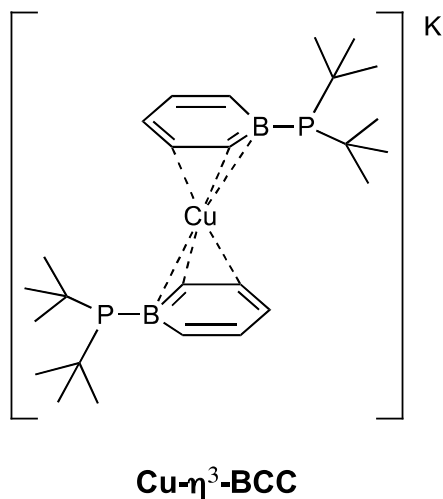


Figure 5.8: Alternative structure proposed for species **5**, $[(\eta^3\text{-DTBB})_2\text{Cu}]\text{K}$ (**Cu- η^3 -BCC**).

On the other hand, evidences of metal bonding in a η^3 -BCC fashion have been observed and are relatively new. Emslie and collaborators made the first reports in 2006 using a phosphine-thioether-borane ligand. This ligand is capable to place the boron atom in proximity to palladium¹⁴¹ but when reacted with certain metal precursors such as $\text{K}[\text{CpFe}(\text{CO})_2]$, an unusual allyl-like Rh-BCC interaction was observed.¹⁴²

Rh- η^3 -BCC $[(\text{TXPB})\text{Rh}(\mu\text{-CO})_2\text{Fe}(\text{CO})\text{Cp}]$ (Figure 5.9) species can be rationalized in two different ways: an η^2 -coordinated phenyl ring and a σ interaction between rhodium and a quasi-planar borane (**XIIa**) or as a conjugated (B-C-C) ligand system (**XIIb**).¹⁴²

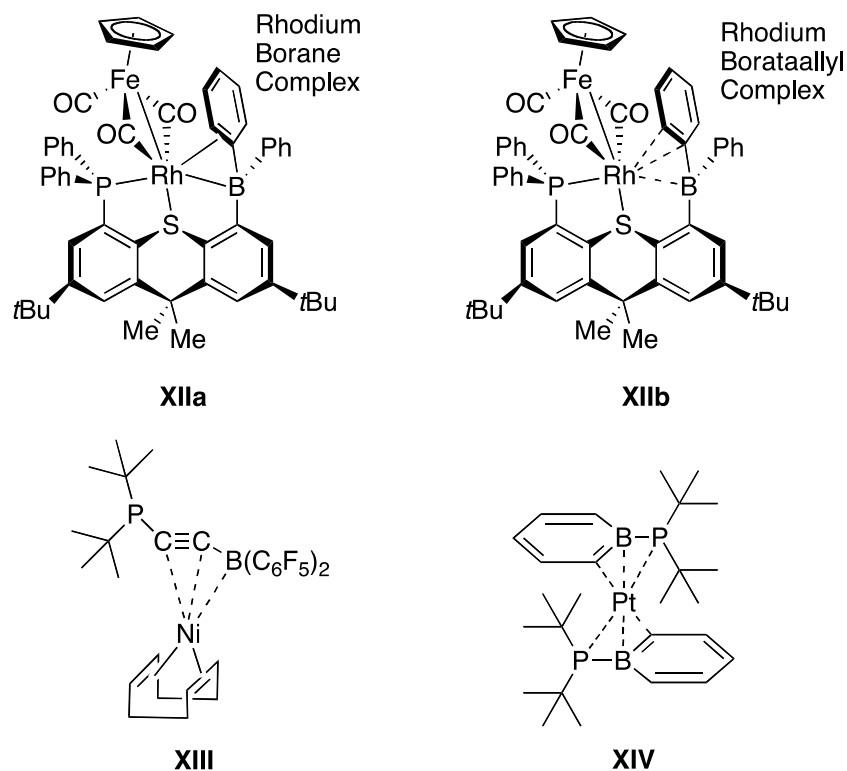


Figure 5.9: $[(\text{TXPB})\text{Rh}(\mu\text{-CO})_2\text{Fe}(\text{CO})\text{Cp}]$ (**X11a** and **X11b**) reported by Emslie,¹⁴² $(\text{tBu}_2\text{PCCB}(\text{C}_6\text{F}_5)_2)\text{Ni}(\text{cod})$ (**X111**),¹⁴³ $(\text{Pt}(\eta^3\text{-DTBB})_2)$ (**X11V**).⁵³

In 2010 Stephan and collaborators reported further evidence on this type of interaction. Figure 5.9 shows a nickel phosphino-alkynyl-borane complex featuring a $\text{Ni}-\eta^3\text{-BCC}$ coordination.¹⁴³ Furthermore Macha and Fontaine⁵³ reported two examples of **DTBB** ligand coordinated to platinum centres featuring the allyl-like interaction (Figure 5.9).

The P-B=C fragment coordinated in a η^3 fashion to platinum (**X11V**, Figure 5.9) exhibits fluxional behaviour at low temperatures. Based on this precedent we decided to carry proton NMR studies at different temperatures, to further investigate the bonding mode of species **5**. However the ^1H NMR at different temperatures did not provide information on any fluxional behaviour, hence a **Cu- $\eta^3\text{-BCC}$** structure could not be confirmed on the basis of NMR spectra. Computational details on the structure of the **Cu- $\eta^3\text{-BCC}$** species and complex **5** are presented and discussed in section 5.2.2.

Nevertheless the change of solvent was observed to have an effect on the NMR splitting of the boratabenzene protons, while three signals corresponding to *ortho*, *meta* and *para* protons are observed in benzene- d_6 and in a mixture of benzene- d_6 /THF, the protons are all inequivalent in toluene- d_8 . This behaviour suggests an interaction of the boratabenzene ring with the solvated K^+ counterion, instead of the formation of a **Cu- η^3 -BCC** species. The affinity of Cu(I) to bind phosphines¹²⁷ seems to be a favourable pathway to coordinate the **DTBB** ligand to the Cu(I) centre, rather than the interaction between the electron rich boratabenzene ring and Cu^+ cation.

Using HR-MS with APPI ionization (Figure 5.10), it was possible to measure the negative ionization, the most abundant molecular ion observed shows a $m/z = 319.06$ corresponding to $[(DTBB)CuCl]^-$ and the second most abundant species corresponds to the molecular ion of $[(DTBB)CuCl_2+H]^-$ ($m/z = 355.10$). Additionally masses corresponding to $[(DTBB)_2Cu]^-$ ($m/z = 505.26$) and bimetallic species of the form $[(DTBB)_2Cu_2Cl_2+H]^-$ ($m/z = 639.20$) and $[(DTBB)_2Cu_2Cl]^-$ ($m/z = 603.15$) were also observed on the mass spectrum and their corresponding isotopic patterns were confirmed by comparison with simulations of the spectra generated in Mmass.⁶⁹

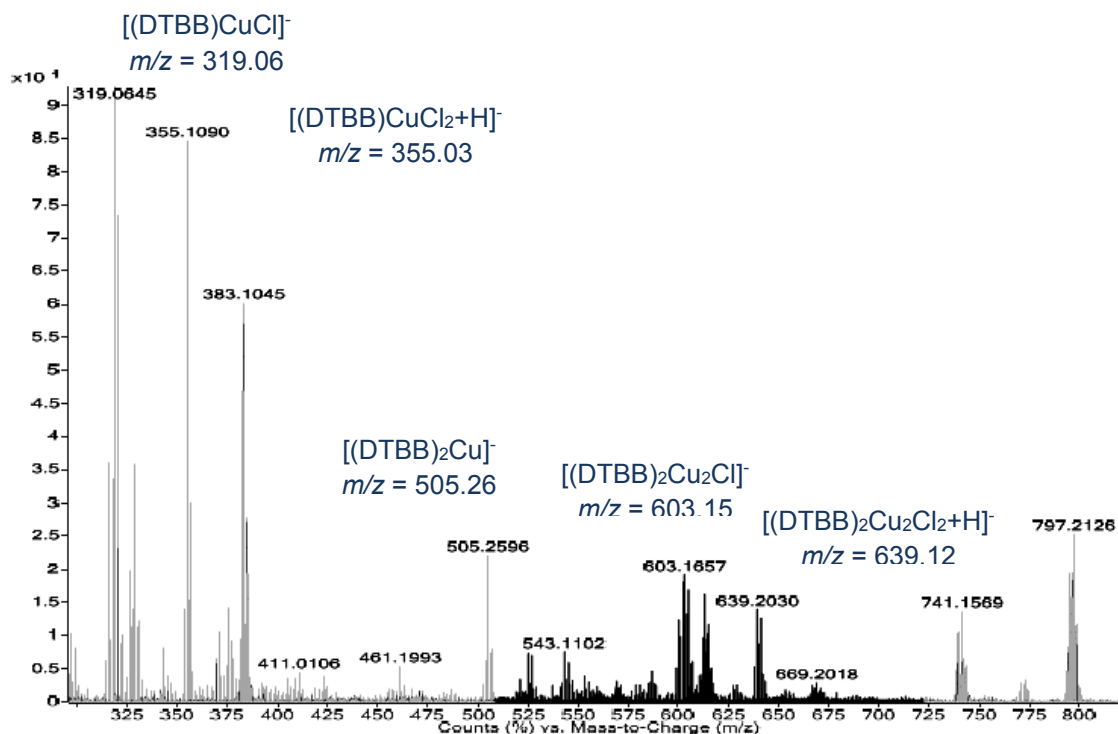


Figure 5.10: Mass spectrum (HR-MS APPI, negative ionization) of a benzene solution of complex **5**: formulas and calculated masses of identified molecular ions.

Figure 5.11 shows the proposed molecular structure of the two main molecular ions found in the spectra. The remaining identified ions could display structures such as those described for copper oligomers in section 5.1.3.

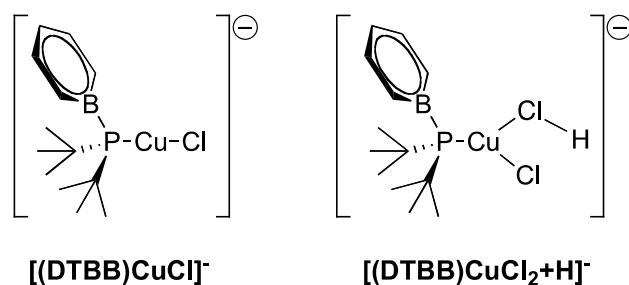
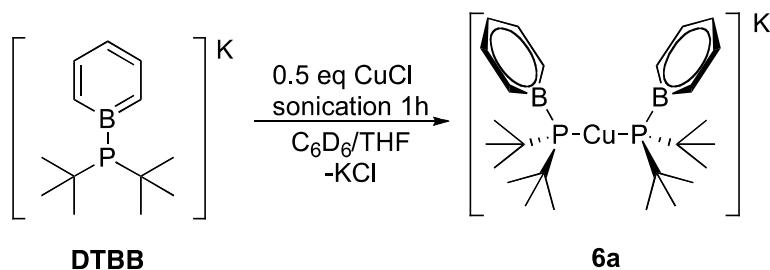


Figure 5.11: Proposed structure of the most abundant molecular ions found by HR-MS APPI.

Interestingly, species **5** seems to undergo a rearrangement in solution. When a reaction mixture of **5** was left at room temperature for a week, the formation of a new copper-boratabenzene species was observed (**6a**, Scheme 5.2). Complex **6a** can also be obtained by sonication of the reaction mixture of **5** for periods longer

than 2 hours, suggesting that species **6a** is the thermodynamically more stable species. Attempts to carry the reaction only in THF resulted as well in the quick formation of species **6a**. Upon heating the reaction mixture of **6a** was shown to decompose by a reduction process since a copper coloured mirror was observed on the glassware. Thus the formation of species **6a** is not reversible.



Scheme 5.2: Synthesis of species **6a** $[\text{Cu}(\eta^1\text{-DTBB})_2]\text{K}$.

The ^1H NMR of species **6a** shows signals at δ 7.45 (*meta*-H), 6.80 (*para*-H), 6.76 (*ortho*-H) and a resonance for the *t*Bu substituents observed as a doublet at 1.26 ppm ($J = 12.9$ Hz). The ^{31}P NMR spectrum displays a broad multiplet at 14 ppm and the ^{11}B NMR shows a broad multiplet at 23.6 ppm.

The formation of species **6a** is consistent with copper's preference to bind phosphines capable to stabilize the unsaturated Cu(I) centre in a linear, two-coordinated arrangement.

HR-MS using APPI ionization showed a molecular ion corresponding to $[\text{Cu}(\text{DTBB})_2]^{-}$ ($m/z = 505.26$), this molecular ion was also observed to be present in the reaction mixture of species **5**. Additionally using the positive ionization the molecular ion $[\text{Cu}(\text{DTBB})_2+\text{H}]^{+}$ ($m/z = 506.62$) was observed. Figure 5.12 shows a comparison between the experimental spectrum and a simulation made with Mmas⁶⁹ confirming the rightful assignation for this species.

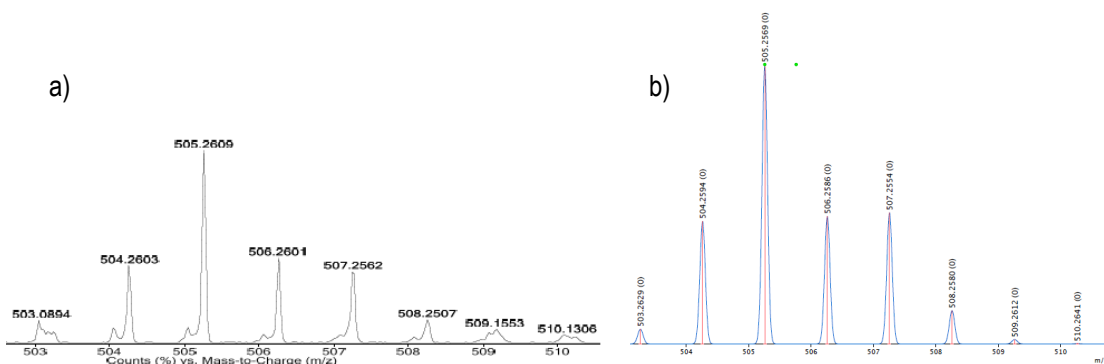
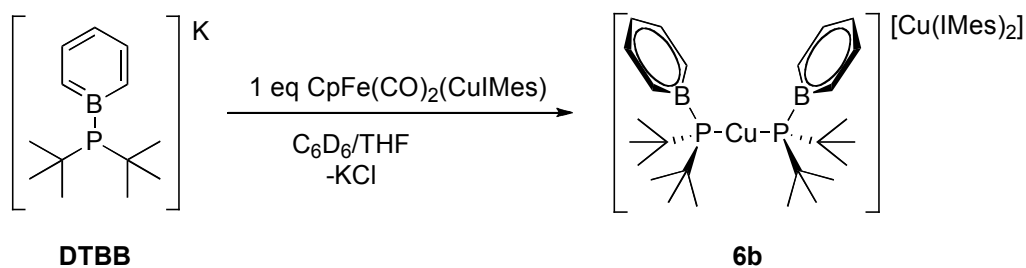


Figure 5.12: a) Experimental HR-MS APPI for **6a**, $m/z = 505.26$ $[\text{Cu}(\text{DTBB})_2]^-$. b) Simulation generated using Mmass.⁶⁹

Species **6** can also be obtained by the reaction of 1 eq of $\text{CpFe}(\text{CO})_2(\text{CuIMes})$ and 1 equiv. of **DTBB** (Scheme 5.3) giving as a result species **6b**, where the counterion is the $[\text{IMes}_2\text{Cu}]^+$ fragment rather than a potassium cation.



Scheme 5.3: Synthesis of species **6b** $[\text{Cu}(\eta^1\text{-DTBB})_2][\text{Cu}(\text{IMes})_2]$.

^1H NMR shows signals for boratabenzene at δ 7.94 (*meta*-H), 7.28 (*ortho*-H), 7.06 (*para*-H), and *t*Bu substituents at 1.17 ppm ($J = 12.5$ Hz). The $[\text{Cu}(\text{IMes})_2]^+$ counterion displays signals at δ 6.71 (*meta*-Mesityl), 5.96 (H-Imidazol), 2.09 (*para*- CH_3), 1.95 (*ortho*- CH_3). ^{31}P NMR shows a broad singlet at 24.3 ppm. The difference in shifts of the phosphorous nuclei in species **6a** and **6b** can be attributed to interactions with the solvent, something that has been observed for Cu^+ cations.^{133b} The ^{11}B NMR of **6b** displays a broad doublet at 26.9 ppm ($J = 72.1$ Hz). To the best of our knowledge, complex **6b** is the only species observed and no evidence of a structure such as complex **5** was observed.

5.2.1 X-ray Structure of **6a** and **6b**

Complex **6a** was crystallized by slow evaporation of a diluted solution in benzene- d_6 . It exhibits a monoclinic, $P2_1/n$ crystal system. Complex **6a** is a 14 electron linear M-L fragment, described by a P-Cu-P interaction (Figure 5.13). Two **DTBB** are coordinated η^1 through the phosphorous lone pair to a Cu(I) metal centre, the charge is balanced by a potassium counterion and the boratabenzene ring remains pendant. An interaction between the boratabenzene ring and the K^+ was observed in solution and is also observed in the crystal structure. Two molecules are present in the unit cell.

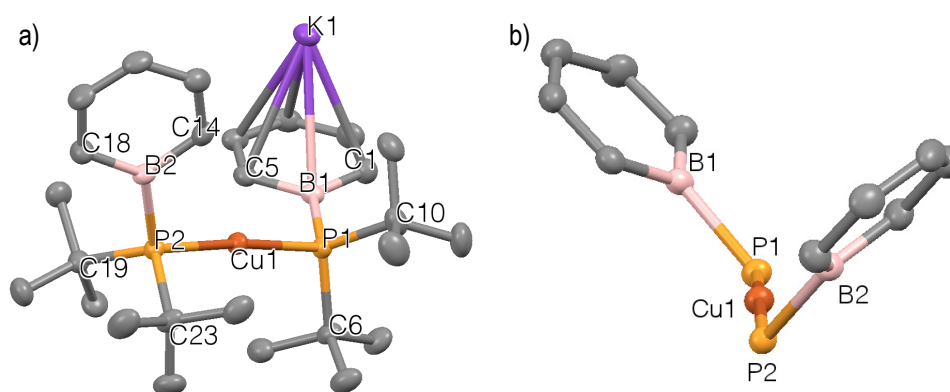


Figure 5.13: a) X-ray structure of **6a**, thermal ellipsoids drawn at the 50% probability level. Hydrogen atoms are omitted for clarity. ($R_1 = 6.42\%$) b) Side view of **6a**, *t*Bu groups and hydrogen atoms are omitted for clarity. Selected bond distances (Å) and angles ($^\circ$): P1-Cu1 2.229(1); P2-Cu1 2.228(1); B1-P1 1.964(5); B2-P2 1.963(6); K1-C_{cent} 2.832(5); P1-Cu1-P2 174.7(1); B1-P1-Cu1 113.9(2); B2-P2-Cu1 115.1(2); Cu1-P1-C10 107.6(2); Cu1-P1-C6 107.3(1); B1-P1-C6 105.3(2); B1-P1-C10 110.6(2); C10-P1-C6 112.1(2); B2-P2-Cu1-P1 138.7(1); B1-P1-Cu1-P2 143.7(1).

The same coordination is observed for species **6b**. Crystals of **6b** were obtained from slow evaporation of a diluted hexane solution in a monoclinic, $C2/c$ crystal system. The overall negative charge of the P-Cu-P fragment is balanced with a $[Cu(IMes)_2]^+$ counterion (Figure 5.14).

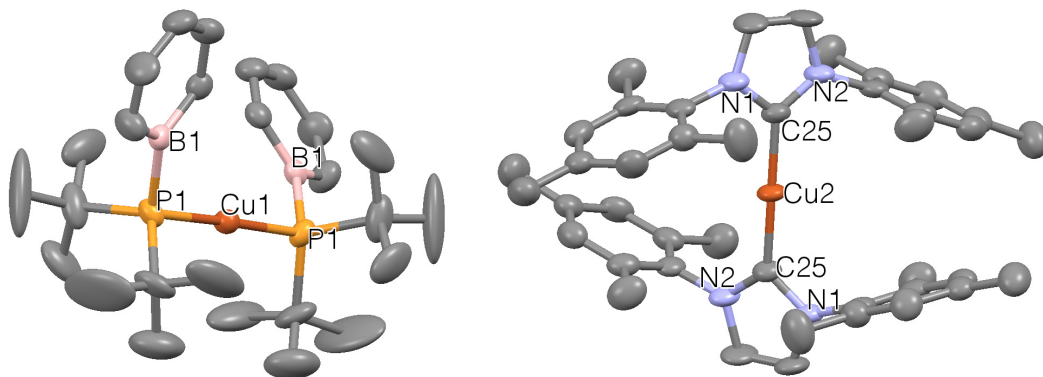


Figure 5.14: X-ray structure of **6b**, thermal ellipsoids drawn at the 50% probability level. Hydrogen atoms are omitted and molecules have been individually rotated for clarity. ($R_1 = 5.24\%$) Selected bond distances (Å) and angles ($^\circ$): P1-Cu1 2.217(1); P1-B1 1.955(4); Cu2-C25 1.876(1); C25-N1 1.361(5); C25-N2 1.343(4); C25-Cu2-C25 177.1(2); P1-Cu1-P1 178.2(3); Cu1-P1-B1 112.0(1); Cu1-P1-C6 108.2(2); Cu1-P1-C10 107.2(2); C6-P1-B1 106.8(2); C10-P1-B1 110.0(2); C6-P1-C10 112.6(2); B1-P1-Cu1-P1 144.6(1).

The P-B distances in both complexes are similar, 1.964(5) Å (**6a**) and 1.955(4) Å (**6b**), these distances are also close to what is observed for the free ligand (1.965(3) Å),⁵³ the B-P-Cu angles are of 113.9(2) $^\circ$ for **6a** and 112.0(1) $^\circ$ for **6b** and the boratabenzene rings are almost aligned facing each other as can be observed on the side view of the structure, Figure 5.13 (b).

The phosphorous atoms from both **DTBB** ligands display a slightly distorted tetrahedral geometry in both species **6a** (B1-P1-Cu1 = 113.9(2); Cu1-P1-C10 = 107.6(2); Cu1-P1-C6 = 107.3(1) $^\circ$) and **6b** (B1-P1-Cu1 = 112.0(1); Cu1-P1-C10 = 107.2(1); Cu1-P1-C6 = 108.2(1) $^\circ$). Interestingly these results correlate with the observations of **DTBB** η^1 -coordinated to Fe presented in Section 4.2.1.

Complex **6b** displays a $[\text{Cu}(\text{IMes})_2]^+$, where the Cu-C_{carb} distance of 1.876(1) Å and C_{carb}-N distances of 1.361(5) and 1.343(4) Å are in accordance with this previously reported cation in $[\text{Cu}(\text{IMes})_2][\text{BF}_4]$ (Cu-C_{carb} 1.884(2); C_{carb}-N 1.349(2) $^\circ$).¹⁴⁴

Complex **6a** displays a Cu-P distance of 2.229(1) Å, similarly the Cu-P distance in **6b** is of 2.217(1) Å. These values are in accordance with other species displaying a P-Cu-P interaction such as a tethered Cu(I) centre (Figure 5.15, **XV**) supported by two diphenyl phosphines on which the P-Cu distance is of 2.214(1) Å. It is important to notice, however that species **XV** features a Cu(I)- π interaction with the

anthracene system.¹⁴⁵ The other example featuring phosphorous bonding copper in a linear fashion is that of the $[\text{Cu}(\text{P}(\text{tBu}_2)_2)]^+$ (**XVI**, Figure 5.15) which shows Cu-P distances of 2.266(4) and 2.246(5) Å.¹⁴⁶

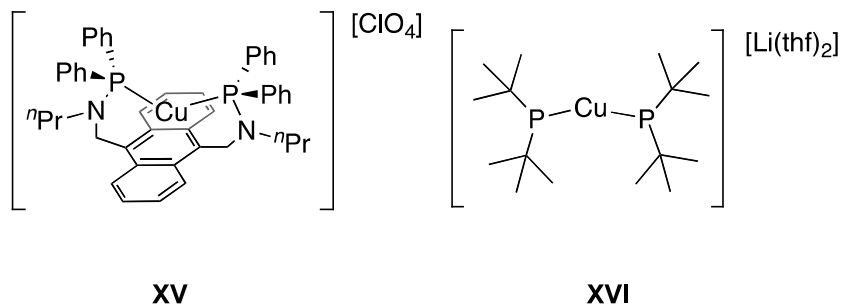


Figure 5.15: Examples of phosphorous two-coordinated linear Cu(I): **XV**,¹⁴⁵ **XVI**.¹⁴⁶

The P-Cu-P angles are close to linearity for complexes **6a** and **6b** at 174.7(1)° and 178.2(3)° respectively. As opposed to the angle observed for the three-coordinated copper center on compound **XV** which P-Cu-P angle is considerably distant from linearity (153.9(7)°) due to its π -interaction with the aromatic ring. However, the P-Cu-P angles observed on **6a/b** resemble those of the phosphido complex **XVI** (176.5(2)°) that is very close from linearity despite repulsion from the free electron pairs on the phosphido ligands.

5.2.2 DFT Calculations

Density functional theory calculations using the hybrid functional B3PW91 and basis set 6-31G(*d,p*), were carried out by Laurent Maron to support the identity of species **5** and **6a**. As expected, calculations showed that species **6** was the most stable compound.

The calculations have shown that **DTBB** ligand engaging in a $\text{M}-\eta^3\text{-P-B=C}$ interaction, as observed for the Pt species (**XIV**, Figure 5.9), does not generate a stable structure with copper and leads to the formation of $\text{Cu}-\kappa^1\text{-P}$ species (**6a/b**). Nevertheless the proposed **Cu- $\eta^3\text{-BCC}$** species was found to be possible but 20 $\text{Kcal}\cdot\text{mol}^{-1}$ less stable than the $\text{Cu}-\kappa^1\text{-P}$ coordination (**6a/b**),¹⁴⁷ which explains why we obtained exclusively crystals of complexes **6a/b**.

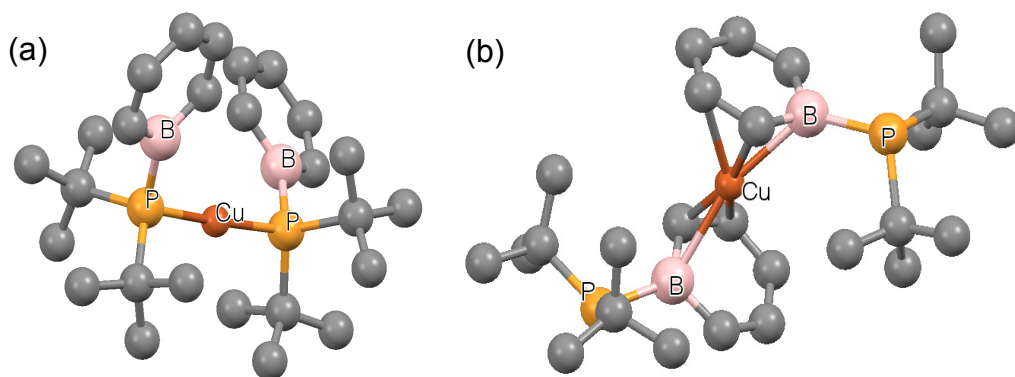


Figure 5.16: Ball and stick representations, structure optimization calculated at the DFT level of theory using the hybrid functional B3PW91, basis set 6-31G(*d,p*). Selected bond distances (Å) and angles (°) a) Cu- κ^1 -P: B-P 1.977; P-Cu 2.276; P-Cu-P 177.8; B-P-Cu 11.8. b) η^3 -B=C-C: B-Cu 2.467; C_{ortho}-Cu 2.052; C_{meta}-Cu 2.512; B-P 1.990; P-B-Cu 125.48; C_{ortho}-B-C_{ortho} 113.46.¹⁴⁷

Figure 5.16 (a) shows the optimised structure of the Cu- η^1 -**DTBB**. The P-B distance observed in the crystal structures of **6a/b** (**6a**: 1.964(5) Å; **6b**: 1.955(4) Å) are well in accordance with the calculations (1.977 Å). The P-Cu distances on **6a** (2.229(1) Å) and **6b** (2.217(1) Å) are slightly shorter than the distance observed on the optimized structure (2.276 Å). Additionally the P-Cu-P angle in **6a** (174.7(1)°) is 4° shorter than the angle observed for **6b** (178.2(3)°) and the angle observed on the optimized structure (177.8°). This suggests an effect of the coordination of K⁺ with the boratabenzene ring present in **6a**, while the counterion in **6b** is not interacting at all with the boratabenzene ring, which is in agreement with the results obtained from the optimized structure in gas phase.

The calculated **Cu- η^3 -BCC** species displays a Cu-B distance of 2.467 Å, if compared to other boratabenzene complexes such as **XIV** (Pt-B = 2.379(4) Å) and **XVII** (2.40(2) Å) (Figure 5.17), it becomes evident by the elongated distance between Cu-B that such interaction is less favoured than the Pt-B observed in stable species **XIV** and **XVII**. In addition, the Cu-B distances on **Cu- η^3 -BCC** range from 2.052 Å for the Cu-C_{ortho} to 2.512 Å for the Cu-C_{meta}. Interestingly the Cu-C_{meta} distance resembles the distance observed between Pt-C_{ortho} in the platinum species (**XIV** = 2.268(3); **XVII** = 2.38(1) Å).

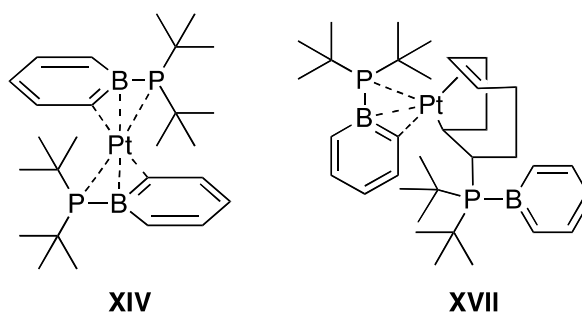


Figure 5.17: η^3 -DTBB species with Pt.

Based on the experimental evidence and the structural data obtained from the calculations, the **DTBB** ligand has a strong tendency to coordinate to Cu through the phosphorous moiety rather than the π system, contrary to what has been observed for the Ni, Pt,⁵³ Fe (Section 4.3.1) and Rh complexes (Chapter 6).

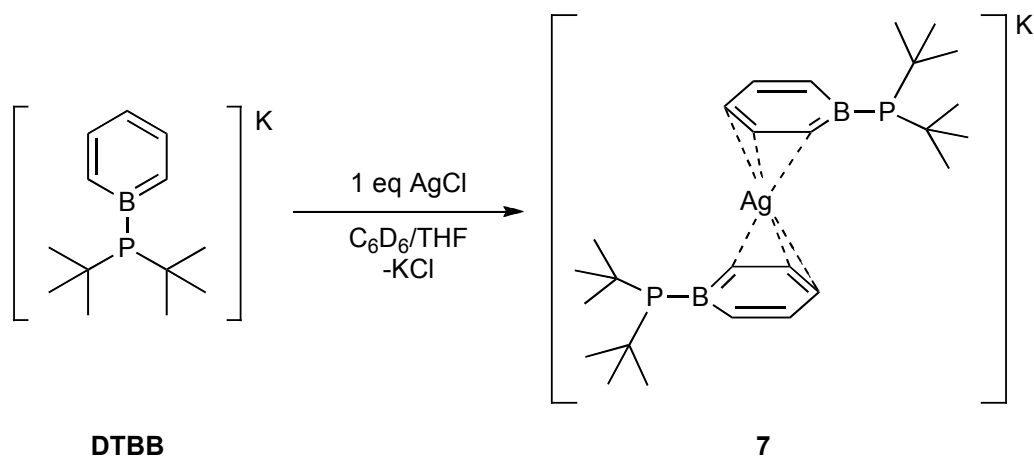
5.3 Boratabenzene Silver Species

In order to better understand the interaction of the **DTBB** ligand with metals such as Cu(I) we decided to expand the study of the ligands coordination to the remaining group 11 metals, which to the best of our knowledge, has never been done for boratabenzene species.

Reaction of 1 equiv of AgCl with **DTBB** in benzene-*d*₆/THF (Scheme 5.4), resulted in a shift of the **DTBB** ligand (δ 7.24 (*meta*-H), 6.92 (*ortho*-H), 6.27 (*para*-H), 1.29 (PtBu₂)) to a lower field 7.52 (*meta*-H), 7.19 (*ortho*-H), 6.55 (*para*-H) (Figure 5.18), while the PtBu₂ protons were not observed due to overlapping with THF.

Additionally, the formation of a brown precipitate in the mixture was observed. Attempts to change the solvent to only benzene-*d*₆, for further characterization, resulted in an increased formation of brown precipitate and decomposition of the sample. Attempts to isolate the sample by recrystallization or precipitation resulted in decomposition. When stored at room temperature or at -30 °C for longer periods than a day, decomposition was also observed. Nevertheless the ³¹P and ¹¹B were recorded in the benzene-*d*₆/THF mixture. The phosphorous NMR shows a resonance at 7.8 ppm, very close to that observed for the free ligand at 8.5 ppm

and a resonance at 19.4 ppm corresponding to free *t*Bu₂PH as a decomposition product (Figure 5.19). The ¹¹B NMR shows very similar results, as a broad multiplet at 34.6 ppm, compared with the free ligand observed at 33 ppm.



Scheme 5.4: Synthesis of Silver-phosphidoboratabenzene complex [Ag(η^3 -DTBB)₂]K (**7**).

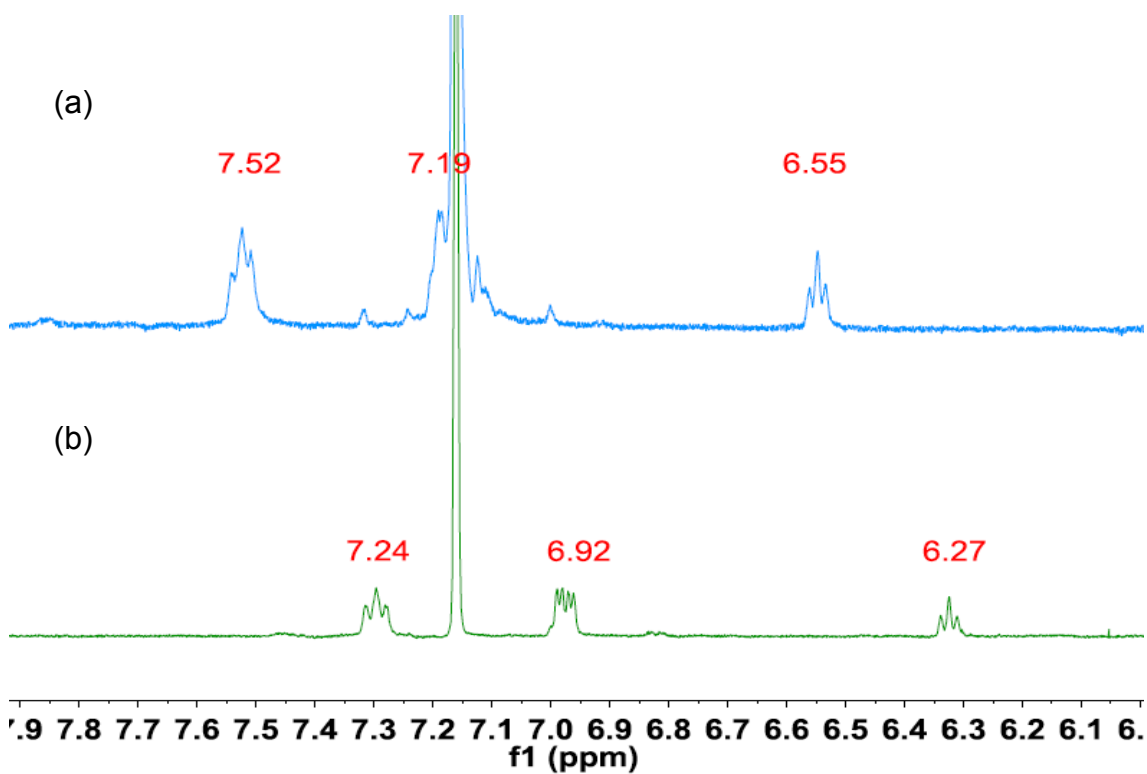


Figure 5.18: ¹H NMR (500 MHz, benzene-*d*₆/THF) a)[Ag(η^3 -DTBB)₂]K (**7**), b) DTBB.

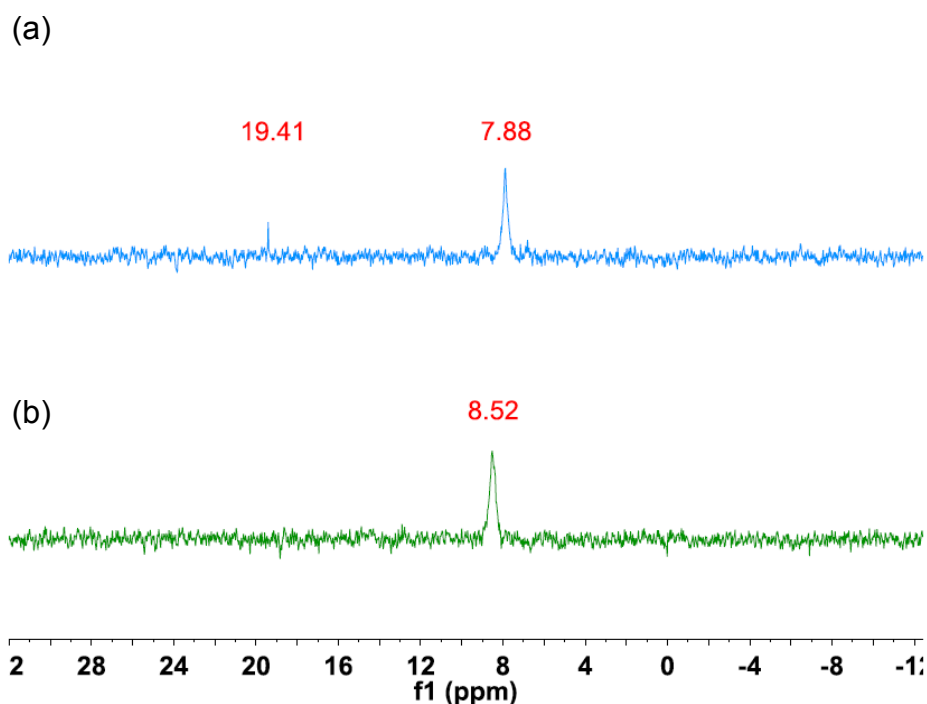


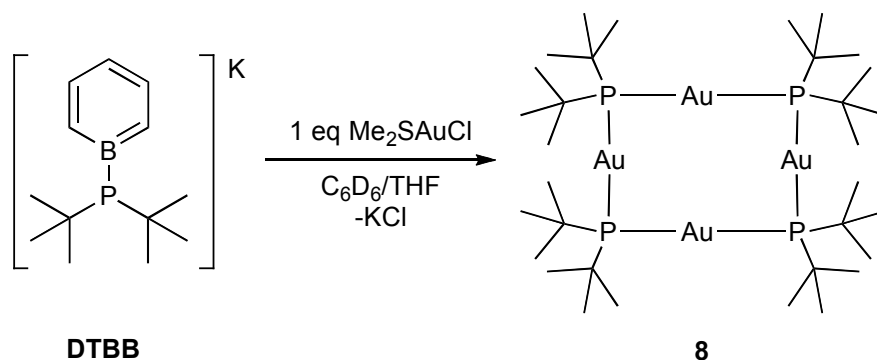
Figure 5.19: ^{31}P NMR (202.40 MHz, benzene- d_6 /THF) a) $[\text{Ag}(\eta^3\text{DTBB})_2]\text{K}$ (7), b) DTBB.

With the precedents of the coordination observed for **DTBB** and Cu(I), the **DTBB** ligand is expected to coordinate Ag(I) either by an η^1 or η^3 fashion. The shift of the signals in the proton NMR, particularly that of the *ortho* proton of boratabenzene which shifts to a lower field, is reminiscent of the behaviour also observed in the Cu(I) complex (**5**). The existence of a $[\text{DTBB-AgCl}]\text{K}$ species can be however disregarded since no significant shift in the ^{31}P or the ^{11}B was observed upon reaction with AgCl, suggesting that either the interaction with these nuclei is very weak or inexistent. Based on this, an interaction between the π system with Ag(I) can then be proposed. The crystal structure would confirm these assumptions, but unfortunately we were not able to obtain a quality crystal for diffraction studies. Moreover, complexes with Ag(I) featuring an intermediate structure between η^3 and η^4 have been reported.¹⁴⁸ Calculations¹⁴⁹ reiterate silver's preference to coordinate η^3 and η^4 to Cp rather than η^5 . These reports support the hypothesis of a weak η^3 interaction between Ag and possibly only a C-C=C fragment of the boratabenzene ring.

5.4 Reactivity of DTBB with Gold

Attempts to obtain the same type of complexes with gold were not as fruitful as with copper and silver, due to gold's strong tendency to form clusters or oligomers. Nevertheless an interesting gold-phosphanyl oligomer was obtained.

Reaction of 1 eq. of **DTBB** with Me_2SAuCl in a mixture of benzene- d_6 /THF, resulted in the formation of a bright yellow solution with quick precipitation of an insoluble red solid.



Scheme 5.5: Reaction of DTBB with Me_2SAu and gold-phosphanyl oligomer (**8**) obtained.

The mixture was then placed inside a J. Young tube and used for NMR spectroscopic analysis. The ^1H NMR spectrum shown in Figure 5.20 (a) was taken 10 min after adding the metal solution to the ligand, Figure 5.20 (b) shows the reaction mixture 5 days after addition and a comparison with the **DTBB** ligand (c).

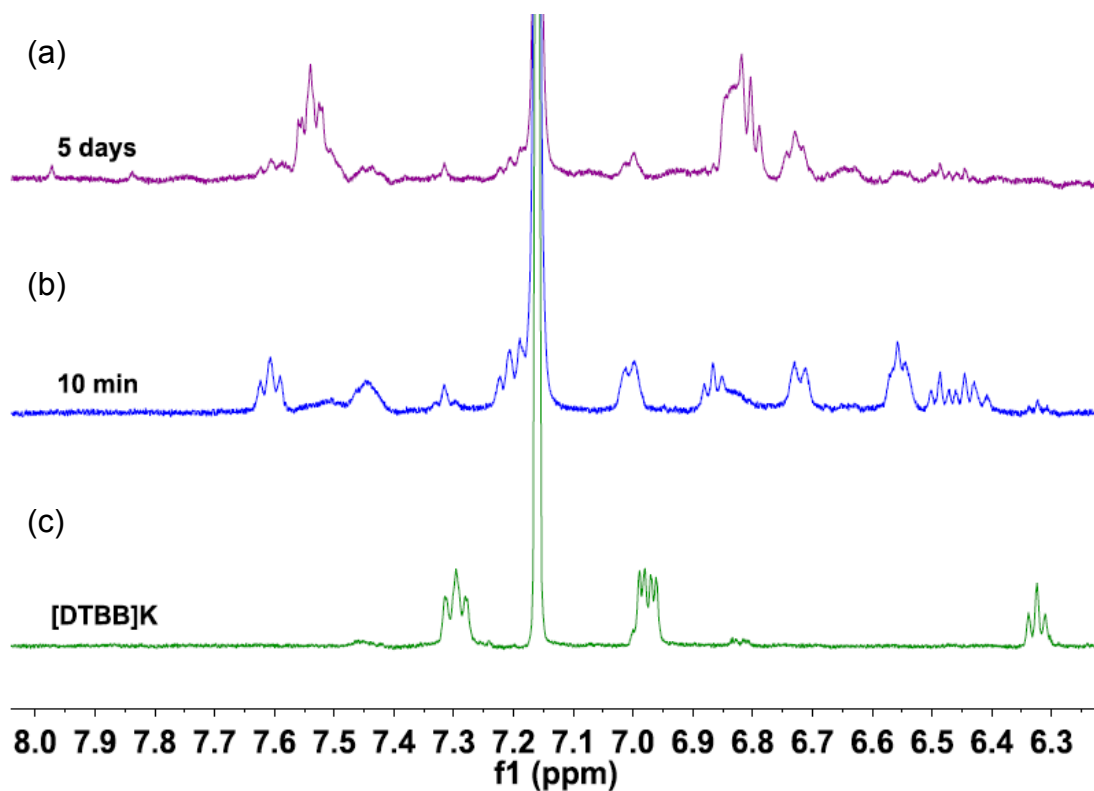


Figure 5.20: ^1H NMR (500 MHz, benzene- d_6 /THF) (a) 5 days after addition of Me_2SAuCl , (b) 10 min after addition and (c) **DTBB** ligand free.

The NMR data suggest that the formation of a gold-boratabenzene complex initially takes place, possibly involving the coordination of both the aromatic ring of boratabenzene and the phosphorous ligand. This can be observed by the multiple sets of aromatic signals for the boratabenzene ring and a shift in the ^{31}P NMR from 8.5 ppm corresponding to **DTBB** ligand, (c, Figure 5.21) to three different signals observed at 49, 48.3 and 44 ppm (a, Figure 5.21) and the progression to the onset of new signals at 95 and 81 ppm (b, Figure 5.21).

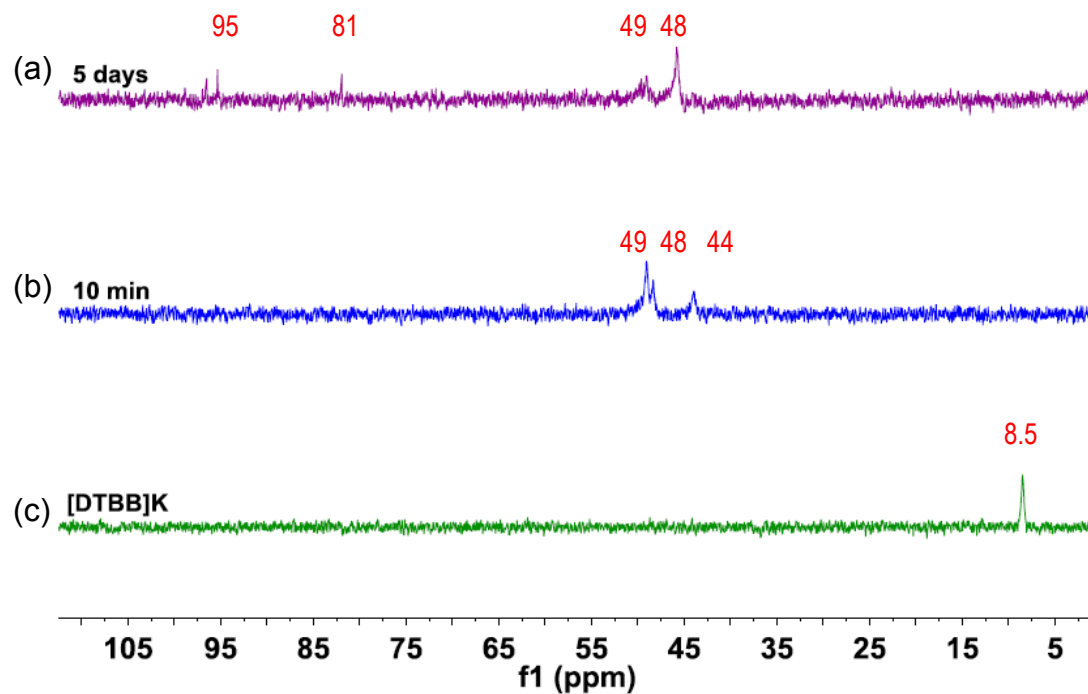


Figure 5.21: ^{31}P NMR (202.40 MHz, benzene- d_6 /THF) (a) 5 days after addition of Me_2SAuCl , b) 10 min after addition and (c) [DTBB]K ligand free.

The reaction mixture was filtered to remove the red solid, but the attempts to solubilize the red powder in common organic solvents were unsuccessful. The slightly yellow solution was left for recrystallization by slow evaporation yielding thin colorless crystals like needles. The X-ray diffraction analysis of the crystals obtained resulted in the oligomeric gold structure shown in Figure 5.23. The structure of species **8** shows the $t\text{Bu}_2\text{P}^-$ groups bridging gold(I) metal centres to form an eight-membered ring with alternating phosphorous and gold atoms.

Gold(I) is known to form oligomers similar to **8**. Indeed, the first gold(I) phosphanyl complex of the type $[\{\text{Au}(\text{PPh}_2)\}_n]$ was reported in 1976.¹⁵⁰ The structure and properties of gold oligomers have sparked the curiosity of many ever since. The aforementioned gold-phosphanyl complex is insoluble and its color, when isolated, depends on the base used in its preparation, which suggests cocrystallization of the base with the complex.¹⁵¹ Nevertheless, to the best of our knowledge and as per September 2015, the structure of **8** has never been reported in the literature.

In 2003 Glueck and collaborators reported the structure of a hexameric cycle with $[t\text{Bu}_2\text{P-Au}]$ units (Figure 5.22).¹⁵² The $\{[\text{Au}(\text{P}t\text{Bu}_2)]_6\}$ complex was formed along with several other species, one of the most abundant secondary products in the reaction mixture was an unidentified species with a ^{31}P resonance at 104.9 ppm. However Glueck *et al* did not provide further details on the structure of such compound.

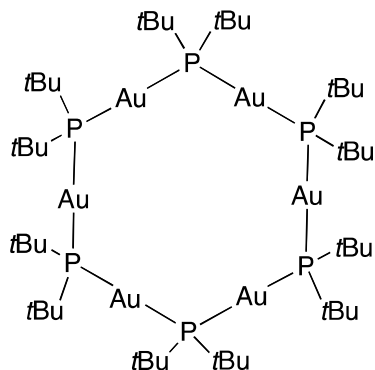


Figure 5.22: Structure of $\{[\text{Au}(\text{P}t\text{Bu}_2)]_6\}$ complex reported by Glueck.¹⁵²

The gold species **8** was obtained by recuperating the colorless crystals from the reaction mixture; these crystals were fully characterized by NMR spectroscopy. Crystals of **8** show a single resonance in ^1H NMR at 1.57 ppm, along with impurities such as $t\text{Bu}_2\text{PH}$, observed by a multiplet at 3.58 ppm. The ^{31}P NMR shows a single resonance at 105.7 ppm, this phosphorous resonance was attributed to the tetrameric species **8**. Interestingly the ^{31}P NMR shift of complex **8** appears to be similar to the unidentified species observed by Glueck.¹⁵²

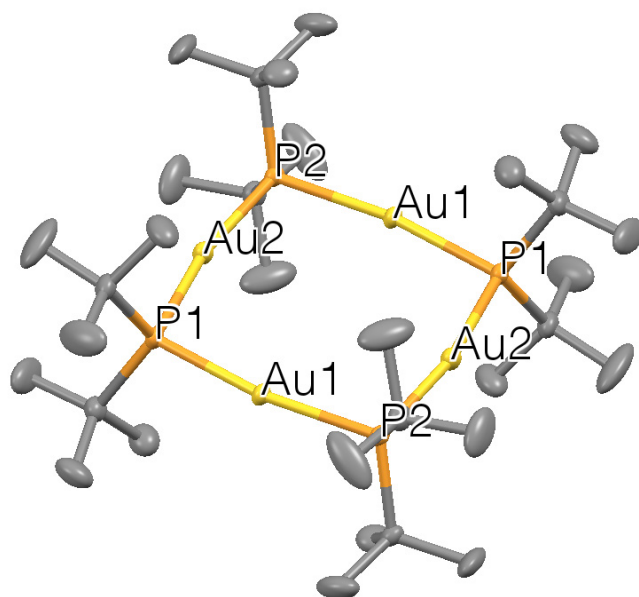


Figure 5.23: X-ray structure of **8**, thermal ellipsoids drawn at the 50% probability level. Hydrogen atoms are omitted for clarity. ($R_1 = 2.62\%$) Selected bond distances (Å) and angles ($^\circ$): P1-Au1 2.328(9); P1-Au2 2.326(1); P2-Au2 2.352(1); Au1-P2 2.328(1); P1-Au1-P2 168.99(4); P2-Au2-P1 168.62(4); C1-P1-C5 114.5(2); C5-P1-Au2 109.5(1); C1-P1-Au1 109.6(1); Au2-P1-Au1 101.88(4); C9-P2-C13 113.3(2); C12-P2-Au2 110.6(1); C9-P2-Au2 110.6(1); Au2-P2-Au1 100.4(5).

The P-Au-P angles are deviating significantly from the linearity, an expected angle for a two coordinated Au(I) species ($168.99(4)$, $168.62(4)^\circ$), which can be attributed to the tension inherent to the oligomeric cycle.¹⁵² The phosphorous atoms display a tetrahedral geometry and the P-Au distances ranging from 2.326(1) to 2.352(1) Å are consistent with the related hexameric species (Figure 5.22).¹⁵²

The distance between Au2-Au2 is of 5.095(1) Å, while that of Au1-Au1 is of 5.075(1) Å, these elongated distances rule out the presence of an aurophilic interaction, which ranges between 2.7 and 3.3 Å.¹⁵³

Details on the nature of the red precipitate, as well as the formation of species **8**, require further investigation. Nevertheless certain trends on gold chemistry can be considered.

Gold has been observed to form π complexes with Cp, however these are supported with a phosphine co-ligand and show an intermediate bonding between η^1 and η^3 .¹⁵⁴ Indeed gold(I) consistently prefers η^1 or η^3 coordination to π systems

over higher hapticities,^{149,155} this is a property that could be explored with boratabenzene ligands, looking for different types of η^1 coordination to gold centres.

On the other hand and unlike the other metals of the group 11, gold(I) has a strong tendency to form metal-metal dimers, oligomers, uni- and multidimensional polymers as well as clusters with almost any donor such as halides, hydroxides, mercaptides, amines, phosphines, arsines, branched alkenes, benzene, carbenium, etc.¹⁵⁶

Moreover heteroleptic L-Au-X compounds can undergo ligand redistribution in solution to form homoleptic isomers $[L_2Au]^+[AuX_2]^-$ which can also form aggregates.¹⁵³ Such interactions can be of interest in the areas of supramolecular chemistry, the formation of braid-like structures¹⁵⁷ as well as the formation of catenanes.¹⁵⁸

5.5 Conclusion

In this chapter we had shown the coordination chemistry of **DTBB** ligand with group 11 metals, a study without precedents.

The discovery of the η^1 -**DTBB** copper complexes further confirms the capability of **DTBB** to stabilize unsaturated metal centres behaving as a highly donor bulky phosphine ligand. The interaction between the phosphorous atom on **DTBB** and the Cu(I) centre is favoured by the soft Lewis acid and base character of both species. The formation of complex **5** featuring a P-Cu-Cl fragment correlates to the well-known affinity of copper to bind phosphine ligands. We had successfully provided spectroscopic characterization of a **DTBB**-CuCl complex; of relevance notably since these species are rarely described in the literature due to their unstable nature.

The linear P-Cu-P interaction observed in **6a** and **6b** sets in evidence the main characteristics of the **DTBB** ligand: the bulkiness and electronic richness of the phosphido-boratabenzene which favours the stabilization of the unsaturated Cu(I) centre in a linear P-Cu-P 14 electron fragment, a scarce geometry observed for copper.

As it has been observed for other Cu(I) species, the stability of the ligand-metal interactions greatly varies according to many factors: the size of the counterions, the inherent properties of the ligand and/or co-ligands present within the coordination sphere and in some cases the interactions with solvent molecules. Hence further investigation on the mechanism of formation of species **5** and its transition to the formation of **6a** is needed.

Silver(I), unlike Cu(I) appears to prefer a coordination to the aromatic ring of boratabenzene rather than through the phosphorous lone pair. The nature of the proposed η^3 interaction might be rooted on the repulsion of the filled *d* orbitals on Ag(I) and the electron rich π system of boratabenzene, as deduced by the proton resonance. The orbitals of the slightly bigger Ag⁺ cation might not overlap with the phosphorous lone pair on **DTBB**, additionally the nature of this interaction is possibly electrostatic, as it has been observed for group 11 species. Hence the

weak interaction with P and B resulting in no observable changes on the ^{31}P and ^{11}B resonances of the reaction mixture. Indeed silver(I) cation is prone to coordination modes such as η^3 or η^4 and it has a very weak preference for higher hapticities such as η^5 .^{148a,149}

Despite the fact that Au(I) preferred coordination mode is consistently η^1 , with a sigma bound organo-gold interaction,^{149,154,159} the reaction of **DTBB** with Au(I) did not afford a metal-bound boratabenzene ligand, instead the P-B bond was cleaved resulting in the formation of **8**, an oligomeric gold complex.

However this result can be correlated with the behaviour observed for the proposed **Cu- η^3 -BCC** species. The calculations show the structure of **Cu- η^3 -BCC** (Section 5.2.2, Figure 5.16) with elongated P-B bonds. This suggest that the complexation of the B=C-C fragment with a group 11 metal would localize the electron density over the allyl-like interaction of the boratabenzene ring. As a result, the electronic density, once shared between the P-B bond, would localize over the B=C-C bonds diminishing the covalent character to the P-B interaction and possibly making the P-B bond labile.

The cleavage of the P-B bond is hence explained by its labilization upon complexation with gold. Using co-ligands to support the metal cation or forcing the interaction by geometrical constraints could possibly lead to stable complexation of boratabenzene moiety to the remaining group 11 elements.

The coordination chemistry of group 11 complexes presented in this chapter is representative of the plethora of interactions between the boratabenzene ligand and transition metals.

5.6 Experimental Details

All manipulations were carried out under inert atmosphere, unless otherwise is specified, using standard Schlenk techniques and inert atmosphere glovebox.

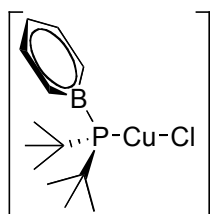
Solvents were distilled under N₂ atmosphere over sodium/benzophenone (THF, hexane) or stirred over Na/K amalgam and vacuum-transferred (benzene-*d*₆), thf-*d*₈ was pre-dried with CaCl₂, degassed using three cycles of freeze-pump-thaw, dried and stored under activated 5 Å molecular sieves. Water used in reactions under inert atmosphere was degassed by three cycles of freeze-pump-thaw prior to bubbling of N₂ for 30 min inside a Schlenk round bottom flask. The volume needed was withdrawn using a purged stainless steel needle and a syringe.

The following reagents were obtained from Sigma Aldrich and used as received: AgCl, Me₂SAuCl, CuCl. The potassium di-*tert*-butyl-phosphidoboratabenzene (**DTBB**) was prepared following the reported procedure.⁵³

Multinuclear NMR spectra were recorded in sealed J. Young NMR tubes on an Agilent Technologies NMR spectrometer, ¹H NMR (500 MHz), ¹³C NMR (125.721 MHz), ³¹P NMR (202.404 MHz), ¹¹B NMR (160.419 MHz). NMR correlation experiments gHSQCAD and gCOSY were used to elucidate ¹³C-¹H, ¹H-¹H correlations. Chemical shifts are quoted in ppm relative to external SiMe₄ (¹H, ¹³C), H₃PO₄ (³¹P), BF₃•Et₂O (¹¹B) references with n-bond *J* couplings being quoted in Hz. NMR signals are referred as (s) singlet, (d) doublet, (t) triplet, (m) multiplet, (dd) double of doublets, etc. It should be noted that due to 3/2 spin of NMR active ¹¹B, the resulting spectra are naturally broad. In addition, spectra of ³¹P nuclei bonded to ¹¹B also experience quadrupolar broadening of their signals, which can often cause imprecise coupling values. Spectroscopic data for **DTBB** can be found in the literature.⁵³

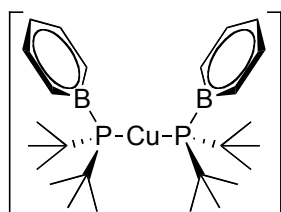
HR-MS spectra were recorded with an Agilent Technologies 6210 LC Time of Flight Mass Spectrometer. Spectra were obtained by direct injection into the nebulizer of solutions of the corresponding species using ESI-MS or APPI-MS ionization in positive and negative modes.

(η^1 -DTBB)CuCl (**5**)



In a vial, inside an inert atmosphere glove box, ligand **DTBB** (4.4 mg, 0.016 mmol) was dissolved in 0.2 mL of THF. In another vial, CuCl (1.7 mg, 0.008 mmol) was dissolved in 0.6 mL of benzene- d_6 . Ligand solution was added to the CuCl suspension using a Pasteur pipette, all at once. Upon addition, the yellow solution was transferred to a J. Young tube and sonicated for 2 h. The solution was then filtered through a Millipore 0.5 μ m filter and transferred to a clean J. Young tube. Volatiles were evaporated and benzene- d_6 was added for characterization. Yield by NMR: 100 %. $^1\text{H NMR}$ (500 MHz, thf- d_8): δ 7.37 (t, J = 8.4, 2H, m -C₅H₄B-*PtBu*₂), 7.07 (d, J = 9.9 Hz, 2H, o -C₅H₄B-*PtBu*₂), 5.51 (t, J = 7.0 Hz, p -C₅H₄B-*PtBu*₂), *tBu*₂-not observed because of overlapping with solvent peak. $^1\text{H NMR}$ (500 MHz, benzene- d_6): δ 7.43 (t, J = 8.7, 8.6 Hz, 2H, m -C₅H₄B-*PtBu*₂), 7.10 (d, J = 9.2 Hz, 2H, o -C₅H₄B-*PtBu*₂), 6.53 (t, J = 6.9, 7.3 Hz, p -C₅H₄B-*PtBu*₂), 1.47 (t, J = 6.5 Hz, 18H, C₅H₄B-*PtBu*₂). $^{13}\text{C NMR}$ (125.72 MHz, benzene- d_6): δ 134.4 (bm, 4C, o -C₅H₄B-*PtBu*₂), 133.3 (t, J = 6.1, 6.4 Hz, 4C, m -C₅H₄B-*PtBu*₂), 115.5 (s, 2C, p -C₅H₄B-*PtBu*₂), 32.8 (t, J = 3.3 Hz, 12C, CH₃), 32.3 (d, J = 6.9 Hz, 2C, C-H). $^{31}\text{P NMR}$ (202.40 MHz, benzene- d_6): δ 17.1 (brs, C₅H₄B-P(*tBu*₂)Cu(*tBu*₂)P-BC₅H₄). $^{11}\text{B NMR}$ (160.41 MHz, benzene- d_6): δ 27.6 (brm, C₅H₄B-P(*tBu*₂)Cu(*tBu*₂)P-BC₅H₄).

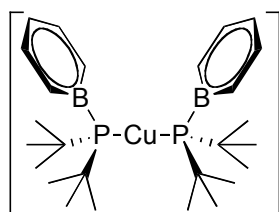
[(η^1 -DTBB)₂Cu]K (**6a**)



Complex **5**, transforms into complex **6a** upon a period of 7 days in benzene- d_6 solution or after 2 hours of sonication the reaction mixture of complex **5**. In a small Schlenk flask, 30 mg (0.135 mmol) of **DTBB** were dissolved in 5 mL of THF. A CuCl (7 mg, 0.068 mmol) solution in C₆H₆ was added by cannula. The reaction mixture was sonicated for 2 hours and all volatiles were removed under vacuum. Yield: 13 mg (35 %). $^1\text{H NMR}$ (500 MHz, benzene- d_6): δ 7.45 (ddd, J = 9.8, 7.1, 2.5 Hz, 4H, m -C₅H₄B-*PtBu*₂), 6.80 (td, J = 7.0, 1.2 Hz, 2H, p -C₅H₄B-*PtBu*₂), 6.76 (dd, J = 9.4, 5.5 Hz, 4H, o -C₅H₄B-*PtBu*₂), 1.26 (d, J = 12.9 Hz, 36H,

$C_5H_4B-PtBu_2$). ^{13}C NMR (125.72 MHz, benzene- d_6): δ 128.3 (signal overlapped with solvent, found by gHSQCAD, $m-C_5H_4B-PtBu_2$), 120.2 (brm, 4C, $o-C_5H_4B-PtBu_2$), 116.1 (s, 2C, $p-C_5H_4B-PtBu_2$), 32.2 (d, $J = 6.48$ Hz, 12C, $C_5H_4B-PtBu_2$), 31.7 (s, 2C, C-H), 31.5 (s, 2C, C-H). ^{31}P NMR (202.40 MHz, benzene- d_6): δ 14.4 (brm, $C_5H_4B-P(tBu_2)Cu(tBu_2)P-BC_5H_4$). ^{11}B NMR (160.41 MHz, benzene- d_6): δ 23.6 (brm, $C_5H_4B-P(tBu_2)Cu(tBu_2)P-BC_5H_4$).

$[(\eta^1-DTBB)_2Cu][Cu(IMes)_2]$ (**6b**)

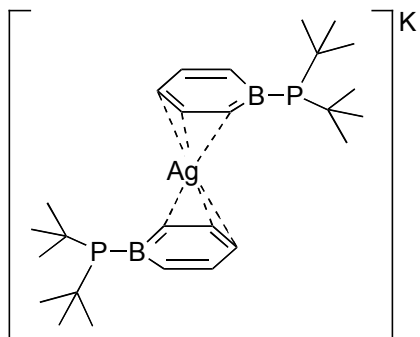


$[Cu(IMes)_2]$ In a vial, inside an inert atmosphere glove box, ligand **DTBB** (5.1 mg, 0.019 mmol) was dissolved in 0.3 mL of THF. In another vial, $(IMes)_2CuCl$ (7.9 mg, 0.019 mmol) was suspended in 0.6 mL of

benzene- d_6 . Ligand solution was added to the metal suspension resulting in a beige solution with a flocculated precipitate. Solid was filtered and solution was evaporated to yield **6b** as a brown powder. Yield by NMR: 100 %. Suitable crystals for X-ray were obtained from a hexane solution at -30 °C.

1H NMR (500 MHz, benzene- d_6): δ 7.94 (m, 4H, $m-C_5H_4B-PtBu_2$), 7.28 (t, $J = 7.1$ Hz, 4H, $o-C_5H_4B-PtBu_2$), 7.06 (t, $J = 8.8$ Hz, 2H, $p-C_5H_4B-PtBu_2$), 6.71 (s, 8H, $m-HMes$), 5.96 (s, 4H, Hmid), 2.09 (s, 12H, p -MethylMes), 1.95 (s, 24H, o -MethylMes), 1.17 (d, $J = 12.5$ Hz, 18H, $C_5H_4B-PtBu_2$). ^{13}C NMR (125.72 MHz, benzene- d_6): δ 134.8 (s, 2C, $p-C_5H_4B-PtBu_2$), 132.9 (d, $J = 14.5$ Hz, 2C, $m-C_5H_4B-PtBu_2$), 129.6 (s, 8C, $m-HMes$), 116.9 (brs, 2C, $o-C_5H_4B-PtBu_2$), 95.1, 32.5 (d, 12C, $J = 6.4$ Hz, $C_5H_4B-PtBu_2$), 32.2 (d, 1C, $J = 6.2$ Hz, $C_5H_4B-PtBu_2$), 32.1 (d, 1C, $J = 16.0$ Hz, $C_5H_4B-PtBu_2$), 21.0 (s, 4C, p -MethylMes), 17.6 (s, 8C, o -MethylMes). ^{31}P NMR (202.40 MHz, benzene- d_6): δ 24.3 (brs, $C_5H_4B-P(tBu_2)Cu(tBu_2)P-BC_5H_4$). ^{11}B NMR (160.41 MHz, benzene- d_6): δ 26.9 (brd, $J = 72.1$ Hz, $C_5H_4B-P(tBu_2)Cu(tBu_2)P-BC_5H_4$).

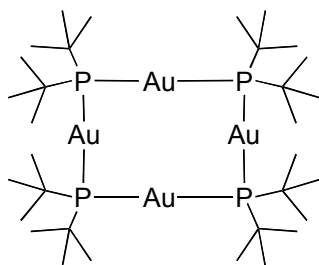
Proposed structure for complex [(DTBB)₂Ag]K (7)



In a vial, ligand **DTBB** (2.9 mg, 0.013 mmol) was dissolved in 0.3 mL of THF. In another vial, AgCl (1.9 mg, 0.013 mmol) was suspended in 0.6 mL of benzene-*d*₆. Ligand solution was added to the metal suspension, resulting in a slightly yellow solution with the presence of a brown precipitate. Upon evaporation of the solvent and re-dissolution in

benzene-*d*₆, decomposition was observed with further formation of brown precipitate. **¹H NMR** (500 MHz, benzene-*d*₆/THF): δ 7.52 (t, *J* = 8.4 Hz, 4H, *m*-C₅H₄B-P*t*Bu₂), 7.19 (m overlapped with solvent, 4H, *o*-C₅H₄B-P*t*Bu₂), 6.55 (t, *J* = 7.0 Hz, 2H, *p*-C₅H₄B-P*t*Bu₂), *t*Bu signals not observed due to overlapping with THF. **³¹P NMR** (202.40 MHz, benzene-*d*₆): δ 7.9 (brs). **¹¹B NMR** (160.41 MHz, benzene-*d*₆): δ 34.6 (brm).

Reaction of DTBB with Me₂SAuCl, [Au₄(μ-η²-PtBu₂)₄] (8)



In a vial, ligand **DTBB** (3.6 mg, 0.013 mmol) was dissolved in 0.3 mL of THF. In another vial, Me₂SAuCl (4.0 mg, 0.013 mmol) was suspended in 0.6 mL of benzene-*d*₆. Ligand solution was added to the metal suspension, resulting in a color change in the solution from pale yellow to bright yellow with instantaneous formation of an

abundant red precipitate. Solid was filtered off and solution was diluted with THF and placed in a diffusion chamber with pentane. Crystals like-needles very thin and transparent were found to be [Au₄(μ-η²-PtBu₂)₄] (**8**). **¹H NMR** (500 MHz, benzene-*d*₆): δ 1.57 (s, 72H, [Au₄(μ-P*t*Bu₂)₄]). **³¹P NMR** (202.40 MHz, benzene-*d*₆): δ 105.7 (s, 4P, [Au₄(μ-P*t*Bu₂)₄]). **¹³C NMR** (125.72 MHz, benzene-*d*₆): δ 110.39, 35.23.

5.6.1 X-Ray Crystallographic Data

Crystals of compounds **6a**, **6b** and **8** were mounted on a glass fibre using Paratone N® hydrocarbon oil. Measurements were made on a Bruker APEX II area detector diffractometer equipped with graphite monochromated MoK α radiation. The program used for retrieving cell parameters and data collection was APEX 2.¹⁶⁰ Data were integrated using the program SAINT,¹⁶¹ and corrected for Lorentz and polarization effects. The structure was solved and refined using SHELXS-97.¹⁶² All non-H atoms were refined anisotropically. The hydrogen atoms were placed at idealized positions.

Crystal data and structure refinement for [Cu(η^1 -DTBB)₂]**K** (6a)

Empirical formula	C ₅₂ H ₉₂ B ₄ Cu ₂ K ₂ P ₄	
Formula weight	1089.65	
Temperature	150(2) K	
Wavelength	0.710773 Å	
Crystal system	Monoclinic	
Space group	P2 ₁ /n	
Unit cell dimensions	a = 17.5823(11) Å	$\alpha = 90^\circ$
	b = 21.9126(14) Å	$\beta = 110.8429(9)^\circ$
	c = 19.5901(12) Å	$\gamma = 90^\circ$
Volume	7053.6(8) Å ³	
Z	4	
Density (calculated)	1.026 mg/m ³	
Absorption coefficient	0.838 mm ⁻¹	
F(000)	2320	
Crystal size	0.320 x 0.220 x 0.200 mm ³	
Theta range for data collection	1.449 to 26.757°	
Index ranges	-22 ≤ h ≤ 22, -27 ≤ k ≤ 27, -24 ≤ l ≤ 24	
Reflections collected	66414	
Independent reflections	150027 [R(int) = 0.0631]	
Completeness to theta = 25.242°	100.0 %	
Absorption correction	Semi-empirical from equivalents	
Max. and min. transmission	0.846 and 0.802	
Refinement method	Full-matrix least-squares on F ²	
Data / restraints / parameters	15027 / 0 / 601	
Goodness-of-fit on F ²	1.002	
Final R indices [I > 2σ(I)]	R1 = 0.0642, wR2 = 0.2088	
R indices (all data)	R1 = 0.0932, wR2 = 0.2325	
Largest diff. peak and hole	2.316 and -0.406 e.Å ⁻³	

Crystal data and structure refinement for [Cu(η^1 -DTBB)₂][Cu(IMes)₂] (6b)

Empirical formula	C ₆₈ H ₉₄ B ₂ Cu ₂ N ₄ P ₂
Formula weight	1178.11
Temperature	150(2) K
Wavelength	0.71073 Å
Crystal system	Monoclinic
Space group	C 2/c
Unit cell dimensions	a = 12.549(2) Å $\alpha = 90^\circ$ b = 35.591(6) Å $\beta = 102.160(3)^\circ$ c = 17.167(3) Å $\gamma = 90^\circ$
Volume	6864(2) Å ³
Z	4
Density (calculated)	1.140 mg/m ³
Absorption coefficient	0.706 mm ⁻¹
F(000)	2512
Crystal size	0.260 x 0.010 x 0.010 mm ³
Theta range for data collection	1742 to 24.990°
Index ranges	-14 ≤ h ≤ 14, -38 ≤ k ≤ 38, -19 ≤ l ≤ 20
Reflections collected	22364
Independent reflections	6032 [R(int) = 0.0646]
Completeness to theta = 25.242°	97.1 %
Absorption correction	Semi-empirical from equivalents
Max. and min. transmission	0.993 and 0.992
Refinement method	Full-matrix least-squares on F ²
Data / restraints / parameters	6032 / 0 / 365
Goodness-of-fit on F ²	1.014
Final R indices [I > 2σ(I)]	R1 = 0.0524, wR2 = 0.1192
R indices (all data)	R1 = 0.0900, wR2 = 0.1351
Largest diff. peak and hole	0.508 and -0.470 e.Å ⁻³

Crystal data and structure refinement for [Au₄(μ-PtBu₂)₄] (8)

Empirical formula	C ₂₃ H ₇₂ Au ₄ P ₄	
Formula weight	1368.64	
Temperature	150(2) K	
Wavelength	0.71073 Å	
Crystal system	Triclinic	
Space group	P-1	
Unit cell dimensions	a = 8.4896(9) Å	α = 68.062(2)°
	b = 11.88717(13) Å	β = 72.623(2)°
	c = 12.2098(14) Å	γ = 84.494(2)°
Volume	1089.2(2) Å ³	
Z	1	
Density (calculated)	2.087 mg/m ³	
Absorption coefficient	13.593 mm ⁻¹	
F(000)	640	
Crystal size	0.20 x 0.02 x 0.02 mm ³	
Theta range for data collection	1.85 to 32.84°	
Index ranges	-12 ≤ h ≤ 12, -17 ≤ k ≤ 18, -18 ≤ l ≤ 18	
Reflections collected	15102	
Independent reflections	7473 [R(int) = 0.0272]	
Completeness to theta = 25.242°	99.9 %	
Absorption correction	Semi-empirical from equivalents	
Max. and min. transmission	0.7622 and 0.729	
Refinement method	Full-matrix least-squares on F ²	
Data / restraints / parameters	7473 / 0 / 193	
Goodness-of-fit on F ²	0.981	
Final R indices [I > 2σ(I)]	R1 = 0.0262, wR2 = 0.0473	
R indices (all data)	R1 = 0.0413, wR2 = 0.0519	
Largest diff. peak and hole	1.407 and -1.050 e.Å ⁻³	

Computational Studies

Calculations were performed using Gaussian 03 suite of programs.¹⁶³ Calculations were carried out at the pseudo relativistic DFT level of theory using the hybrid functional B3PW91,¹⁶⁴ and the basis set 6-311G(*p,d*).¹⁶⁵ Geometry optimizations were carried out without any symmetry restrictions, and the nature of the extremum (minimum) was verified with analytical frequency calculations.

6 Chapter 6 Phosphidoboratabenzene-Rhodium(I) Complexes as Catalysts for the Hydrogenation of Alkenes at Room Temperature and Atmospheric Pressure

The results presented in the following chapter have been accepted for publication in the journal *Dalton Transactions* (*Dalton Trans.*, **2016**, *45*, 2130-2137). Modifications on the numbering of the compounds, figures and tables of the paper have been done in order to fit the sequence of the dissertation.

6.1 Context of the Research

Within the framework of this dissertation we have shown how the **DTBB** ligand has a variety of coordination modes and how this can be modulated accordingly to the metal precursor in terms of its electronic needs and steric effects from the ligand. Interestingly unlike the η^1 species presented in Chapter 5, the Rh(I) center is stabilized by the **DTBB** capability to coordinate through the aromatic ring as well as through the phosphorous atom, yielding a dimeric structure. The hemilability of the ligand has also been demonstrated in Chapter 4 with the iron ferrocenyl like phosphine.

Considering that only Ni and Pt complexes of **DTBB** are known, it becomes clear that the study of the coordination chemistry and reactivity of **DTBB** ligand has not been fully explored yet, in fact to the best of our knowledge only the coordination with group 10 metals, reported by our group, exist in the literature, while similar ligands such as **DPB** had been reported to coordinate with Zr, Fe, Rh and more recently with Sm.¹⁶⁶

Moreover, the reactivity of **DTBB** with group 9 metals has not been previously studied. It is however interesting considering the number of catalytic applications group 9 metals like rhodium have in relevant chemical transformations. Additionally with the promise of the expansion of the catalytic applications of boratabenzene complexes to other than polymerization, the use of a rhodium complex to carry the

hydrogenation of alkenes and alkynes at room temperature and atmospheric pressure becomes an interesting alternative.

6.2 Abstract

The di-*tert*-butylphosphido-boratabenzene ligand (**DTBB**) reacts with $[(C_2H_4)_2RhCl]_2$ yielding the dimeric species $[(C_2H_4)_2Rh(DTBB)]_2$ (**9**). This species was fully characterized by multinuclear NMR and X-ray crystallography. Complex **9** readily dissociates ethylene in solution and upon exposure to 1 atm of H_2 is capable of carrying out the hydrogenation of ethylene. The characterization of two Rh-H species by multinuclear NMR spectroscopy is provided. The reactivity of **9** towards the catalytic hydrogenation of alkenes and alkynes at room temperature and 1 atm of H_2 is reported and compared to the activity of Wilkinson's catalyst under the same reaction conditions.

6.3 Résumé

Le ligand di-*tert*-butylphosphido-boratabenzene (**DTBB**) réagit avec $[(C_2H_4)_2RhCl]_2$ donnant le dimère $[(C_2H_4)_2Rh(DTBB)]_2$ (**9**). Cette espèce a été totalement caractérisée par RMN multinucléaire et cristallographie des rayons X. Le complexe **9** est capable de dissocier l'éthylène facilement en solution et après l'exposition à 1 atm de H_2 est capable d'effectuer l'hydrogénation de l'éthylène. La caractérisation de deux espèces Rh-H par spectroscopie RMN multinucléaire est fournie. La réactivité du complexe **9** vers l'hydrogénation catalytique d'alcènes et d'alcynes à la température ambiante et 1 atm de H_2 est rapportée et comparée à l'activité de catalyseur de Wilkinson dans les mêmes conditions de réaction.

6.4 Introduction

Since the first report of a boratabenzene complex by Herberich,³¹ this heterocyclic moiety has been coordinated to most transition metals, either as a neutral borabenzene^{34,167} or an anionic boratabenzene ligand (Figure 6.1, **I** and **II**).¹⁶⁸ Borabenzene derivatives and their metal complexes have been shown to be active in the polymerization of alkenes,^{55a,d,e,f,57,169} the cyclotrimerization of alkynes and nitriles,⁵⁴ E-H bond activation,^{58,60} acting as a chirality source¹⁷⁰ and generating interesting optoelectronic materials.^{41,158b,171}

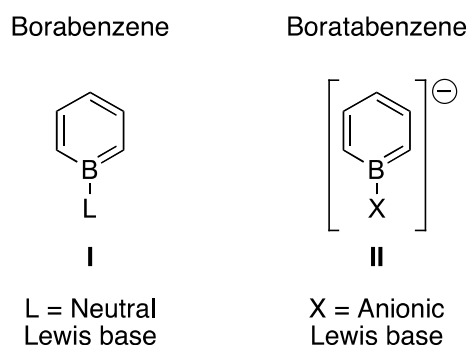


Figure 6.1: Neutral and anionic boron heterocycles.³¹⁻³⁸

The boratabenzene framework is an isoelectronic analogue of the cyclopentadienyl ligand and as such, interacts with transition metals by its π system and usually adopts a η^6 -coordination mode.^{32b,37b,45,172} Ring slippage to the η^5 -coordination where the boron is away from the metal centre is however frequent, specially when facilitated by π -donating¹⁷³ or bulky substituents on boron.⁴⁴ Other types of hapticities are more scarce and include η^3 -allylic-like coordination^{47,53} and η^1 -coordination where the substituent on boron interacts with the transition metal. Two different boratabenzene moieties have been shown to exhibit the latter coordination mode, including species **III** (Figure 6.2) having a unique Pt-Cl-B interaction.⁴⁸ Upon addition of a Lewis base, the Cl-boratabenzene anion can dissociate and undergo ligand exchange⁴⁹ or coordinate to other transition metals.⁴³ This atypical coordination mode is also observed for the diphenylphosphido-boratabenzene, first reported by Fu,²³ an anionic analogue of

the ubiquitous PPh_3 , where the lone pair on phosphorous remains available for σ -donation, as observed in Rh complex **IV** (Figure 6.2).

Our group reported in 2012 the synthesis of di-*tert*-butylphosphido-boratabenzene (**DTBB**), a ligand designed to act as a bulky and anionic phosphine. It was shown that the **DTBB** fragment does not coordinate in a purely η^1 -mode on electronically unsaturated metal centres. Instead, in addition to the phosphine binding one metal, it was possible to coordinate the **DTBB** ligand by the aromatic ring in a η^6 -fashion on another nickel centre in species **VI**. **DTBB** also coordinated in a η^3 allylic-like mode, through a P-B-C interaction with Pt(II) (**V**).⁵³ It is precisely the hemilability of the **DTBB** and its donor capability as a bulky phosphine that makes it an attractive framework for catalytic applications.¹⁷⁴ Herein we report the synthesis and characterization of a rhodium di-*tert*-butyl-phosphidoboratabenzene complex and its catalytic activity towards alkene hydrogenation at room temperature and atmospheric pressure.

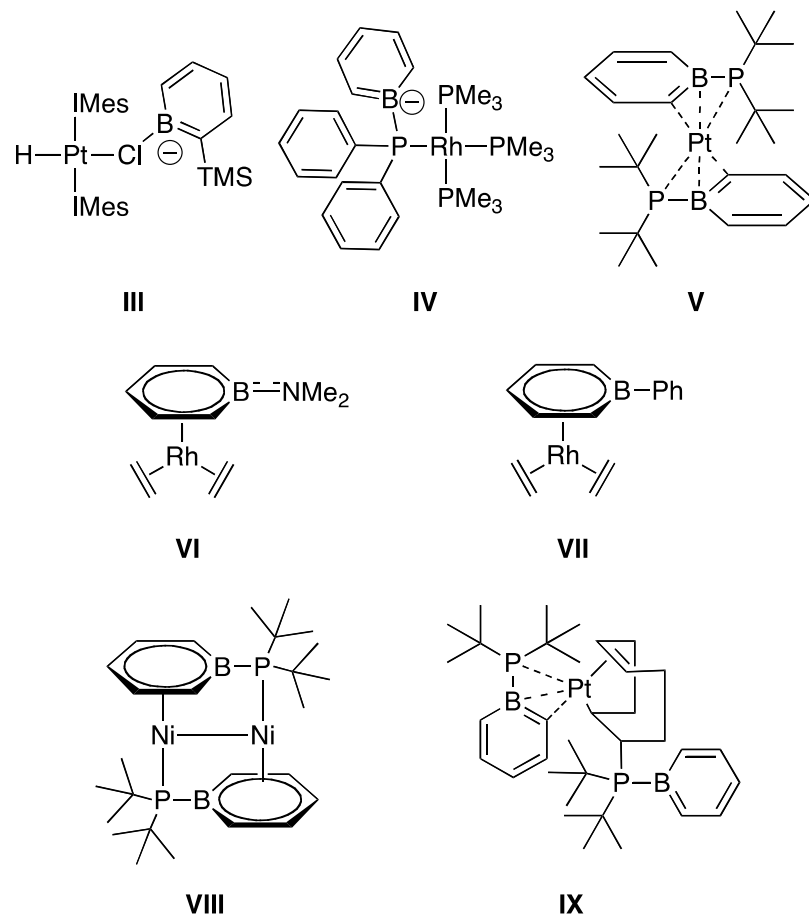
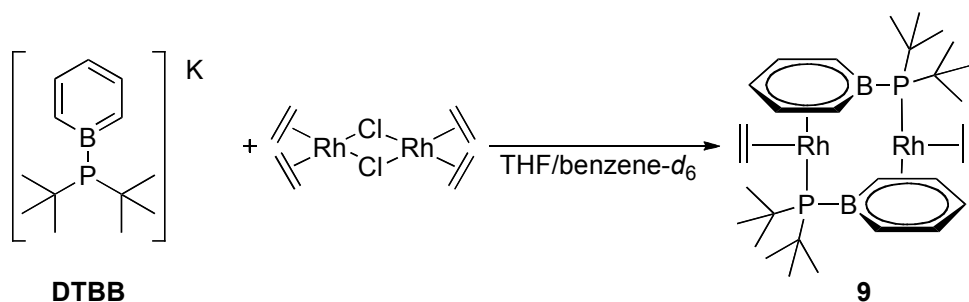


Figure 6.2: Some borabenzene species related to this study: $[(\text{IMes})_2\text{Pt}(\text{H})(1\text{-Cl-2-SiMe}_3\text{-BC}_5\text{H}_4)]$ (**III**),⁴⁸ $\text{Rh}(\text{PMe}_3)_3(\text{DPB})$ (**IV**),²³ $\text{Pt}(\text{DTBB})_2$ (**V**),⁴⁷ $[(\text{C}_2\text{H}_4)_2\text{Rh}(\text{C}_5\text{H}_5\text{B-NMe}_2)]$ (**VI**),⁵⁸ $[(\text{C}_2\text{H}_4)_2\text{Rh}(\text{C}_5\text{H}_5\text{B-Ph})]$ (**VII**),⁵⁸ $[\text{Ni}_2(\text{DTBB})_2]$ (**VIII**) and $[\eta^3\text{-(C,B,P)-C}_5\text{H}_5\text{BP}(\text{tBu})_2(\kappa\text{-}\eta^2\text{:}\eta^1\text{-C}_8\text{H}_{12}(\text{P}(\text{tBu})_2\text{BC}_5\text{H}_5)\text{Pt})]$ (**IX**).⁵³

6.5 Results and Discussion

The reaction of 2.2 equiv. of ligand **DTBB** with $[\text{RhCl}(\text{C}_2\text{H}_4)_2]_2$ in a benzene/THF mixture at room temperature, followed by removal of volatiles and extraction with diethyl ether, provided complex **9** as a red-brown crystalline powder in 40% yield (Scheme 6.1).



Scheme 6.1: Synthesis of $[(\text{C}_2\text{H}_4)\text{Rh}(\text{DTBB})]_2$ (**9**).

Crystalline red needles, suitable for X-ray diffraction studies were obtained from the slow evaporation of a benzene- d_6 solution of **9**. The bimetallic complex crystallized in a monoclinic $P2_1/n$ space group (Table S2, Supporting Information, also available in Section 6.7). Species **9** was confirmed to be a centrosymmetric dimer where each of the two **DTBB** ligands bridges two rhodium(I) centres, with the boratabenzene moiety binding in a η^6 -fashion to one Rh(I) and the lone pair of the phosphine coordination the other metal centre. A η^2 -ethylene molecule is completing the 18-electron count of each rhodium (Figure 6.3).

The homobimetallic species has a B-Rh distance of 2.510(4) Å, which is larger than in related π -boratabenzene complex $[(\text{C}_5\text{H}_5\text{BPh})\text{Rh}(\text{CH}_2\text{CH}_2)_2]$ (**IX**) which has a B-Rh distance of 2.398(4) Å.⁴⁷ The B-Rh distance in **9** is somewhat comparable to species $[(\text{C}_5\text{H}_5\text{BNMe}_2)\text{Rh}(\text{CH}_2\text{CH}_2)_2]$ (**VIII**), which has a B-Rh bond length of 2.521(2) Å,⁵⁸ despite the fact that there is no π -bonding between P-B since the lone pair on phosphorous is engaged in a bond with one metal centre.⁵⁰ Interestingly, complex **9** displays some asymmetry in the coordination of the boratabenzene moiety since one of the Rh-C_{ortho} bond is significantly elongated (Rh-C(1) = 2.435(3) Å) compared to the other Rh-C_{ortho} bond (Rh-C(5) = 2.237(3) Å), suggesting that the heterocyclic moiety might be closer to an η^4 -coordination

rather than a typical η^6 -coordination (Figure 6.3).^{32,76,175} The C=C bond length for the ethylene molecule is 1.370(6) Å and the Rh-C_{ethylene} distances are very similar (2.121(4) and 2.140(4) Å). These values compare well to those observed in species **IX** (Rh-C_{ethylene} = 2.145(4), 2.143(4) Å and C=C = 1.385(6) Å).⁵⁸ Finally, the Rh-bound phosphine ligand retains its tetrahedral geometry, as expected. Whereas most of the angles around phosphorous are close to the expected value for a tetrahedral centre, the B-P-C(8) angle of 97.2(2)° is smaller than 109° and diverts significantly from the related angle in the metal-free ligand (108.6(2)°).⁵³

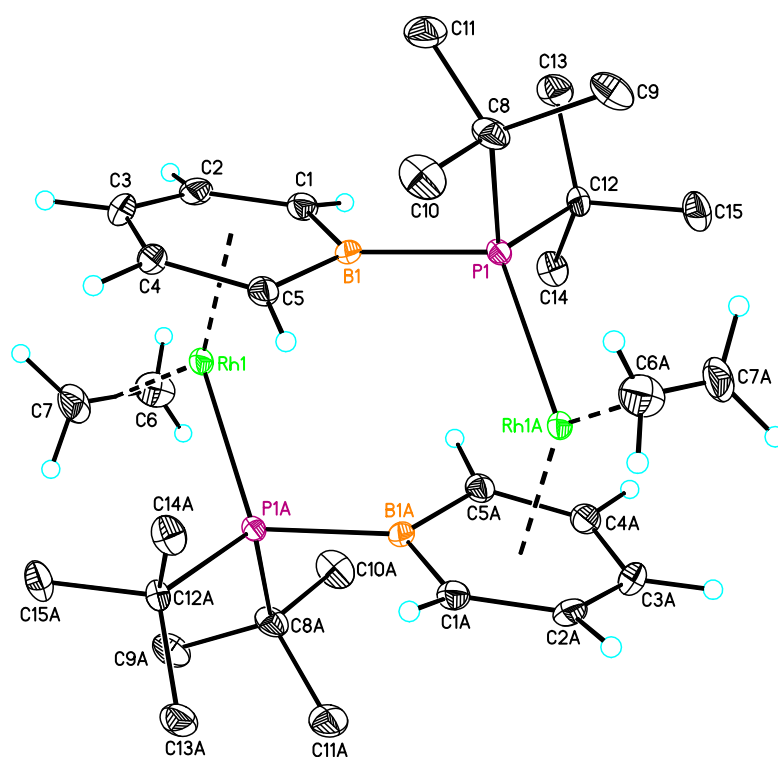


Figure 6.3: ORTEP plot of **9** with thermal ellipsoids set at the 50% probability level. H atoms are shown as spheres with arbitrary radii. H atoms on all methyl groups are omitted for clarity. Symmetry transformations used to generate equivalent atoms: A: $-x+1, -y, -z+1$. Selected bond distances [Å] and angles [deg]: P1-B1 1.962(4), B1-Rh1 2.510(4), Rh1-P1 2.3226(9), Rh1-C1 2.435(3), Rh1-C2 2.267(4), Rh1-C3 2.259(3), Rh1-C4 2.259(4), Rh1-C5 2.237(3), Rh1-C6 2.140(4), Rh1-C7 2.131(4); Rh1-P1-C12 110.8(1), Rh1-P1-C8 118.4(1), Rh-P1-B1 112.4(1), C8-P1-C12 108.6(2), B1-P1-C8 97.2(2), B1-P1-C12 108.6(2), C7-Rh1-P1 97.8(1), C6-Rh1-P1 100.3(1), Rh1-B1-P1 145.3(2), B1-Rh1-P1 100.63(9), C1-B1-C5 113.9(3), B1-Rh1-C7 161.2(1), B1-Rh1-C6 133.6(1).

The multinuclear NMR characterization confirmed the presence of **9** in solution. The similarity between the boratabenzene proton resonances in the ^1H NMR spectrum for **9** at $\delta = 5.95$, 5.55 and 4.48 for the *ortho*, *meta* and *para* positions, respectively, with the ones observed for rhodium complexes **VII** ($\delta = 5.82$ *ortho*, 4.87 *meta*, 4.27 *para*) and **IX** ($\delta = 6.0$ *ortho* and *meta*, 4.34 *para*) suggest similar η^6 coordination modes.⁵⁸ Both the *ortho* and *meta* protons appear as a single resonance in the ^1H NMR spectrum, as expected for a symmetric coordination of the heterocycles to the metal centre in **9**, suggesting that the asymmetry present at the solid-state is not observed in solution at room temperature. As expected, the *t*Bu₂P- fragment is present as a doublet at 1.34 ppm ($^3J_{\text{HP}} = 11.6$ Hz). Two resonances observed at 3.00 ($J = 11.7, 2.2$ Hz) and 2.74 ppm ($J = 12.0, 2.2$ Hz) put in evidence the presence of an ethylene ligand in the coordination sphere. Regardless of the high donor capability of **DTBB**, which should allow the metal to be more electron rich and engaging more efficiently into back-donation with a π -coordinated alkene ligand, the ethylene protons on complex **9** are observed to be less shielded compared to those previously reported for Rh(I)- η^6 -boratabenzene species ($\delta = 2.19$ for **VIII** and $1.22, 2.82$ for **IX**).

The broad doublet observed in the ^{31}P NMR spectrum at 23.7 ppm and the J_{PRh} value of 160 Hz support the coordination of the phosphorous atom on a rhodium(I) centre. Only one resonance is observed because of the presence of a centre of symmetry on the complex. The chemical shift is significantly different than the one observed for the nickel species **VIII** (-8.9 ppm). In contrast, the complexes where the **DTBB** ligand is η^3 -coordinated to Pt exhibit similar resonances at 31.9 and 37.2 ppm for **V** and **VII**, respectively.

Boratabenzene species **VIII** and **IX**, having ethylene ligands, were shown to exhibit dynamic behaviour attributed to the rotation of ethylene, as confirmed by variable temperature NMR experiments.⁵⁸ However, it was not possible to observe ethylene rotation with species **9** because of the dissociation of the ethylene molecules observed when dissolved in solution. When the solution reached 40 °C, the broadening of the aromatic and ethylene resonances was observed but the rate of ethylene dissociation was significant as suggested by the increase in intensity of

the singlet at 5.2 ppm. Traces of unidentified products were observed spectroscopically along with some precipitate, suggesting that degradation was taking place. Therefore complex **9** was stored at -30 °C and protected from light, since Rh ethylene species such as $\text{CpRh}(\text{C}_2\text{H}_4)_2$ have been shown to undergo rearrangements under photochemical conditions.^{176,177}

6.5.1 Reactivity of **9** with H_2

Whereas some preliminary studies have been done on the reactivity of species **IV** and $[(\text{COD})\text{Rh}(\text{C}_5\text{H}_5\text{B-L})][\text{OTs}]$ ($\text{L} = \text{Py}$, PMe_3 ; $\text{OTs} = \text{CH}_3\text{C}_6\text{H}_4\text{SO}_3^-$) with hydrogen suggesting that rhodium hydride species have been generated, no details were given on the characterization and reactivity of these compounds.^{23,178}

We were able to show that complex **9** reacts with 1 atm of H_2 to generate free ethylene and ethane, observed as resonances at $\delta = 5.20$ and 0.90, respectively, by ^1H NMR spectroscopy. As mentioned above, it should be noted that free ethylene is always observed when **9** is dissolved in solution, along with uncharacterized species. When H_2 is allowed to react with **9** over a period of 3 h in an airtight J.-Young NMR tube, two hydride resonances, attributed to two different species, were observed at -13.94 (**10**) and -17.83 ppm (**11**), along with new aromatic resonances. It was unfortunately impossible in our hand to isolate these two compounds in the solid state. It should be noted that even when handled under strict anhydrous and air free conditions, the presence of precipitate was observed (evidenced by a modification in the integration for the *t*Bu moieties by ^1H NMR) along with small amounts of the phosphine oxide $t\text{Bu}_2\text{PH}(\text{O})$ ($^{31}\text{P}\{^1\text{H}\} \delta = 61.6$; ^1H (benzene- d_6) = 0.99 (d, 18H, *t*Bu₂), 5.82 (d, 1H, *t*Bu₂PH)),¹⁰⁴ which might be caused by traces of water or oxygen in the molecular hydrogen. It is however possible to obtain selectively each hydride as main species in solution depending on the reaction conditions. When left for a period of 3 days under a hydrogen atmosphere, species **10** was the main species observed in solution. However, when the solvent of a solution containing both **10** and **11** was removed under reduced pressure and the oily solid residue was dissolved back under a nitrogen atmosphere, only species **11** was observed. It proved impossible to revert from **11**

to **10** under atmosphere of hydrogen. All attempts to obtain a crystalline solid from solutions of **10** and **11** failed.

As mentioned above, a hydride resonance appearing as a doublet of doublets at δ -13.94 with two distinct coupling constants of 23.3 and 21.3 Hz is characteristic of species **10** by ^1H NMR spectroscopy (Figure 6.4). Aromatic resonances were also observed at δ = 6.00 (t, *meta*), 5.78 (dd, *ortho*) and 5.38 (t, *para*), along with a doublet at 1.35 ppm. The integration ratio of the hydride and of the aromatic resonances demonstrates that there are two hydrides per boratabenzene moiety. The similarity of the splitting pattern of **11** shows a very broad multiplet at \approx 52 ppm. The lack of intensity of the $^{31}\text{P}\{^1\text{H}\}$ resonance, even after an acquisition of 1 hour at -90 °C, suggests that in addition of the broadness caused by the ^{11}B quadrupolar moment and the coupling with the ^{103}Rh nuclei, some rapid fluxional process also takes place. The same problem was observed by $^{11}\text{B}\{^1\text{H}\}$ NMR spectroscopy where after 12 hour of acquisition (over 34 000 scans) no discernible resonance was observed. It should be noted that the difficulty in acquiring good ^{11}B NMR spectra has been previously observed for boratabenzene complexes.⁴⁸ Nevertheless, it was possible to confirm that the $^{31}\text{P}\{^1\text{H}\}$ resonance at 52 ppm was indeed for species **10** by the acquisition of a $^1\text{H}\{^{31}\text{P}\}$ spectrum with selective decoupling at the latter frequency. Indeed, the hydride resonance at -13.94 ppm was observed as a doublet of 23.4 Hz, attributed to a Rh-H interaction, therefore confirming that the 21.2 Hz coupling constant corresponds to a $J_{\text{P-H}}$. It was further confirmed that the *ortho* proton of the boratabenzene moiety, previously observed as a triplet, was now a doublet of 9.3 Hz and that the doublet at 1.37 ppm for the *t*Bu groups was now a singlet.

The ^1H NMR hydride resonance at -17.83 ppm for species **11** (Figure 6.4) also exhibits two distinct coupling constants of 21.5 and 14.6 Hz. However, five distinct resonances at δ = 6.25 (overlapped, 2H), 6.03, 4.95 and 4.80, can be observed for the boratabenzene moiety, suggesting a loss of symmetry of the complex in solution. It is noteworthy to mention that the integration ratio observed is now of 1:1 between the hydride and the boratabenzene resonances. Carrying a $^1\text{H}\{^{31}\text{P}\}$ NMR experiment by selectively decoupling the ill-defined ^{31}P resonance of **5** at 54 ppm

did show that the doublet of doublets at -17.83 ppm in the ^1H NMR spectrum now appeared as a doublet of 15.9 Hz, which can be attributed to a $J_{\text{Rh-H}}$. Additionally, two resonances in the aliphatic region, attributed to the *t*Bu groups, were observed as singlets at 1.46 and 1.29 ppm rather than doublets.

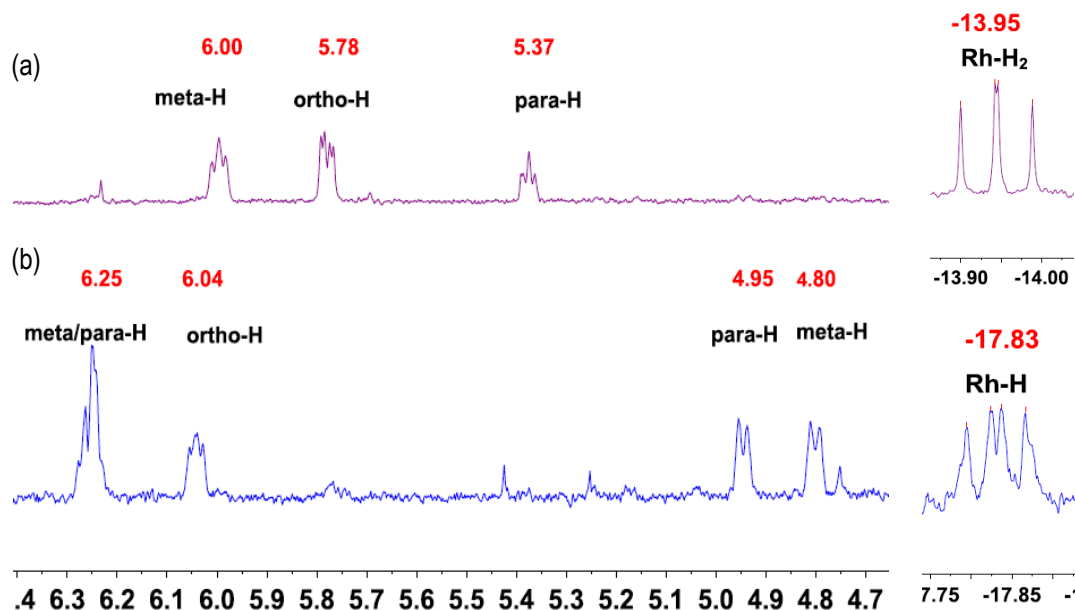


Figure 6.4: Selected region of the ^1H NMR spectra (benzene- d_6 , 500 MHz) for the boratabenzene and high field Rh-H resonances for hydride **10** (a) and **11** (b).

It should also be noted that it was very difficult to obtain good NMR spectra for the elements other than proton regardless of the concentration of the sample and the acquisition time.

For example, when carrying $^{13}\text{C}\{^1\text{H}\}$ NMR experiments with 12 hour acquisition for **10** and **11**, no resonance other than the one for the *t*Bu group were observed. HSQCAD and gHMBCAD correlation experiments also proved unsuccessful for both hydride species.

T_1 measurements were nevertheless informative regarding the bonding mode of hydrogen to metal centres since they can help discriminating between bridging and terminal hydrides, or put in evidence non-classical sigma bonded H_2 .^{65a,67b179} Species **10** shows a minimum T_1 of 4.49 s at 183 K in toluene- d_8 on a 500 MHz spectrometer. At 283 K, the T_1 value was 8.62 s. On the other hand, the minimum

T_1 value for **11** is 6.35 s at 183 K in toluene- d_8 and a maximum of 6.75 s at 295 K (Table 6.1). Dipole-dipole relaxation for classical metal hydrides lies in the range of seconds, while dihydrogen complexes show a much shorter T_1 in the range of 4-100 ms.^{177,179,180} On this basis, because **10** and **11** display long T_1 dipole relaxation times, the existence of a H-H bond can be ruled out.

Table 6.1: T_1 (s) measurements for complexes [(DTBB)Rh(H) $_2$] $_2$ (**10**) and [(DTBB)Rh(H)] $_2$ (**11**) at different temperatures. This table was originally included in the supported information of the publication.

Temperature (K)	10 T_1 (s) ^a	11 T_1 (s) ^a
183	4.49	4.81
193	5.30	5.35
203	5.70	6.41
213	6.58	6.02
223	6.77	6.16
233	7.91	6.25
243	7.42	5.38
253	7.56	5.60
263	7.75	6.18
273	8.13	7.01
283	8.62	6.34
295	0.87 ^b	6.75

^aAll measurements were carried in a 500 MHz NMR in toluene- d_8 , 5 seconds were allowed between each pulse to avoid NOE effects. ^bMeasurement in benzene- d_6 .

Based on its spectral properties and on the structure of precursor **9**, one can propose **10** to be a classical Rh(III) dihydride species [(DTBB)Rh(H) $_2$] $_2$ (Figure 6.5).

Indeed, the spectral properties of the hydride at -13.94 ppm with a $J_{\text{H-Rh}}$ coupling constant of 23.2 Hz are very similar to those of $[\text{Cp}^*\text{Rh}(\text{PMe}_3)(\text{H})_2]$ (-13.65 PPM, dd, $J_{\text{Rh-H}} = 29.8$ Hz, $J_{\text{P-H}} = 41.8$ Hz)^{181a,b} and $[\text{CpRh}(\text{P}i\text{Pr}_3)(\text{H})_2]$ (-14.73 ppm, dd, $J_{\text{Rh-H}} = 27.5$ Hz, $J_{\text{P-H}} = 33.5$ Hz).^{181c}

It should be noted that only species **11** remains when a mixture of **10** and **11** are put under reduced pressure. Interestingly, species **11** is shown to have two hydrogen atoms less than species **10** according to ^1H NMR spectroscopy. The ^1H NMR chemical shift of the hydride is more shielded and the $J_{\text{Rh-H}}$ coupling of **11** is significantly smaller compared to **10**. Several cyclopentadienyl rhodium hydride species have been shown to have similar spectroscopic features when the complexes were cationic^{180c,182} or when the hydrides were bridging,^{180a,181c} which is not expected to occur for **11** since no ionization source was added and triplet would be observed in the case of a hydride bridging two active ^{103}Rh centres. The most likely speculation as for the structure of **11** (Figure 6.5) would be a dimeric Rh(II) species having a Rh-Rh interaction and one hydride on each metal. Because of the Rh-Rh interaction and the limited flexibility one might imagine for such complex, the asymmetry observed in the coordination mode of the boratabenzene moiety in the crystal structure of **9** could be present in **11** and kept “locked” in solution, something that was not observed for the ethylene complex. Thereby, a centre of symmetry might be present for **11** but each proton of the boratabenzene would remain inequivalent. However, several other conformations are possible for this species, especially since **DTBB** was shown to have very rich coordination chemistry.

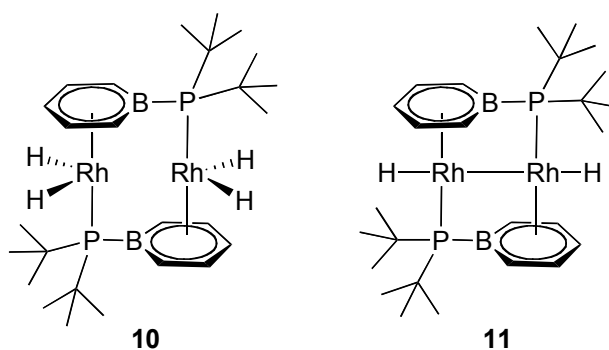
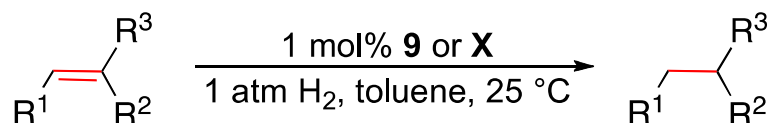


Figure 6.5: Proposed molecular structures for hydride species $[(\text{DTBB})\text{Rh}(\text{H})_2]_2$ (**10**) and $[(\text{DTBB})\text{Rh}(\text{H})]_2$ (**11**).

6.5.2 Hydrogenation of Alkenes by Complex **9**

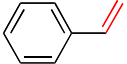
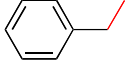
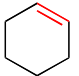
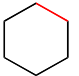
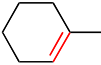
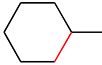


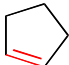
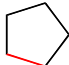
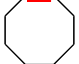



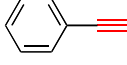
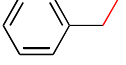
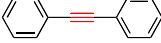
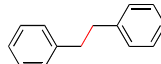
Boratabenzene complexes reported by Bazan⁵⁸ were shown to effectively catalyze the C-H activation of octane. However the activity quickly decays overtime due to the low thermal stability of the complex. Because of the activity of species **9** at ambient temperature and pressure with hydrogen, we were interested in looking at the possibility for **9** to act as an alkene hydrogenation catalyst (Scheme 6.2). Although several rhodium complexes are known to be efficient catalysts for the hydrogenation of olefins, to our knowledge no boratabenzene complex has been studied for such transformation. Furthermore, very few studies have been done in the homogeneous hydrogenation of alkenes at ambient temperature and pressure.¹⁸³ For comparison purpose, the activity of Wilkinson's catalyst $\text{CIRh}(\text{PPh}_3)_3$ (**X**) was also investigated in the same mild conditions.



Scheme 6.2: Catalytic hydrogenation of alkenes.

Table 6.2 shows the activity of catalyst **9** and **X** for the hydrogenation of alkenes and alkynes, at room temperature and ≈ 1 atm of H₂. It can be observed that for most of the substrates the conversions obtained for the hydrogenation of alkenes are similar when comparing **9** to **X**. In the case of styrene and cyclohexene the conversion yields are of 29 and 20%, respectively, using **9** as a catalyst (entries 1 and 2).

Table 6.2: Hydrogenation of alkenes and alkynes using **9** and Wilkinson's catalyst (**X**).

Entry	Substrate	Product	% Conversion ^a
(1)			9 : 29% X : 27%
(2)			9 : 20% X : 30%
(3)			9 : 84% X : 100%
(4)			9 : 73% X : 100%
(5)			9 : 43% X : 90%
(6)			9 : 12% X : 19%
(7)			9 : 24% X : 26%
(8)			9 : 2% X : 3%
(9)			9 : 21% X : 13%

^a Conversion determined by GC-FID after 24 h of reaction.

The conversion is significantly higher with 1-methyl-cyclohexene and 1-octene, with 84% and 73% yield, although the conversion is complete when using Wilkinson's catalyst in both entries (entries 3 and 4). A significant difference is observed for the hydrogenation of cyclopentene, where the hydrogenation using **9** is half of what is observed using **X** (43 vs. 90%, respectively; entry 5). In the case of cyclooctene, both catalyst **9** and **X** give poor yields (entry 6). The hydrogenation of alkynes is also possible, although the conversion is relatively low (2 and 21 % for phenyl- and diphenylacetylene, respectively). It should be noted that it is

possible to observe by NMR spectroscopy that the alkenes are generated during the hydrogenation of alkynes, suggesting that the hydrogenation is occurring through sequential steps. Therefore, the reactivity of species **9** as a precatalyst for the hydrogenation of alkenes and alkynes follow the trend reported for Wilkinson's catalyst.^{183b} It should be noted that according to ¹H NMR species **10** is no longer present when catalysis starts whereas species **11** remains throughout catalysis. However, since some degradation products are present throughout catalysis, it is difficult to confirm which species is acting as catalyst.

6.6 Conclusions

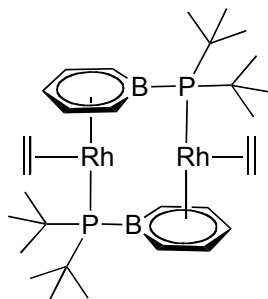
We have carried out the synthesis of species $[(C_2H_4)Rh(DTBB)]_2$ where the **DTBB** moiety bridges two rhodium centre by a η^6 -coordination of the boratabenzene moiety and by the lone pair on phosphorous. In the latter complex, the ethylene ligand proves to be quite labile. Under a hydrogen atmosphere, complex **9** transforms into complex **10** and **11** having respectively two and one hydride per metal centre, according to multinuclear NMR spectroscopy. Interestingly, complex **9** can serve as a precatalyst for the hydrogenation of alkenes and alkynes at ambient temperature and pressure. Interestingly, the activity observed is very similar to the one observed for Wilkinson's catalyst in similar conditions, even if formally the metal in **9** does not exhibit the same unsaturation observed for the ubiquitous $CIRh(PPh)_3$ catalyst. It can be therefore proposed that in order for catalysis to occur, the **DTBB** ligand needs to present some hemilability in order to open up coordination sites. Although the **DTBB** exhibits a rich and diverse coordination chemistry, its usefulness as a ligand for catalysis seems to be impeded by the sensitivity of the P-B bond to hydrolysis and/or oxidation, which we are currently studying in more detail.

6.7 Experimental Section

General Considerations

All manipulations were carried under inert atmosphere of nitrogen using either Schlenk line techniques or a MBraun glovebox. THF and Et₂O were distilled under N₂ atmosphere over sodium/benzophenone; toluene, benzene, benzene-*d*₆, toluene-*d*₈, alkenes, alkynes and alkanes were pre-treated with Na/K alloy and vacuum transferred or distilled. **DTBB** was prepared according to a literature precedent.⁴⁷ Wilkinson catalyst, alkenes and alkanes were purchased from Sigma-Aldrich [RhCl(C₂H₄)₂]₂ was purchased from Praxair. NMR spectra were recorded in a sealed J.-Young quartz NMR tube on an Agilent Technologies NMR spectrometer, ¹H NMR (500 MHz), ¹³C NMR (125.721 MHz), ³¹P NMR (202.404 MHz), ¹¹B NMR (160.419 MHz). The coupling constants (*J*) should be considered as an average with standard deviation of ±0.2 Hz. 2D NMR *g*HSQCAD, and *g*COSY experiments were used to elucidate ¹³C-¹H and ¹H-¹H correlations. FTIR spectra were obtained with a Nicolet Bomem Magna-850. The solid was suspended in Nujol previously degassed by bubbling N₂ and the sample was prepared inside an inert atmosphere glove box. GC-FID was carried out using a Thermo Scientific trace GC ultra coupled with an ITQ 900 mass spectrometer using electronic impact ionization (EI), standard curves of the corresponding alkanes were used to calculate the concentration in ppm, internal standards were used and yields were calculated against the theoretical yield for each substrate. All species exhibited decomposition and did not give satisfactory elemental analysis.

Synthesis of [Rh(C₂H₄)(DTBB)]₂ (9)



DTBB (0.073 g, 0.28 mmol) was dissolved in 6 mL of THF. To the yellow solution was added 4 mL of [ClRh(C₂H₄)₂]₂ (0.050 g, 0.13 mmol) solution in benzene. The resulting red solution was stirred at room temperature for 2h. The reaction mixture was evaporated to dryness. The remaining red solid was washed with 2 x 8 mL of Et₂O and dried under vacuum.

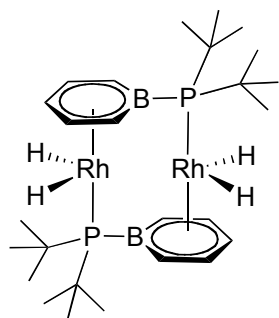
Yield = 0.066 g, 40%. ¹H NMR (500 MHz, benzene-*d*₆): δ 5.96 (m, 4H, *o*-C₅H₄B),

5.55 (t, $J = 6.5$ Hz, 4H, m -C₅H₄B), 4.48 (t, $J = 5.8$ Hz, 2H, p -C₅H₄B), 3.00 (dd, $J = 11.7$ and 2.2 Hz, 4H, C₂H₄), 2.74 (dt, $^1J = 12.0$ and 2.2 Hz, 4H, C₂H₄), 1.34 (d, $J = 11.6$ Hz, 36H, t Bu₂). **¹³C{¹H} NMR** (125.72 MHz, benzene-*d*₆): δ 101.4 (m -C₅H₄B), 99.6 (o -C₅H₄B), 91.8 (p -C₅H₄B), 36.4 (d, $J = 12.8$ Hz, C- t Bu₂), 33.2 (d, $J = 3.2$ Hz, CH₃ t Bu₂), 32.9 (dd, $J = 13.7$ and 1.6 Hz, C₂H₄). **³¹P{¹H} NMR** (202.40 MHz, benzene-*d*₆): δ 23.7 (br d, $J = 160$ Hz, [Rh(C₂H₄)(DTPBB)]₂). **¹¹B{¹H} NMR** (160.41 MHz, benzene-*d*₆): δ 31.

Reaction of [Rh(C₂H₄(DTBB)]₂ (9) with H₂

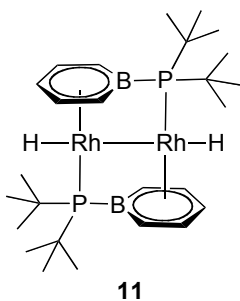
In a sealed J-Young NMR tube (0.002 g, 2.8 μ mol) were dissolved in 0.6 mL of benzene-*d*₆, the yellow solution was degassed by 3 cycles of freeze-pump-thaw in a liquid nitrogen bath and ≈ 1 atm of H₂ was added by removing the liquid nitrogen bath and opening the valve to H₂ flow for 30 seconds. The sample was then allowed to reach room temperature slowly. The NMR spectrum recorded after 3 h displayed the signals for two different hydrides along with some of the starting material. After 3 days only species **10** was observed in solution. Removal of the hydrogen atmosphere generates species **11**. **FT-IR** (cm⁻¹): 3663, 3308, 3196, 3107, 3063, 3035, 2919, 2849, 2662, 2351, 2291, 2161, 2084, 1979, 1753, 1679, 1591, 1567, 1453, 1375, 1240, 1116, 1084, 1027, 968, 895, 869, 810, 796, 774.

Hydride 10



¹H NMR (500 MHz, benzene-*d*₆): δ 6.00 (t, $J = 7.5$ Hz, 2H, m -C₅H₄B), 5.78 (dd, $J = 8.9$ and 4.1 Hz, 2H, o -C₅H₄B), 5.38 (t, $J = 6.0$ Hz, 1H, p -C₅H₄B), 1.37 (d, $J = 12.7$ Hz, Pt Bu₂), -13.94 (dd, $J = 23.3$ and 21.3 Hz, 2H, Rh-H). **¹H{³¹P} NMR** (51.8 ppm) (500 MHz, benzene-*d*₆): δ 6.00 (dd, $J = 9.3$ and 5.8 Hz, 2H, m -C₅H₄B), 5.78 (d, $J = 8.6$ Hz, 2H, o -C₅H₄B), 5.38 (t, $J = 6.0$ Hz, 1H, p -C₅H₄B), 1.37 (s, Pt Bu₂), -13.94 (d, $J = 23.4$ Hz, 2H, Rh-H). **³¹P{¹H} NMR** (202.40 MHz, benzene-*d*₆): δ 51 (br).

Hydride 11



^1H NMR (500 MHz, benzene- d_6): δ 6.25 (m, 2H), 6.04 (m, 1H), 4.95 (d, J = 8.9 Hz, 2H), 4.80 (d, J_{23} = 9.7 Hz, 2H), 1.46 (d, J = 12.8 Hz, 18H), 1.29 (d, J = 12.3 Hz, 20H), 0.99 (d, J = 14.5 Hz, 4H), -17.83 (dd, J = 21.32, 14.7 Hz, 1H, Rh-H). **$^1\text{H}\{^{31}\text{P}\}$ NMR** (54.2 ppm) (500 MHz, benzene- d_6): δ 6.25 (m, 4H), 6.04 (dd, J = 8.4, 6.1 Hz, 2H), 4.95 (d, J = 8.5 Hz, 2H), 4.80 (d, J = 9.2 Hz, 1H) 1.46 (s, 36H, PtBu_2), 1.29 (s, 54H, PtBu_2), -17.83 (d, J = 15.9 Hz, 1H, Rh-H). **$^{31}\text{P}\{^1\text{H}\}$ NMR** (202.40 MHz, benzene- d_6): δ 54 (br).

X-ray Crystallography of 9

A red crystal of **9** (0.26 x 0.10 x 0.08 mm³) was mounted on a glass fibre using Paratone N hydrocarbon oil. Measurements were made at 150(2) K on a Bruker APEX II area detector diffractometer equipped with graphite monochromated MoK α radiation. The program used for retrieving cell parameters and data collection was APEX 2.¹⁸⁴ Data were integrated using the program SAINT,¹⁸⁵ and corrected for Lorentz and polarization effects. The structure was solved and refined using SHELXS-97.¹⁸⁶ All non-H atoms were refined anisotropically. The hydrogen atoms were placed at idealized positions. Crystallographic data have been deposited at CCDC (CCDC no. 1415613). The crystallographic details are presented in Table S1 (ESI). This data can be obtained upon request from the Cambridge Crystallographic Data Centre.

Crystal data and structure refinement for [(C₂H₄)Rh(DTBB)]₂ (9)

Empirical formula	C ₃₀ H ₅₄ B ₂ P ₂ Rh ₂	
Formula weight	704.11	
Temperature	150(2) K	
Wavelength	0.71073 Å	
Crystal system	Monoclinic	
Space group	P 2 ₁ /n	
Unit cell dimensions	a = 8.3211(8) Å	α = 90°
	b = 19.9816(19) Å	β = 110.3513(14)°
	c = 9.8002(10) Å	γ = 90°
Volume	1527.8(3) Å ³	
Z	2	
Density (calculated)	1.531 Mg/m ³	
Absorption coefficient	1.203 mm ⁻¹	
F(000)	728	
Crystal size	0.260 x 0.100 x 0.080 mm ³	
Theta range for data collection	2.038 to 28.291°	
Index ranges	-11 ≤ h ≤ 11, -26 ≤ k ≤ 26, -13 ≤ l ≤ 13	
Reflections collected	16042	
Independent reflections	3786 [R(int) = 0.0561]	
Completeness to theta = 25.242°	100.0 %	
Absorption correction	Semi-empirical from equivalents	
Max. and min. transmission	0.908 and 0.866	
Refinement method	Full-matrix least-squares on F ²	
Data / restraints / parameters	3786 / 0 / 185	
Goodness-of-fit on F ²	1.037	
Final R indices [I > 2σ(I)]	R1 = 0.0346, wR2 = 0.0758	
R indices (all data)	R1 = 0.0551, wR2 = 0.0849	
Largest diff. peak and hole	1.079 and -0.438 e.Å ⁻³	

General procedure for hydrogenation reactions

Hydrogenation reactions were carried out in Schlenk flasks over 24 h of continuous flow of H₂, at room temperature. Aliquots of 0.1 mL were withdrawn after 1, 6, 12 and 24 h of reaction, filtered through a 1 cm silica plug and diluted with 0.3 mL of toluene. All liquids were measured with automated pipets. In a typical hydrogenation reaction substrate, internal standard, 1 mol % of catalyst and 10 mL of toluene were loaded into a 18 mL Schlenk flask, equipped with a magnetic stirring bar.

Acknowledgements

The authors acknowledge the Natural Sciences and Engineering Research Council of Canada (NSERC), the Canada Foundation for Innovation (CFI), the Fonds de Recherche Nature et Technologies (FQRNT), the Centre de Catalyse et Chimie Verte (C3V-Université Laval) for financial support. P. Audet is also acknowledged for his aid on NMR characterization and GC spectroscopy. W. Bi is acknowledged for his help on X-ray diffraction.

Electronic Supplementary Information (ESI) available: Multinuclear NMR characterization for complex **9** and hydride species **10** and **11**, 2D NMR and crystallographic data for **9**. This material is available free of charge via the Internet at <http://pubs.rsc.org>. See DOI: 10.1039/C5DT03109E.

7 Chapter 7 On the Stability of the P-B Bond and Two New Ligands

The present chapter is a compilation of experiments that provide important observations on the stability of the P-B bond in both phosphido-borates and phosphido-boratabenzene and the advantages of using one or the other. Additionally the synthesis of two new ligands: di-*iso*-propylphosphido-triphenylborate (**DiPB**) and the *ansa*-phosphido-bis-boratabenzene (***ansa*-DTBB**), obtained from the cleavage of the P-B bond in **DTBB** are presented. The chapter is divided in two main subjects, the **DiPB** ligand and the ***ansa*-DTBB** ligand, a brief introduction is provided at the beginning of each section, followed by the results. The conclusion of the chapter summarizes key concepts on the two ligands described.

7.1 The Di-*iso*-propylphosphido-triphenylborate Ligand (DiPB)

In the previous chapters we have demonstrated that the **DTBB** ligand can coordinate in a η^1 -fashion accordingly to the metal precursor used and the surrounding ligands. However we decided to investigate an alternative way to obtain negatively charged phosphido-borates without using the boratabenzene framework.

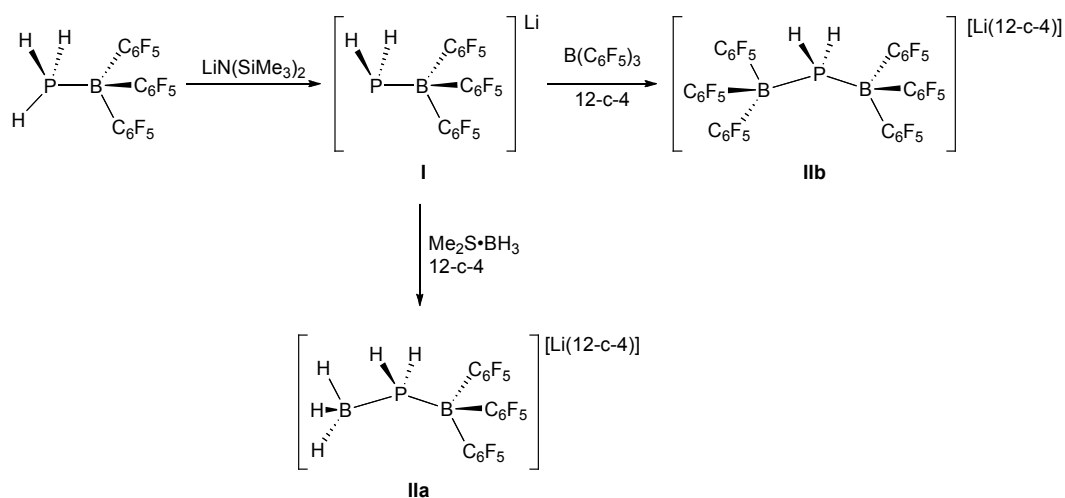
7.1.1 Introduction: Precedents on Phosphine-boranes

The formation of phosphine-borane adducts of the type R_3P-BH_3 has been widely investigated, notably for their use in the synthesis of phosphines, where the borane serves as a protecting group.¹⁸⁷ Recently the use of phosphine-borane adducts on dehydrocoupling reactions arises as a promising alternative to H_2 production.¹⁸⁸ Phosphino-boranes have also found applications as reducing agents,¹⁸⁹ in hydrophosphination,¹⁹⁰ and in olefin reduction reactions.¹⁹¹

However when sterically encumbered species are used, as Stephan first reported,¹⁹² the P-B interactions do not occur between the bulky phosphine and a

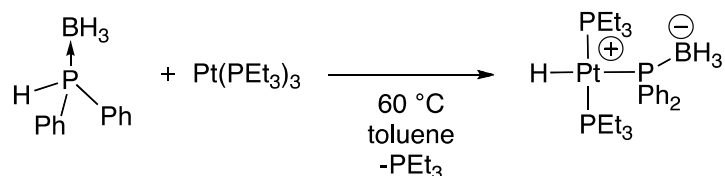
Lewis acidic borane, instead these species form Frustrated Lewis pairs, which can carry transformations involving the activation of small molecules such as hydrogen.¹⁹³

While the neutral phosphino-boranes have been widely studied, the monophosphido anions of such species have been less investigated. Few examples have been reported such as that of a phosphido-borate anion obtained by deprotonation of a $\text{H}_3\text{P}\cdot\text{B}(\text{C}_6\text{F}_5)_3$ adduct. The Lithium phosphido-borate (**I**) is capable to form phosphido-diborates (**IIa**) when reacting with $\text{Me}_2\text{S}\cdot\text{BH}_3$ or by reaction with a second equivalent of $\text{B}(\text{C}_6\text{F}_5)_3$ (**IIb**) (Scheme 7.1).¹⁹⁴ These anionic phosphido-borates were designed for applications on polymerization catalysis.¹⁹⁵



Scheme 7.1: Synthesis of $[\text{H}_3\text{P}\cdot\text{B}(\text{C}_6\text{F}_5)_3]\text{Li}$ and phosphido-diborates with BH_3 and $\text{B}(\text{C}_6\text{F}_5)_3$.¹⁹⁴

In 2003 Manners reported the synthesis of a Pt bonded phosphido-borate using phosphino-boranes as a precursor and carrying an oxidative addition of the P-H bond to a $\text{Pt}(0)(\text{PEt}_3)_3$ species. Manners Pt-phosphino-borate is capable to undergo ligand exchange in the presence of other phosphino-borane adducts of the type $\text{Ph}_2\text{PH}\cdot\text{BH}_3$ or $\text{PhPH}_2\cdot\text{BH}_3$.²²



Scheme 7.2: Synthesis of $(Et_3P)_2Pt(H)(Ph_2P-BH_3)$ by Manners.²²

Other phosphido-borate species have been prepared such as the lithium species (**III**, Figure 7.1) reported by Manners and used in the preparation of linear hybrid aminoborane/ phosphanylborane chains.¹⁹⁶ Species **III** was revisited by Wagner as part of a systematic study of the basicity of such species reported in 2006. Wagner had compared species **III** and **IV** spectroscopically in order to better understand the properties of these molecules as ligands. In this study, Wagner *et al* had concluded that the negatively charged $[Ph_2PBH_3]^-$ fragment is more Lewis basic towards the BH_3 Lewis acid to form $[Ph_2P(BH_3)_2]^-$ species than neutral fragments of the type $P(CH_3)Ph_2$.¹⁹⁷

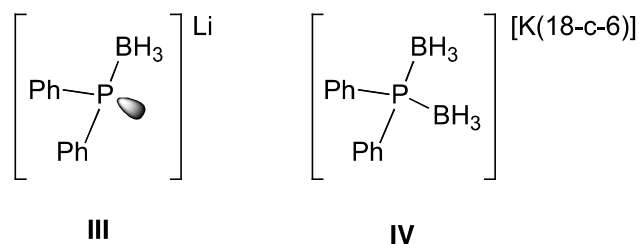


Figure 7.1: Anionic phosphino-boranes: $[Ph_2PBH_3]Li$ (**III**)¹⁹⁶ and $[Ph_2P(BH_3)_2][K(18-c-6)]$ (**IV**).¹⁹⁷

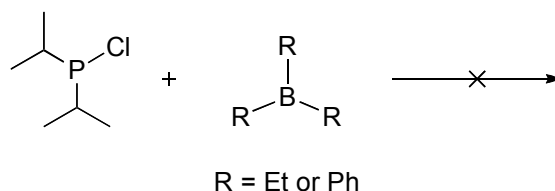
The observations reported by Wagner on the basicity of phosphido-borates as ligands have stimulated our interest on the coordination chemistry of such molecules to metals, an area that has been poorly explored except for examples of complexes with Fe, Pd, Pt,^{81,198} and main group elements such as Li and Al.¹⁹⁹

7.1.2 Synthesis of Lithium Di-*iso*-propylphosphido-*tri*-phenylborate (DiPB)

Previous reports by B. Macha, showed that the boratabenzene ring in the **DTBB** ligand is so electron rich that the preferred coordination mode is η^6 , similar to Cp rings, instead of the desired η^1 -coordination through the phosphorous.

With these precedents we decided to investigate whether the replacement of the boratabenzene ring would lead to η^1 coordination of a phosphido-borate ligand.

Our first attempt to achieve the synthesis of a phosphido-borate was to react the neat $i\text{Pr}_2\text{P-Cl}$ with the borane to obtain a neutral adduct that could be reduced by alkali metals to produce the phosphido-borate salt. However the adduct formation between the $i\text{Pr}_2\text{P-Cl}$ does not form a P-B adduct with BEt_3 or with BPh_3 , due to steric preclusion.



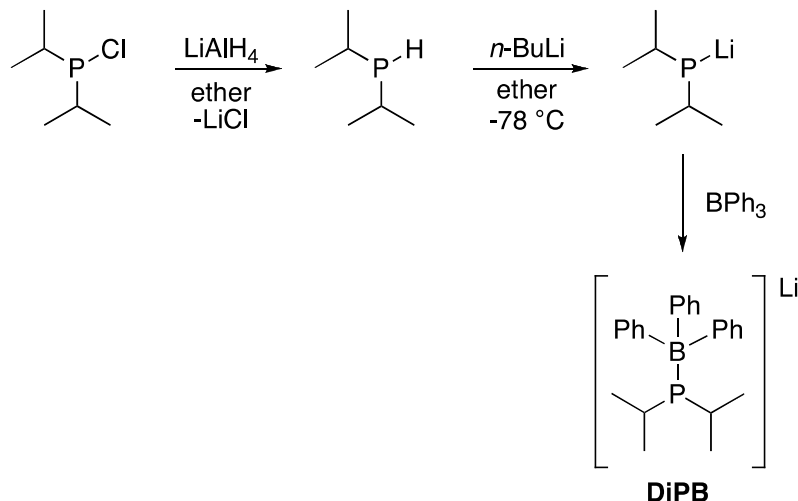
Scheme 7.3: Attempted adduct formation between $i\text{Pr}_2\text{P-Cl}$ and BR_3 (R = Et or Ph) neat.

This behaviour has been well documented for other alkyl phosphines and boranes and is the key concept of FLP chemistry.^{85,200}

A strategy to overcome the steric hindrance of bulky phosphines such as tBuPH_2 and force the interaction with a borane is by using a very Lewis acidic borane like $\text{B}(\text{C}_6\text{F}_5)_3$, such interaction has been confirmed by X-ray crystallography.²⁰¹ Another alternative is to increase the strength of the P-B interaction by turning the phosphine more nucleophilic that is using a phosphide to carry a nucleophilic attack on a borane, overcoming the steric impediments without withdrawing much electron density from the phosphine by using a very electron deficient borane.

The synthesis of **DiPB** (Scheme 7.4) was carried using $i\text{Pr}_2\text{P-Cl}$ as starting material, a chlorophosphine commercially available and more affordable than the reduced phosphine. Reduction of the Cl-phosphine with LiAlH_4 resulted in $i\text{Pr}_2\text{P-H}$.²⁰² The ethereal solution of $i\text{Pr}_2\text{P-H}$ can then be deprotonated with $n\text{-BuLi}$, yielding the lithium di-*iso*-propyl phosphide.²⁰³ The lithium phosphide is a very

reactive species and must be used in the following step as soon as the reaction mixture reaches room temperature. Using *i*Pr₂P-Li to carry a nucleophilic attack on the BPh₃ it became possible to isolate the **DiPB** lithium as a colorless powder.



Scheme 7.4: Synthesis of **DiPB** ligand

¹H NMR of the powder showed resonances at 7.76 (*ortho*-H), 7.28 (*meta*-H) and 7.10 ppm (*para*-H) corresponding to the aromatic protons of the three phenyl substituents on boron, the integration is in agreement with the presence of two *iso*-propyl groups displaying a multiplet at 2.21 ppm for the methyne and two multiplets at 1.17 and 1.03 ppm, accounting for the methyl groups. Interestingly one molecule of Et₂O seems to remain coordinated to the lithium cation, even after several hours of drying under vacuum. ³¹P NMR shows a broad multiplet at -14.1 ppm. The phosphorous signal shifts to a lower frequency compared to *i*Pr₂P-Cl (132 ppm)²⁰⁴ or *i*Pr₂P-H (16.4 ppm),²⁰² as a result of the negative charge imposed upon it.¹⁹⁴ ¹¹B NMR shows a broad multiplet at -7.6 ppm and a second signal, a sharp singlet (-9.3 ppm), which accounts for one tenth of the broad signal. The second signal was assigned to a Ph₃B•OEt₂ adduct formed between the borane and the solvent, the presence of unreacted Ph₃B was ruled out by the absence of a signal at 67.4 ppm.²⁰⁵

By heating an ethereal solution and allowing slow cooling to room temperature, single crystals of **DiPB** ligand were obtained as colorless needles of a monoclinic

crystal system and point group $P2_1$ (Figure 7.2). Two molecules are found within the unit cell.

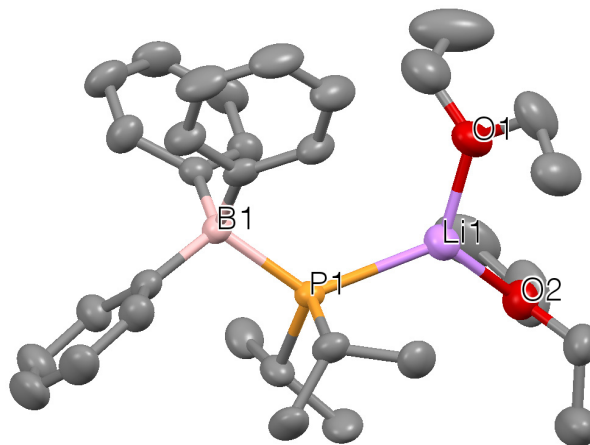


Figure 7.2: X-ray structure of **DiPB**, thermal ellipsoids drawn at the 50% probability level. Hydrogen atoms are omitted. ($R_1 = 4.19\%$) Selected bond distances (Å) and angles ($^\circ$): B1-P1 2.042(2); P1-Li1 2.575(4); C1-B1 1.636(3); C7-B1 1.642(3); C13-B1 1.630(3); C19-P1 1.867(2); C22-P1 1.886(2); B1-P1-Li1 125.1(1) Phosphine angles: B1-P1-C19 108.03(9); C10-P1-C22 103.67(9); C22-P1-B1 103.59(9); Borate angles: C1-B1-C7 104.9(2); C1-B1-C13 112.4(2); C7-B1-C13 112.4(2).

P-B distances on **DiPB** (2.042(2) Å) correspond to an intermediate between a covalent (1.90 – 2.00 Å)⁸⁶ and a dative interaction (2.15 – 2.50 Å).^{85,200}

The phosphine atom displays a distorted tetrahedral geometry (angles of 108.03(9); 103.67(9); 103.59(9) $^\circ$), placing the borate on the apex, while the boron atom assumes a tetrahedral geometry. This geometry is also observed on phosphine-borane adducts where the boron centre displays a tetrahedral geometry due to the sp^3 hybridization of the newly populated empty orbital on boron.¹⁸⁷

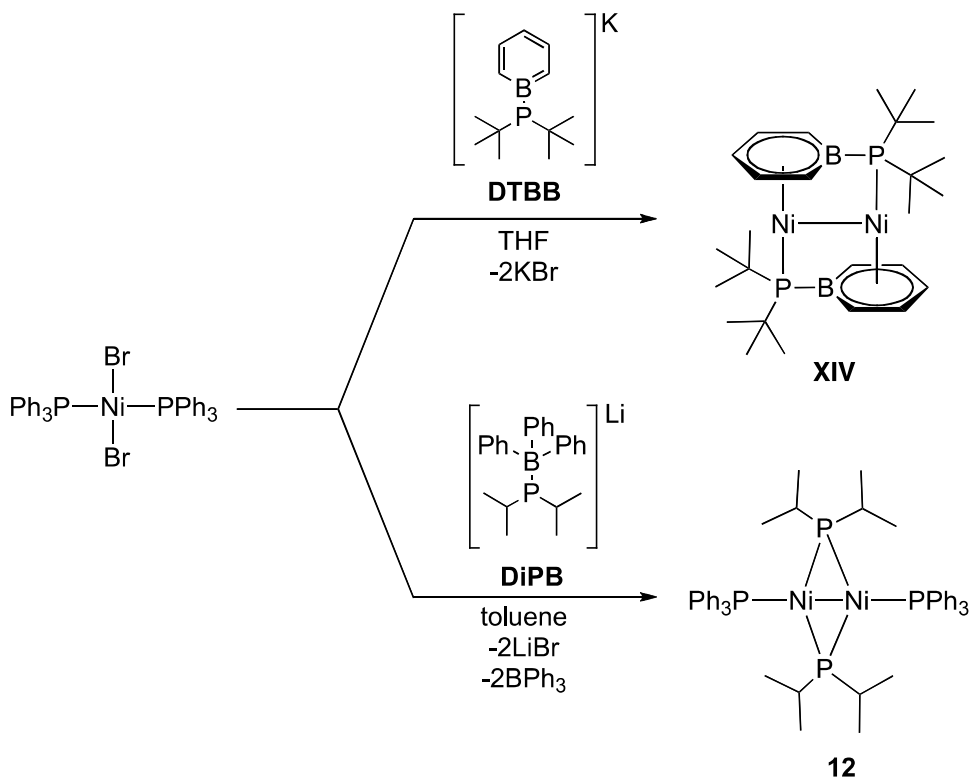
Interestingly the lithium counterion appears to be located over the phosphide (P-Li 2.575(4) Å). For the case of neutral phosphino-borane adducts, if electronegativity is considered, there is a partial negative charge on phosphorous, while boron remains electron deficient even after the phosphorous electron pair is populating the empty orbital of boron,²⁰⁶ hence the lithium cation remains localized over the partial negative charge on the phosphorous on **DiPB** ligand in solid state.

7.1.3 DiPB Reaction with Metals of the Group 10

DiPB ligand was expected to coordinate η^1 through the phosphorous lone pair. However when reacted with group 10 metals, only the cleavage of the P-B bond was observed. These results are contrasting with the **DTBB** coordination chemistry, where the metal complexes are stabilized by the coordination through the aromatic ring of boratabenzene and/or involving the exocyclic phosphide substituent.

Scheme 7.5 shows the reaction of $(\text{PPh}_3)_2\text{NiBr}_2$ with **DTBB** and with **DiPB**. As mentioned above the **DTBB** framework forms a dimer with a Ni-Ni bond and two **DTBB** ligands coordinated η^6 (**XIV**).⁵³

However when the same metal precursor was reacted with **DiPB**, the product obtained didn't contain the borate functionality. Instead the PPh_3 ligands remained attached to the metal and two $\mu\text{-}i\text{-Pr}_2\text{P}$ - fragments are bridging both Ni nuclei (**12**).



Scheme 7.5: Comparison of the reaction of $(\text{PPh}_3)_2\text{Ni}(\text{Br})_2$ with **DTBB**⁵³ and **DiPB**.

Crystals were obtained from slow evaporation of a benzene solution of the reaction mixture. Cuboidal pink crystals were found to crystalize in a triclinic crystal system of the P-1 point group (Figure 7.3).

Complex **12** displays a Ni-Ni distance of 2.381(2) Å, similar complexes featuring bridging ligands such as $[\{\text{Ni}(\text{dppe})\}_2(\mu\text{-H})_2][\text{BPh}_4]$ display an actual Ni-Ni interaction of 2.316(5) Å,²⁰⁷ however when bulky substituents are present such as *t*Bu₂P, Ni-Ni bond can be as long as 2.559(2) Å.²⁰⁸

A linear arrangement is observed for the atoms P1-Ni1-Ni1-P1, the angle described by P2-Ni1-P2 is of 122.63(3)°, indicative of a trigonal planar geometry on the nickel centre. The bridging *i*Pr₂P- on complex **12** displays Ni1-P1 distances of 2.166(7) Å, slightly longer than a similar complex of formula $[\text{Ni}(\mu\text{-}i\text{Bu}_2\text{P})(\text{PMe}_3)]_2$ (2.136(5) Å),²⁰⁹ while the equatorial PMe₃ ligand displays Ni1-P2 distances 2.174(3), a distance longer than that observed for complex **12** (2.131(6) Å) due to the steric bulk of both the *i*Pr and PPh₃ ligands.

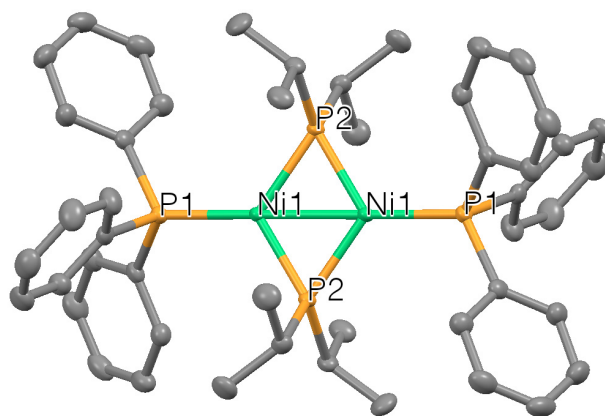
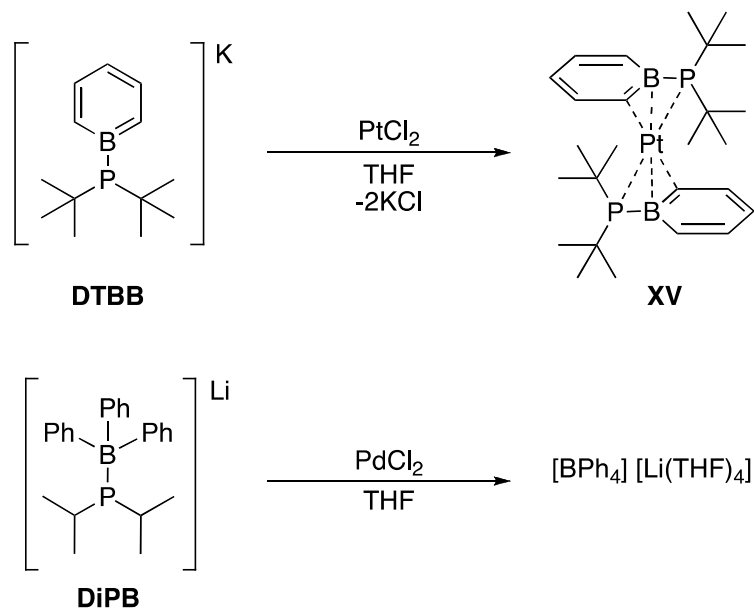


Figure 7.3: X-ray structure of **12**, thermal ellipsoids drawn at the 50% probability level. Hydrogen atoms are omitted. (R1 = 3.10%) Selected bond distances (Å) and angles (°): Ni1-Ni1 2.381(3); Ni1-P1 2.131(6); Ni1-P2 2.166(7); Ni1-P2-Ni1 66.70(2); P2-Ni1-P2 113.30(3); P2-Ni1-P1 122.63(3); P1-Ni1-Ni1-P1 180.0(7).

In a similar way, the P-B interaction of the **DIPB** ligand is cleaved when reacted with PdCl₂ in toluene. In contrast with the **DTBB** which is capable to coordinate in an η³ fashion through the P-B=C bond to other metals of the group 10 such as Pt(II) (**XV**, Scheme 7.6). From the reaction of **DIPB** with PdCl₂, a borate

[BPh₄][Li(THF)₄] (Scheme 7.6) was obtained as crystals found in the reaction mixture when left for slow evaporation.



Scheme 7.6: Synthesis of [Pt(DTBB)]⁵³ and reaction of DiPB with PdCl₂.

The crystal structure of compound [BPh₄][Li(THF)₄] has been reported as a private communication in 1999.²¹⁰

7.2 The Discovery of an *ansa*-boratabenzene Ligand (*ansa*-DTBB)

The *ansa*-DTBB was found as a result of the cleavage of the P-B bond on DTBB ligand in the presence of Zr. In the following sections an introduction to the *ansa*-metallocenes chemistry, the motivation behind the Zr reaction and the synthesis of *ansa*-DTBB are presented.

7.2.1 Introduction: Metallocenes and Phosphorous Bridged *ansa*-ligands

Metallocene derivatives of early transition metals (**V**, Figure 7.4) have been widely used as precatalyst in olefin polymerization.²¹¹ Soon after the first reports of such compounds, structural modifications with an impact on the activity and stability of these type of complexes was the subject of many scientific publications.²¹²

Modifications such as the bridging of the Cp rings with linkers contributed to a better understanding of their mechanism of action as catalyst. Bridged metallocenes are better known as *ansa*-metallocenes, Luttringhaus and Kullick first coined the term *ansa*,²¹³ which comes from the Latin word for “*handle*”.²¹⁴

The bridge enforces the bending of the ring and pinches open the wedge between the rings so the metal centre remains accessible to interact with substrates. The bridge also prevents rotation of the cyclopentadienyl rings about the metal axis so conformational mobility is restricted. These features have a major impact on the composition, length and conformation of the polymeric chains obtained as product of the catalytic reaction.^{212,215}

Ansa-ligands with bridges that vary in nature and size have been reported. Bridging groups such as carbon linkers,^{211a,216} silicon,^{211,217} boron²¹⁸ and phosphorous²¹⁹ have been used (**VI**, Figure 7.4). Alternatively a more sophisticated approach has been undertaken by combining the donor/acceptor (D/A) functionality on the bridging group as observed on species **VII** in Figure 7.4.²²⁰

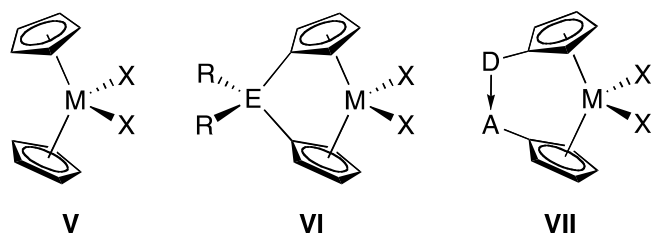


Figure 7.4: Metallocenes: non-bridged,²¹¹ *ansa*-bridged with main group atoms^{211,217-219} and *ansa*-with a donor/acceptor (D/A) bridge²²⁰ (E = C, Si, P, B; R = H, Me, Ph, SMe₂, PMe₃; X = Cl; M = Ti, Zr, Hf; D = NR₂, PR₂, SbR₂, OR, F, C; A = BR₂, AlR₂, GaR₂).

A wide variety of donor and acceptor groups provide the chance to effectively tailor the activity of such catalysts. D/A *ansa*-metallocenes act as effective catalyst for ethylene polymerization producing high molecular weight polyethylene. Moreover they are thermally stable, they provide excellent regio and stereocontrol of the polymeric products as well as access to sequence polymers and long chain branching.²²⁰

The modification of the linker as well as the structure and composition of the ring has been also extended to the use of boron-containing heterocycles. Bazan and Ashe first approached polymerization catalysis using zirconocene **VIII** (Figure 7.5) featuring a (C₅H₅B-NiPr₂) ligand.^{55e,d}

Later on an *ansa* amido-boratabenzene featuring a silicon linker (**IX**, Figure 7.5) was reported by Ashe.²²¹ When activated with an excess of methylaluminoxane (MAO), complex **IX** is capable to carry the polymerization of ethylene. However the presence of the bulky substituents on boron, located at the front of the metal wedge, decrease the activity of the catalyst due to steric congestion. As an alternative, Ashe had proposed to change the bridging position in order to push the boron substituent to the side of the wedge, diminishing the steric congestion in the front.²²¹

More recently this work has been extended by Chen with the *ansa*-heteroborabenzene divalent ytterbium amide (**X**, Figure 7.5) obtained as a product of the C-H cleavage of PMe₃ and featuring a dative P-B bond, notably both boratabenzene rings are coordinated to a YbN(SiMe₃)₂ fragment.²²²

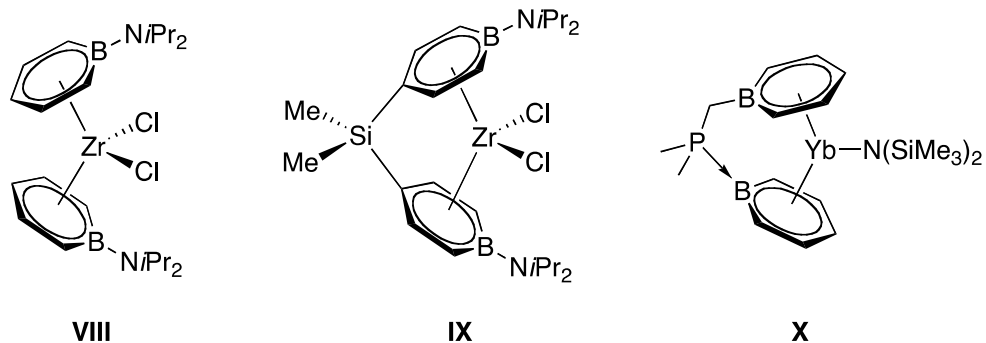


Figure 7.5: Metallocenes complexes of boratabenzene ligands: $[(C_5H_5B-NiPr_2)_2ZrCl_2]$ (**VIII**),^{55e,d} $[Me_2Si(C_5H_5B-NiPr_2)_2ZrCl_2]$ **IX**²²¹ and $[(C_5H_5B-(CH_3)_2P-BC_5H_5)Yb(N(SiMe_3)_2)]$ **X**.²²²

The structure of the *ansa* ligand **X** is not only exceptional due to the D/A interaction but it has also led to the observation of borabenzene's capacity to interact through a η^3 - η^6 ring slippage with lanthanides such as Yb. Moreover reaction of **X** with alkali salts of organic nucleophiles (Cp^*K), leads to coordination of the neutral borabenzene to an alkali ion, an interaction never observed before for neutral borabenzene adducts (**XI**, Figure 7.6).²²³

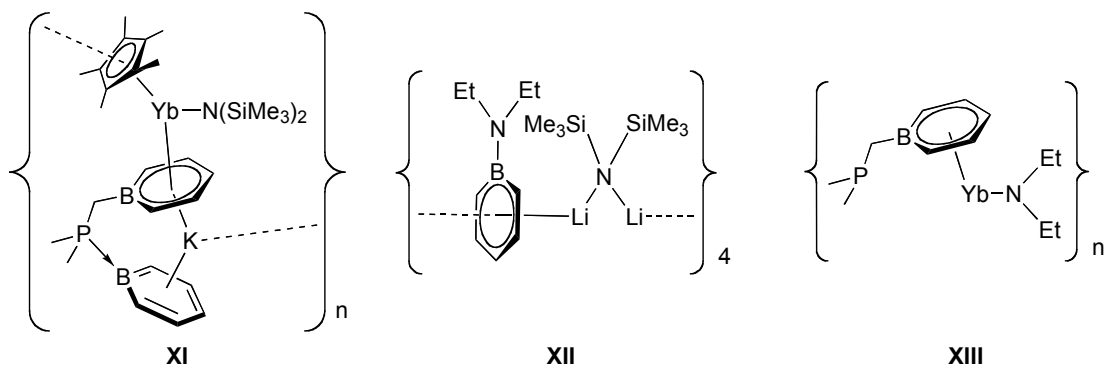


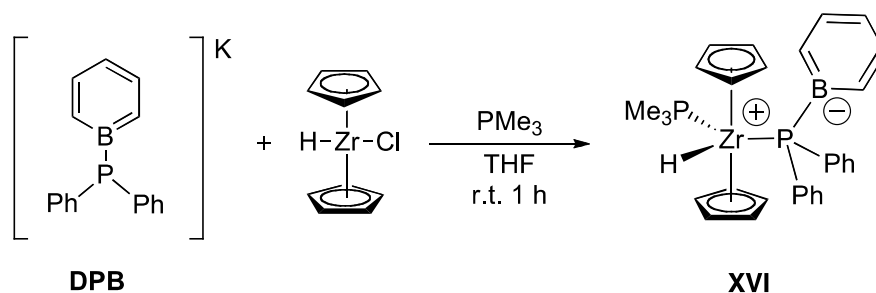
Figure 7.6: Structures of *ansa* ligand coordinated to Yb and K (**XI**), first evidence of a neutral borabenzene coordinated to an alkali metal (**XII**) and product of the dissociation of neutral borabenzene from *ansa* ligand (**XIII**).²²³

Further investigations on species **X**, revealed that a ligand displacement could be carried on the Yb atom by using sigma donor ligands without disturbing the dative P-B bond.^{223,224} However when bases such as $[NEt_2]^-$ are added, the cleavage of

the dative P-B bond by a nucleophilic attack of the base on boron is observed to generate species **XII** and **XIII** (Figure 7.6).²²³

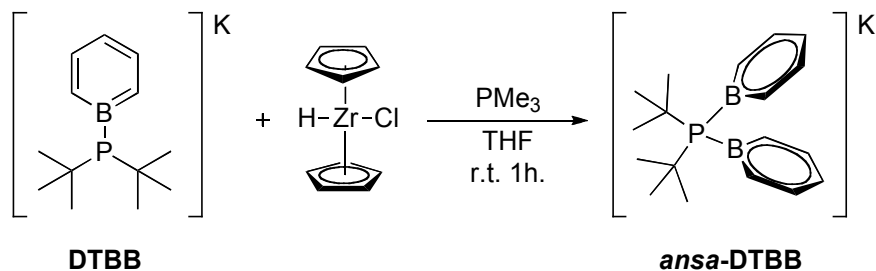
7.2.2 The Cleavage of the P-B Bond and The Discovery of an *ansa*-Boratabenzene Ligand

In 1996 Fu and collaborators reported the first evidences of the **DPB** ligand to coordinate η^1 to metal centres. Among the examples reported was the reaction of $\text{Cp}_2\text{Zr}(\text{H})(\text{Cl})$ with **DPB** in the presence of PMe_3 , by displacement of the chloride ligand yielding the $\text{Cp}_2\text{Zr}(\text{H})(\text{PMe}_3)(\text{DPB})$ (**XVI**, Scheme 7.7) which features a **DPB** ligand acting as a σ -donor to Zr.²³ Fu and collaborators observed that Zr species **XVI** is slightly unstable as a solid at room temperature and in solution it is unstable in the absence of excess PMe_3 .



Scheme 7.7: Synthesis of $\text{Cp}_2\text{Zr}(\text{H})(\text{PMe}_3)(\text{DPB})$ (**XVI**) reported by Fu.²³

While exploring the coordination chemistry of **DTBB** by analogy with **DPB** ligand, our interest turned to the reaction of **DTBB** with $\text{Cp}_2\text{Zr}(\text{H})(\text{Cl})$ following the reaction conditions previously described by Fu.²³ To our surprise instead of coordination of **DTBB** ligand to Zr by a ligand displacement, the formation of a new *ansa*-**DTBB** ligand was observed. The cleavage of the P-B bond of one molecule of **DTBB** led to the formation of a free borabenzene ring, the free borabenzene ring forms an adduct with the lone pair on phosphorous of a second molecule of **DTBB**.



Scheme 7.8: Reaction of **DTBB** and $\text{Cp}_2\text{Zr}(\text{H})(\text{Cl})$ and **ansa-DTBB**.

Although the NMR studies showed a complicated mixture of several species, the ^{31}P NMR of the reaction mixture showed the presence of $t\text{Bu}_2\text{PH}$ and other unidentified decomposition products.

The reaction mixture was stored at $-30\text{ }^\circ\text{C}$ and the formation of colorless needles-like crystals ($P2_1/c$ space group) for X-ray diffraction studies allowed for the characterization of one of the products.

The crystal structure confirmed the formation of an *ansa*-type ligand featuring a **DTBB** unit with another borabenzene ring coordinated to the lone pair on phosphorous.

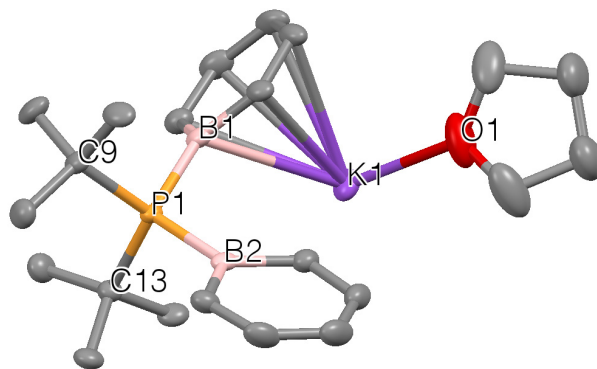


Figure 7.7: X-ray structure of **ansa-DTBB**, thermal ellipsoids drawn at the 50% probability level. Hydrogen atoms are omitted. ($R_1 = 3.87\%$) Selected bond distances (\AA) and angles ($^\circ$): P1-B1 1.957(2); P1-B2 1.959(2); C9-P1 1.885(2); C13-P1 1.885(2); K1-C_{cent} 2.848(5); B1-K1 3.189(2); K1-O1 2.694(2); B1-P1-B2 111.1(9); C9-P1-B1 105.3(9); C13-P1-B2 106.2(9); C9-P1-C13 111.8(9); C9-P1-B2 111.2(9); C13-P1-B1 111.1(9).

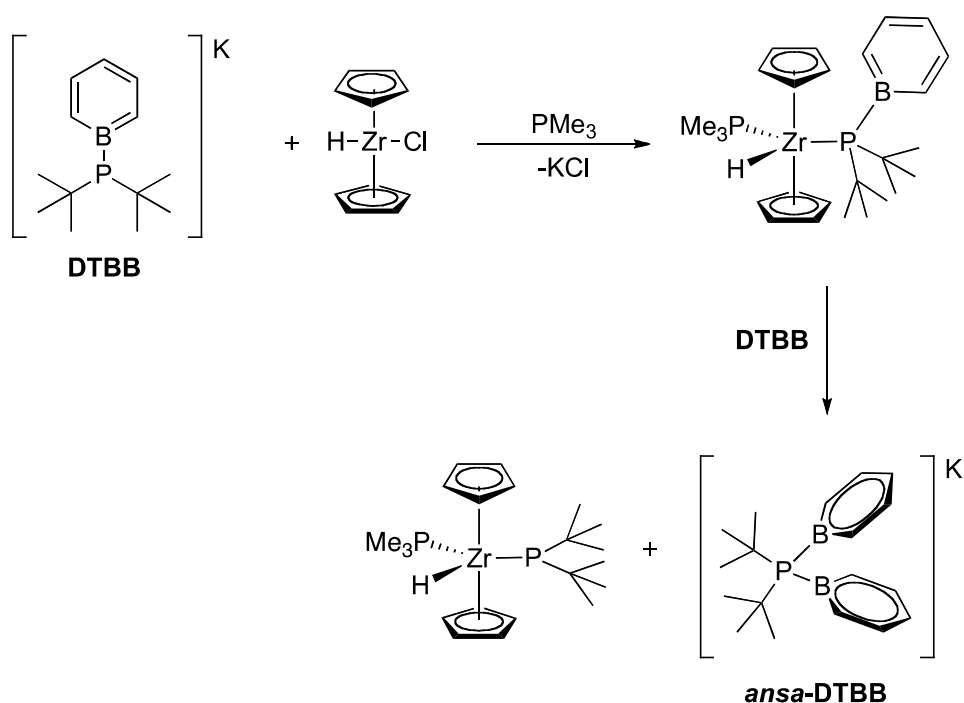
The P-B distances in the **ansa-DTBB** ligand differ by 0.002 Å (P-B1 = 1.957(2) Å; P-B2 = 1.959(2) Å), both distances fall within the range of covalent P-B bonds (1.90 to 2.00 Å).^{85,86} The short difference between the two P-B bonds has also been observed for a similar bis-borate phosphido species such as [Ph₂P(BH₃)₂][K(18-c-6)] (**IV**, Figure 7.1) (1.931(3); 1.940(2) Å).¹⁹⁷ Interestingly the P-B bonds on the *ansa* ligand are slightly shorter than that observed for the **DTBB** (1.965(3) Å)⁵³ and the **DPB** ligand (1.968(7) Å)⁵⁰ despite the increase in the steric constraint by the presence of a second borabenzene ring.

The phosphorous atom in **ansa-DTBB** displays a distorted tetrahedral geometry. The B1-P1-B2 angle of 111.1(8)° appears to be shorter than that observed for species **IV** (116.3(1)°) (Section 7.1.1, Figure 7.1), while the angle described by the *t*Bu groups and the phosphorous atom (C9-P1-C13) on the *ansa* ligand (111.8(9)°) is larger than the angle observed for the phenyl groups on **IV** (100.2(1)°).

Within the unit cell each borabenzene ring is coordinated to a K⁺ cation, forming a coordination network with another molecule of **ansa-DTBB** ligand. Due to coordination with K⁺ the borabenzene rings are not aligned face-to-face in a sandwich arrangement. The borabenzene ring containing B1 displays elongated distances between the boron, *ortho* and *meta* carbons and the K⁺ cation K-B1 (3.189(2) Å), C1 (3.138(2) Å) and C2 (3.165(2) Å), against the distances for C3 (3.199(2) Å), C4 (3.211(2) Å) and C5 (3.212(2) Å). This is suggestive of a ring slippage from η⁶-η³ as observed for species such as the *ansa* ligand **X**.²²² Likewise the ring containing B2 displays elongated distances between the K and B2 (1.189(2) Å), C_{*ortho*} (1.522(2) Å) and C_{*meta*} (3.188(2) Å). Interestingly in both rings the shortest distance observed is that corresponding to one of the *ortho* carbons and the potassium cation. This suggests that the way both rings are oriented apart from each other is a result of repulsion of the partial negative charge located over the *ortho* carbons, such a behaviour has been observed for the iron species **4** presented in section 4.4.

The formation of the **ansa-DTBB** can be proposed in the following way: a salt metathesis reaction between **DTBB** and the zirconocene lead to the precipitation of

KCl and coordination of **DTBB** in a η^1 fashion through phosphorous along with the coordination of a PMe_3 ligand to stabilize the Zr centre. Upon formation of a species $[\text{Cp}_2\text{Zr}(\text{PMe}_3)(\text{H})(\text{DTBB})]$, a couple of considerations must be taken into account. First, the Zr centre might withdraw electron density thus weakening the P-B interaction and favouring the nucleophilic attack on boron by a second **DTBB** molecule. Secondly the inherent bulkiness of the complex might also contribute to weakening the P-B bond in order to favour the cleavage to stabilize the Zr centre into an 18 electron $[\text{Cp}_2\text{Zr}(\text{PMe}_3)(\text{H})(\text{tBu}_2\text{P})]$ species featuring a phosphido ligand instead of a **DTBB** (Scheme 7.9).



Scheme 7.9: Proposed pathway for the formation of *ansa*-DTBB.

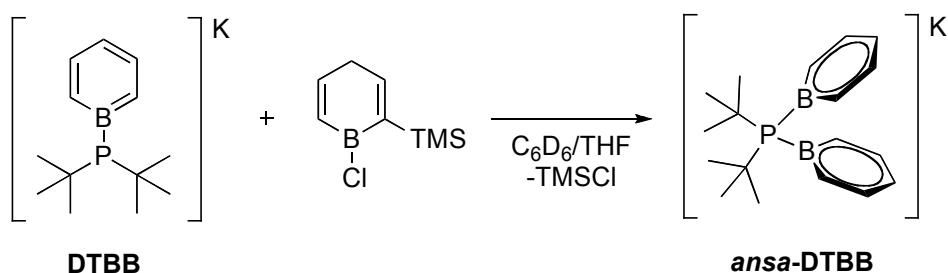
At this point, our attention turned to the discovery of alternative synthetic pathways to obtain the *ansa*-DTBB in order to study its coordination chemistry.

While no further investigations on the mechanism of formation of the *ansa* ligand with Zr were undertaken, it is important to note that reactional pathways, other than the one described herein, could be taking place to form the *ansa* ligand in the presence of Zr.

Boron to ligand redistribution, which can occur by two mechanisms: direct boron-to-boron migration, observed for perfluoroaryl borates or a metal assisted mechanism.²²⁵ Moreover, a similar ligand exchange such as that observed for tetrahaloborates cannot be disregarded. Tetrahaloborates are capable to carry a ligand exchange via dissociation followed by a S_N2 attack of the halide on another borate molecule.²²⁶

Additionally, the formation of decomposition products such as dimers or tetramers of $[\text{Cp}_2\text{Zr}]$ units could take place.^{227a} These species could be reacting with N_2 forming side-on or end-on N_2 complexes.^{227b}

In previous reports, Wagner observed that phosphido-borates of the type $[\text{Ph}_2\text{PBH}_3]^-$ appear to be more Lewis basic towards Lewis acids such as BH_3 than neutral R_3P species.¹⁹⁷ Moreover our group has demonstrated that Cl-boracycle(TMS) species can be used as precursors to obtain borabenzene adducts via a ligand exchange and elimination of TMSCl .³⁶ Based on these evidences and stating that the **DTBB** is indeed nucleophilic enough to carry an attack on boron, the independent synthesis of **ansa-DTBB** was undertaken by reacting the **DTBB** with one equivalent of Cl-boracycle(TMS). Similar to the reactional pathway to obtain **DTBB**, aromatization of the Cl-boracycle(TMS) is achieved by elimination of a molecule of TMSCl upon the nucleophilic attack on boron.



Scheme 7.10: Synthesis of **ansa-DTBB** ligand.

Characterization by ^1H NMR spectroscopy shows both borabenzene rings to be equivalent and display the same chemical shift $\delta = 8.03$ (*ortho*-H), 7.41 (*para*-H), 7.27 (*meta*-H), while the *t*Bu₂ groups can be observed as a doublet at 0.92 ppm and the byproduct TMSCl can be observed at 0.16 ppm. Figure 7.8 shows a

comparison between the **ansa-DTBB** and the **DTBB** ligand, notably the aromatic signals of the *ansa* ligand appear at a lower field than those of the precursor. Considering the observations from the crystal structure of the **ansa-DTBB**, both P-B distances differ by only 0.002 Å, this distance is only 0.02 Å shorter than the distance observed for free **DTBB** ligand. Furthermore the P-B distances are representative of an intermediate between a dative and a covalent interaction; this behaviour appears to be retained both in solution and in solid state.

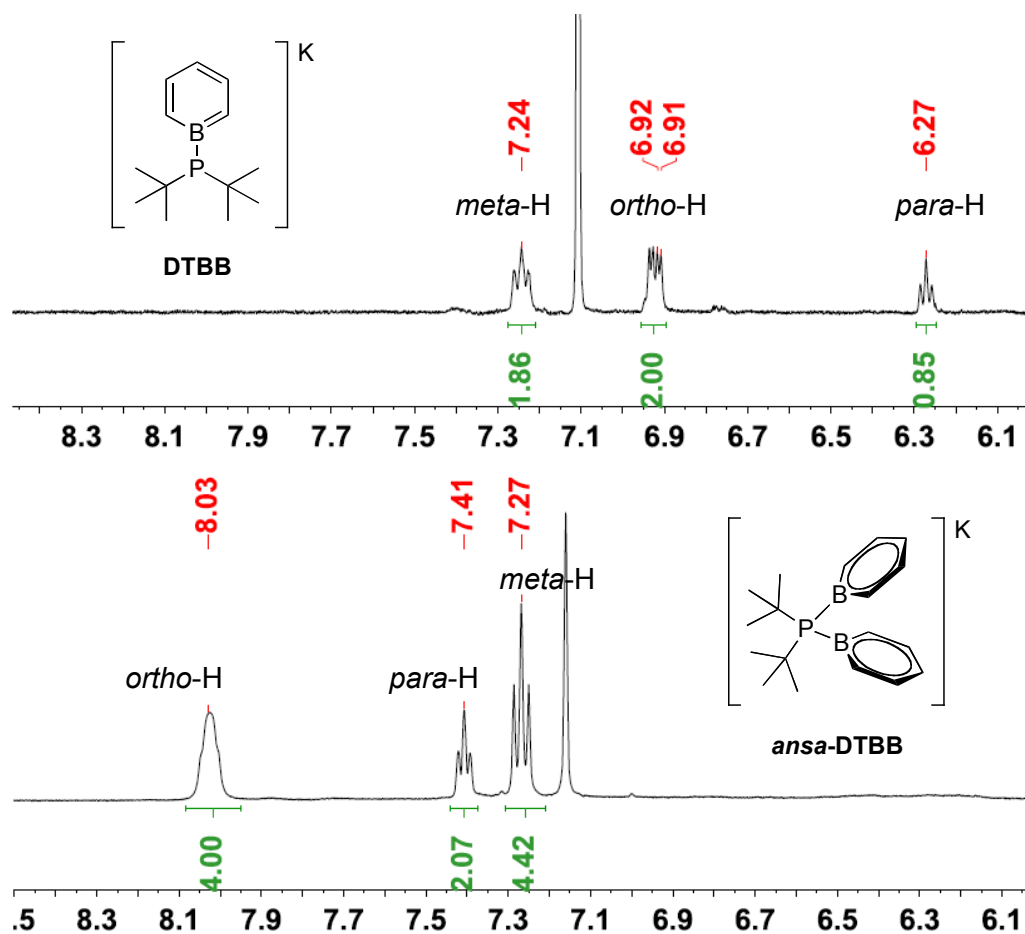


Figure 7.8: ¹H NMR spectra showing a comparison between the **DTBB** and **ansa-DTBB** ligands.

The ³¹P NMR of **ansa-DTBB** shows a broad quadruplet at 33.5 ppm ($J_{P-B} = 178.2$ Hz) and an ¹¹B resonance at 19.2 ppm (broad signal) considerably different than the resonances observed for the **DTBB** precursor (³¹P = br s, 8.5 ppm; ¹¹B = br m, 33.5 ppm). It is important to notice that the low resolution on ¹¹B NMR was

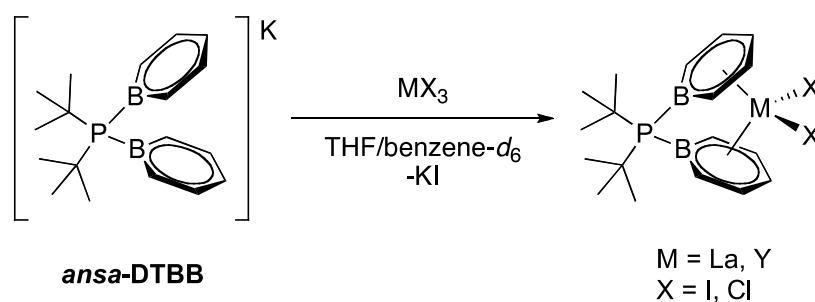
improved by using apodization, which resulted in a substantial difference between coupling constants on the ^{31}P and ^{11}B NMR for the **ansa-DTBB**; hence measuring the P-B on the ^{11}B NMR was not possible.

Other similar ligands display very different phosphorous and boron shifts, the P-B coupling constants of the **ansa-DTBB** seem to fall within the range of species such as $[\text{Ph}_2(\text{Me})\text{P}\cdot\text{BH}_3]$ (^{31}P = -9.2 ppm, $J_{\text{P-B}}$ = 150 Hz; ^{11}B = 33.5 ppm, $J_{\text{P-B}}$ = 150 Hz),¹⁹⁷ $[\text{Ph}_2\text{P}(\text{BH}_3)_2]\text{K}$ (**IV**, Figure 7.1) (^{31}P = -11.1 ppm; ^{11}B = -34.6 ppm, $J_{\text{P-B}}$ = 64 Hz),¹⁹⁷ $[(\text{C}_5\text{H}_5\text{B}-(\text{CH}_3)_2\text{P}-\text{BC}_5\text{H}_5)\text{Yb}(\text{N}(\text{SiMe}_3))] (\mathbf{X}, \text{Figure 7.5})$ (^{31}P = -14.6 ppm, $J_{\text{P-B}}$ = 101.4 Hz; ^{11}B = 25.8 ppm, $J_{\text{P-B}}$ = 99 Hz),²²² $[\text{Cp}^*(\text{N}(\text{SiMe}_3))\text{Yb}(\text{C}_5\text{H}_5\text{B}-(\text{CH}_3)_2\text{P}-\text{BC}_5\text{H}_5)\text{K}]_n (\mathbf{XI}, \text{Figure 7.6})$ (^{31}P = -12.1 ppm, $J_{\text{P-B}}$ = 126 Hz; ^{11}B = 24 ppm).²²³

7.2.3 Preliminary Studies on the Coordination and Reactivity of **ansa-DTBB**

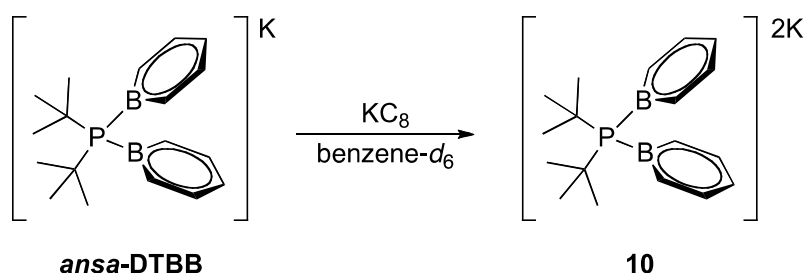
Motivated by Chen's ansa ligand coordinated to lanthanides²²²⁻²²⁴ and because the boratabenzene chemistry with lanthanides has not been extensively studied.²²⁸ We decided to carry preliminary studies on the **ansa-DTBB** coordination to lanthanides in 3^+ and 2^+ oxidation states as well as potential coordination to transition metals from the group 3.

Scheme 7.11 shows the proposed coordination of **ansa-DTBB** to metals of the lanthanum series. Although some preliminary studies have been carried on the coordination with LaI_3 and YCl_3 , indeed the **ansa-DTBB** seems to coordinate through the aromatic ring to La without disturbing the P-B bonds. The ^1H NMR shows signals for the aromatic protons of **ansa-DTBB** (δ = 8.03 (*ortho*-H), 7.41 (*para*-H), 7.27 (*meta*-H)) to be shifted towards the high field: δ = 7.73 (*ortho*-H), 7.11 to 7.09 (*para/meta*-H). Further characterization of the lanthanum and yttrium species by recrystallization is in progress.



Scheme 7.11: Proposed coordination of **ansa-DTBB** to metals of the lanthanide series.

Furthermore, our interest turned to the second reduction on the **ansa-DTBB** ligand in order to obtain a dianionic *ansa* ligand. The reduction was attempted by sonication of a benzene- d_6 yellow solution containing **ansa-DTBB** with bronze coloured scales of KC_8 (Scheme 7.12). As the reaction proceeds, the solution of ligand **10** turns deep yellow and precipitation of a dark powder (graphite) is observed. Attempts to analyze the solution by NMR failed, only broad and large signals were observed. Crystallization attempts for ligand **10** are in progress.



Scheme 7.12: Reduction of **ansa-DTBB** with KC_8 .

When a solution of **10** was reacted with LaI_3 , the 1H NMR spectrum shows signals with a similar shift as those observed from the reaction of **ansa-DTBB** with LaI_3 . Further characterization of these species is in progress.

7.3 Conclusion: On the Stability of the P-B Bond and the Advantages of Having Boratabenzene

While **DTBB** is capable to coordinate η^6 to nickel, the **DiPB** ligand fails to do so. As it has been observed for phosphino-borane adducts, the stability of the P-B bond is greatly influenced by many factors: the Lewis acidity of the borane and the Lewis basicity of the phosphine, as well as the steric constraints created by the substituents on both P and B nuclei. For example, the presence of alkyl chains on boron has a destabilizing effect on the adduct formation, because it decreases the strength of the dative bond. On the other hand, the presence of alkyl chains on phosphorous increases the strength of the dative bond, stabilizing the adduct interaction.¹⁸⁷ However, as the steric bulk increases the adduct stability decreases, affecting the interaction of the phosphorous and boron centers to approach and interact by formation of a dative bond.

Additionally the formation and stability of adducts featuring a P-B interaction will be greatly influenced by two factors: the capability of the Lewis base to direct charge density towards the acceptor orbital (lone pair of high p character) and the capability of the Lewis acid to undergo pyramidalization.¹⁹⁷ This explains why the formation of an adduct between iPr_2PCl and BPh_3 was not observed, such interaction had to be rather forced by increasing the nucleophilicity on the phosphine, hence increasing the p character on the lone pair of phosphorous.

The coordination of the **DiPB** ligand through the free electron pair on phosphorous, was proposed as an alternative to that observed for **DPB** and **DTBB** ligands (Figure 7.9). Unfortunately this was not possible to achieve by complexation with Ni and Pd metal precursors.

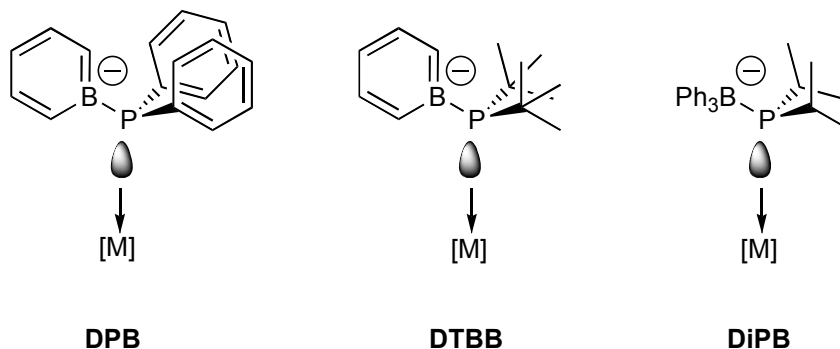


Figure 7.9: Proposed coordination modes of the **DPB** ligand reported by Fu, the **DTBB** and the **DiPB** ligands reported by us.

Nevertheless the **DiPB** ligand demonstrates that the use of bulky phosphido-borates for the synthesis of zwitterionic complexes poses a challenge due to the stability of the P-B bond in such species. Indeed this puts forward the importance of the stabilization of the P-B bond by the presence of an aromatic ring like boratabenzene and its capability to bear and sequester the charge over the π -system.

In order to better understand the reactivity of **DiPB** ligand and further investigate the stability of the P-B bond, which can be easily cleaved under certain conditions, using metal precursors in zero oxidation state, metal precursors from the group 11 or the formation of complexes of **DiPB** followed by reduction of the metal center are synthetic alternatives worth to be explored.

Moreover the discovery of the **ansa-DTBB** ligand, sets in evidence that despite the stability of the P-B interaction in **DTBB** ligand, the bond can be cleaved under certain conditions, as has been observed in the reaction with zirconocene.

The lability of the P-B bond has also been described in chapter 4, the iron boratabenzene species obtained are proof of the sensitivity of the P-B interaction to traces of moisture, however this situation has not been observed with other metals such as Cu(I) and Rh(I) described in chapters 5 and 6. This sets forward that the choice of metal precursor and the reaction conditions are key on the control of the coordination modes and reactivity of **DTBB** complexes.

Interestingly, preliminary results on the ***ansa*-DTBB** with LaI_3 show that it is in fact possible to preserve the P-B interaction and achieve coordination of the π system to a metal. Furthermore the possibility of the second reduction to obtain a dianionic ligand increases the number of chances to stabilize metals in a high oxidation state. This results open up the possibilities to use ***ansa*-DTBB** ligands in a series of catalytic applications as polymerization catalyst⁵⁷ or in the dehydrocoupling of amine-boranes.^{60,228e}

7.4 Experimental Details

All manipulations were carried out under inert atmosphere, unless otherwise is specified, using standard Schlenk techniques and inert atmosphere glovebox.

Solvents were distilled under N₂ atmosphere over sodium/benzophenone (THF, ether, hexane, toluene) or stirred over Na/K amalgam and vacuum-transferred (benzene-*d*₆), thf-*d*₈ was pre-dried with CaCl₂, degassed using three cycles of freeze-pump-thaw, dried and stored under activated 5 Å molecular sieves. Water used in reactions under inert atmosphere was degassed by three cycles of freeze-pump-thaw prior to bubbling of N₂ for 30 min inside a Schlenk round bottom flask. The volume needed was withdrawn using a purged stainless steel needle and a syringe.

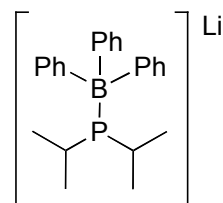
The following reagents were obtained from Sigma Aldrich and used as received: *t*Bu₂PCl, *i*Pr₂PCl, Ph₃B, LiAlH₄, Br₂Ni(PPh₃)₃, LaI₃, YCl₃, Cp₂Zr(H)(Cl). The potassium di-*tert*-butyl-phosphidoboratabenzene (**DTBB**)⁵³ and 1-chloro-2-(trimethylsilyl)boracyclohexa-2,5-diene (Cl-boracycle(TMS))³⁴ were prepared following the reported procedures.

Multinuclear NMR spectra were recorded in sealed J.-Young NMR tubes on an Agilent Technologies NMR spectrometer, ¹H NMR (500 MHz), ¹³C NMR (125.721 MHz), ³¹P NMR (202.404 MHz), ¹¹B NMR (160.419 MHz). NMR correlation experiments *g*HSQCAD and *g*COSY were used to elucidate ¹³C-¹H, ¹H-¹H correlations. Chemical shifts are quoted in ppm relative to external SiMe₄ (¹H, ¹³C), H₃PO₄ (³¹P), BF₃•Et₂O (¹¹B) references with n-bond *J* couplings being quoted in Hz. NMR signals are referred as (s) singlet, (d) doublet, (t) triplet, (m) multiplet, (dd) double of doublets, etc. It should be noted that due to 3/2 spin of NMR active ¹¹B, the resulting spectra are naturally broad. In addition, spectra of ³¹P nuclei bonded to ¹¹B also experience quadrupolar broadening of their signals, which can often cause imprecise coupling values. Spectroscopic data for **DTBB**⁵³ and Cl-boracycle(TMS)³⁴ are available in the literature.

HR-MS spectra were recorded with an Agilent Technologies 6210 LC Time of Flight Mass Spectrometer. Spectra were obtained by direct injection into the

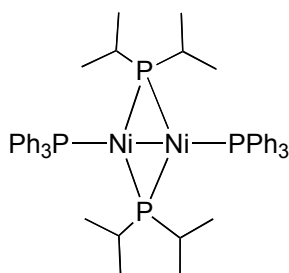
nebulizer of solutions of the corresponding species using ESI-MS or APPI-MS ionization in positive and negative modes.

Lithium di-*iso*-propylphosphido-tri-phenylborate (DiPB)



In a 15 mL Schlenk tube equipped with a magnetic stirrer, iPr_2PCl (1.0 g, 6.3 mmol) was dissolved in 10 mL of Et_2O . In a 100 mL Schlenk tube, equipped with a magnetic stirrer, $LiAlH_4$ (0.6 g, 14.5 mmol) was suspended in 20 mL of Et_2O , this suspension was then cooled to 0 °C in an ice-water bath. Chloro-phosphine was added to the $LiAlH_4$ drop wise over 7 min. The reaction mixture was kept at 0 °C for 30 min and kept stirring at room temperature overnight. The resulting iPr_2PH/Et_2O solution was vacuum-transferred to another 100 mL Schlenk tube. This solution was then cooled down to -80 °C in an acetone-liquid nitrogen bath. Addition of 2.5 mL $n-BuLi$ (2.5 M solution in hexanes) was added drop wise with syringe over 7 min. The reaction mixture was kept stirring at -80 °C for 1 h. Once the cold bath was removed, solution was allowed to reach room temperature, upon a color change from colorless to yellow. Solution of iPr_2PLi was immediately added drop wise over 5 min to a solution of Et_3B (1.5 g, 6.3 mmol) in 10 mL of Et_2O previously cooled to -80 °C, reaction mixture was kept for 30 min at -80 °C. Solution was then allowed to warm up to room temperature for 10 min. Isolation of the product was carried by recrystallization of a yellow slurry at -80 °C in Et_2O . Crystals were washed with cold Et_2O twice and dried under vacuum. A white powder was obtained: 1.1 g, 38 % yield. **1H NMR** (500 MHz, benzene- d_6): δ 7.76 (2, 6H, *o*-Ph), 7.28 (t, 6H, *p*-Ph), 7.10 (t, 3H, *p*-Ph), 2.98 (q, 8H, Et_2O -coord), 2.21 (sext, 2H, C-H), 1.17 (dd, 6H, CH_3), 1.03 (t, 6H, CH_3), 0.82 (t, 12H, Et_2O -coord). **^{13}C NMR** (125.72 MHz, benzene- d_6): δ 135.4 (d, 6C, *o*-Ph), 127.4 (*m*-Ph, signal overlapped with solvent, found by *g*HSQC), 124.2 (s, 3C, *p*-Ph), 65.6 (s, 4C, Et_2O -coord), 26.2 (d, 2C, CH_3), 26.6 (s, 2C, CH_3), 22.0 (s, 2C, C-H), 14.9 (s, 4C, Et_2O -coord). **^{31}P NMR** (202.40 MHz, benzene- d_6): δ -13.7 to -14.6 (brm, iPr_2P-BEt_3Li). **^{11}B NMR** (160.41 MHz, benzene- d_6): δ -7.6 (brm, iPr_2P-BEt_3Li).

[(PPh₃)₂Ni(μ-P*i*Pr₂)₂] (12)



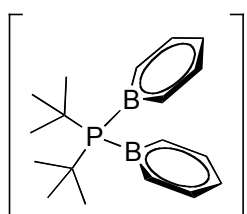
Nickel dimer **12** was isolated from the reaction mixture of ligand **DiPB** (0.08 g, 0.15 mmol) and (PPh₃)NiBr₂ (0.06 mg, 0.08 mmol) were placed inside a small Schlenk and ≈ 10 mL of toluene were added to the mixture of solids. Solution turned brown dark with the presence of a precipitate.

Solution was filtered through cannula and volatiles were removed under vacuum. Crystals were obtained from slow evaporation of a saturated solution of toluene.

[BPh₄][Li(THF)₄]

[BPh₄][Li(THF)₄] was isolated from the reaction of ligand **DiPB** (0.08 g, 0.16 mmol) dissolved in ≈ 5 mL of toluene and added to a 5 mL red solution of PdCl₂ (0.01 g, 0.08 mmol), mixture turned colorless with the presence of a black precipitate, reaction was allowed to stir overnight at room temperature. Upon 24 h of stirring solution turns green-dark, solid was filtered out through cannula and yellow solution was evaporated to dryness. Crystals were obtained from a saturated solution in THF.

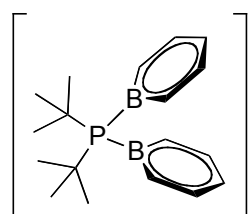
Potassium ditertbutylphosphido-bisboratabenzene (*ansa*-DTBB)



In a 15 mL Schlenk tube equipped with a magnetic stirrer, **DTBB** ligand (0.02 g, 0.08 mmol) was dissolved in 5.0 mL of THF. This yellow solution was added drop wise over 5 min to a colorless solution of Cl-boracycle(TMS) (0.01 g, 0.08 mmol) dissolved in 2.5 mL of THF. The reaction mixture became deep yellow, after evaporation of volatiles. The yellow oil was triturated with hexane. The volatiles were removed and trituration with hexane was repeated twice. A pale yellow powder was obtained. Yield 100% by NMR. ¹H NMR (500 MHz, benzene-*d*₆): δ 8.03 (brs, 4H, *o*-C₅H₄B-*PtBu*₂), 7.41 (t, *J* = 7.3 Hz, 2H, *p*-C₅H₄B-*PtBu*₂), 7.27 (t, *J* = 8.9 Hz, 4H, *m*-C₅H₄B-*PtBu*₂), 0.92 (d, *J* = 14.4 Hz, 18H, C₅H₄B-*PtBu*₂). ¹³C (125.72 MHz, benzene-*d*₆): δ 133.8 (d, *J* = 16.2 Hz, 2C, *o*-C₅H₄B-*PtBu*₂), 132.2 (*ortho*

carbon not observed, found by HSQCAD), 120.4 (*para* carbon not observed, found by HSQCAD), 31.2 (s, 1C, *PtBu*₂), 30.9 (s, 1C, *PtBu*₂), 29.0 (d, *J* = 2.8 Hz, 6C, CH₃- *PtBu*₂). ³¹P NMR (202.40 MHz, benzene-*d*₆): δ 33.5 (q, *J*_{P-B} = 178.2 Hz, B-P-B). ¹¹B NMR (160.41 MHz, benzene-*d*₆): δ 19.2 (d, *J*_{P-B} = 96.2 Hz). HR-MS (ESI): *m/z* = 291.21 [(C₅H₄B)₂-*PtBu*₂]⁻.

Dipotassium ditertbutylphosphido-bisboratabenzene (13)



2K A freshly prepared yellow solution of ***ansa*-DTBB** in THF/benzene-*d*₆ (0.02 g, 0.005 mmol) was added to a vial containing K_{C₈} (0.001 g, 0.012 mmol), mixture was transferred to a J-Young tube and left for sonication for 1h. After sonication, the yellow solution turned deep yellow with graphite as a black precipitate. Solution was then filtered and used for characterization. No peaks were observed by NMR.

X-Ray Crystallography Data

Crystals of compounds **DiPB**, **12** and ***ansa*-DTBB** were mounted on a glass fibre using Paratone N® hydrocarbon oil. Measurements were made on a Bruker APEX II area detector diffractometer equipped with graphite monochromated MoK α radiation. The program used for retrieving cell parameters and data collection was APEX 2.²²⁹ Data were integrated using the program SAINT,²³⁰ and corrected for Lorentz and polarization effects. The structure was solved and refined using SHELXS-97.²³¹ All non-H atoms were refined anisotropically. The hydrogen atoms were placed at idealized positions.

Crystal data and structure refinement for [iPr₂P-BPh₃Li (DiPB)

Empirical formula	C ₃₂ H ₄₉ BLiO ₂ P	
Formula weight	524.43	
Temperature	200(2) K	
Wavelength	0.71073 Å	
Crystal system	Monoclinic	
Space group	P21	
Unit cell dimensions	a = 11.0666(4) Å	α = 90°
	b = 23.6638(7) Å	β = 93.589(2)°
	c = 12.1432(4) Å	γ = 90°
Volume	3173.80(18) Å ³	
Z	4	
Density (calculated)	1.077 mg/m ³	
Absorption coefficient	0.111 mm ⁻¹	
F(000)	1120	
Crystal size	0.24 x 0.12 x 0.08 mm ³	
Theta range for data collection	1.72 to 26.38°	
Index ranges	-13 ≤ h ≤ 13, -26 ≤ k ≤ 26, -15 ≤ l ≤ 15	
Reflections collected	63853	
Independent reflections	12987 [R(int) = 0.0404]	
Completeness to theta = 25.242°	99.8 %	
Absorption correction	Semi-empirical from equivalents	
Max. and min. transmission	0.881 and 0.859	
Refinement method	Full-matrix least-squares on F ²	
Data / restraints / parameters	12987 / 1 / 667	
Goodness-of-fit on F ²	1.019	
Final R indices [I > 2σ(I)]	R1 = 0.0419, wR2 = 0.1048	
R indices (all data)	R1 = 0.0509, wR2 = 0.1111	
Largest diff. peak and hole	0.527 and -0.233 e.Å ⁻³	

Crystal data and structure refinement for [(PPh₃)₂Ni₂(μ-PiPr₂)₂] (12)

Empirical formula	C ₄₈ H ₅₈ Ni ₂ P ₄	
Formula weight	876.24	
Temperature	150(2) K	
Wavelength	0.71073 Å	
Crystal system	Triclinic	
Space group	P-1	
Unit cell dimensions	a = 8.6885(2) Å	α = 109.9590(10)°
	b = 10.3384(3) Å	β = 91.5840(10)°
	c = 14.4128(4) Å	γ = 111.4940(10)°
Volume	1114.85(5) Å ³	
Z	1	
Density (calculated)	1.305 mg/m ³	
Absorption coefficient	1.020 mm ⁻¹	
F(000)	462	
Crystal size	0.46 x 0.24 x 0.16 mm ³	
Theta range for data collection	1.19 to 28.31°	
Index ranges	-9 ≤ h ≤ 10, -12 ≤ k ≤ 12, -18 ≤ l ≤ 18	
Reflections collected	12822	
Independent reflections	4204 [R(int) = 0.0180]	
Completeness to theta = 25.242°	92.3 %	
Absorption correction	Semi-empirical from equivalents	
Max. and min. transmission	0.849 and 0.745	
Refinement method	Full-matrix least-squares on F ²	
Data / restraints / parameters	4204 / 0 / 248	
Goodness-of-fit on F ²	1.032	
Final R indices [I > 2σ(I)]	R1 = 0.0310, wR2 = 0.0717	
R indices (all data)	R1 = 0.0428, wR2 = 0.0803	
Largest diff. peak and hole	0.644 and -0.364 e.Å ⁻³	

Crystal data and structure refinement for [tBu₂P-(BC₅H₅)₂]K (*ansa*-DTBB)

Empirical formula	C ₂₂ H ₃₆ B ₂ KOP	
Formula weight	408.20	
Temperature	150(2) K	
Wavelength	0.71073 Å	
Crystal system	Monoclinic	
Space group	P 2 ₁ /c	
Unit cell dimensions	a = 14.729(3) Å	α = 90°
	b = 13.555(2) Å	β = 100.381(2)°
	c = 12.1257(18) Å	γ = 90°
Volume	2381.4(6) Å ³	
Z	4	
Density (calculated)	1.139 mg/m ³	
Absorption coefficient	0.299 mm ⁻¹	
F(000)	880	
Crystal size	0.22 x 0.16 x 0.08 mm ³	
Theta range for data collection	2.06 to 26.38°	
Index ranges	-18 ≤ h ≤ 18, -16 ≤ k ≤ 16, -15 ≤ l ≤ 15	
Reflections collected	21427	
Independent reflections	4865 [R(int) = 0.0535]	
Completeness to theta = 25.242°	99.9 %	
Absorption correction	Semi-empirical from equivalents	
Max. and min. transmission	0.9765 and 0.9371	
Refinement method	Full-matrix least-squares on F ²	
Data / restraints / parameters	4865 / 0 / 250	
Goodness-of-fit on F ²	1.036	
Final R indices [I > 2σ(I)]	R1 = 0.0387, wR2 = 0.0941	
R indices (all data)	R1 = 0.0545, wR2 = 0.1039	
Largest diff. peak and hole	0.459 and -0.371 e.Å ⁻³	

8 Chapter 8 Conclusion and Perspective

The aim of this dissertation has been to investigate the unusual coordination modes of the di-*tert*-butylphosphido-boratabenzene ligand (**DTBB**). The **DTBB** ligand has proved to be able to coordinate in a η^1 fashion to transition metals through the lone pair of phosphorous. Thus **DTBB** acts as a bulky anionic phosphine capable to stabilize unsaturated metal centres. We had demonstrated the flexibility boratabenzene offers as a hemilabile ligand in order to fulfill the electronic needs of a metal centre and successfully obtain zwitterionic metal complexes with catalytic applications.

In Chapter 4 we reported a structural analysis of the donating capability of **DTBB** against other donor ligands by coordination to an iron centre, affording the first example of the **DTBB** ligand coordinated η^1 to a transition metal. These results highlight the electron richness of this ligand and provide experimental evidences on the calculations carried previously by our group. The **DTBB** demonstrates to be a highly donating ligand and its steric bulk contributes to its nucleophilicity as an anionic phosphine. Additionally **DTBB** is capable to rearrange its coordination mode from η^1 to η^6 when coordinated to iron, generating a pendant phosphidoboratabenzene. The discovery of the pendant phosphine and its high reactivity against moisture are further evidence of the nucleophilicity of the **DTBB** when coordinated to a metal centre. The interaction of the exocyclic Lewis base on boron with moisture and its synergic interaction with the boron itself have been set in evidence by the formation of hydrolysis products of the pendant phosphidoboratabenzene.

This work was extended to the synthesis of boratabenzene complexes with metals of the group 11, which to the best of our knowledge has no precedents in the literature. We had provided the characterization of two Cu(I)- η^1 -**DTBB** species. The monophosphine and the bisphosphine species display a P-Cu σ interaction, which is evidenced by the η^1 coordination. Unlike the Cu species, the Ag cation appears to interact weakly with the aromatic ring on **DTBB**, as a result of this weak interaction the stability of the complex is compromised, despite **DTBB**'s σ -donating

strength. The reactivity with gold resulted in the labilization of the P-B interaction, forming a structurally relevant phosphido-gold(I) tetramer. This labilization offers insights into the stability of the P-B bond under certain conditions and the possibilities to apply this into the discovery of a B-M interaction, the formation of an unprecedented σ -bonded boratabenzene ring to a metal.

Contrary to the η^1 interaction which appears to be favoured for the metals of the group 11, the formation of a dimeric Rh(I)-**DTBB** complex shows a boratabenzene ring coordinated η^6 through the π system, a well known coordination mode for boratabenzene ligand. This interaction however proved to be convenient as the boratabenzene ligand stabilizes the reactive Rh(I) centre and allows for it to carry the catalytic hydrogenation of alkenes and alkynes under mild conditions. The identification of two Rh-H species sets up questions on what the active species is and the mechanism of the reaction, as well as the role of boron and the Lewis base on boron over the catalytic activity.

Finally the extension of the main goal of the project, the synthesis of highly donating bulky anionic phosphine ligands, was undertaken by replacing the boratabenzene moiety for a borate. This resulted in a new di-*iso*-propylphosphido-tetraphenylborate molecule (**DiPB**), which demonstrates P-B cleavage upon reaction with metals, which widely differs from what was observed for the **DTBB** ligand. These results set in place the importance of the stabilization by the aromatic ring of boratabenzene and the singularity of the P-B interaction in boratabenzene ligands.

The possibility to cleave the P-B interaction in **DTBB** was evidenced by the reaction with zirconocene. The P-B bond was broken resulting in the formation of a free borabenzene ring captured by another molecule of **DTBB** (**ansa-DTBB**). The discovery of the **ansa-DTBB** ligand has provided new insights on the lability of the P-B interaction as well as provided a new ligand with promising coordination chemistry and future applications in catalysis.

Overall this work demonstrates that boratabenzene ligands are useful tools in the synthesis of zwitterionic complexes with promising catalytic applications. The results obtained from the comparison of the **DPB**, **DiPB** and **DTBB** ligands had allowed us to evaluate and better understand the nature and strength of the P-B interaction. The synthesis of η^1 bonded **DTBB** complexes was achieved as well, including the discovery of a new family of complexes from the group 11, which are possible to isolate due to the presence of the η^1 coordination.

Previous research from our group on the coordination modes of **DTBB** have shown evidence of a variety of hapticities such as a Ni- η^6 -**DTBB** dimer and two examples of Pt- η^3 -**DTBB** complexes. The results presented herein shed light onto the reach coordination chemistry of **DTBB** ligand, as put in evidence by the transitions from η^1 – η^6 observed on the iron complexes, the observed Cu- η^1 -**DTBB** species and the proposed η^3 species with silver.

In the following paragraphs, a description of what has been learned about the possible coordination modes of the **DTBB** ligand will be presented. While some of these ideas are based on previous work, they are supported in evidences presented in this dissertation.

- The **DTBB** ligand is a highly donating anionic phosphine

Our study of the CpFe(CO)₂DTBB (**1**) species had demonstrated in a qualitative way that the **DTBB** ligand is more donating than the related **DPB** and other very good donors such as carbenes. In fact the **DTBB** donating capability resembles that of phosphide ligands.

Also, it was possible to isolate Cu(I) complexes, as stable linear M-L fragments of mono and bis-**DTBB** species. These 14 electron complexes could potentially find a variety of applications in catalysis.

- The **DTBB** is a hemilabile ligand

We observed that the CO ligands on species **1**, are susceptible to photodissociation, generating a ferrocenyl-like pendant phosphine CpFeDTBB (**2**). Due to its rich variety of coordination modes and the hemilability inherent to the ligand, the use of boratabenzene frameworks would be an asset to the stabilization of reactive intermediates involved in catalytic processes, similarly to the role of the Cp ligand.

The **DiPB** ligand featuring a P-B interaction between an alkyl phosphide and an aryl borate, demonstrated that the P-B bonding did not withstand the coordination to group 10 metals, setting forward a relative increased stability on the P-B interaction that comes with the presence of the aromatic boratabenzene ring.

However considering the evidences withdrawn from the reaction of **DTBB** with zirconocene, which resulted in the formation of the **ansa-DTBB** and the formation of species such as CpFe(C₅H₅B-OH) (**3**) and CpFe(C₅H₅B)-O-(BC₅H₅)FeCp (**4**) with a B-O-B bridge, had demonstrated that the P-B on **DTBB** can be susceptible to cleavage under certain conditions and upon coordination to the metal. Additionally the cleavage of the P-B bond in the presence of Au(I), resulted in the formation of an phosphido-gold oligomeric complex, providing a wider perspective on the stability of such interaction.

- Overall, the **DTBB** offers a very rich coordination chemistry, which is unique in the field of borabenzene research

8.1 Future Work

8.1.1 Iron Boratabenzene Complexes

In order to overcome the difficulties on the isolation of the CpFeDTBB (**2**) species, an alternative to its enhanced reactivity with moisture would be to protect the pendant phosphine by forming an HBF₄ adduct, as has been observed for other ferrocenyl-like phosphines.²³² Moreover protonation of the phosphine, generating a naked boron centre could generate unprecedented B-M species.

Other difficulties to be addressed are the big scale synthesis of **2**. Perhaps changing the metal precursor using a ligand that can be easily displaced such as solvent molecules, might lead to the formation of the pendant ferrocenyl-like phosphine.

In contrast to what was reported by Wen,⁷⁸ the conversion from the μ -oxo B-O-B species to B-OH does not happen in the case of the iron-coordinated species **3** and **4**. A systematic study on the mechanism of formation of the iron species should be undertaken in order to better understand the formation of such species. Attempts for the protonation of the B-O-B bridge with acid might lead to the formation of the B-OH (**3**) species, however the synthesis of the B-O-B (**4**) species still is a subject to be assessed. The reactivity with water reported for the ruthenium species does not hold true for the iron species.

Interest must also be put onto the catalytic applications of the species mentioned in chapter 4, i.e.:

- Explore the catalytic applications of CpFe(CO)₂DTBB (**1**) in reductive amination as reported for similar species with very donor phosphines.²³³ The species proposed to date for such catalytic process, are cationic complexes. Hence a zwitterionic species should provide an enhanced catalytic activity, avoiding ion-pairing effects. Additionally the presence of a highly donating phosphine ligand could increase the activity, if the conversion to the η^6 -coordination does not hinders the reaction.

- Alternatively, applications in the dehydrocoupling of amino boranes are of relevance due to their use as hydrogen storage materials. It should be then appropriate to explore the ligand displacement on the $\text{CpFe}(\text{CO})_2\text{DTBB}$ (**1**) by reaction with a strong donor such as PMe_3 under photolytic conditions. By looking at the possibility of one of the CO ligands to be displaced by a highly basic PMe_3 . Interestingly this reaction could cleave the P-B interaction, but if the P-B bond is left undisturbed upon reaction with a donor phosphine, such reactivity could result in the use of the iron carbonyl species as a dehydrocoupling catalyst.

8.1.2 Copper Boratabenzene Complexes

One of the most interesting results obtained during the course of this work was the isolation and characterization of a $\text{Cu}(\text{I})-\eta^1\text{-DTBB}$ species. The use of such species to activate small molecules such as CO, CO_2 and H_2 are catalytic alternatives of interest. Notably $\text{Cu}(\text{I})$ species can also be useful to the bioinorganic chemist as models for metalloenzymes that feature L-Cu-L linear geometries.

Further essays on the use of co-ligands and possibly employing other metal precursors for $\text{Ag}(\text{I})$ and $\text{Au}(\text{I})$, could lead to interesting coordination chemistry and open up new avenues in catalytic transformations as it has been observed for other organometallic complexes of this group.

Additionally, the preference for η^1 coordination for metals such as gold, could lead to interesting interactions between borabenzene and $\text{Au}(\text{I})$ metal centre, such as $\eta^1\text{-B}$ observed by Bourissou.²³⁴ Therefore taking advantage of the labilization of the P-B bond, the so long desired B-M interaction, which has never been observed for borabenzene ligands, but could potentially be stabilized by gold's preference for η^1 coordination and the *d* filled orbitals, might result into a boratabenzene ring base-free, featuring a B-M bond. The relevance of the B-M interaction as a depart species for several transformations, including the formation of C-C bonds¹³⁸ is indeed a valuable and interesting possibility to be explored.

8.1.3 Rhodium Boratabenzene Complexes

Boratabenzene ligand has been used as a chiral ligand for stereoselective catalytic reactions. In order to expand the substrate scope of the Rh hydrogenation chemistry, competition experiments between stereoisomers should be carried to looking for selectivity influenced by the bulkiness of the phosphine.

Furthermore, the possibility of the rhodium dimer to carry the C-H activation and display an enhanced activity due to the role of the available lone pair on phosphorous might overpass the activity of the piano stool complexes of amido-boratabenzene reported by Bazan.⁵⁸ The major drawback of this application is the instability of the species at high temperatures.

Further work on the isolation of the metal hydride species will bring a better understanding on the mechanism of the hydrogenation. Moreover, the use of high pressures of hydrogen to carry hydrogenation at room temperature and high pressure H₂ and ethylene, could also help overcoming the temperature limitations.

8.1.4 The DiPB and *ansa*-DTBB Ligands

The most important aspect into possible applications for the **DiPB** ligand in coordination chemistry is to look for transition metals that will bind the ligand while preserving the P-B interaction.

In order to achieve this goal, the use of group 11 metals is proposed, based on the results observed with **DTBB** ligand. Metals such as Cu would be a first hand choice of metal precursor. Copper has shown to have a weak interaction with B and displays a preference to coordinate through a σ interaction of the type L-M-L generating also a species of the type R₃P-MCl. Results on the behaviour of the **DiPB** ligand would provide further data to compare the differences and relevance of the ligands containing the boratabenzene framework.

One of all the interesting molecules obtained from this work is the ***ansa*-DTBB** ligand. Further research on the formation of complexes using group 3 and group 4 transition metals is worth of a systematic exploration.

Investigations on the stability of the P-B interaction by looking at the possibility of using the **ansa-DTBB** as a source of base free borabenzene to generate a metal supported borabenzene with a direct M-B interaction is of main interest due to the scarcity of M-B σ -interactions. Furthermore, the use of group 11 metals, which could potentially stabilize the M-B interaction, is recommended.

Carrying DFT calculations to obtain the structure optimization of the **ansa-DTBB** would give a perspective on the dimensions of the $C_{\text{cent}}\text{-M-C}_{\text{cent}}$ angle, enabling the optimal choice of metal centre to achieve coordination through the aromatic rings or the boratabenzene ligands.

On a last word, one has to mention the main complication in using borabenzene derivatives as ligands for transition metals. The long synthetic pathways to obtain this boron heterocycle, limit its applications at a larger scale. However this should rather be a motivation to design relatively stable boratabenzene metal complexes with excellent catalytic activity.

8.2 Final Words

Ever since the first reports of the boratabenzene ligand in the 70s, it has been clear that it is a promising framework to work with. However boratabenzene chemistry still holds secrets to us. As we observed, the role of the exocyclic substituent can provide additional functionalities to the complexes. The reactivity and applications are still a challenge to undertake by future boron chemist. The stabilization of the boratabenzene moiety with the appropriate Lewis base will help mediate the reactivity to find a middle point between the two edges of unreactive and extremely reactive boratabenzene species. Despite the fact that boratabenzene ligands are a challenging target molecule to work with, the nature of its interactions with metal centres and substrates and the role these interactions may have on catalytic applications are worth the challenge. We hope that the results of our research will continue to encourage other chemists on their quest to shape the fundamental aspects of the boratabenzene research into affordable and meaningful industrial applications.

9 Bibliography

¹<http://resources.schoolscience.co.uk/johnsonmatthey/index.htm>, consulted on September **2015**.

²<http://www.acs.org/content/acs/en/pressroom/newsreleases/2011/november/aming-catalysts-american-chemical-societys-latest-prized-science-video.html>, consulted on September **2015**.

³Crabtree, R.H. *The Organometallic Chemistry of the Transition Metals*; 5th Ed. John Wiley & Sons: USA **2009**.

⁴Anastas, P.T.; Warner, J.C. *Green Chemistry, Theory and Practice*; Oxford University Press: USA **2000**.

⁵a) Heck, R.F. Nobel Lecture: Palladium Reactions for Organic Syntheses. nobelprize.org. Nobel Media AB 2014. Consulted December **2015**.

http://www.nobelprize.org/nobel_prizes/chemistry/laureates/2010/heck-lecture.html

b) Negishi, E.-I. Nobel Lecture: Magical Power of Transition Metals: Past, Present and Future. *The Nobel Prizes 2010*. Ed. Karl Grandin, Nobel Foundation, Stockholm: **2011**. c) Susuki, A. Nobel Lecture: Cross-coupling Reactions of Organoboranes: An Easy Way for C-C Bonding. *The Nobel Prizes 2010*. Ed. Karl Grandin, Nobel Foundation, Stockholm: **2011**.

⁶a) Chauvin, Y. Nobel Lecture: Olefin metathesis: The Early Days. *The Nobel Prizes 2005*. Ed. Karl Grandin, Nobel Foundation, Stockholm, **2006**. b) Grubs, R.H. Nobel Lecture: Olefin Metathesis Catalysts for the Preparation of Molecules and Materials. *The Nobel Prizes 2005*. Ed. Karl Grandin, Nobel Foundation, Stockholm, **2006**. c) Schrock, R.R. Nobel Lecture: Multiple Metal-Carbon bonds for Catalytic Metathesis Reactions. *The Nobel Prizes 2005*. Ed. Karl Grandin, Nobel Foundation, Stockholm, **2006**.

⁷a) Knowles, W.S. Nobel Lecture: Asymmetric Hydrogenations. *The Nobel Prizes 2001*. Ed. Tore Frangsmyr, Nobel Foundation, Stockholm, **2002**. b) Noyori, R. Nobel Lecture: Asymmetric Catalysis: Science and Technology. *The Nobel Prizes 2001*. Ed. Tore Frangsmyr, Nobel Foundation, Stockholm, **2002**. c) Sharpless, K.B. Nobel Lecture: The Search for New Chemical Reactivity. *The Nobel Prizes 2001*. Ed. Tore Frangsmyr, Nobel Foundation, Stockholm, **2002**.

⁸Thomas, C.M.; Suss-Fink, G. *Coord. Chem. Rev.*, **2003**, 243, 125-142.

⁹a) Piers, W. *Chem. Eur. J.*, **1998**, 4, 13-18; b) Erker, G. *Acc. Chem. Res.*, **2001**, 34, 309-317.; c) Erker, G. *Chem. Commun.*, **2003**, 1469-1476.

¹⁰IUPAC. Compendium of Chemical Terminology, 2nd ed. (the "Gold Book"). Compiled by A. D. McNaught and A. Wilkinson. Blackwell Scientific Publications, Oxford, **1997**. XML on-line corrected version: <http://goldbook.iupac.org> (2006-) created by M. Nic, J. Jirat, B. Kosata; updates compiled by A. Jenkins. ISBN 0-9678550-9-8.doi:10.1351/goldbook. Last updated on: **2014**.

¹¹Chauvin, R. *Eur. J. Inorg. Chem.*, **2000**, 577-5591.

-
- ¹²Rankin, M.A.; McDonald, R.; Ferguson, M.J.; Stradiotto, M. *Organometallics*, **2005**, *24*, 4981-4994.
- ¹³Bianchini, C.; Frediani, P.; Sernaue, V. *Organometallics*, **1995**, *14*, 5458-5459.
- ¹⁴Stradiotto, M.; Hesp, K.D.; Lundgren, R.J. *Angew. Chem. Int. Ed.*, **2010**, *49*, 494-512.
- ¹⁵Ibrahim, I.; Alper, H. *J. Am. Chem. Soc.*, **1990**, *112*, 3674-3677.
- ¹⁶Macchioni, A. *Chem. Rev.*, **2005**, *105*, 2039-2073.
- ¹⁷Peters, J.C.; Feldman, J.D.; Tilley T.D. *J. Am. Chem. Soc.* **1999**, *121*, 9871-9872.
- ¹⁸Thomas, J.C.; Peters, J.C. *J. Am. Chem. Soc.*, **2002**, *123*, 5501-5101.
- ¹⁹Thoma, C.M.; Peters, J.C. *Inorg. Chem.*, **2004**, *43*, 8-10.
- ²⁰Beach, M.T.; Walker, J.M.; Larocque, T.G.; Deagle, J.L.; Wang, R.; Spivak, G.J. *J. Organomet. Chem.*, **2008**, *693*, 2921-2928.
- ²¹Granville, S.L.; Welch, G.C.; Stephan, D.W. *Inorg. Chem.*, **2012**, *51*, 4711-4721.
- ²²Jaska, C.A.; Dorn, H.; Lough, A.J.; Manners, I. *Chem. Eur. J.* **2003**, *9*, 271-281.
- ²³Hoic, D.A.; Davis, W.M.; Fu, G.C. *J. Am. Chem. Soc.*, **1996**, *118*, 8176-8177.
- ²⁴Emsley, J. RSC: Boron, Element information, properties and uses. Periodic table. <http://www.rsc.org/periodic-table/element/5/boron>, Consulted October **2015**.
- ²⁵Thomas Jefferson National Accelerator Facility - Office of Science Education, [It's Elemental - The Periodic Table of Elements](#), Consulted October **2015**.
- ²⁶Hosmane, N.S. Boron Science, New Technologies and Applications; Taylor & Francis Group: USA **2012**. P.p. 91, 147.
- ²⁷Borates by use, Rio Tinto Minerals, Borax. <http://www.borax.com/about-borates/borates-by-use>, Consulted October 2015.
- ²⁸Thomas, S.E. *Organic Synthesis, The Roles of Boron and Silicon*; Oxford University Press: USA **1991**.
- ²⁹Sivaev, I.B.; Bregadze, V.I. *Coord. Chem. Rev.*, **2014**, *270-271*, 75-88.
- ³⁰Miessler, G.L. *Inorganic Chemistry*; 3rd Ed. Pearson, Prentice Hall: **2003**.
- ³¹Herberich, G.E.; Greiss, G.; Heil, H.F. *Angew. Chem. Int. Ed.*, **1970**, *9*, 805-806.
- ³²a) Raabe, G.; Baldofski, M. *Aust. J. Chem.*, **2011**, *64*, 957-964.; b) Fu, G.C. *Adv. Organomet. Chem.*, **2001**, *47*, 101-119.
- ³³Ashe, A.J.; Shu, P. *J. Am. Chem. Soc.*, **1971**, *93*, 1804-1805.
- ³⁴Hoic, D.A.; Robbins, J.W.; Davis, W.M.; Fu, G.C. *Organometallics*, **1996**, *15*, 1315-1318.
- ³⁵Qiao, S.; Hoic, D.A.; Fu, G.C. *J. Am. Chem. Soc.*, **1996**, *118*, 6329-6330.
- ³⁶Légaré, M.-A.; Bélanger-Chabot, G.; De Robillard, G.; Languérand, A.; Maron, L.; Fontaine, F.-G. *Organometallics*, **2014**, *33*, 3596-3606.
- ³⁷a) Herberich, G.E.; Ohst, H. *Adv. Organomet. Chem.*, **1986**, *52*, 199-236.; b) Allen, C.W.; Palmer, D.E. *J. Chem. Edu.*, **1978**, *55*, 497-500.
- ³⁸Hoic, D.A.; Davis, W.M.; Fu, G.C. *J. Am. Chem. Soc.*, **1995**, *117*, 8480-8481.

-
- ³⁹Herberich, G.E.; Zheng, X.; Rosenplanter, J.; Englert, U. *Organometallics*, **1999**, *18*, 4747-4752.
- ⁴⁰Herberich, G.E.; Englert, U.; Ganter, B.; Lamertz, C. *Organometallics*, **1996**, *15*, 5236-5241.
- ⁴¹Hagenau, U.; Heck, J.; Hendrickx, E.; Persoons, A.; Schuld, T.; Wong, H. *Inorg. Chem.*, **1996**, *35*, 7863-7866.
- ⁴²Bélanger-Chabot, G.; Rioux, P.; Maron, L.; Fontaine, F.-G. *Chem. Commun.*, **2010**, *46*, 6816-6818.
- ⁴³Perez, V.; Barnes, S.; Fontaine, F.-G. *Eur. J. Inorg. Chem.*, **2014**, *33*, 5698-5702.
- ⁴⁴Mushtaq, A.; Bi, W.; Légaré, M.-A.; Fontaine, F.-G. *Organometallics*, **2014**, *33*, 3173-3181.
- ⁴⁵Ashe III, A.J.; Al-Ahmad, S.; Fang, X. *J. Organomet. Chem.*, **1999**, *581*, 92-97.
- ⁴⁶Rabee, E., *Dissertation*, Rheinisch-Westfälische Technische Hochschule, Aachen, **1984**.
- ⁴⁷Herberich, G.E.; Englert, U.; Fischer, A.; Ni, J.; Schmitz, A. *Organometallics*, **1999**, *18*, 5496-5501.
- ⁴⁸Langerand, A.; Barnes, S.S.; Bélanger-Chabot, G.; Maron, L.; Berrouard, P.; Audet, P.; Fontaine, F.-G. *Angew. Chem. Int. Ed.*, **2009**, *48*, 6695-6698.
- ⁴⁹Barnes, S.S.; Légaré, M.-A.; Maron, L.; Fontaine, F.-G. *Dalton Trans.*, **2011**, *40*, 12439-12442.
- ⁵⁰Hoic, D.A.; DiMare, M.; Fu, G.C. *J. Am. Chem. Soc.*, **1997**, *119*, 7155-7156.
- ⁵¹Tolman, C.A. *Chem. Rev.*, **1977**, *77*, 313-348.
- ⁵²Gusev, D.G. *Organometallics*, **2009**, *28*, 763-770.
- ⁵³Macha, B.B.; Boudreau, J.; Maron, L.; Maris, T.; Fontaine, F.-G. *Organometallics*, **2012**, *31*, 6428-6437.
- ⁵⁴Bonnemann, H.; Brijoux, W.; Brinkmann, R.; Meurers, W. *Helv. Chimica Acta*, **1984**, *67*, 1616-1624.
- ⁵⁵a) Banhart, R.W.; Bazan, G.C. *J. Am. Chem. Soc.*, **1998**, *120*, 1082-1083.; b) Rogers, J.S.; Bazan, G.C.; Sperry, C.K. *J. Am. Chem. Soc.*, **1997**, *119*, 9305-9306.; c) Tobisch, S.; Ziegler, T. *Organometallics*, **2005**, *24*, 256-265.; d) Bazan, G.C.; Rodriguez, G. *Organometallics*, **1997**, *16*, 2492-2494.; e) Bazan, G.C.; Rodriguez, G. *J. Am. Chem. Soc.*, **1996**, *118*, 2291-2292.; f) Komon, Z.J.A.; Rogers, J.S.; Bazan, G.C. *Organometallics*, **2002**, *21*, 3189-3195.
- ⁵⁶Wang, X.; Peng, W.; Cui, P.; Leng, X.; Xia, W.; Chen, Y. *Organometallics*, **2013**, *32*, 6166-6169.
- ⁵⁷Wang, X.; Leng, X.; Chen, Y. *Dalton Trans.*, **2015**, *44*, 5771-5776.
- ⁵⁸Woodmansee, D.H.; Bu, X.; Bazan, G.C. *Chem. Commun.*, **2001**, 619-620.
- ⁵⁹Yuan, Y.; Chen, Y.; Li, G.; Xia, W. *Organometallics*, **2008**, *27*, 6307-6312.
- ⁶⁰Lu, E.; Yuan, Y.; Chen, Y.; Xia, W. *ACS Catal.*, **2013**, *3*, 521-524.
- ⁶¹Schlenk W. in *Methoden Org. Chem.*; Houben-Weyl, **1924**, *4*, 720-978.

-
- ⁶²Shriver, D.F.; Drezdon, M.A., *The manipulation of air-sensitive compounds*, 2nd Ed., Wiley: New York, **1986**.
- ⁶³Armarego, W.L.F.; Chai, C.L.L. *Purification of Laboratory Chemicals*, 5th Ed., Butterworth-Heinemann, Elsevier Science: USA, **2003**.
- ⁶⁴<http://web.mit.edu/specplab/www/Facility/nmrfreq.html>, Consulted on August **2015**.
- ⁶⁵a) Ammann, C.; Isaia, F.; Pregosin, P. S. *Magn. Reson. Chem.* **1988**, *26*, 236-238.; b) Cotton, F.A.; Luck, R.L.; Root, D.R.; Walton, R.A. *Inorg. Chem.* **1990**, *29*, 43-47.
- ⁶⁶Crabtree, R.H.; Lavin, M. *J. Chem. Soc., Chem. Commun.*, **1985**, 1661-1662.
- ⁶⁷a) Heinekey, D.M.; Oldham, W.J.J. *Chem.Rev.*, **1993**, *93*, 913-926.; b) Desrosiers, P.J.; Cai, L.; Lin, Z.; Richards, R.; Halpern, J. *J. Am. Chem. Soc.* **1991**, *113*, 4173-4184.
- ⁶⁸Pregosin, P. *NMR in organometallic chemistry*, Wiley-VCH Verlag & Co: Weinheim, Germany, **2012**.
- ⁶⁹a) Strohal M., Hassman M., Košata B., Kodíček M. *Rapid Commun. Mass Spec.*, **2008**, *22*, 905-908; b) Strohal M., Kavan D. Novák P, Volný M., Havlíček V., *Anal. Chem.*, **2010**, *82*, 4648-4651.
- ⁷⁰Koch, W.; Holthausen, M.C. *A Chemist Guide to Density Functional Theory*, 2nd Ed., Wiley-VCH: Germany, **2007**.
- ⁷¹a) Hohenberg, P. *Phys. Rev.*, **1964**, *136*, B 864-B871.; b) Kohn, W.; Sham, L.J. *Phys. Rev.*, **1965**, *140*, A 1133-A 1138.; c) Kohn, W. *Rev. Mod. Phys.*, **1999**, *71*, 1253-1266.
- ⁷²Schuman, H. *J. Organomet. Chem.*, **1987**, *320*, 145-162.
- ⁷³Zheng, J.; Misal Castro, L.C.; Roisnel, T.; Darcel, C.; Sortais, J.-B. *Inorg. Chim. Acta*, **2012**, *380*, 301-307.
- ⁷⁴Bézier, D.; Venkanna, G.T.; Misal Castro, L.C.; Zheng, J.; Roisnel, T.; Sortais, J.-B.; Darcel, C. *Adv. Synth. Catal.*, **2012**, *354*, 1879-1884.
- ⁷⁵Lee, K; Clark, T.J.; Lough, A.J.; Manners, I. *Dalton Trans.*, **2008**, 2732-2740.
- ⁷⁶Herberich, G.E.; Basu Baul, T.S.; Englert, U. *Eur. J. Inorg. Chem.*, **2002**, 43-48.
- ⁷⁷Herberich, G.E.; Hebner, B. *Chem. Ber.*, **1982**, *115*, 3115-3127.
- ⁷⁸Li, T.; Fu, C.; Liu, Z.; Guo, S.; Liu Z.; Wen, T.-B. *Organometallics*, **2015**, *34*, 3292-3302.
- ⁷⁹Ashe, A.J. III; Butler, W.; Sandford, H.F. *J. Am. Chem. Soc.*, **1979**, *101*, 7066-7067.
- ⁸⁰Kuckmann, T.I.; Dornhaus, F.; Bolte, M.; Lerner, H.-W.; Hotlhausen, M.C.; Wagner, M. *Eur. J. Inorg. Chem.*, **2007**, 1989-2003.
- ⁸¹a) Lee, K; Clark, T.J.; Lough, A.J.; Manners, I. *Dalton Trans.*, **2008**, 2732-2740.; b) Angerer, W.; Sheldrick, W.S.; Malisch, W. *Chem. Ber.*, **1985**, *118*, 1261-1266.
- ⁸²Lorenz, I.-P.; Murschel, P.; Pohl, W.; Polborn, K. *Chem. Ber.*, **1995**, *128*, 413-416.

- ⁸³a) Riley, P.E.; Davis, R.E.; *Organometallics*, **1983**, *2*, 286-292.; b) Davison, A.; Green, M.L.H.; Wilkinson, G. *J. Chem. Soc.*, **1961**, 3172-3177.
- ⁸⁴Burckett-St. Laurent, J.C.T.R.; Haines, R.J.; Nolte, C.R.; Steen, N.D.C.T. *Inorg. Chem.*, **1980**, *19*, 577-587.
- ⁸⁵Bontemps, S.; Bouhadir, G.; Dyer, P.W.; Miqueu, K.; Bourissou, D. *Inorg. Chem.*, **2007**, *46*, 5149-5151.
- ⁸⁶Paine, R.T.; Noth, H. *Chem. Rev.*, **1995**, *95*, 343-379.
- ⁸⁷a) Nyulaszi, L. *Chem. Rev.*, **2001**, *101*, 1229-1246.; b) Cloke, F.G.N.; Hitchcock, P.B.; Hunnable, P.; Nixon, J.F.; Nyulaszi, L.; Niecke, E.; Thelen, V. *Angew. Chem. Int. Ed.*, **1998**, *37*, 1083-1086.
- ⁸⁸[CpFe(CO)₂(PPh₃)]Cl•3H₂O (*P1*; 2.0%), CpFe(CO)₂(DPB) (*C2/c*; 6.49%), CpFe(CO)₂(PtBu₂•BH₃) (*P2₁2₁2₁*; 2.70%), CpFe(CO)₂(PPh₂•BH₃) (*P2₁/n*; 3.77%), CpFe(CO)₂(SiPPh₂Me) (*P2₁2₁2₁*; 2.23%), CpFe(CO)₂(DTBB) (*C2/c*; 3.16%).
- ⁸⁹Azevedo, C.G.; Calhorda, M.J.; Carrondo, M.A.A.F.C.T.; Dias, A.R.; Duarte, M.T.; Galvao, A.M.; Gamelas, C.A.; Gonçalves, I.S.; Piedade, F.M.; Romao, C.C. *J. Organomet. Chem.*, **1997**, *544*, 257-276.
- ⁹⁰Mayor-López, M.J.; Weber, J.; Mannfors, B.; Cunningham, A.F.Jr. *Organometallics*, **1998**, *17*, 4983-4991.
- ⁹¹a) Huttner, G.; Britzinger, H.H.; Bell, L.G.; Friedrich, P.; Bejenke, V.; Neugebauer, D. *J. Organomet. Chem.*, **1978**, *145*, 329-333.; b) Ascenco, J.R.; Azevedo, C.G.; Gonçalves, I.S.; Herdtweck, E.; Moreno, D.S.; Pessanha, M.; Romao, C.C. *Organometallics*, **1995**, *14*, 3901-3919.; c) Monkeberg, S.; Raaij, E.; Kiesele, H.; Brintzinge, H.H. *J. Organomet. Chem.*, **1989**, *365*, 285-295.
- ⁹²Gonçalves, I.S.; Herdweck, E.; Romao, C.C.; Royo, B. *J. Organomet. Chem.*, **1999**, *580*, 169-177.
- ⁹³Basolo, F. *Coord. Chem. Rev.*, **1982**, *43*, 7-15.
- ⁹⁴Caldwell, H.; Isseponi, S.; Pregosin, P.S.; Albinati, A.; Rizzato, S. *J. Organomet. Chem.*, **2007**, *692*, 4043-4051.
- ⁹⁵Luck, R.L.; Morris, R.H.; Sawyer, J.F. *Organometallics*, **1984**, *3*, 247-255.
- ⁹⁶Wang, X.; Kehr, G.; Daniluc, C.G.; Erker, G. *J. Am. Chem. Soc.*, **2014**, *136*, 3293-3303.
- ⁹⁷Kataoka, N.; Shelby, Q.; Stambuli, J.P.; Hartwig, J.F. *J. Org. Chem.*, **2002**, *67*, 5553-5566.
- ⁹⁸Cowie, B.E.; Emslie, D.J.H. *Chem. Eur. J.*, **2014**, *20*, 16899-16912.
- ⁹⁹**3** (*P32*; 3.28 %), **XXIV** (*P-1*; 3.13 %), **4** (*P2₁/c*; 4.67%), **XXV** (*P-1*; 5.01%), **XX** (*P2₁/c*; 7.90%).
- ¹⁰⁰Wells, A.F. *Structural Inorganic Chemistry*; 5th Ed. Clarendon Press, Oxford Press: Great Britain, **1984**. P.p.: 1066, 1080.
- ¹⁰¹Herberich, G.E.; Klein, W.; Spaniol, T.P. *Organometallics*, **1993**, *12*, 2660-2667.
- ¹⁰²Herberich, G.E.; Pahlmann, W. *J. Organomet. Chem.*, **1975**, *97*, C51-C53.

-
- ¹⁰³Herberich, G.E.; Engelke, C.; Pahlmann, W. *Chem. Ber.*, **1979**, *112*, 607-624.
- ¹⁰⁴Dornhaus, F.; Lerner, H.-W.; Bolte, M. *Acta Crystallogr., Sect. E: Struct. Rep. Online*, **2005**, *E61*, 0657-0658.
- ¹⁰⁵Bruker (**2005**). APEX 2 Version 2.0.2. Bruker AXS Inc., Madison, Wisconsin, USA.
- ¹⁰⁶Bruker (**2003**). SAINT Version 7.07a. Bruker AXS Inc., Madison, Wisconsin, USA.
- ¹⁰⁷Sheldrick, G.M. (**1997**). SHELXS-97 and SHELXL-97. Programs for the refinement of crystal structures. University of Gottingen, Germany.
- ¹⁰⁸Dolomanov, O.V.; Bourhis, L.J.; Gildea, R.J.; Howard, J.A.K.; Puschmann, H. *J. Appl. Cryst.*, **2009**, *42*, 339-341.
- ¹⁰⁹Sheldrick, G.M.; *Act. Cryst.*, **2008**, *a64*, 112-122.
- ¹¹⁰a) Posner, G.H. *Substitution Reactions Using Organocopper Reagents. Organic Reactions*; John Wiley & Sons: **2011**.; b) Surry, D.S.; Spring, D.R. *Chem. Soc. Rev.*, **2006**, 218-225.; c) Pearson, R.G.; Gregory, C.D. *J. Am. Chem. Soc.*, **1976**, *98*, 4098-4104.; d) House, H.O.; Respass, W.L.; Whitesides, G.M. *J. Org. Chem.*, **1966**, *31*, 3128-3141.; e) Corey, E.J.; Posner, G.H. *J. Am. Chem. Soc.*, **1967**, *89*, 3911-3912.
- ¹¹¹Calvin, M.; Wilmarth, W.K. *J. Am. Chem. Soc.*, **1956**, *78*, 1301-1305.
- ¹¹²a) Power, P.P. *Chem. Rev.*, **2012**, *112*, 3482-3507.; b) Angels, C.M.; Novoa, J.J.; Alvarez, S. *J. Am. Chem. Soc.*, **2004**, *126*, 1465-1477.
- ¹¹³Power, P.P. *J. Organomet. Chem.*, **2004**, *689*, 3904-3919.
- ¹¹⁴a) Power, P.P. *Comments Inorg. Chem.*, **1989**, *8*, 177-202.; b) Kays, D.L. *Dalton Trans.*, **2011**, *40*, 769-778.
- ¹¹⁵a) Karlin, K.D.; Zubieta, J. *Copper Coordination Chemistry: Biochemical and inorganic Perspectives*. Adenine Press: New York, **1983**.; b) Karlin, K.D.; Tyeklar, Z. *Bioinorganic Chemistry of Copper*. Springer: Netherlands, **1993**.
- ¹¹⁶Krause, N. *Modern Organocopper Chemistry*. Wiley-VCH: Germany, **2002**.
- ¹¹⁷Wilkinson, G.; Gillard, R.D.; Mcleverty, J.A. *Comprehensive Coordination Chemistry*, 5ed, Vol. 5. Pergamon: Great Britain, **1987**. P.p.: 591-534.
- ¹¹⁸Clainche, L.L.; Giorgi, M.; Reinaud, O. *Eur. J. Inorg. Chem.*, **2000**, 1931-1933.
- ¹¹⁹a) Stollenz, M.; John, M.; Gehring, H.; Dechert, S.; Frosse, C.; Meyer, F. *Inorg. Chem.*, **2009**, *48*, 10049-10059.; b) Himes, R.A.; Park, G.Y.; Barry, A.N.; Blackburn, N.J.; Karlin, K.D. *J. Am. Chem. Soc.*, **2007**, *129*, 5352-5353.; c) Du, J.-M.; Kang, D.J. *Chemistry Letters*, **2007**, *36*, 168.; d) Hubin, T.J.; Alcock, N.W.; Clase, H.J.; Busch, D.H. *Acta Crystallogr.*, **1999**, *C55*, 1402-1404.; e) Furlan, S.; Hureau, C.; Faller, P.; La Penna, G. *J. Phys. Chem. B*, **2010**, *114*, 15119-15133.; f) Ray, A.; Rosair, G.M.; Rajeev, R.; Sunoj, R.B.; Rentschler, E.; Mitra, S. *Dalton Trans.*, **2009**, 9510-9519.; g) Chou, C.-C. Liu, H.-J.; Chao, L.H.-C.; Yang, C.-C.

New J. Chem., **2015**, *39*, 1260-1266.; h) Peck, K.L.; Clewett, H.S.; Schmitt, J.C.; Shearer, J. *Chem. Commun.*, **2013**, *49*, 4797-4799.

¹²⁰Lum, J.S.; Tahsini, L.; Golen, J.A.; Moore, C.M Rheingold, A.L.; Doerrer, L.H. *Chem. Eur. J.*, **2003**, *19*, 5374-6384.

¹²¹Fernandes, T.A.; Carvalho, M.F.; Galvao, A.M.; Bandeir, N.A.G.; Calhorda, M.J.; Botelho do Rego, A.M. *J. Polym. Sci., A: Polym. Chem.*, **2012**, *50*, 1102-1110.

¹²²a) Mascal, M.; Kerdelhué, J.-L.; Blake, A.J.; Cooke, P.A. *Angew. Chem. Int. Ed.*, **1999**, *38*, 1968-1971.; b) Ferrara, S.J.; Mague, J.T.; Donahue, J.P. *Inorg. Chem.*, **2012**, *51*, 6567-6576.

¹²³a) Gierz, V.; Seyboldt, A.; Maichle-Mossmer, C.; Tornroos, K.W.; Speidel, M.T.; Speiser, B.; Eichele, K.; Kunz, D. *Organometallics*, **2012**, *31*, 7893-7901.; b) Amendola, V.; Bergamaschi, G.; Boiocchi, M.; Fabbrizzi, L.; Fuscoa, N. *Dalton Trans.*, **2011**, *40*, 8367-8376.; c) Petz, W.; Neumuller, B.; Klein, S.; Frenking, G. *Organometallics*, **2011**, *30*, 3330-3339.

¹²⁴Luck, R.; Morris, R.H. *Inorg. Chem.*, **1984**, *23*, 1489-1491.

¹²⁵a) Mee, S.P.H.; Lee, V.; Bladwin, J.E. *Angew. Chem. Int. Ed.*, **2004**, *43*, 1132-1136.; b) Casado, A.L.; Espinet, P. *Organometallics*, **2003**, *22*, 1305-1309.; c) Farina, V.; Kapadia, S.; Krishnan, B.; Wang, C.; Liebeskind, L.S. *J. Org. Chem.*, **1994**, *59*, 5905-5911.; d) Liebeskind, L.S.; Fengl, R.W. *J. Org. Chem.*, **1990**, *55*, 5359-5364.; e) Han, X.; Stoltz, B.M.; Corey, E.J. *J. Am. Chem. Soc.*, **1999**, *121*, 7600-7605.

¹²⁶a) Schulz, M.D.; Atkinson, M.B.J.; Elsey, R.J.; Thuo, M.M. *Transition Met. Chem.*, **2014**, *39*, 763-767.; b) Ulman, M.; Grubbs, R.H. *J. Org. Chem.*, **1999**, *64*, 7202-7207.; c) Dias, E.L.; Grubbs, R.H. *Organometallics*, **1998**, *17*, 2758-2767.; d) Dias, E.L.; Nguyen, S.T.; Grubbs, R.H. *J. Am. Chem. Soc.*, **1997**, *119*, 3887-3897.

¹²⁷a) Churchill, M.R.; Kalra, K.L. *Inorg. Chem.*, **1974**, *13*, 1065-1071.; b) Churchill, M.R.; DeBoer, B.G.; Mendak, S.J. *Inorg. Chem.*, **1975**, *14*, 2041-2047.

¹²⁸Schmidbaur, H.; Adlkofer, J.; Schwirten, K. *Chem. Ber.*, **1972**, *105*, 3382-3388.

¹²⁹a) Churchill, M.R.; Rotella, F.J. *Inorg. Chem.*, **1979**, *18*, 166-171.; b) Moers, F.G.; Op Het Veld, P.H. *J. Inorg. Nucl. Chem.*, **1970**, *22*, 3225-3228.

¹³⁰a) Dougherty, D.A. *Science*, **1996**, *271*, 163-168, b) Ma, J.C.; Dougherty, D.A. *Chem. Rev.*, **1997**, *97*, 1303-1324.

¹³¹Zacharias, N.; Dougherty, D.A. *Trends Pharma. Sci.*, **2002**, *23*, 281-287.

¹³²Gokel, G.; *Chem. Commun.*, **2003**, 2847-2852.

¹³³a) Zaric, S.D.; *Eur. J. Inorg. Chem.*, **2003**, 2197-2209.; b) Zhang, S.-L.; Liu, L.; Fu, Y.; Guo, Q.-X. *J. Molec. Struct.: TEOCHEM*, **2005**, *757*, 37-46.

¹³⁴a) Dines, M.B.; Bird, P.H. *J. Chem. Soc. Chem. Commun.*, **1973**, *12*.; b) Turner, R.W.; Amma, E.L.; *J. Am. Chem. Soc.*, **1966**, *88*, 1877-1882.

¹³⁵Wright, A.M.; Irving, B.J.; Wu, G.; Meijer, A.J.H.M.; Hayton, T.W. *Angew. Chem. Int. Ed.*, **2015**, *54*, 3088-3091.

-
- ¹³⁶a) Cotton, F.A.; Marks, T.J. *J. Am. Chem. Soc.*, **1970**, *92*, 5114-5117.; b) Cotton, F.A.; Takats, J. *J. Am. Chem. Soc.*, **1970**, *92*, 2353-2358.
- ¹³⁷Sircoglou, M.; Bontemps, S.; Bouhadir, G.; Saffon, N.; Miqueu, K.; Gu, W.; Merci, M.; Chen, C.-H.; Foxman, B.M.; Maron, L.; Ozerov, O.V.; Bourissou, D. *J. Am. Chem. Soc.*, **2008**, *130*, 16729-16738.
- ¹³⁸Laitar, D.S.; Tsui, E.Y.; Sadighi, J.P. *Organometallics*, **2006**, *25*, 2405-2408.
- ¹³⁹Sircoglou, M.; Bontemps, S.; Mercy, M.; Miqueu, K.; Ladeira, S.; Saffon, N.; Maron, L.; Bouhadir, G.; Bourissou, D. *Inorg. Chem.*, **2010**, *49*, 3983-3990.
- ¹⁴⁰Perez, V.; Bi, W.; Fontaine, F.-G. *Unpublished results*, **2014**.
- ¹⁴¹Emslie, D.J.H.; Blackwell, J.M.; Britten, J.F.; Harrington, L.E. *Organometallics*, **2006**, *25*, 2412-2414.
- ¹⁴²Oakley, S.R.; Parker, K.D.; Emslie, D.J.H.; Vargas-Baca, I.; Robertson, C.M.; Harrington, L.E.; Britten, J.F. *Organometallics*, **2006**, *25*, 5835-5838.
- ¹⁴³Zhao, X.; Otten, E.; Song, D.; Stephan, D.W. *Chem. Eur. J.*, **2010**, *16*, 2040-2044.
- ¹⁴⁴Díez-González, S.; Stevens, E.D.; Scott, N.M.; Petersen, J.L.; Nolan, S.P. *Chem. Eur. J.*, **2008**, *14*, 158-168.
- ¹⁴⁵Xu, F.-B.; Li, Q.-S.; Wu, L.-Z.; Leng, X.-B.; Li, Z.-C.; Zeng, X.-S.; Chow, Y.L.; Zhang, Z.-Z. *Organometallics*, **2003**, *22*, 633-640.
- ¹⁴⁶Cowley, A.H.; Giolando, D.M.; Jones, R.A.; Nunn, C.M.; Power, J.M. *J. Chem. Soc., Chem. Commun.*, **1988**, 208-209.
- ¹⁴⁷Maron, L. Personal Communication, **2015**.
- ¹⁴⁸a) Stammler, H.-G.; Jutzi, P.; Wieland, W.; Neumann, B. *Acta Crystallogr.*, **1998**, *C54*, 64-66.; b) Gee, D.R.; Wan, J.K.S. *Can. J. Chem.*, **1971**, *49*, 160-163.; c) Traynham, J.G.; Olechowski, R. *J. Am. Chem. Soc.*, **1959**, *81*, 571-574.
- ¹⁴⁹Budzelaar, P.H.; Engelberts, J.J.; Lenthe, J.H. *Organometallics*, **2003**, *22*, 1562-1576.
- ¹⁵⁰Puddephatt, R.J., Thompson, P.J., *J. Organomet. Chem.*, **1976**, *117*, 395-403.
- ¹⁵¹a) Vicente, J.; Chicote, M.T.; Jones, P.G. *Inorg. Chem.*, **1993**, *32*, 4960-4964.; b) Vicente, J.; Chicote, M.T.; Saura-Llamas, I.; Lagunas, M.-C. *J. Chem. Soc., Chem. Commun.*, **1992**, 915-916.; c) Annan, T.A.; Kumar, R.; Tuck, D.G. *J. Chem. Soc., Dalton Trans.*, **1991**, 11-18.; d) Dyson, D.B.; Parish, R.V.; McAuliffe, C.A.; Pritchard, R.G.; Fields, R.; Beagley, B. *J. Chem. Soc., Dalton Trans.*, **1989**, 907-914.; e) Annan, T.A.; Kumar, R.; Tuck, D.G. *J. Chem. Soc., Chem. Commun.*, **1988**, 446-448.; f) Dyson, D.B.; Parish, R.V.; McAuliffe, C.A.; Fields, R. *Hyperfine Interact.*, **1988**, *40*, 327-330.
- ¹⁵²Stefanescu, D.M.; Yuen, H.F.; Glueck, D.S.; Golen, J.A.; Rheingold, A.L. *Angew. Chem. Int. Ed.*, **2003**, *42*, 1046-1048.
- ¹⁵³Schmidbaur, H. *Gold Bull.*, **2000**, *33*, 3-10.

-
- ¹⁵⁴Werner, H.; Otto, H.; Ngo-Khac, T.; Burschka, Ch. *J. Organomet. Chem.*, **1984**, *262*, 123-136.
- ¹⁵⁵Himmelspach, A.; Finze, M.; Raub, S. *Ange. Chem. Int. Ed.*, **2011**, *50*, 2628-2631.
- ¹⁵⁶Schmidbaur, H. *Chem. Soc. Rev.*, **1995**, 391-400.
- ¹⁵⁷a) Van Calcar, P.M.; Olmstead, M.M.; Balch, A.L. *J. Chem. Soc., Chem. Commun.*, **1995**, 1773-1774.; b) Van Calcar, P.M.; Olmstead, M.M.; Balch, A.L. *Inorg. Chem.*, **1997**, *36*, 5231-5238.
- ¹⁵⁸a) Puddephatt, R.J. *J. Organomet. Chem.*, **2015**, *792*, 13-24.; b) Wiseman, M.R.; Marsh, P.A.; Bishop, P.T.; Brisdon, B.J.; Mahon, M.F. *J. Am. Chem. Soc.*, **2000**, *122*, 12598-12599.
- ¹⁵⁹a) Baukova, T.V.; Slovokhotov, Y.L.; Struchkov, Y.T. *J. Organomet. Chem.*, **1981**, *220*, 125-137.; b) Ortaggi, G. *J. Organomet. Chem.*, **1974**, *80*, 275-279.
- ¹⁶⁰Bruker (2005). APEX 2 Version 2.0.2. Bruker AXS Inc., Madison, Wisconsin, USA.
- ¹⁶¹Bruker (2003). SAINT Version 7.07a. Bruker AXS Inc., Madison, Wisconsin, USA.
- ¹⁶²Sheldrick, G.M. (1997). SHELXS-97 and SHELXL-97. Programs for the refinement of crystal structures. University of Gottingen, Germany.
- ¹⁶³Frisch, M.J.; Trucks, G.W.; Schlegel, H.B.; Scuseria, G.E.; Robb, M.A.; Cheeseman, J.R.; Montgomery, J.A.Jr.; Vreven, T.; Kudin, K.N.; Burant, J.C.; Millam, J.M.; Iyengar, S.S.; Tomasi, J.; Barone, V.; Mennucci, B.; Cossi, M.; Scalmani, G.; Rega, N.; Petersson, G.A.; Nakatsuji, H.; Hada, M.; Ehara, M.; Toyota, K.; Fukuda, R.; Hasegawa, J.; Ishida, M.; Nakajima, T.; Honda, Y.; Kitao, O.; Nakai, H.; Klene, M.; Li, X.; Knox, J.E.; Hratchian, H.P.; Cross, J.B.; Bakken, V.; Adamo, C.; Jaramillo, J.; Gomperts, R.; Stratmann, R.E.; Yazyev, O.; Austin, A.J.; Cammi, R.; Pomelli, C.; Ochterski, J.W.; Ayala, P.Y.; Morokuma, K.; Voth, G.A.; Salvador, P.; Dannenberg, J.J.; Zakrzewski, V.G.; Dapprich, S.; Daniels, A. D.; Strain, M.C.; Farkas, O.; Malick, D.K.; Rabuck, A.D.; Raghavachari, K.; Foresman, J.B.; Ortiz, J.V.; Cui, Q.; Baboul, A.G.; Clifford, S.; Cioslowski, J.; Stefanov, B.B.; Liu, G.; Liashenko, A.; Piskorz, P.; Komaromi, I.; Martin, R. L.; Fox, D.J.; Keith, T.; Al-Laham, M.A.; Peng, C.Y.; Nanayakkara, A.; Challacombe, M.; Gill, P.M.W.; Johnson, B.; Chen, W.; Wong, M.W.; Gonzalez, C.; Pople, J.A. Gaussian 03, Revision C.02; Gaussian, Inc.: Wallingford, CT, **2004**.
- ¹⁶⁴a) Perdew, J.P.; Wang, Y. *Phys. Rev. B*, **1992**, *45*, 284.; b) Becke, A.D. *J. Chem. Phys.*, **1993**, *98*, 5648-5652.
- ¹⁶⁵a) McLean, A.D.; Chandler, G.S. *J. Chem. Phys.*, **1980**, *72*, 5639-5648.; (b) Krishnan, R.; Binkley, J.S.; Seeger, R.; Pople, J.A.J. *J. Chem. Phys.*, **1980**, *72*, 650-654. c) Clark, T.; Chandrasekhar, J.; Spitznagel, G.W.; Schleyer, P.B.R. *J. Comput. Chem.*, **1983**, *4*, 294-301.; d) Wachters, A.J.H. *J. Chem. Phys.*, **1970**, *52*,

- 1033–1036.; e) Hay, P.J. *J. Chem. Phys.*, **1977**, *66*, 4377–4384.; f) Frisch, M.J.; Pople, J.A.; Binkley, J.S. *J. Chem. Phys.*, **1984**, *80*, 3265–3269.
- ¹⁶⁶Cui, P.; Chen, Y.; Zeng, X.; Sun, J.; Li, G.; Xia, W. *Organometallics*, **2007**, *26*, 6519–6521.
- ¹⁶⁷a) Schulman, J.M.; Disch, R.L. *Organometallics*, **1989**, *8*, 733–737.; b) Cioslowski, J.; Hay, P.J. *J. Am. Chem. Soc.*, **1990**, *112*, 1707–1710.; c) Zheng, X.; Herberich, G.E. *Organometallics*, **2000**, *19*, 3751–3753.
- ¹⁶⁸For synthesis of boratabenzene species see references: 31, 33, 35, 38, a) Herberich, G.E.; Schmidt, B.; Englert, U. *Organometallics*, **1995**, *14*, 471–480.
- ¹⁶⁹a) Rogers, J.S.; Bu, S.; Bazan, G.C. *J. Am. Chem. Soc.*, **2000**, *122*, 730–731.; b) Rogers, J. S.; Bu, X.; Bazan, G.C. *Organometallics*, **2000**, *19*, 3948–3956.
- ¹⁷⁰a) Tweddell, J.; Hoic, D. A.; Fu, G. C. *J. Org. Chem.*, **1997**, *62*, 8286–8287.; b). Herberich, G. E.; Ganter, B.; Pons, M. *Organometallics*, **1998**, *17*, 1254–1256.; c) Herberich, G. E.; Englert, U.; Ganter, B.; Pons, M. *Eur. J. Inorg. Chem.*, **2000**, 976–986.
- ¹⁷¹a) Behrens, U.; Meyer-Friedrichsen, T.; Heck, J. Z. *Anorg. Allg. Chem.*, **2003**, *629*, 1421–1430.; b) Jaska, C. A.; Emslie, D. J. H.; Bosdet, M. J. D.; Piers, W. E.; Sorensen, T. S.; Parvez, M. *J. Am. Chem. Soc.*, **2006**, *128*, 10885–10896.; c) Wood, T. K.; Piers, W. E.; Keay, B. A.; Parvez, M. *Angew. Chem. Int. Ed.*, **2009**, *48*, 4009–4012.; d) Wood, T. K.; Piers, W. E.; Keay, B. A.; Parvez, M. *Chem. Eur. J.*, **2010**, *16*, 12199–12206.; e) Emslie, D. J. H.; Piers, W. E.; Parvez, M. *Angew. Chem. Int. Ed.*, **2003**, *42*, 1252–1255.; f) Tan, W.B.; Hongmei, J.; Yang, S.-W.; Xu, G.Q. *Nanoscale*, **2012**, *4*, 7557–7562.
- ¹⁷²Herberich, G.E.; Ohst, H. *Adv. Organomet. Chem.*, **1986**, *25*, 199–236.
- ¹⁷³a) Putzer, M.A.; Rogers, J.S.; Bazan, G.C. *J. Am. Chem. Soc.*, **1999**, *121*, 8112–8113.; b) Bazan, G.C.; Cotter, W.D.; Komon, Z.J.A.; Lee, R.A.; Lachicotte, R.J. *J. Am. Chem. Soc.*, **2000**, *122*, 1371–1380.; c) Sperry, C.K.; Rodriguez, G.; Bazan, G.C. *J. Organomet. Chem.*, **1997**, *548*, 1–7.
- ¹⁷⁴a) Sperry, C. K.; Bazan, G. C.; Cotter, W. D. *J. Am. Chem. Soc.*, **1999**, *121*, 1513–1523.; b) Ashe, A.J.; Al-Ahmad, S.; Fang, X. *J. Organomet. Chem.*, **1999**, *581*, 92–97.
- ¹⁷⁵a) Herberich, G. E.; Boveleth, W.; Hessner, B.; Koch, W.; Raabe, E.; Schmitz, D. *J. Organomet. Chem.*, **1984**, *265*, 225–235.; b) Raabe, G.; Baldofski, M. *Aust. J. Chem.*, **2011**, *64*, 957–964.
- ¹⁷⁶Belt, S. T.; Haddleton, V.; Perutz, R. N.; Smith, B. P. H.; Dixon, A. J. *J. Chem. Soc., Chem. Commun.*, **1987**, 1347–1349.
- ¹⁷⁷Duckett, S. B.; Haddleton, D. M.; Jackson, S. A.; Perutz, R. N.; Poliakoff, M.; Upmacis, R. K. *Organometallics*, **1988**, *7*, 1526–1532.
- ¹⁷⁸Hoic, D. A. Ph.D. thesis, Massachusetts Institute of Technology, **1998**.

¹⁷⁹T1 measurements at different temperatures are recommended in order to find a minimum relaxation time. a) Hamilton, D.G.; Crabtree, R.H. *J. Am. Chem. Soc.*, **1998**, *110*, 4126-4133.; b) Jessop, P.G.; Morris, R. *Coord. Chem. Rev.*, **1992**, *121*, 155-248.

¹⁸⁰a) Taw, F.L.; Mellows, H.; White, P.S.; Hollander, F.J.; Bergman, R.G.; Brookhart, M.; Heinekey, D.M. *J. Am. Chem. Soc.*, **2002**, *124*, 5100-5108.; b) Oldham Jr, W.J.; Hinkle, A.S.; Heinekey, D.M. *J. Am. Chem. Soc.*, **1997**, *119*, 11028-11036.; c) Janowicz, A.H.; Bergman, R.G. *J. Am. Chem. Soc.*, **1983**, *105*, 3929-3939.

¹⁸¹a) Periana, R. A.; Bergman, R. G. *J. Am. Chem. Soc.*, **1986**, *108*, 7332-7346.; b) Isobe, K.; Bailey, P.M.; Maitlis, P. M. *J. Chem. Soc., Dalton Trans.*, **1981**, 2003-2008; c) Werner, H.; Wolf, J. *Angew. Chem. Int. Ed.*, **1982**, *21*, 296-297.

¹⁸²Heinekey, D.M.; Millar, J.M.; Koetzle, T.F.; Payne, N.G.; Zilm, K.W. *J. Am. Chem. Soc.*, **1990**, *112*, 909-919.

¹⁸³For homogenous catalysts see: a) Osborn, J.A.; Jardine, F.H.; Young, J.F.; Wilkinson, G. *Chem. Commun.*, **1965**, 131-132.; b) Osborn, J.A.; Jardine, F.H.; Young, J.F.; Wilkinson, G. *J. Chem. Soc. A*, **1966**, 1711-1732.; c) Kitamura, K.; Shigeta, M.; Maezawa, Y.; Watanabe, Y.; Hsu, D.-S.; Ando, Y.; Matsumoto, T.; Susuki, K. *J. Antibiot.*, **2013**, *66*, 131-139.; d) Jourdan, A.; Gonzáles-Zamora, E.; Zhu, J. *J. Org. Chem.*, **2002**, *67*, 3163-3164.; e) Duckett, S. B.; Newell, C.L.; Eisenberg, R. *J. Am. Chem. Soc.*, **1994**, *116*, 10548-10556.; f) Iwami, T.; Yoshida, T.; Sato, M. *J. Chem. Soc. Japan*, **1976**, *10*, 1652-1653.; g) Guoi, X.; Scott, P.J.; Rempel, G.L. *J. Mole. Catal.*, **1992**, *72*, 193-208.; h) Furstner, A.; Nagano, T. *J. Am. Chem. Soc.*, **2007**, *129*, 1906-1907.; i) Mercadente, M.A.; Kelly, C.B.; Lee, C. Leadbeater, N.E. *Org. Process Res. Dev.*, **2012**, *16*, 1064-1068.; j) Bugoni, S.; Boccato, D.; Porta, A.; Zanoni, G.; Vidari, G. *Chem. Eur. J.*, **2015**, *21*, 791-799.; For heterogeneous catalysts see: k) Singha, N.K.; Sivaram, S.; Talwar, S.S. *Rub. Chem. Technol.*, **1995**, *68*, 281-286.; l) Singha, N.K.; Sivaram, S.; Talwar, S.S. *Polym. Sci.*, **1994**, *1*, 181-185.; m) Kovtunov, K.V.; Zhivonitko, V.V.; Skovpin, I.V.; Barskiy, D.A.; Salnikov, O.G.; Koptug, I.B. *J. Phys. Chem. C*, **2013**, *117*, 2287-22893.

¹⁸⁴Bruker (2005). APEX 2 Version 2.0.2. Bruker AXS Inc., Madison, Wisconsin, USA.

¹⁸⁵Bruker (2003). SAINT Version 7.07a. Bruker AXS Inc., Madison, Wisconsin, USA.

¹⁸⁶Sheldrick, G.M. (1997). SHELXS-97 and SHELXL-97. Programs for the refinement of crystal structures. University of Göttingen, Germany.

¹⁸⁷Staubitz, A.; Robertson, A.P.M.; Sloan, M.E.; Manners, I. *Chem. Rev.*, **2010**, *110*, 4023-4078.

-
- ¹⁸⁸Taylor, L.J.; Surgenor, B.A.; Wawrzyniak, P.; Ray, M.J.; Cordes, D.B.; Slawin, A.M.Z.; Kilian, P. *Dalton Trans.*, **2016**, *Advance Article* DOI: 10.1038/C5DT02539G
- ¹⁸⁹a) Hetzer, R.H.; Gais, H.-J.; Raabe, G. *Synthesis*, **2008**, *7*, 1126-1132.; b) Schlieve, C.R.; Tam, A.; Nilsson, B.L.; Lieven, C.J.; Raines, R.T.; Levin, L.A. *Exp. Eye. Res.*, **2006**, *83*, 1252-1259.
- ¹⁹⁰a) Brunel, J.M.; Faure, B.; Maffe, M. *Coord. Chem. Rev.*, **1998**, *170-180*, 665-698.; b) Gaumont, A.-C.; Gulea, M.; Levillain, J. *Chem. Rev.*, **2009**, *109*, 1371-1401.; c) Glueck, D.S. *Chem. Eur. J.*, **2008**, *14*, 7108-7117.
- ¹⁹¹Barban, J.A.; Roberts, B.P. *J. Chem. Soc., Perkin Trans. 2*, **1988**, 1195-1200.
- ¹⁹²Stephan, D.W. *Dalton Trans.*, **2009**, 3129-3136.
- ¹⁹³a) Spies, P.; Kehr, G.; Bergander, K.; Wibbeling, B.; Frohlich, R.; Erker, G. *Dalton Trans.*, **2009**, 1534-1541.; b) Geie, S.; Stephan, D.W. *Chem. Commun.*, **2010**, *46*, 1026-1028.; c) Geier, S.J.; Gilbert, T.M.; Stephan, D.W. *J. Am. Chem. Soc.*, **2008**, *130*, 12632-12633.
- ¹⁹⁴Fuller, A.-M.; Mountford, A.J.; Scott, M.L.; Coles, S.J.; Horton, P.N.; Hughes, D.L.; Hursthouse, M.B.; Lancaster, S.J. *Inorg. Chem.*, **2009**, *48*, 11474-11482.
- ¹⁹⁵a) Lancaster, S.J.; Walker, D.A.; Thornton-Pett, M.; Bochman, M. *Chem. Commun.*, **1999**, 1533-1534.; b) LaPointe, R.E.; Roof, G.R.; Abboud, K.A.; Klosin, J. *J. Am. Chem. Soc.*, **2000**, *122*, 9560-9561.; c) Zhou, J.; Lancaster, S.J.; Walker, D.A.; Beck, S.; Thornton-Pett, M.; Bochman, M. *J. Am. Chem. Soc.*, **2001**, *123*, 223-237.; d) Lancaster, S.J.; Rodriguez, A.; Lara-Sanchez, A.; Hannant, M.D.; Walker, D.A.; Hughes, D.H.; Bochman, M. *Organometallics*, **2002**, *21*, 451-453.; e) Hannant, M.H.; Wright, J.A.; Lancaster, S.J.; Hughes, D.L.; Horton, P.N.; Bochman, M. *Dalton Trans.*, **2006**, 2415-2426.
- ¹⁹⁶Jaska, C.A.; Lough, A.J.; Manners, I. *Inorg. Chem.*, **2004**, *43*, 1090-1099.
- ¹⁹⁷Dornhaus, F.; Bolte, M.; Lerner, H.-W.; Wagner, M. *Eur. J. Inorg. Chem.*, **2006**, 1777-1785.
- ¹⁹⁸a) Gaumont, A.-C.; Brown, J.M.; Hursthouse, M.B.; Coles, S.J. *Chem. Commun.*, **1999**, 63-64.; b) Dorn, H.; Jaska, C.A.; Singh, R.A.; Lough, A.J.; Manners, I. *Chem. Commun.*, **2000**, 1041-1042.
- ¹⁹⁹Muller, G.; Brand, J. *Organometallics*, **2003**, *22*, 1463-1467.
- ²⁰⁰a) Gilbert, T.M. *Dalton Trans.*, **2012**, 9046-9055.; b) Neu, R.C.; Lough, A.; Stephan, D.W. *Chem. Sci.*, **2011**, 170-176.; c) Skara, G.; Pinter, B.; Top, J.; Geerlings, P.; De Proft, F.; De Vleeschouwer, F. *Chem. Eur. J.*, **2015**, *21*, 5510-5519.
- ²⁰¹Bradley, D.C.; Harding, I.S.; Keefe, A.D.; Motevalli, M.; Zheng, D.H. *J. Chem. Soc., Dalton Trans.*, **1996**, 3931-3936.
- ²⁰²Zhu, K.; Achord, P.D.; Zhang, X.; Krogh-Jespersen, K.; Goldman, A.S. *J. Am. Chem. Soc.*, **2004**, *126*, 13044-13053.

-
- ²⁰³Wolfsberger, W.; Burkart, W.; Bauer, S.; Hampp, A.; Wolf, J.; Werner, H. Z. *Naturforschung*, **1994**, *49b*, 1659-1673.
- ²⁰⁴ACD-A: Sigma-Aldrich, Spectral data were obtained from Advanced Chemistry Development, Inc.
- ²⁰⁵Brown, H.C.; Racherla, U.S. *J. Org. Chem.*, **1986**, *51*, 427-432.
- ²⁰⁶Haaland, A. *Angew. Chem. Int. Ed.*, **1989**, *28*, 992-1007.
- ²⁰⁷Tenorio, M.J.; Puerta, M.C.; Valerga, P. *J. Chem. Soc., Dalton Trans.*, **1996**, 1305-1308.
- ²⁰⁸Jones, R.A.; Norman, N.C.; Seeberger, M.H.; Atwood, J.L.; Hunter, W.E. *Organometallics*, **1983**, *2*, 1629-1634.
- ²⁰⁹Jones, R.A.; Stuart, A.L.; Atwood, J.L.; Hunter, W.E.; Rogers, R.D. *Organometallics*, **1982**, *1*, 1721-1723.
- ²¹⁰Theopold, K.H.; Rheingold, A.L.; Incarvito, C.D. CCDC 137580: *Experimental Crystal Structure Determination*, **1999**, DOI: 10.5517/cc4m52z. Deposited on: 2/12/1999. Data available at <http://www.ccdc.cam.ac.uk/>.
- ²¹¹a) Britzinger, H.H.; Fischer, D.; Mulhaupt, R.; Rieger, B.; Waymouth, R.M. *Angew. Chem. Int. Ed.*, **1995**, *34*, 1143-1170.; b) Gladysz, J.A. *Chem. Rev.*, **2000**, *100*, 1167-1168.
- ²¹²a) Wang, B. *Coord. Chem. Rev.*, **2006**, *250*, 242-258.; b) Braunsweig, H.; Breitling, F.M. *Coord. Chem. Rev.*, **2006**, *250*, 2691-2720.
- ²¹³Luttringhaus, A.; Kullick, W. *Angew. Chem.*, **1958**, *70*, 438.
- ²¹⁴Morwood, J. *The Pocket Oxford Latin Dictionary: Latin-English*, 3rd Ed., Oxford University Press: *online version*, **2012**. <http://www.oxfordreference.com/view/10.1093/acref/9780191739583.001.0001/acref-9780191739583>, Consulted online on November **2015**.
- ²¹⁵Yang, H.; Fang, X.; Kampf, J.W.; Ashe, A.J. *Polyhedron*, **2005**, *24*, 1280-1288.
- ²¹⁶a) Gibson, V.C.; Spitzmesser, S.K. *Chem. Rev.*, **2003**, *103*, 283-316.; b) Shaltout, R.M.; Corey, J.Y.; Rath, N.P. *J. Organomet. Chem.*, **1995**, *503*, 205-212.
- ²¹⁷a) Spaleck, W.; Antbert, M.; Rohrmann, J.; Winter, A.; Bachmann, B.; Kiprof, P.; Behm, J.; Hermann, W. *Angew. Chem. Int. Ed.*, **1992**, *31*, 1347-1350.; b) Hermann, W.; Rohrmann, J.; Herdtweck, E.; Spaleck, W.; Winter, A. *Angew. Chem. Int. Ed.*, **1989**, *28*, 1511-1512.
- ²¹⁸a) Bajgur, C.S.; Tikkanen, W.; Petersen, J.L. *Inorg. Chem.*, **1985**, *24*, 2539-2546.; b) Larkin, S.A.; Golden, J.T.; Shapiro, P.J.; Yap, G.P.A.; Ming Jin Foo, D.; Rheingold, A.L. *Organometallics*, **1996**, *15*, 2393-2398.; c) Stelck, D.S.; Shapiro, P.J.; Basicckes, N. *Organometallics*, **1997**, *16*, 4546-4550.
- ²¹⁹a) Bourissou, D.; Freund, C.; Martin-Vaca, B.; Bouhadir, G. *C. R. Chimie*, **2006**, *9*, 1120-1142.; b) Leyser, N.; Schmidt, K.; Brintzinger, H.-H. *Organometallics*, **1998**, *17*, 2155-2161.; c) Kauffmann, T.; Ennen, J.; Berghus, K. *Tetrahedron Lett.*, **1984**, *25*, 1971-1974.

-
- ²²⁰a) Ostoja-Starzewski, A.; Kelly, W.M.; Stumpf, A.; Freitag, D. *Angew. Chem. Int. Ed.*, **1999**, *38*, 2439-2443.; b) Ostoja-Starzewski, A. *Macromol. Symp.*, **2004**, *213*, 47-55.; c) Braunschweig, H.; Bera, H.; Stellwag, S.; Schwarz, S.; Hemberger, Y.; Radacki, K. *Z. Anorg. Allg. Chem.*, **2007**, *633*, 2314-2320.
- ²²¹Ashe, A.J.; Al-Ahmad, S.; Fang, X.; Kampf, J.W. *Organometallics*, **1998**, *17*, 3883-3888.
- ²²²Cui, P.; Chen, Y.; Li, G.; Xia, W. *Angew. Chem. Int. Ed.* **2008**, *47*, 9944-9947.
- ²²³Cui, P.; Chen, Y.; Li, G.; Xia, W. *Organometallics*, **2011**, *30*, 2012-2017.
- ²²⁴Cui, P.; Chen, Y.; Zhang, Q.; Li, G.; Xia, W. *J. Organomet. Chem.*, **2010**, *695*, 2713-2719.
- ²²⁵Dioumaev, V.K.; Harrod, J.F. *Organometallics*, **1997**, *16*, 2798-2807.
- ²²⁶Lockhart, J.C. *Chem. Rev.*, **1965**, *65*, 131-151.
- ²²⁷a) Kopf, H.; Klapotke, T. *Z. Naturforschung*, **1985**, *40b*, 447-449.; b) Peigné, B.; Cano, J.; Aullón, G. *Eur. J. Inorg. Chem.*, **2012**, 797-806.
- ²²⁸a) References 56, 57, 60, 166, 173; b) Yuan, Y.; Chen, Y.; Li, G.; Xia, W. *Organometallics*, **2010**, *29*, 3277-3728.; c) Cui, P.C.; Chen, Y.; Wang, G.; Li, G.; Xia, W. *Organometallics*, **2008**, *27*, 4013-4016.; d) Yuan, Y.; Wang, X.; Li, Y.; Fan, L.; Xu, X.; Chen, Y.; Li, G.; Xia, W. *Organometallics*, **2011**, *30*, 4330-4341.; e) Wang, C.; Leng, X.; Chen, Y. *Organometallics*, **2015**, *34*, 3216-3221.
- ²²⁹Bruker (**2005**). APEX 2 Version 2.0.2. Bruker AXS Inc., Madison, Wisconsin, USA.
- ²³⁰Bruker (**2003**). SAINT Version 7.07a. Bruker AXS Inc., Madison, Wisconsin, USA.
- ²³¹Sheldrick, G.M. (**1997**). SHELXS-97 and SHELXL-97. Programs for the refinement of crystal structures. University of Gottingen, Germany.
- ²³²Qu, B.; Haddad, N.; Han, Z.S.; Rodriguez, S.; Lorenz, J.C.; Grinberg, N.; Lee, H.; Busacca, C.A.; Krishnamurthy, D.; Senanayake, C.H. *Tetrahedron Lett.*, **2009**, *50*, 6126-6129.
- ²³³Jaafar, H.; Li, H.; Misal Castro, L.C.; Zheng, J.; Roisnel, T.; Dorcet, V.; Sortais, J.-B.; Darcel, C. *Eur. J. Inorg. Chem.*, **2012**, 3546-3550.
- ²³⁴Sircoglou, M.; Bontemps, S.; Mercy, M.; Saffon, N.; Takahashi, M.; Bouhadir, G.; Maron, L.; Bourissou, D. *Angew. Chem. Int. Ed.*, **2007**, *46*, 8583-8586.